Universidade Federal de Juiz de Fora

Programa de Pós-Graduação em

Engenharia Elétrica

Pablo Carlos de Siqueira Furtado

CONTRIBUTIONS TO POWER CONDITIONING TECHNIQUES IN TWO-PHASE
THREE-WIRE ELECTRIC NETWORKS

Doctoral Thesis

Juiz de Fora

2019

Pablo Carlos de Siqueira Furtado

CONTRIBUTIONS TO POWER CONDITIONING TECHNIQUES IN TWO-PHASE
THREE-WIRE ELECTRIC NETWORKS

<div style="margin-left:50%">

Doctoral thesis presented to the Electrical Engineering Program, area of Electronic Systems, of the Federal University of Juiz de Fora in partial fulfilment of the requirements for the degree of Doctor in Electrical Engineering.

</div>

Supervisor: Prof. Pedro Gomes Barbosa, D.Sc.

Juiz de Fora

2019

Pablo Carlos de Siqueira Furtado

CONTRIBUTIONS TO POWER CONDITIONING TECHNIQUES IN TWO-PHASE THREE-WIRE ELECTRIC NETWORKS

Doctoral thesis presented to the Electrical Engineering Program, area of Electronic Systems, of the Federal University of Juiz de Fora in partial fulfilment of the requirements for the degree of Doctor in Electrical Engineering.

Presented on 26th July 2019 .

EXAMINATION BOARD:

Prof. Pedro Gomes Barbosa, D.Sc.
Universidade Federal de Juiz de Fora, UFJF
Supervisor

Prof. Guilherme Márcio Soares, Dr.Eng.
Universidade Federal de Juiz de Fora, UFJF

Prof. Pedro Machado de Almeida, Dr.Eng.
Universidade Federal de Juiz de Fora, UFJF

Prof. Luís Fernando Corrêa Monteiro, D.Sc.
Universidade do Estado do Rio de Janeiro, UERJ

Prof. Danilo Iglesias Brandão, Dr.Eng.
Universidade Federal de Minas Gerais, UFMG

To all living beings.

ACKNOWLEDGEMENTS

"I know that I know nothing."

Socrates

ABSTRACT

This doctoral thesis deals with power conditioning applications in two-phase three-wire electric circuits derived from three-phase four-wire systems. This kind of application can be useful in modern electricity networks, specially for residential and small commercial consumers. An adaptation of the *pq* Theory is proposed to use the concepts of instantaneous powers in two-phase three-wire circuits. A linear transformation is proposed to map two-phase voltages and currents into an orthogonal $\alpha\beta$ reference frame. Time-domain mathematical analyses are used to present the behaviour and interpretation of two-phase instantaneous powers, comparing the proposed definitions with single-phase and three-phase instantaneous powers theories found in the literature. The concepts of two-phase instantaneous powers are used to design algorithms to control a shunt grid-connected converter, specially to be used as active power filter. It is also proposed an algorithm to detect fundamental-frequency positive-sequence voltages by measuring only two phase-voltages of the grid. Two different strategies are presented to control the shunt active power filter: double single-phase strategy and zero neutral current strategy. The adapted two-phase positive-sequence detector is implemented in a laboratory prototype and experimental results validate the effectiveness of the proposed positive-sequence detector. Simulation studies are also performed to validate the proposed control algorithms for two-phase power conditioning equipment. The obtained results confirm the effectiveness of the two proposed control strategies to compensate load reactive power and currents' harmonic components and unbalances. Furthermore, the zero-neutral current strategy shows to be suitable to avoid or reduce zero-sequence unbalances in distribution grids and microgrids. Proposals for future studies include further experimental implementation, active power injection applications and field measurements to evaluate the influence of zero-sequence voltage unbalances in the proposed controllers.

Keywords: Power conditioning, active power filters, power quality, *p–q* theory.

RESUMO

Esta tese de doutorado trata de aplicações de condicionamento de energia em circuitos elétricos bifásicos a três fios oriundos de sistemas trifásicos a quatro fios. Esse tipo de aplicação pode ser útil no futuro em redes modernas de energia, em especial para consumidores residenciais e pequenas instalações comerciais. Uma adaptação da Teoria pq é proposta como forma de utilizar os conceitos de potências instantâneas em circuitos bifásicos a três fios. Uma transformação linear é proposta para mapear tensões e correntes bifásicas para o sistema de coordenadas ortogonais $\alpha\beta$. Análises matemáticas no domínio do tempo são utilizadas como forma de apresentar o comportamento das potências instantâneas bifásicas, bem como sua interpretação, sendo comparadas com conceitos encontrados na literatura de potências instantâneas monofásicas e trifásicas. Os conceitos de potências bifásicas são utilizados para projetar algoritmos de controle conversores conectados em paralelo à rede elétrica, especialmente para realizar funções de filtro ativo de potência. É também proposto um algoritmo de detecção da tensão de sequência positiva, na frequência fundamental através da medição de duas tensões de fase apenas. Duas diferentes estratégias de controle são apresentadas para controle do filtro ativo paralelo: estratégia de operação duplo monofásico e a estratégia de mitigação da corrente de neutro. O detector de sequencia positiva adaptado para sistemas bifásicos foi implementado em um protótipo de laboratório e os resultados experimentais obtidos são usados como validação da estrutura proposta. Estudos de simulação foram também realizados para avaliar os algoritmos de controle propostos como um todo. Os resultados obtidos confirmaram a eficácia das estratégias de controle propostas para compensação de correntes harmônicas, potência reativa e desequilíbrios de correntes causados pela carga bifásica. Além disso, é mostrado que a estratégia de compensação para corrente de neutro zero é útil para evitar ou reduzir desequilíbrios de sequência zero em redes de distribuição e microrredes. As propostas para a continuação desta pesquisa incluem o aprofundamento da implementação experimental, aplicações de injeção de potência ativa na rede elétrica e medições de campo para quantificar a influência de desequilíbrios de sequência zero nos sistemas de controle propostos.

Palavras-chave: Condicionamento de energia, filtros ativos de potência, qualidade de energia, teoria p–q.

LIST OF FIGURES

LIST OF TABLES

LIST OF ACRONYMS AND ABBREVIATIONS

APF Active Power Filter

AC Alternating Current

ANEEL Agência Nacional de Energia Elétrica

DC Direct Current

DG Distributed Generation

DSC Digital Signal Controller

DSOGI Dual Second-Order Generalized Integrator

DSPS Double Single-Phase Strategy

ESS Energy Storage System

FFT Fast Fourier Transform

ICE Internal Combustion Engine

MPC Model Predictive Controller

MPPT Maximum Power Point Tracking

MRI Multiple Ressonant Integrators

NAEP Power Electronics and Automation Group (in Portuguese, *Núcleo de Automação e Eletrônica de Potência*)

PEV Plug-in Electric Vehicle

PEC Power Electronic Converter

PF Power Factor

PI Proportional-Integral

PLL Phase-Locked Loop

PV Photovoltaic

PC Power Conditioning

PCC Point of Common Coupling

PSC Positive-Sequence Calculation

QSG Quadrature Signal Generator

SG Smart Grid

SMC Sliding-Mode Controller

SRF Synchronous Reference Frame

THD Total Harmonic Distortion

UPS Uninterrupted Power Supply

UPQC Unified Power Quality Conditioner

RES resonant integrator

rms root mean square

SOGI Second-Order Generalized Integrator

SVM Space Vector Modulation

VSC Voltage Sourced Converter

UFJF Federal University of Juiz de Fora (in Portuguese, *Universidade Federal de Juiz de Fora, Brasil*)

V2G Vehicle-to-Grid

ZNCS Zero Neutral Current Strategy

CONTENTS

1 INTRODUCTION

The development and modernization of electric power systems is continuously pursued since the beginning of electricity distribution. The advances achieved intend to make electric systems more efficient, reliable, safe, cost-effective and adequate according to power quality requirements and demand needs. Nowadays, efforts and investments in grid modernization are also strongly motivated by concerns regarding sustainability and environment conservation. As new technologies are developed, new improvements and functionalities can be applied to power grids and loads. Therefore, the evolution of several technologies and their application in electric power systems has led researchers, governments, industry and utility companies to develop the concept of smart electricity networks, commonly referred as Smart Grids (SGs).

The expression *smart grids* can be understood in many ways. According to Bollen et al. (2010), SGs can be seen as the way power systems are operated, namely by applying communication, power electronics and energy storage technologies to match electrical energy production and consumption. From another point of view, the SG concept *"is emerging as a convergence of information technology and communication technology with power system engineering"* (FARHANGI, 2010). The definition presented by the U.S. Department of Energy (2016) states that a SG is the power network which *"uses digital technology to improve reliability, resiliency, flexibility, and efficiency (both economic and energy) of the electric delivery system"*. A typically European way to understand SGs regards electric networks capable of integrating all connected users (*i.e.*, generators, consumers, storage, etc.) to provide efficient, sustainable, economic and reliable electric services (CLASTRES, 2011). Despite such diversity in definitions, there is a consensus that power grids must evolve to face energy-related challenges of the 21th century, such as the environment conservation, reduction of fossil fuel economic dependence and meeting the increasing energy demand.

There are several technologies and functionalities currently related to the development of smart power grids. From operation and management point of view, efforts and investments on SGs development relies on the improvement of monitoring, analysis, optimization, decision-making and control technologies (FANG et al., 2012). Smart meters, for instance, aim to allow

two-way communication of time-sensitive measurements such as demand, local energy generation capacity and power quality index. Smart meters are also supposed to provide communication services (*e.g.*, as price changes) to commercial and residential energy management systems (NEENAN & HEMPHILL, 2008). The concept of demand response serve as an example of information technology applied to SGs. It is a management tool that allows the operator to regulate generation and consumption using available control technologies such as dynamic pricing, and not only by adjusting generation as in conventional power grids (FANG et al., 2012).

1.1 POWER CONDITIONING APPLICATIONS IN SMART GRIDS

Another important field in the evolution of power grids is the research and development of Power Conditioning (PC) technology (YU et al., 2011). Power conditioning is also referred as power processing in technical literature and throughout this text. In the context addressed in this work, PC is referred as actions aiming to process and control the flow of electric energy by using voltage and/or current waveforms that are optimally suited for each application and equipment (MOHAN; UNDELAND & ROBBINS, 1995). Power Electronic Converters (PECs) are currently *"the technology that enables the efficient and flexible interconnection of different players [...] to the electrical power system"* (TEODORESCU; LISERRE & RODRIGUEZ, 2011). Therefore, the research and development of applications, topologies and control systems for PECs play an essential role in the improvement of electric power networks. This work deals specifically with the control of PEC for PC functions in electric networks, as the in the applications briefly commented in the following subsections.

1.1.1 DISTRIBUTED GENERATION

In conventional power systems, most of the electric energy is generated by large power plants. These plants are installed in geographical locations that are apropriate for generation purposes. Thus, long distance transmission lines are commonly necessary to transport the generated energy to consumer centres. But nowadays, the decentralized generation of electric energy is seen as a better way to deliver a reliable and efficient power supply. The concept of Distributed Generation (DG) also embraces the intensive usage of renewable and alternative energy resources like Photovoltaic (PV) panels, wind turbines, hydrogen fuel cells, small hydro and others (GUERRERO et al., 2010).

In Brazil, where this thesis is developed, DG is regulated since the National Electric Energy Agency (in Portuguese, *Agência Nacional de Energia Elétrica*) released the normative resolution No. 482/2012. This document established general grid-connection requirements for

micro-generation (up to 75 kVA) and mini-generation systems (between 75 kVA and 3 MVA). The resolution No. 482/2012 also creates a credit system that allows users to sell surplus energy to the utility (ANEEL, 2012). The installation of rooftop PV systems is, since then, becoming more popular in Brazil.

Each kind of DG technology presents its own generation patterns, which commonly differ from consumer demand needs. There are also undesired characteristics such as intermittent generation and uncertain availability. The integration of DG to electric power grids is considered the key to properly explore these resources. Therefore, PECs are fundamental to match the characteristics of DG resources with grid connection requirements such as frequency, voltage, harmonic levels and active/reactive power flow control (BLAABJERG; CHEN & KJAER, 2004).

The main function of grid-interface converters in PV and fuel cell systems is to transform the generated energy from Direct Current (DC) into the Alternating Current (AC) form. Other functions commonly required for these inverters include voltage boosting, Maximum Power Point Tracking (MPPT), anti-islanding and grid synchronization (TEODORESCU; LISERRE & RODRIGUEZ, 2011; CHAKRABORTY; SIMÕES & KRAMER, 2013). In wind turbine systems, grid converters must perform an AC/AC power conversion. Power converters also allow generator control and output power regulation in this application, which are important functions for the proliferation of wind energy (TEODORESCU; LISERRE & RODRIGUEZ, 2011). As shown by Fogli (2014), PECs can also be employed to connect diesel-generators to the grid. In this case, the PEC is useful for grid-synchronization, stand-alone operation and mitigation of power oscillations in the generator.

1.1.2 PLUG-IN ELECTRIC VEHICLES

Most of present transportation facilities have their propulsion systems based on Internal Combustion Engines (ICEs). This technology presents several undesired characteristics. Low efficiency, emission of air-polluting gases and a strong dependence on fossil fuels as energy source can be cited as some deficiencies (EMADI, 2011). The adoption of Plug-in Electric Vehicles (PEVs) is emerging as an option to handle such issues in transportation. In this context, transportation electrification is seen as a practical opportunity to improve the use of available energy resources for transportation. The expression PEVs is used generically to refer to vehicles with electric propulsion and grid-connection capability (GALUS et al., 2013; YILMAZ & KREIN, 2013a; RICHARDSON, 2013; RODRIGUES et al., 2014).

Plug-in Electric Vehicles present several advantages over conventional ICE-based vehicles. For their high-efficiency, PEVs may reduce the overall emission of air-polluting gases, con-

sidering all emissions between fuel production and vehicle operation (RODRIGUES et al., 2014). Also, the energy necessary for electric transportation can be obtained from renewable and DG resources (IEA, 2011). Low noise emission and relatively low cost of electric motors are other pros of PEVs (IEA, 2011). In addition to such great advantages over ICE vehicles, other great interesting aspect of PEV technology rely on PECs used to interface vehicles and power grid, as discussed in the following paragraphs.

Motor driving and battery charging are the main functions performed by on-board power converters in PEVs (YILMAZ & KREIN, 2013a). The development of modern SGs creates new opportunities that improve the way such functions are performed. For example, proper communication and control may allow vehicle owners to choose how and when to charge PEV batteries. Therefore, vehicle owners could choose fast or slow charging, time-scheduled charging, to charge when energy costs are interesting, during peak generation hours or other possibilities (RICHARDSON, 2013). Furthermore, the employment of bidirectional on-board PECs also allows vehicles to return stored energy back to the grid, which is commonly referred as Vehicle-to-Grid (V2G) operation.

By properly controlling bidirectional on-board PECs, the power flow between grid and vehicle can be controlled aiming to perform additional functions in SGs or local microgrids (YILMAZ & KREIN, 2013b; GALUS et al., 2013). Many works found in technical literature report several different ancillary services that can be provided by PEVs in future SGs. For example, harmonic filtering and reactive power compensation in residential installations (RODRIGUES, 2014; TANAKA et al., 2013), backup power supply and load demand shaping (demand side management), renewables and DG integration and support, frequency regulation and voltage support (YILMAZ & KREIN, 2013b; RICHARDSON, 2013; GALUS et al., 2013).

1.1.3 ENERGY STORAGE SYSTEMS

The development of modern power networks, with high penetration of DG and PEVs, challenges operators to keep grid stability, reliability, efficiency and power quality. As Ribeiro et al. (2001) states, advancements on Energy Storage Systems (ESSs) and power electronics are making the application of energy storage technologies an useful tool to deal with modern system operation issues. Power converters are used to integrate ESSs to the grid, performing charge and discharge functions (VAZQUEZ et al., 2010). Also, PECs operate to meet, simultaneously, storage device characteristics and grid connection requirements. As literature review indicates, batteries, supercapacitors, flyweels, compressed air, superconducting magnetic systems are examples of energy storage technologies that may suit several advanced functions in SGs (RIBEIRO et al.,

2001; VAZQUEZ et al., 2010; KOOHI-KAMALI et al., 2013).

Energy storage plays a vital role on technical and economical aspects of transportation electrification. The autonomy and performance of PEVs are directly related to the characteristics of on-board ESS (FERREIRA, 2007). Two or more storage devices may be combined in a single vehicle aiming to extend their lifespan and improve the power quality provided to propulsion system (FERREIRA, 2007). For example, it is interesting to combine supercapacitors and batteries in road electric vehicles (FERREIRA, 2007; VAZQUEZ et al., 2010). Several ancillary V2G services, such as backup power supply and frequency regulation, also depend on energy storage capacity to be implemented (VAZQUEZ et al., 2010; GALUS et al., 2013).

Renewable energy and DG resources are also supported by ESSs. A high penetration of PV and wind systems, for example, may cause voltage and frequency oscillations due to intermittent generation characteristics. Also, these power sources commonly generate more energy out of peak demand periods (VAZQUEZ et al., 2010). Therefore, ESSs may be applied to smooth power outputs and store energy during peak generation to be used later when necessary (ROBERTS & SANDBERG, 2011).

As Vazquez et al. (2010) summarized, energy storage may also contribute in different applications regarding grid stability and control. For example ESSs help levelling demand curves, absorbing energy at peak generation and delivering at peak consumption, which is called peak-shaving. In this way, new infrastructure investments to meet load peaks may be postponed. In frequency regulation, high-capacity energy storage can serve as permanent resources, whereas low- and medium-capacity ESSs suit transient support (VAZQUEZ et al., 2010). In literature there are several proposals for other applications of ESSs(KOOHI-KAMALI et al., 2013; VAZQUEZ et al., 2010; RIBEIRO et al., 2001).

1.1.4 MICROGRIDS

An efficient and safe coordination of a whole SG, integrating a large number of DG resources, PEVs and ESSs, is a daunting task for a centralized grid operator. This challenge may be addressed by the concept of microgrids, which refers to a more decentralized management of SG resources (HATZIARGYRIOU et al., 2007). Therefore, microgrids are expected to increase renewable DG penetration in power grids, as well as to improve power quality by mitigating disturbances and reducing outages (USTUN; OZANSOY & ZAYEGH, 2011). In this aim, several works reported in literature are dedicated to the development of both DC and AC microgrid systems (JUSTO et al., 2013).

Essentially, microgrids can be understood as small-scale power-grid assemblies that group

loads and generators combined with storage resources, as well as management, control and protection systems. By summarizing, a microgrid can be seen as a single unity that behaves according to grid-connection constraints and provides ancillary services to the utility (USTUN; OZANSOY & ZAYEGH, 2011).

Microgrids shall operate in grid-connected and disconnected (islanded) modes. The control of PECs must meet specific requirements for each operation mode. In grid-connected mode, power converters are controlled for proper grid synchronization, power flow control and DG and ESSs integration. Islanding detection is also important for microgrid controllers in this operating condition. On the other hand, when a microgrid operates in islanded mode, PECs may perform to provide serveral features as, for example, voltage and frequency regulation, independent local energy flow management and DG and ESSs integration. Microgrid controllers are also supposed to monitor grid conditions for reconnection when possible or desired (JUSTO et al., 2013; USTUN; OZANSOY & ZAYEGH, 2011).

1.1.5 *ACTIVE POWER FILTERS*

Active Power Filters (APFs), or simply active filters, are static power converters connected to an electric grid to perform PC functions such as load balancing, harmonic filtering, power factor correction, voltage unbalance mitigation and others. Active filters operate in real-time, detecting load changes and adjusting compensation quantities. Another interesting feature is the flexible operation of APFs, which may perform PC functions simultaneously. Compared to traditional passive filters, APFs also present advantages regarding performance and volume (AKAGI, 2005).

In technical literature, several different topologies and control techniques of active filters have been discussed (AKAGI, 2005; EMADI; NASIRI & BEKIAROV, 2005; SINGH; AL-HADDAD & CHANDRA, 1999). Basically, regarding the type of grid connection, APFs can be shunt (parallel) or series filters. Shunt filters usually act as current sources, whereas series filters work as voltage sources in the grid. The union of shunt and series APF into a single equipment is commonly referred as Unified Power Quality Conditioner (UPQC). From constructive point of view, active filters are also classified as pure or hybrid. Pure APFs are composed by power converters, *i.e.*, more commonly Voltage Sourced Converters (VSCs). Hybrid APFs combine power converters and passive components as inductors, capacitors and resistors (AKAGI, 2005; EMADI; NASIRI & BEKIAROV, 2005; SINGH; AL-HADDAD & CHANDRA, 1999).

Active filters, specially those presenting shunt connection, can be found in commercial use all over the world (AKAGI; WATANABE & AREDES, 2007). Recent works in this field of appli-

cation dedicate to describing active filtering functions as additional features for grid-connected converters such as those in electric vehicles (RODRIGUES, 2014; TANAKA et al., 2013) and PV systems (NOROOZIAN & GHAREHPETIAN, 2013). Power electronic converters connected to the grid may be controlled to perform active power filtering functions. This concept may contribute to popularize the dissemination of active filters in distribution networks, contributing to the power quality improvement, as well as incrementing the aggregated value of commercial products.

As previously discussed in this work, it can be noted that power processing is a fundamental issue for modern electric power networks. The current interest of research groups in this area, as noted in recently published works, show that PC technology is under development and new applications continue to emerge. The research proposals and results in this work also takes part on the development of techniques for PC in modern electric networks. More specifically, this work deals with power conditioning in two-phase three-wire networks.

1.2   TWO-PHASE THREE-WIRE CIRCUITS

In distribution power grids one may note several circuit configurations. The reasons for choosing a topology are related to local load and urban characteristics, legislation, costs and other challenges at the time of system planning. The main distribution system layouts are the North American and the European, as illustrated in Figure 1 (SHORT, 2014). North American primary networks typically present a multi-grounded three-phase four-wire configuration. The phase and ground are used to connect single-phase transformers with center-tapped secondaries. Each transformer supplies a few consumers only. In the European layout, primary circuits are three-phase three-wire. Step down transformers are commonly connected in *delta-wye* (Δ–Y) and the neutral is grounded at the transformer location and at each consumer installation. In comparison with American grids, a greater number of consumers is supplied by each transformer. In specific cases, as rural areas for instance, two phases are commonly used together with center-tapped transformers (SHORT, 2014). Urban distribution grids in Brazil, where this research is developed, are typically based on the European grids layout (AMPLA, 2011; LIGHT, 2014; AES ELETROPAULO, 2014; COPEL, 2016; CEMIG, 2013; CPFL, 2012; CELG-D, 2008).

Low-voltage distribution circuits typically present different configurations and ramifications at which consumers are connected:

   i. three-phase three-wire, composed by three phase conductors;

   ii. three-phase four-wire, formed by three phases and one neutral conductor;

iii. single-phase two-wire, with one phase and neutral or two phase conductors;

iv. single-phase three-wire, formed by two live wires and one neutral in the secondary of a center tap transformer, with line-to-neutral voltages displaced by 180°; and

v. two-phase three-wire $(2\phi3w)$, a derivation of two phases and one neutral conductors from a three-phase four-wire grid (SHORT, 2014).

Figure 1 – North American and European distribution layouts.

Fundamentals of Distribution Systems
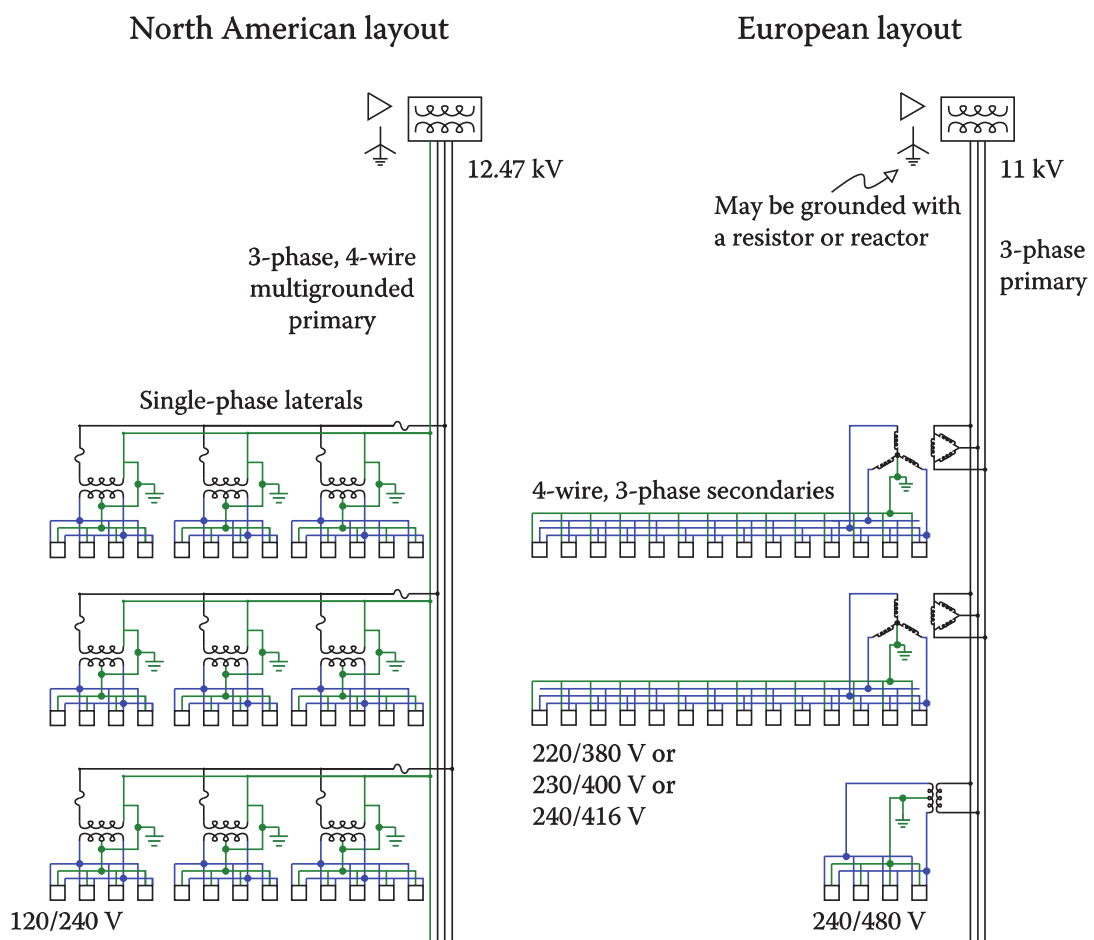
Source: Short (2014)

The reader should pay attention to avoid misunderstandings between two-phase three-wire circuits and single-phase circuits composed by two phase conductors. For convenience, the expression *"two-phase three-wire"* is also referred as *"two-phase"* in this work.

The type of power supply (single-phase, two-phase or three-phase) a consumer receives from the utility depends on the local grid configuration and consumer power demand. High-power loads often are supplied through three-phase circuits, whereas single-phase supplies are

typically applied for low-power applications. Additionally, electricity distribution companies in diverse countries employ $2\phi3w$ circuits to feed low power electrical consumers as residences and small business, for instance. This work focus in this kind of circuit. Such grid topology is also observed in several countries as, for example, Australia (ESSENTIAL ENERGY, 2011; POWERWATER CORPORATION, 2008; WESTERN POWER DISTRIBUTION AU & HORIZON POWER AU, 2015), United Kingdom (ANTONIOU; TZIMAS & ROWLAND, 2015; WESTERN POWER DISTRIBUTION UK, 2016), North America (WISCONSIN ELECTRIC POWER COMPANY, 2012) and Brazil (ABNT, 2008; AMPLA, 2011; LIGHT, 2014; AES ELETROPAULO, 2014; COPEL, 2016; CEMIG, 2013; CPFL, 2012; CELG-D, 2008).

Two-phase power supplies are a simple and economic option that allows consumers to use two voltage levels to connect single-phase loads. It is usual to feed ordinary wall sockets and lighting circuits with phase-neutral circuits. Equipment with higher rated power, such as electric showers and heaters, are preferably connected in phase-to-phase circuits. The main conditions to provide $2\phi3w$ power supplies, as defined by some of the utility companies in Brazil, are described in Table 1 (AMPLA, 2011; LIGHT, 2014; AES ELETROPAULO, 2014; COPEL, 2016; CEMIG, 2013; CPFL, 2012; CELG-D, 2008).

Table 1 – Conditions of low-voltage two-phase power supplying in Brazil.

Utility Company	Voltage (V)	Power (kVA)
AES Eletropaulo	127/220	≤ 20
	120/208	≤ 20
	115/230	> 5
CEMIG	127/220	< 15
	127/254	
COPEL	127/220	< 14
CPFL Paulista	127/220	$12 - 25$
	220/380	$15 - 25$
Light	127/220	< 8
Ampla	127/220	$8 - 10$
CELG-D	220/380	$12,1 - 25$

The basic network configuration considered in this work is shown in Figure 2. It illustrates a generic $2\phi3w$ installation (or group of installations) supplied by a low-voltage three-phase four-wire distribution grid.

Figure 2 – Basic $2\phi3w$ system topology.
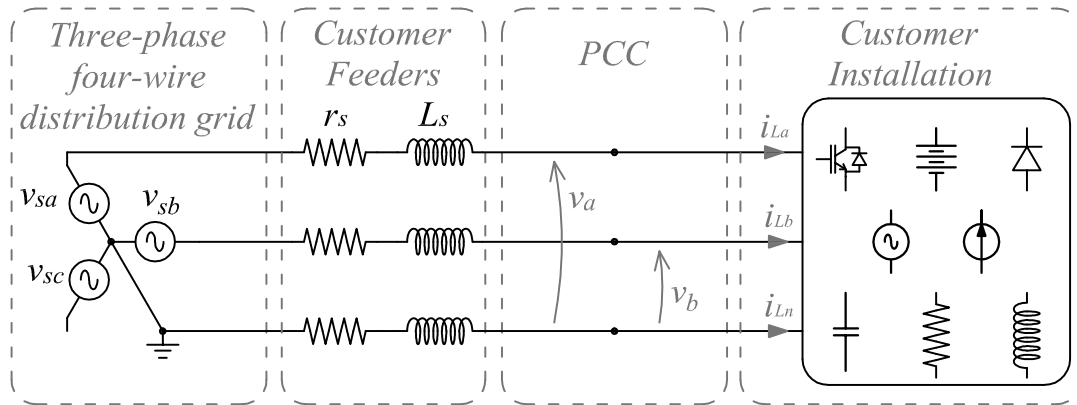
Source: Own authorship.

Electrical installations in general are referred as *"load"* and *"consumer"* in this text, even though they may also behave as energy sources due to local generation. The point at which the consumer installation is connected to the power system is called the Point of Common Coupling (PCC). The installation feeder comprises three conductors: two phases (*a* and *b* in this example) and a grounded neutral. It is important to highlight that two-phase installations have no physical access to the third phase, even though it exists in the grid. For simplicity, this work considers that neutral and phase conductors have the same dimensions and characteristics (r_s and L_s). Considering the power level of two-phase installations, this consideration is reasonable in most practical cases (ABNT, 2008).

Two-phase three-wire residential loads are typically composed of single-phase circuits, which can be connected phase-to-phase (*a-b*) or phase-to-neutral (*a-n* or *b-n*). It is also common that one phase be more loaded than the other. Moreover, the load may present linear or non-linear characteristics, with resistive and reactive elements (WATSON; SCOTT & HIRSCH, 2009; HARDIE & WATSON, 2010; GIL-DE-CASTRO et al., 2013). These characteristics are known by causing power losses, ageing and overheating in transformers and cables, resonances, interferences in communication systems, bad operation of power meters and protection equipment (FURTADO; RODRIGUES & BARBOSA, 2015b; IEEE, 2014).

Two-phase consumers typically represent relatively small loads to the power system, typically rating a few tens of kVA, as shown in Table 1. But, despite their small installed load, these consumers are found in large number on distribution networks. The aggregate effects of a large number of small installations may reach concerning levels (WATSON; SCOTT & HIRSCH, 2009; HARDIE & WATSON, 2010; GIL-DE-CASTRO et al., 2013). As discussed in the previous section, power processing applications may take part on the mitigation of such issues to improve

power quality, as well as providing other functionalities such as grid integration of PV and PEV systems.

1.3 TOPOLOGIES OF TWO-PHASE THREE-WIRE GRID-CONNECTED VOLTAGE-SOURCED CONVERTERS

At the time when this research was done, different converter topologies were analysed for power processing applications in $2\phi3w$ networks, specially for shunt APF functionalities. For this reason, the topologies shown in this section are regarded as APFs, even though they may also be used for other applications.

As previously reported by Furtado (2014b), the first studied approach was the use of two single-phase power converters as shown in Figure 4.

Figure 3 – Two-phase shunt compensation with two independent single-phase APF.
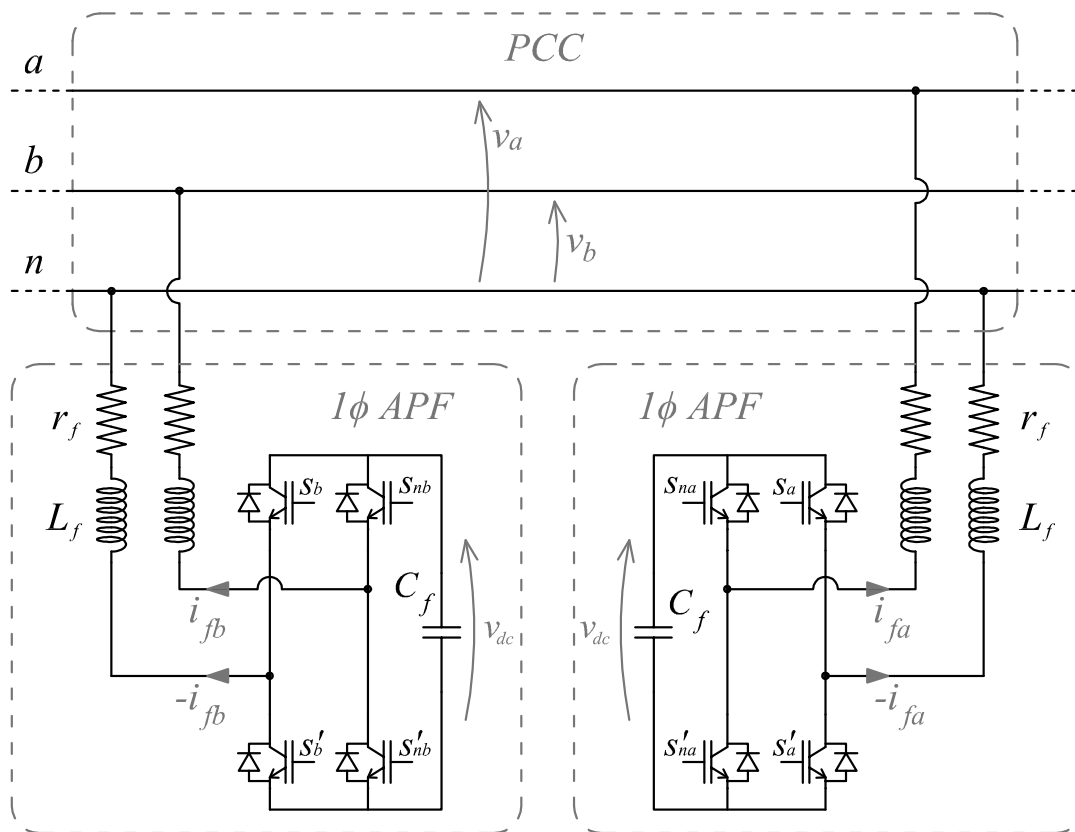
Source: Own authorship.

Each converter is composed of a DC-link voltage, semiconductor switching branches and inductive-resistive output filters. In this topology, the control of each converter can be completely independent and its use is well-known in technical

Figure 4 – Two-phase shunt compensation with two independent single-phase APF.
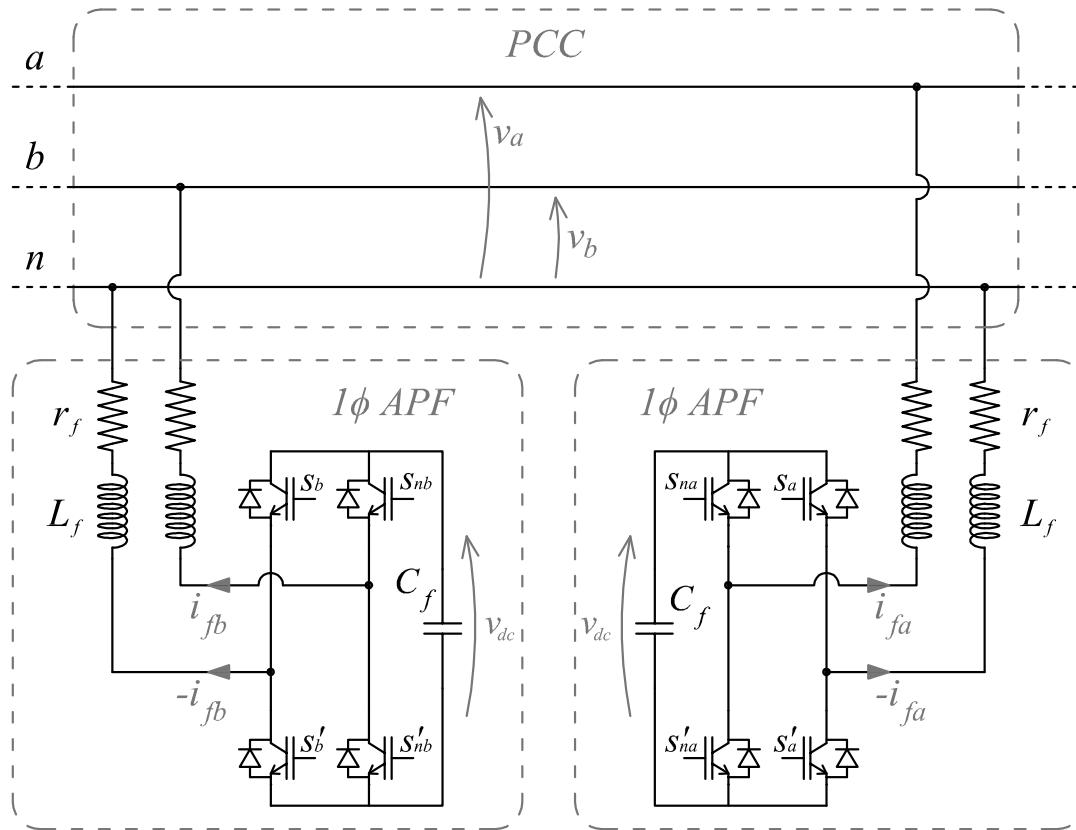
Source: Own authorship.

literature (ASIMINOAEL; BLAABJERG & HANSEN, 2007; KHADKIKAR; CHANDRA & SINGH, 2009; MONFARED & GOLESTAN, 2012; COLAK et al., 2011). However, this scheme requires four branches of static switches and two isolated DC-link voltages. Also, the independent control of these converters may not guarantee the compensation of load imbalances.

These converters can also be integrated by sharing the same DC-link voltage. The resulting topology, presenting a single capacitor, is illustrated in Figure 5. Also, the DC-voltage control can be done by one of the single-phase converters which form this topology or, alternatively, shared by both converters. Although the DC bus is shared, current control loops for each converter in this topology is also independent.

Figure 5 – Two-phase shunt compensation with two single-phase APF sharing the same DC busbar.

Source: Own authorship.

It can be observed the converter topologies in Figure 4 and Figure 5 have two branches connected to the same wire at the PCC, *i.e.*, the neutral conductor. These branches can be integrated in a single branch which synthesize simultaneously both currents $-i_{fa}$ and $-i_{fb}$. In this case, the current that flows through the neutral branch is:

$$i_{fn} = -\left(i_{fa} + i_{fb}\right). \tag{1.1}$$

The resulting topology leads to the use of typical three-phase VSC, as illustrated in Figure 6. This integration reduces the number of static switches, as well as measurement, drive and protection circuits. There is also the possibility of using well established current control methods, as discussed in Chapter 4 of this work.

Figure 6 – Two-phase three-wire shunt APF with a single DC busbar and neutral leg.
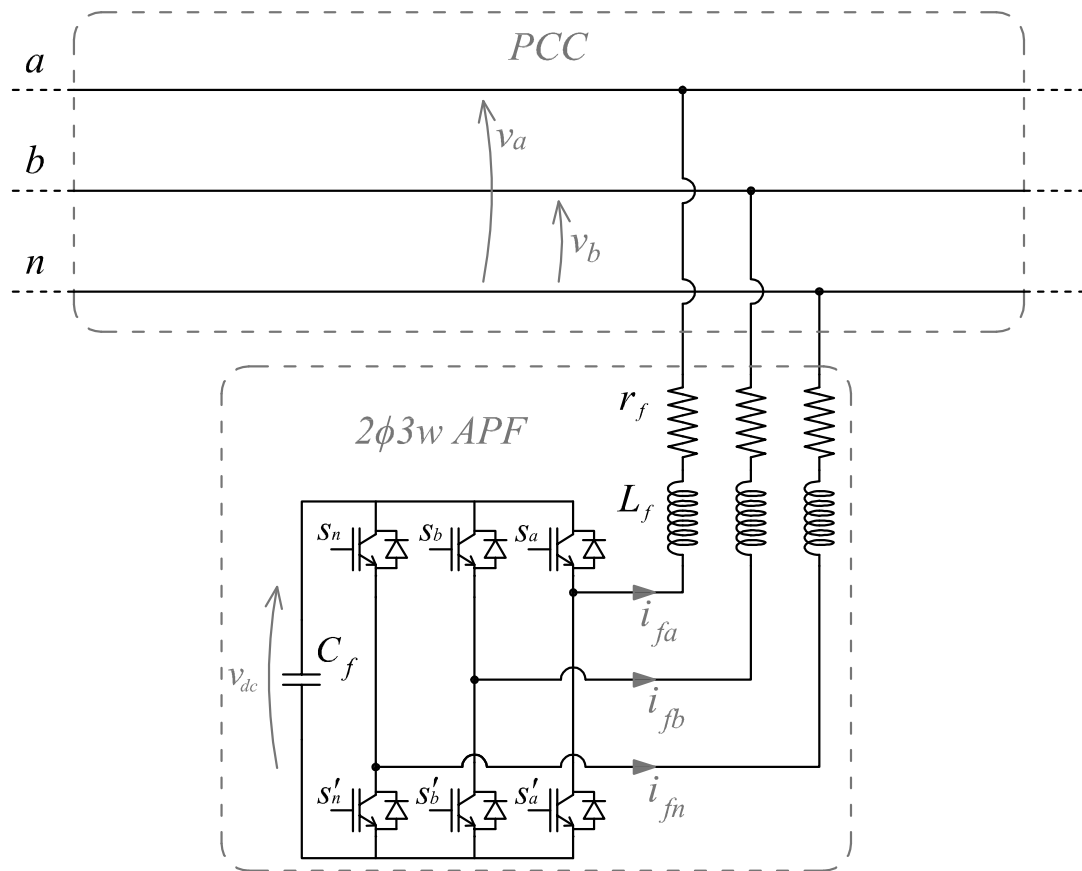
Source: Own authorship.

The converter topology of Figure 6 was already used in this research and is also adopted in this work. The main challenge in this research is the development and improvement of control techniques to properly integrate this converter topology into $2\phi3w$ networks to perform power conditioning features.

1.4 MOTIVATION

The majority of PC-related works report applications developed for single-phase and three-phase power networks. Teodorescu, Liserre and Rodriguez (2011) and Chakraborty, Simões and Kramer (2013), for example, describe a wide variety of PECs for renewable energy systems, always addressing single-phase and three-phase topologies. Yazdani and Iravani (2010) describe in detail a wide variety of converters and applications in power systems, always dedicated to single-phase and three-phase PECs. Akagi (2005) also states that *"active filters can be divided into single and three-phase active filters"*. A survey on APFs technology, published by Singh, Al-Haddad and Chandra (1999), classifies active filters as *"two-wire (single-phase), three-wire*

(three-phase without neutral) and four-wire (three-phase with neutral)". Another review on harmonic detection methods for APF control also deals with single-phase and three-phase techniques (ASIMINOAEL; BLAABJERG & HANSEN, 2007). In general terms, the vast majority of technical works reported in literature deal with single-phase and three-phase electric circuits.

There are only a few scientific works addressing two-phase PC applications and control techniques. Early works focused on specific applications such as the shunt active compensation of welding equipment (HOJABRI & MOKHTARI, 2006) and rail transportation (WU et al., 2012). The objective in these works was to compensate all current harmonics and reactive power demanded by $2\phi3w$ loads. Emadi, Nasiri and Bekiarov (2005) also mentions the possible use of back-to-back converters in Uninterrupted Power Supplies (UPSs) to feed $2\phi3w$ loads from a single-phase power supply. In all cases, single-phase control techniques were adapted to deal with $2\phi3w$ systems as the superposition of two single-phase circuits (HOJABRI & MOKHTARI, 2006; WU et al., 2012; EMADI; NASIRI & BEKIAROV, 2005).

The research related to this doctoral thesis proposal started in 2013, during the author Master's studies, when a conference paper was published (FURTADO et al., 2013). The first paper discussed general principles of $2\phi3w$ shunt compensation and described a control algorithm for reference currents extraction in $2\phi3w$ compensation. The control algorithm was based on *pq* Theory concepts applied for single-phase circuits. In the following year, experimental results were also published (FURTADO et al., 2014). Afterwards, some other advancements were reported, describing the integration of photovoltaic energy resources into $2\phi3w$ networks (FURTADO et al., 2015a), a two-phase shunt compensation strategy with neutral current mitigation capability (FURTADO; RODRIGUES & BARBOSA, 2015b) and also a comparison of two possible $2\phi3w$ compensation strategies (FURTADO et al., 2015c). Details of the control algorithms used in these works are briefly reviewed in Chapter 2.

Another research group has also recently published works addressing the usage of a $2\phi3w$ APF to compensate nonlinear residential loads. Bueno et al. (2014) described the application of a multilevel VSC to compensate current harmonics of $2\phi3w$ nonlinear loads. Also in this context, Fajardo et al. (2015) described a method to estimate and equalize capacitor voltages at the multilevel VSC. These works also adapted single-phase techniques aiming to fully compensate current harmonics and reactive power.

The works currently found in literature addressed two-phase PC applications using single-phase approaches. Two-phase networks were analysed as two independent single-phase circuits and single-phase techniques were adapted to control two-phase converters. Recently, Furtado, Rodrigues and Barbosa (2015d) published a work showing that two-phase networks can be

analysed as an unity and not only as two single-phase circuits. This approach simplifies the implementation of control algorithms. The proposed two-phase analysis technique could be applied to control power an APF and can be used in other PC applications as well.

In this context, the main motivation of this work is to describe new advancements on the analysis and control of $2\phi3w$ PECs, specially APFs. These advancements can be useful in widening the adoption of SG technologies by a large number of $2\phi3w$ consumers in countries like Brazil. Two-phase power conditioning can contribute to a proper integration of SG resources and functionalities into two-phase residential and commercial installations, which includes PV systems, electric vehicles, active filters, smart meters, UPSs and others. As previously discussed, the proper and wide adoption of such technologies aims, in a broad perspective, to improve modern power networks in efficiency, reliability, safety, cost-effectiveness and quality in power delivery.

1.5 OBJECTIVES

In the discussed context, the main objectives of this work are to study and to propose new techniques for analysis and control of $2\phi3w$ networks and power conditioning equipment. Aiming to achieve the main goals, the following specific objectives are pursued in this work:

i. To discuss the main applications of power conditioning in $2\phi3w$ networks;

ii. To review concepts and techniques applied for power conditioning in single-phase and three-phase networks;

iii. To present pq Theory concepts applied to two-phase three-wire circuits;

iv. To propose and to describe control techniques for power electronic converters connected to $2\phi3w$ networks;

v. To propose controllers and to implement the proposed $2\phi3w$ power conditioning techniques; and

vi. To validate the proposed concepts by presenting simulation and experimental results.

1.6 TEXT OUTLINE

A literature review regarding instantaneous powers concepts for both three-phase and single-phase systems is presented in Chapter 2. The proposed use of the pq Theory concepts for two-

phase three-wire circuits is presented and discussed in Chapter 3. A time-domain analysis is also presented to allow the interpretation of two-phase quantities in the proposed definitions.

Based on the proposed concepts of two-phase instantaneous powers, techniques were developed to control $2\phi3w$ shunt power conditioning equipment. The proposed control systems are described in detail in Chapter 4. Simulation studies were performed aiming to validate the control systems proposed in this work. The simulated system is described and results are presented and discussed in Chapter 5. Part of proposed control systems were tested in laboratory and preliminary experimental results are also presented.

Chapter 6 presents conclusions achieved in this thesis and a list of the works published during the development of this research. The proposals of new studies for future works are also presented in Chapter 6, followed by bibliographical references. Appendix A and Appendix B contain mathematical expressions of instantaneous powers obtained in time-domain analyses discussed in Chapter 2 and Chapter 3, respectively. Finally, the Appendix C discusses the choice of the method used in this work for voltage measurement.

2   INSTANTANEOUS POWER THEORY: CONCEPTS REVIEW

This chapter aims to at briefly reviewing the main studies that constitute the background for the development of this research. These concepts are discussed in this work aiming to ease the understanding of the proposed definitions of two-phase instantaneous powers discussed in Chapter 3, as well as allowing the drawn of parallels between the proposed $2\phi3w$ powers and the power definitions already present in technical literature.

2.1   *THE INSTANTANEOUS POWER THEORY*

The instantaneous power theory, or simply *pq* Theory, is a set of three-phase time-domain power definitions initially developed and originally published in a conference by Akagi, Kanazawa and Nabae (1983) and later in a journal publication (AKAGI; KANAZAWA & NABAE, 1984). These definitions were generalized after some time by Watanabe, Stephan and Aredes (1993) to comprise three-phase four-wire systems, considering zero-sequence voltages and currents. Several works found in literature show that other authors also contributed to the analysis, development and generalization of instantaneous powers concepts (KIM & AKAGI, 1999; KIM & AKAGI, 1997; PENG & LAI, 1996). This wide set of concepts and applications related to the *pq* Theory were brought together and didactically presented in a book by Akagi, Watanabe and Aredes (2007).

Since its first presentation, the *pq* Theory proved to be a powerful tool for analysis, design and control of PC equipment. Furthermore, the definitions of the *pq* Theory also provide a physical interpretation of power quantities in three-phase systems, including non-linear characteristics (AKAGI; WATANABE & AREDES, 2007). Whereas conventional power definitions are based on *rms* and/or average values for steady-state and sinusoidal conditions, the *pq* Theory uses instantaneous values of voltages and currents to calculate power quantities. This approach is specially useful to deal with electric powers in non-linear circuits in steady-state or transient conditions (AKAGI; WATANABE & AREDES, 2007).

The Clarke transformation is used in the *pq* Theory to represent three-phase voltages and

currents from their natural (abc) coordinates into an orthogonal reference frame named $\alpha\beta0$. The Clarke transformation is expressed as:

$$\begin{bmatrix} x_\alpha \\ x_\beta \\ x_0 \end{bmatrix} = \sqrt{\frac{2}{3}} \begin{bmatrix} 1 & -\frac{1}{2} & -\frac{1}{2} \\ 0 & \frac{\sqrt{3}}{2} & -\frac{\sqrt{3}}{2} \\ \frac{1}{\sqrt{2}} & \frac{1}{\sqrt{2}} & \frac{1}{\sqrt{2}} \end{bmatrix} \begin{bmatrix} x_a \\ x_b \\ x_c \end{bmatrix}, \tag{2.1}$$

where the triplets (x_a, x_b, x_c) and (x_α, x_β, x_0) stand for the quantities in the *abc* and $\alpha\beta0$ reference frames, respectively. The factor $\sqrt{\frac{2}{3}}$ is used to provide power invariance between *abc* and $\alpha\beta$ powers (AKAGI; WATANABE & AREDES, 2007).

The $\alpha\beta$ quantities obtained with (2.1) can be understood as the orthogonal projections of an space vector denoted as $\vec{x}$. Under balanced sinusoidal conditions, $\vec{x}$ presents constant amplitude, performing a circular trajectory in the $\alpha\beta$ plane, as illustrated in Figure 7. If the *abc* quantities presents the phase sequence *a–b–c*, then the space vector rotates in the counter clockwise direction, that is, in the α–β phase sequence (AKAGI; WATANABE & AREDES, 2007).

Figure 7 – Space vector representation in the *abc* (a) and $\alpha\beta$ (b) reference frames.

(a)　　　　　　　　　　　　　　　(b)
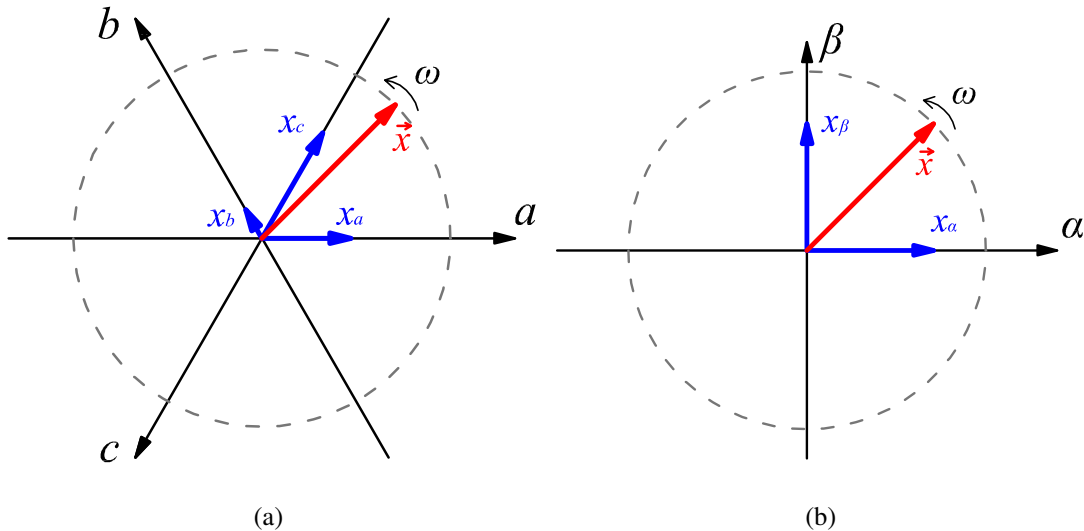
Source: Own authorship.

The three-phase instantaneous powers are defined, in terms of $\alpha\beta0$ voltages and currents, as:

$$
\begin{bmatrix} p \\ q \\ p_0 \end{bmatrix} = \begin{bmatrix} \bar{p} + \tilde{p} \\ \bar{q} + \tilde{q} \\ \bar{p}_0 + \tilde{p}_0 \end{bmatrix} = \begin{bmatrix} v_\alpha & v_\beta & 0 \\ v_\beta & -v_\alpha & 0 \\ 0 & 0 & v_0 \end{bmatrix} \begin{bmatrix} i_\alpha \\ i_\beta \\ i_0 \end{bmatrix}, \tag{2.2}
$$

where p is the instantaneous real power, q is the imaginary power and p_0 is called zero-sequence power. Each of the instantaneous power components can be decomposed in an average ($\bar{p}$, $\bar{q}$ and $\bar{p}_0$) and an oscillating zero-averaged components ($\tilde{p}$, $\tilde{q}$ and $\tilde{p}_0$) (AKAGI; WATANABE & AREDES, 2007).

Next section briefly discusses the resulting instantaneous powers for different voltage and current conditions, as also treated by Akagi, Watanabe and Aredes (2007). The understanding of these results is important in the context of this work.

2.1.1 TIME-DOMAIN ANALYSIS OF THE *PQ* THEORY

2.1.1.1 SINUSOIDAL BALANCED CONDITIONS

A set of sinusoidal balanced three-phase voltages and currents can be respectively expressed as

$$
\begin{cases} v_a = \sqrt{2}\, V_+ \sin(\omega t) \\ v_b = \sqrt{2}\, V_+ \sin(\omega t - 2\pi/3) \\ v_c = \sqrt{2}\, V_+ \sin(\omega t + 2\pi/3) \end{cases} \tag{2.3}
$$

and

$$
\begin{cases} i_a = \sqrt{2}\, I_+ \sin(\omega t + \phi_{i_+}) \\ i_b = \sqrt{2}\, I_+ \sin(\omega t - 2\pi/3 + \phi_{i_+}) \\ i_c = \sqrt{2}\, I_+ \sin(\omega t + 2\pi/3 + \phi_{i_+}) \end{cases}, \tag{2.4}
$$

where V_+ and I_+ represent root mean square (rms) value of positive-sequence voltages and currents, respectively.

The application of Equation 2.1 to transform these quantities into the $\alpha\beta 0$ reference frame results in

$$
\begin{cases} v_\alpha = \sqrt{3}\, V_+ \sin(\omega t) \\ v_\beta = -\sqrt{3}\, V_+ \cos(\omega t) \\ v_0 = 0 \end{cases} \tag{2.5}
$$

and

$$
\begin{cases} i_\alpha = \sqrt{3}\, I_+ \sin(\omega t + \phi_{i_+}) \\ i_\beta = -\sqrt{3}\, I_+ \cos(\omega t + \phi_{i_+}) \\ i_0 = 0 \end{cases}, \tag{2.6}
$$

Finally, substituting (2.5) and (2.6) into (2.2), the result obtained for the instantaneous powers is mathematically expressed as

$$
\begin{cases}
p = \bar{p} = 3V_+ I_+ \cos\left(\phi_{i_+}\right) \\
q = \bar{q} = -3V_+ I_+ \sin\left(\phi_{i_+}\right) \\
p_0 = 0
\end{cases}
\tag{2.7}
$$

This condition is illustrated in the following example waveforms. Figure 8 and Figure 9 show three-phase balanced sinusoidal voltages and currents with $V_+ = 127$ V and $I_+ = 35$ A, respectively.

Figure 8 – Three-phase *abc* balanced voltages with $V_+ = 127$ V.
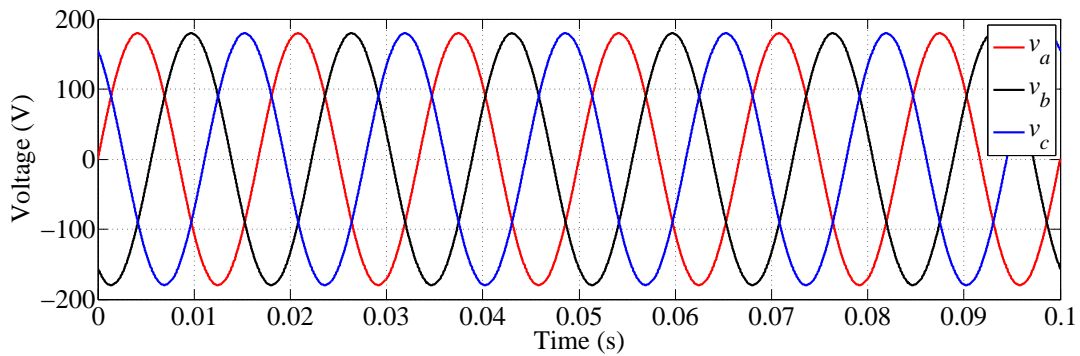
Source: Own authorship.

Figure 9 – Three-phase *abc* balanced currents with $I_+ = 35$ A and $\phi_{i_+} = -\dfrac{\pi}{6}$ rad.
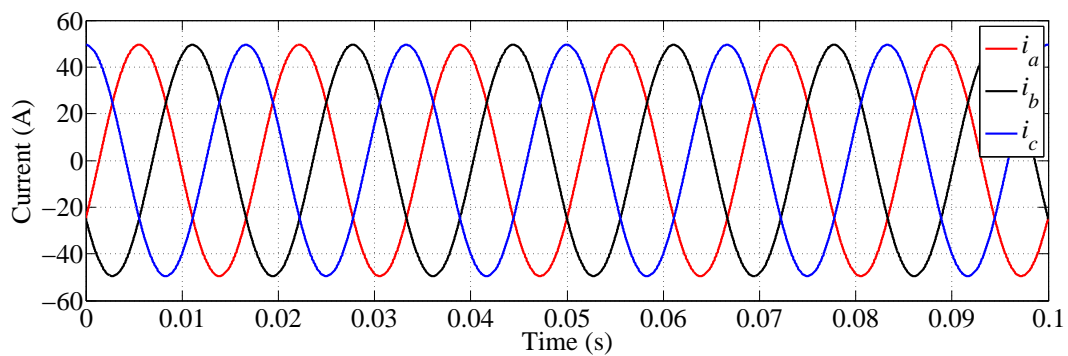
Source: Own authorship.

The waveforms in Figure 10 and Figure 11 illustrate the three-phase example quantities represented in the $\alpha\beta0$ reference frame through the application of the Clarke transformation (2.1).

Figure 10 – Three-phase balanced voltages in the $\alpha\beta0$ reference frame.
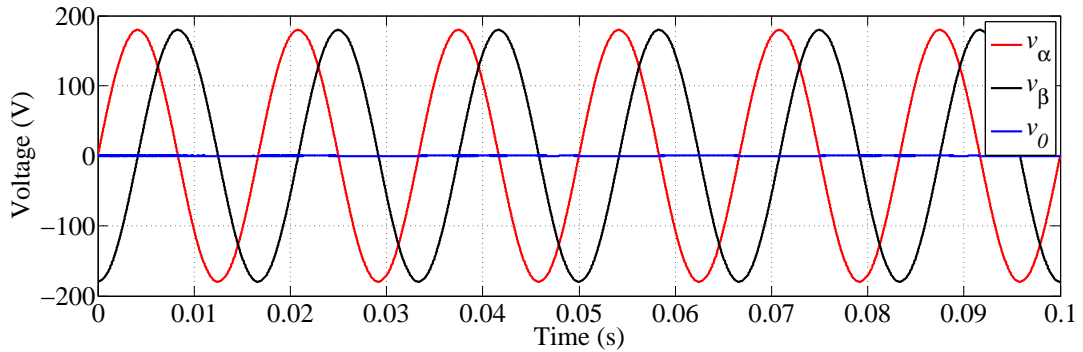
Source: Own authorship.

Figure 11 – Three-phase balanced currents in the $\alpha\beta0$ reference frame.
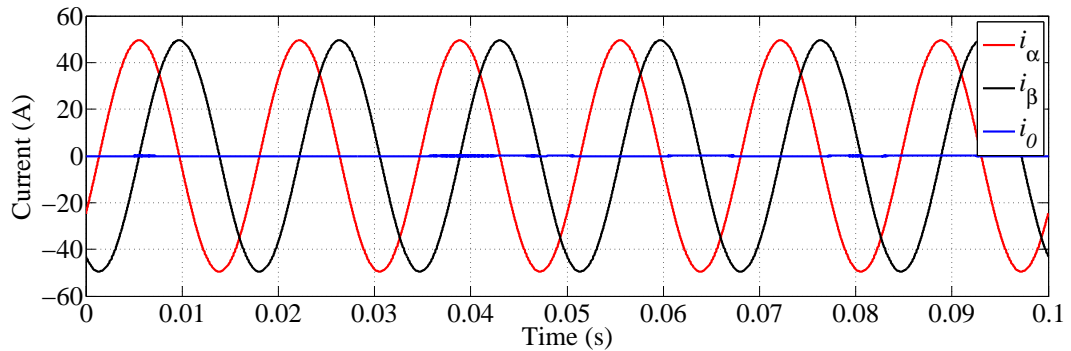
Source: Own authorship.

Figure 12 shows graphically the constant behaviour of the instantaneous powers obtained in this example, which matches with the expression in (2.7).

Figure 12 – Three-phase instantaneous powers under sinusoidal balanced conditions.
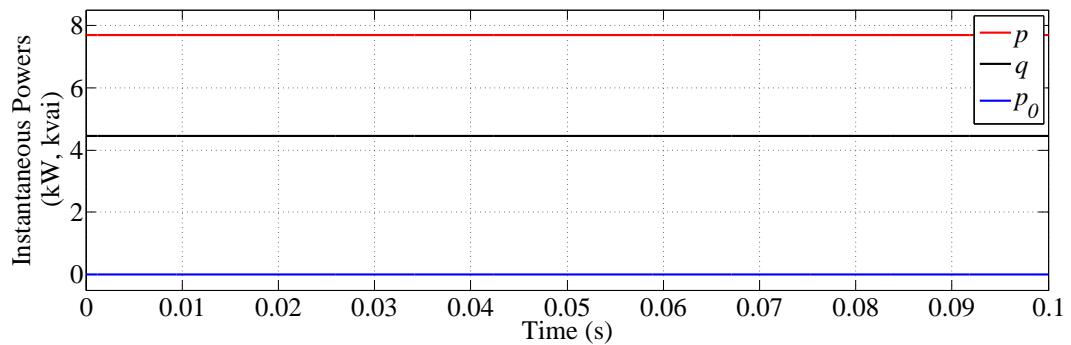
Source: Own authorship.

These results match the conventional power definitions, as described by (AKAGI; WATAN-ABE & AREDES, 2007). The instantaneous powers p and q equal the three-phase active and

reactive powers denoted as $P_{3\phi}$ and $Q_{3\phi}$, respectively. This result confirms the power invariance between the *pq* Theory and conventional definitions for sinusoidal balanced conditions (AKAGI; WATANABE & AREDES, 2007).

2.1.1.2 SINUSOIDAL UNBALANCED CONDITIONS

Through the symmetrical components introduced by Fortescue, any set of unbalanced three-phase quantities can be decomposed into three sets of balanced quantities called positive-, negative and zero-sequence components (GRAINGER & STEVENSON, 1994). Therefore, unbalanced voltages and currents of a three-phase system can be generically expressed as

$$
\begin{cases}
v_a = & \sqrt{2}\,V_+\sin\left(\omega t\right) + \sqrt{2}\,V_-\sin\left(\omega t + \phi_{v_-}\right) + \\
& +\sqrt{2}\,V_0\sin\left(\omega t + \phi_{v_0}\right) \\
v_b = & \sqrt{2}\,V_+\sin\left(\omega t - 2\pi/3\right) + \sqrt{2}\,V_-\sin\left(\omega t + 2\pi/3 + \phi_{v_-}\right) + \\
& +\sqrt{2}\,V_0\sin\left(\omega t + \phi_{v_0}\right) \\
v_c = & \sqrt{2}\,V_+\sin\left(\omega t + 2\pi/3\right) + \sqrt{2}\,V_-\sin\left(\omega t - 2\pi/3 + \phi_{v_-}\right) + \\
& +\sqrt{2}\,V_0\sin\left(\omega t + \phi_{v_0}\right)
\end{cases}
\tag{2.8}
$$

and

$$
\begin{cases}
i_a = & \sqrt{2}\,I_+\sin\left(\omega t + \phi_{i_+}\right) + \sqrt{2}\,I_-\sin\left(\omega t + \phi_{i_-}\right) + \\
& +\sqrt{2}\,I_0\sin\left(\omega t + \phi_{i_0}\right) \\
i_b = & \sqrt{2}\,I_+\sin\left(\omega t - 2\pi/3 + \phi_{i_+}\right) + \sqrt{2}\,I_-\sin\left(\omega t + 2\pi/3 + \phi_{i_-}\right) + \\
& +\sqrt{2}\,I_0\sin\left(\omega t + \phi_{i_0}\right) \\
i_c = & \sqrt{2}\,I_+\sin\left(\omega t + 2\pi/3 + \phi_{i_+}\right) + \sqrt{2}\,I_-\sin\left(\omega t - 2\pi/3 + \phi_{i_-}\right) + \\
& +\sqrt{2}\,I_0\sin\left(\omega t + \phi_{i_0}\right)
\end{cases}
,
\tag{2.9}
$$

where V_+, V_- and V_0 are the rms values of positive-, negative- and zero-sequence voltages. Analogous definitions are adopted for I_+, I_- and I_0.

By applying the Clarke transformation to these quantities, the resulting $\alpha\beta 0$ components can be written as

$$
\begin{cases}
v_\alpha = & \sqrt{3}\,V_+\sin\left(\omega t\right) + \sqrt{3}\,V_-\sin\left(\omega t + \phi_{v_-}\right) \\
v_\beta = & -\sqrt{3}\,V_+\cos\left(\omega t\right) + \sqrt{3}\,V_-\cos\left(\omega t + \phi_{v_-}\right) \\
v_0 = & \sqrt{6}\,V_0\sin\left(\omega t + \phi_{v_0}\right)
\end{cases}
\tag{2.10}
$$

and

$$
\begin{cases}
i_\alpha = & \sqrt{3}\,I_+\sin\left(\omega t + \phi_{i_+}\right) + \sqrt{3}\,I_-\sin\left(\omega t + \phi_{i_-}\right) \\
i_\beta = & -\sqrt{3}\,I_+\cos\left(\omega t + \phi_{i_+}\right) + \sqrt{3}\,I_-\cos\left(\omega t + \phi_{i_-}\right) \\
i_0 = & \sqrt{6}\,I_0\sin\left(\omega t + \phi_{i_0}\right)
\end{cases}
.
\tag{2.11}
$$

It can be noted that the Clarke transformation separates zero-sequence voltages and currents. Therefore, these components are not expected to take part in p and q, but only in p_0. Indeed, applying the *pq* Theory definitions, the resulting instantaneous powers are given by:

$$\begin{cases} \bar{p} = & 3V_+I_+ \cos\left(\phi_{i_+}\right) + 3V_-I_- \cos\left(\phi_{v_-} - \phi_{i_-}\right) \\ \tilde{p} = & -3V_+I_- \cos\left(2\omega t + \phi_{v_+} + \phi_{i_-}\right) - 3V_-I_+ \cos\left(2\omega t + \phi_{v_-} + \phi_{i_+}\right) \end{cases}, \tag{2.12}$$

$$\begin{cases} \bar{q} = & -3V_+I_+ \sin\left(\phi_{i_+}\right) - 3V_-I_- \sin\left(\phi_{v_-} - \phi_{i_-}\right) \\ \tilde{q} = & -3V_+I_- \sin\left(2\omega t + \phi_{v_+} + \phi_{i_-}\right) + 3V_-I_+ \sin\left(2\omega t + \phi_{v_-} + \phi_{i_+}\right) \end{cases}, \tag{2.13}$$

and

$$\begin{cases} \bar{p}_0 = & 3V_0I_0 \cos\left(\phi_{v_0} - \phi_{i_0}\right) \\ \tilde{p}_0 = & -3V_0I_0 \cos\left(2\omega t + \phi_{v_0} + \phi_{i_0}\right) \end{cases}. \tag{2.14}$$

Aiming to illustrate these conditions, Figure 13 and Figure 14 present example waveforms of three-phase unbalanced sinusoidal voltages and currents, respectively.

Figure 13 – Three-phase *abc* unbalanced sinusoidal voltages with $V_+ = 127$ V, $V_- = 10$ % of V_+ and $V_0 = 5$ % of V_+.
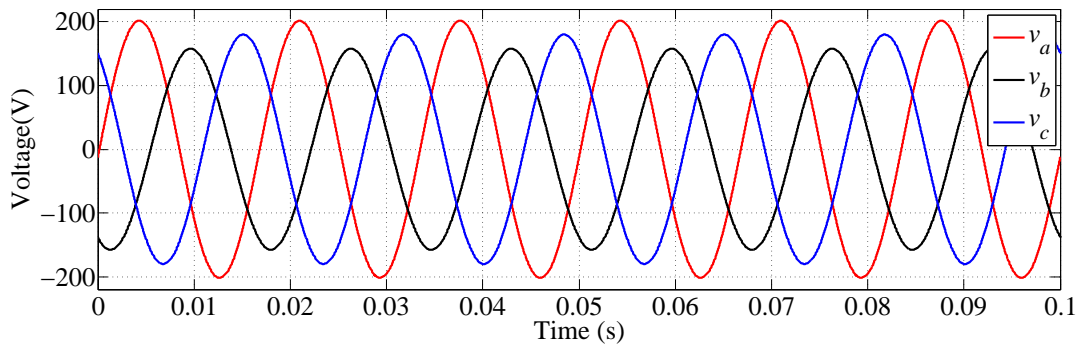
Source: Own authorship.

Figure 14 – Three-phase *abc* unbalanced sinusoidal currents with $I_+ = 35$ A, $I_- = 20$ % of I_+ and $I_0 = 5$ % of I_+.
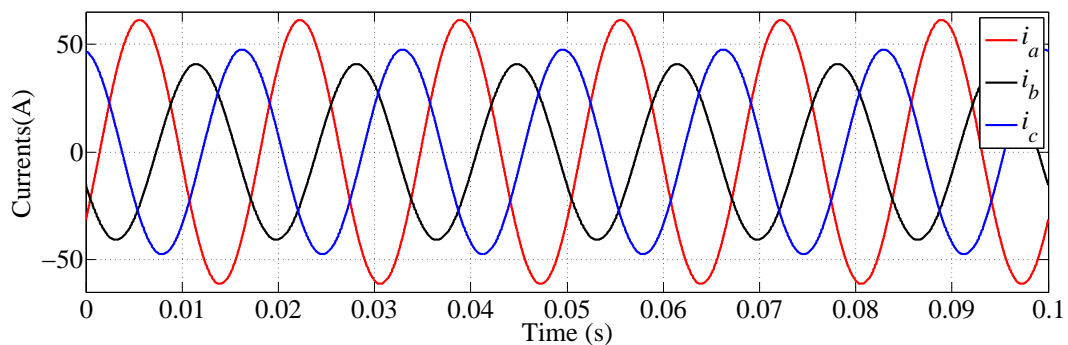
Source: Own authorship.

Figure 15 and Figure 16 illustrate the example unbalanced three-phase quantities represented in the $\alpha\beta0$ reference frame.

Figure 15 – Three-phase sinusoidal unbalanced voltages in the $\alpha\beta0$ reference frame.
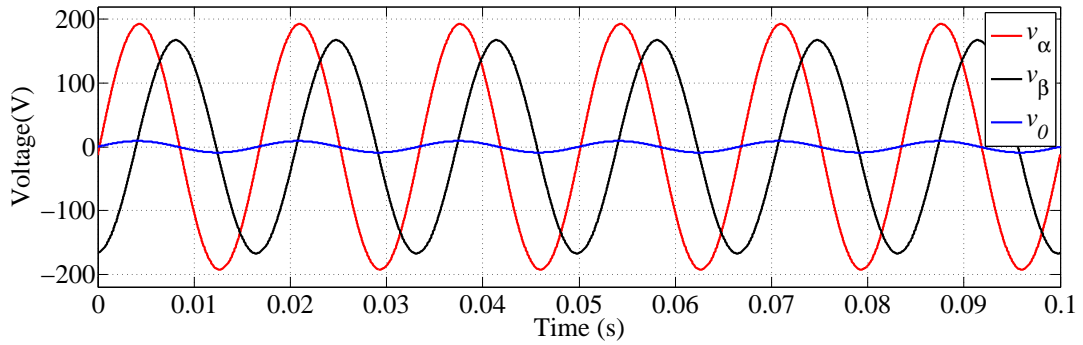
Source: Own authorship.

Figure 16 – Three-phase sinusoidal unbalanced currents in the $\alpha\beta0$ reference frame.
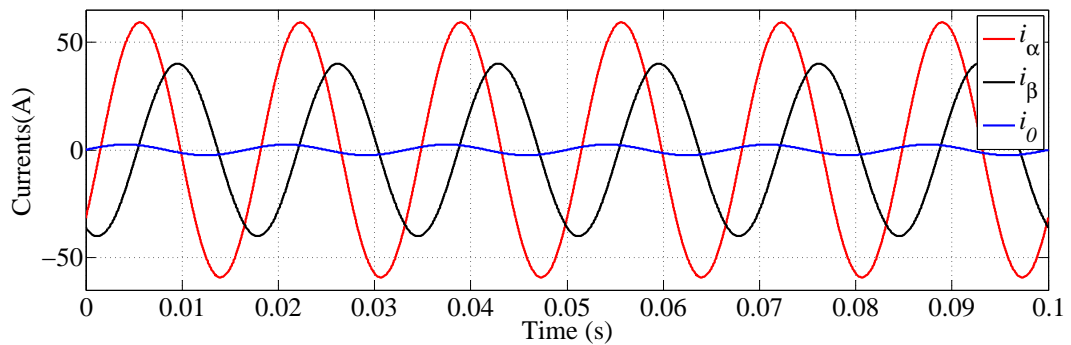
Source: Own authorship.

Finally, instantaneous powers obtained with these quantities are shown graphically in Figure 17, at which is possible to observe that p, q and p_0 oscillate with 2ω frequency around a constant non-zero value.

Figure 17 – Three-phase instantaneous powers under sinusoidal unbalanced conditions.
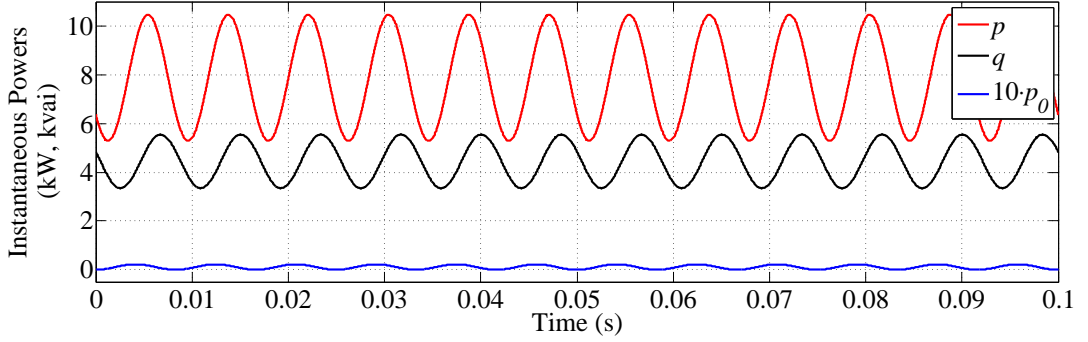
Source: Own authorship.

As discussed by Akagi, Watanabe and Aredes (2007), $\bar{p}$ and $\bar{q}$ result from interactions of voltages and currents with the same symmetrical component, whereas $\tilde{p}$ and $\tilde{q}$ result from voltages and currents with different symmetrical components. The zero-sequence power $\bar{p}_0$ exists only if there are both zero-sequence voltage and current, which is possible only in three-phase four-wire circuits. Zero-sequence power always present both average an oscillating components.

2.1.1.3 UNBALANCED AND HARMONIC DISTORTED CONDITIONS

The most general case occurs when both, voltages and currents, contain harmonic components and, additionally, unbalances in harmonic frequencies. Aiming to analyse instantaneous powers under these conditions, three-phase quantities can be expressed as:

$$
\begin{cases}
v_a = \sum_{h=1}^{\infty} \sqrt{2} V_{h_+} \sin\left[h\left(\omega t\right) + \phi_{v_{h+}}\right] + \sum_{h=1}^{\infty} \sqrt{2} V_{h_-} \sin\left[h\left(\omega t\right) + \phi_{v_{h-}}\right] + \\
\qquad + \sum_{h=1}^{\infty} \sqrt{2} V_{h_0} \sin\left[h\left(\omega t\right) + \phi_{v_{h0}}\right] \\
v_b = \sum_{h=1}^{\infty} \sqrt{2} V_{h_+} \sin\left[h\left(\omega t - 2\pi/3\right) + \phi_{v_{h+}}\right] + \sum_{h=1}^{\infty} \sqrt{2} V_{h_-} \sin\left[h\left(\omega t + 2\pi/3\right) + \phi_{v_{h-}}\right] + \\
\qquad + \sum_{h=1}^{\infty} \sqrt{2} V_{h_0} \sin\left[h\left(\omega t\right) + \phi_{v_{h0}}\right] \\
v_c = \sum_{h=1}^{\infty} \sqrt{2} V_{h_+} \sin\left[h\left(\omega t + 2\pi/3\right) + \phi_{v_{h+}}\right] + \sum_{h=1}^{\infty} \sqrt{2} V_{h_-} \sin\left[h\left(\omega t - 2\pi/3\right) + \phi_{v_{h-}}\right] + \\
\qquad + \sum_{h=1}^{\infty} \sqrt{2} V_{h_0} \sin\left[h\left(\omega t\right) + \phi_{v_{h0}}\right]
\end{cases}
$$

$$(2.15)$$

and

$$
\begin{cases}
i_a = \displaystyle\sum_{h=1}^{\infty} \sqrt{2}I_{h_+} \sin\left[h\left(\omega t\right)+\phi_{i_{h+}}\right] + \sum_{h=1}^{\infty} \sqrt{2}I_{h_-} \sin\left[h\left(\omega t\right)+\phi_{i_{h-}}\right] + \\
\qquad + \displaystyle\sum_{h=1}^{\infty} \sqrt{2}I_{h_0} \sin\left[h\left(\omega t\right)+\phi_{i_{h0}}\right] \\
i_b = \displaystyle\sum_{h=1}^{\infty} \sqrt{2}I_{h_+} \sin\left[h\left(\omega t - 2\pi/3\right)+\phi_{i_{h+}}\right] + \sum_{h=1}^{\infty} \sqrt{2}I_{h_-} \sin\left[h\left(\omega t + 2\pi/3\right)+\phi_{i_{h-}}\right] + \\
\qquad + \displaystyle\sum_{h=1}^{\infty} \sqrt{2}I_{h_0} \sin\left[h\left(\omega t\right)+\phi_{i_{h0}}\right] \\
i_c = \displaystyle\sum_{h=1}^{\infty} \sqrt{2}I_{h_+} \sin\left[h\left(\omega t + 2\pi/3\right)+\phi_{i_{h+}}\right] + \sum_{h=1}^{\infty} \sqrt{2}I_{h_-} \sin\left[h\left(\omega t - 2\pi/3\right)+\phi_{i_{h-}}\right] + \\
\qquad + \displaystyle\sum_{h=1}^{\infty} \sqrt{2}I_{h_0} \sin\left[h\left(\omega t\right)+\phi_{i_{h0}}\right]
\end{cases} .
$$

$$(2.16)$$

The respective $\alpha\beta 0$ components obtained through the Clarke transformation are:

$$
\begin{cases}
v_\alpha = \displaystyle\sum_{h=1}^{\infty} \sqrt{3}\,V_{h_+} \sin\left[h\left(\omega t\right)+\phi_{v_{h+}}\right] + \sum_{h=1}^{\infty} \sqrt{3}\,V_{h_-} \sin\left[h\left(\omega t\right)+\phi_{v_{h-}}\right] \\
v_\beta = -\displaystyle\sum_{h=1}^{\infty} \sqrt{3}\,V_{h_+} \cos\left[h\left(\omega t\right)+\phi_{v_{h+}}\right] + \sum_{h=1}^{\infty} \sqrt{3}\,V_{h_-} \cos\left[h\left(\omega t\right)+\phi_{v_{h-}}\right] \\
v_0 = \displaystyle\sum_{h=1}^{\infty} \sqrt{6}\,V_{h_0} \sin\left[h\left(\omega t\right)+\phi_{v_{h0}}\right]
\end{cases} \quad (2.17)
$$

and

$$
\begin{cases}
i_\alpha = \displaystyle\sum_{h=1}^{\infty} \sqrt{3}\,I_{h_+} \sin\left[h\left(\omega t\right)+\phi_{i_{h+}}\right] + \sum_{h=1}^{\infty} \sqrt{3}\,I_{h_-} \sin\left[h\left(\omega t\right)+\phi_{i_{h-}}\right] \\
i_\beta = -\displaystyle\sum_{h=1}^{\infty} \sqrt{3}\,V_{h_+} \cos\left[h\left(\omega t\right)+\phi_{v_{h+}}\right] + \sum_{h=1}^{\infty} \sqrt{3}\,I_{h_+} \cos\left[h\left(\omega t\right)+\phi_{i_{h-}}\right] \\
i_0 = \displaystyle\sum_{h=1}^{\infty} \sqrt{6}\,I_{h_0} \sin\left[h\left(\omega t\right)+\phi_{i_{h0}}\right]
\end{cases} . \quad (2.18)
$$

In the context of this work, it is important to note that $\alpha\beta$ components obtained through the Clarke transformation are always orthogonal, even including harmonic terms. For each harmonic frequency, β lags α by $\dfrac{\pi}{2}$ rad. This property guarantees orthogonality. Another property to be highlighted is that α and β components obtained through the Clarke Transformation have no influence of zero-sequence components at any harmonic frequency.

The calculation of instantaneous powers as defined in (2.2) leads to the following results:

$$
\begin{cases}
\bar{p} = \displaystyle\sum_{h=1}^{\infty} 3V_{h_+}I_{h_+}\cos\left(\phi_{v_{h+}} - \phi_{i_{h+}}\right) + \sum_{h=1}^{\infty} 3V_{h_-}I_{h_-}\cos\left(\phi_{v_{h-}} - \phi_{i_{h-}}\right) \\[2ex]
\tilde{p} = \displaystyle\sum_{h\neq k} 3V_{h_+}I_{k_+}\cos\left[(h-k)\,\omega t + \phi_{v_{h+}} - \phi_{i_{h+}}\right] + \\[2ex]
\qquad + \displaystyle\sum_{h\neq k} 3V_{h_-}I_{k_-}\cos\left[(h-k)\,\omega t + \phi_{v_{h-}} - \phi_{i_{h-}}\right] + \\[2ex]
\qquad + \displaystyle\sum_{h=1}^{\infty}\sum_{k} -3V_{h_+}I_{k_-}\cos\left[(h+k)\,\omega t + \phi_{v_{h+}} + \phi_{i_{h-}}\right] + \\[2ex]
\qquad + \displaystyle\sum_{h=1}^{\infty}\sum_{k} -3V_{h_-}I_{k_+}\cos\left[(h+k)\,\omega t + \phi_{v_{h-}} + \phi_{i_{h+}}\right]
\end{cases}
\tag{2.19}
$$

$$
\begin{cases}
\bar{q} = \displaystyle\sum_{h=1}^{\infty} 3V_{h_+}I_{h_+}\sin\left(\phi_{v_{h+}} - \phi_{i_{h+}}\right) - \sum_{h=1}^{\infty} 3V_{h_-}I_{h_-}\sin\left(\phi_{v_{h-}} - \phi_{i_{h-}}\right) \\[2ex]
\tilde{q} = \displaystyle\sum_{h\neq k} 3V_{h_+}I_{k_+}\sin\left[(h-k)\,\omega t + \phi_{v_{h+}} - \phi_{i_{h+}}\right] + \\[2ex]
\qquad + \displaystyle\sum_{h\neq k} -3V_{h_-}I_{k_-}\sin\left[(h-k)\,\omega t + \phi_{v_{h-}} - \phi_{i_{h-}}\right] + \\[2ex]
\qquad + \displaystyle\sum_{h=1}^{\infty}\sum_{k} -3V_{h_+}I_{k_-}\sin\left[(h+k)\,\omega t + \phi_{v_{h+}} + \phi_{i_{h-}}\right] + \\[2ex]
\qquad + \displaystyle\sum_{h=1}^{\infty}\sum_{k} 3V_{h_-}I_{k_+}\sin\left[(h+k)\,\omega t + \phi_{v_{h-}} + \phi_{i_{h+}}\right]
\end{cases}
\tag{2.20}
$$

and

$$
\begin{cases}
\bar{p}_0 = \displaystyle\sum_{h=1}^{\infty} 3V_{h_0}I_{h_0}\cos\left(\phi_{v_{h0}} - \phi_{i_{h0}}\right) \\[2ex]
\tilde{p}_0 = \displaystyle\sum_{h\neq k} 3V_{h_0}I_{h_0}\cos\left[(h-k)\,\omega t + \phi_{v_{h0}} - \phi_{i_{h0}}\right] + \\[2ex]
\qquad + \displaystyle\sum_{h=1}^{\infty}\sum_{k} -3V_{h_0}I_{h_0}\cos\left[(h+k)\,\omega t + \phi_{v_{h0}} + \phi_{i_{h0}}\right]
\end{cases}
\tag{2.21}
$$

It can be observed that constant power parcels $\bar{p}$, $\bar{q}$ and $\bar{p}_0$ are always generated by voltages and currents at the same voltage and phase sequence and frequency. Interactions between quantities in different frequencies and/or phase sequences produce oscillating power components $\tilde{p}$, $\tilde{q}$ and $\tilde{p}_0$ (AKAGI; WATANABE & AREDES, 2007). These characteristics are useful in power conditioning applications. As broadly shown by Akagi, Watanabe and Aredes (2007), by separating p and q in their oscillating and average parcels, it becomes possible to obtain the voltage and/or current components which produce each power parcel. The three-phase instantaneous powers obtained in the example used in this section are illustrated in Figure 22.

These conditions are exemplified in voltage and current waveforms in Figure 18 and Figure 19, respectively. These figures show three-phase quantities with unbalances and harmonic distortions.

Figure 18 – Three-phase unbalanced and distorted voltages with $V_{1_+} = 127$ V, $V_{1_-} = 10$ % of V_{1_+} and $V_{3_+} = 5$ % of V_{1_+}.
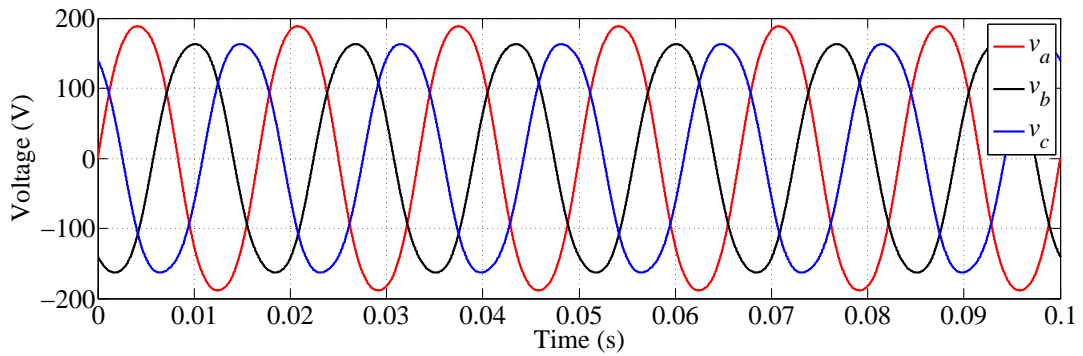
Source: Own authorship.

Figure 19 – Three-phase unbalanced and distorted currents with $I_{1_+} = 35$ A, $I_{1_-} = 20$ % of I_{1_+}, $I_{3+} = 10$ % of I_{1_+} and $I_{5+} = 5$ % of I_{1_+}.
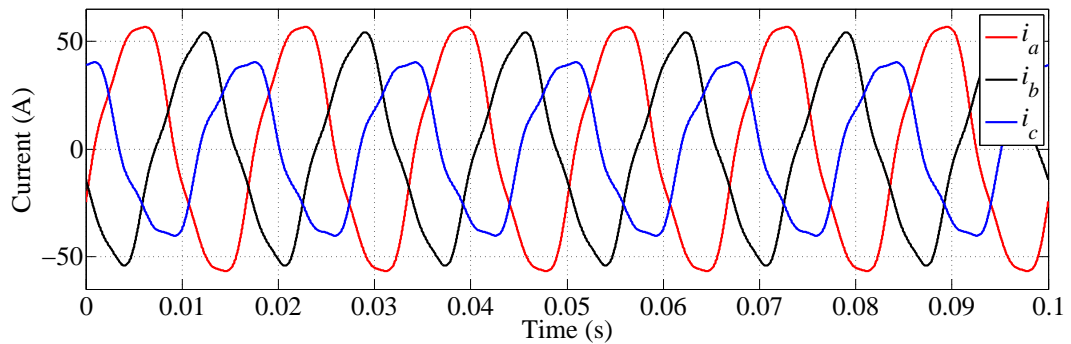
Source: Own authorship.

The application of the Clarke transformation Equation 2.1 result in the $\alpha\beta0$ voltages and currents illustrated in Figure 20 and Figure 21, respectively.

Figure 20 – Example waveforms of three-phase unbalanced and harmonic distorted voltages in the $\alpha\beta0$ reference frame.
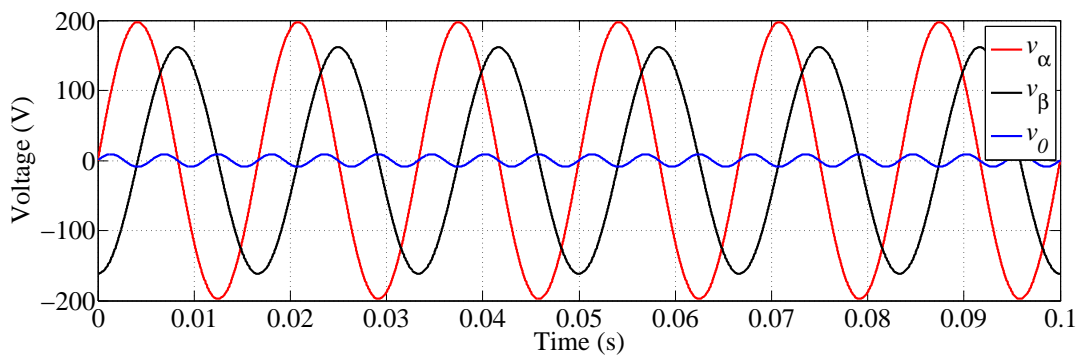
Source: Own authorship.

Figure 21 – Example waveforms of three-phase unbalanced and harmonic distorted currents in the $\alpha\beta 0$ reference frame.
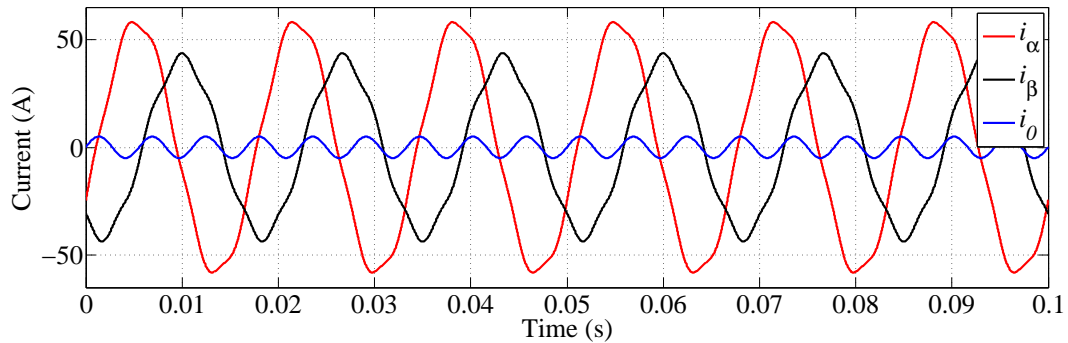
Source: Own authorship.

Finally, Figure 22 illustrates the instantaneous powers obtained with the example quantities. It is possible to observe the existence of a p_0 power due to 3rd order harmonics present in both voltages and currents. Also, p and q present average values and oscillations caused by interactions between different phase sequences and frequency harmonic components.

Figure 22 – Three-phase instantaneous powers under unbalance and harmonic distortion conditions.
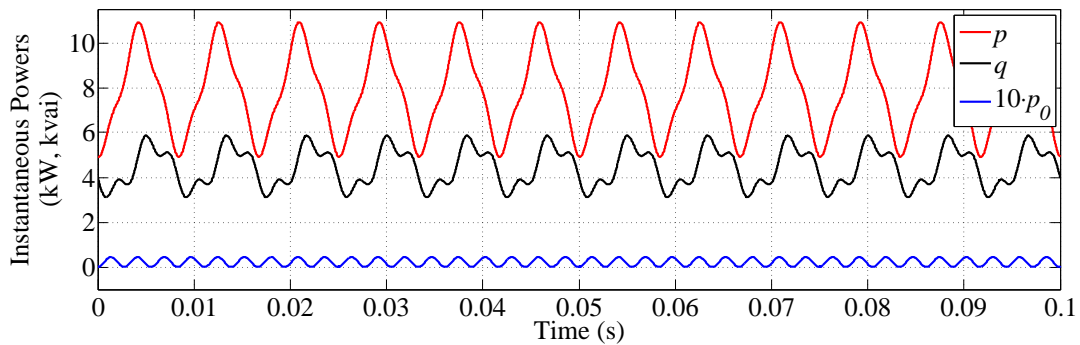
Source: Own authorship.

The concepts and expressions discussed in this section are useful in Chapter 3, which compares the results of the *pq* Theory and the concepts of two-phase instantaneous powers proposed in this work.

2.2 SINGLE-PHASE INSTANTANEOUS POWERS

As previously mentioned, the concepts of The *pq* Theory were originally conceived for three-phase systems. The successful application of the *pq* Theory attracted the attention of researchers for applications in single-phase power conditioning. In this context, adaptations of

the *pq* Theory were proposed aiming to employ its concepts to deal with power conditioning applications in single-phase circuits. It must be kept in mind that the concepts of single-phase $\alpha\beta$ powers are a mathematical approach that showed to be useful to extract reference signals for static power compensators (LIU; YANG & WANG, 1999; HAQUE, 2002b; KHADKIKAR; CHANDRA & SINGH, 2009; FURTADO et al., 2013). However, this approach do not guarantee a proper physical interpretation of power flow process in single-phase circuits. The cited works do not treat this aspect of single-phase $\alpha\beta$ instantaneous powers.

Liu, Yang and Wang (1999) presented a single-phase harmonic detection method based on the *pq* Theory and described its application in hybrid active filters. In such approach, single-phase voltage and current were represented in virtual two-phase $\alpha\beta$ orthogonal system. Then, single-phase instantaneous powers can be calculated in terms of single-phase $\alpha\beta$ voltages and currents as:

$$\begin{bmatrix} p_{1\phi} \\ q_{1\phi} \end{bmatrix} = \begin{bmatrix} \bar{p}_{1\phi} + \tilde{p}_{1\phi} \\ \bar{q}_{1\phi} + \tilde{q}_{1\phi} \end{bmatrix} = \begin{bmatrix} v_\alpha & v_\beta \\ v_\beta & -v_\alpha \end{bmatrix} \begin{bmatrix} i_\alpha \\ i_\beta \end{bmatrix}. \tag{2.22}$$

Haque (2002a), Haque (2002b), Saitou and Shimizu (2002) published works describing similar concepts in the control of single-phase hybrid filters for harmonic currents and reactive power compensation. Similarly as what Liu, Yang and Wang (1999) presented, Haque (2002a), Haque (2002b), Saitou and Shimizu (2002) based their works on a virtual two-phase orthogonal representation of single-phase voltage and current. The single-phase instantaneous powers were also calculated according to (2.22). The proposed single-phase approach of instantaneous powers was named as the *"Single-phase pq Theory"*. Haque (2002a), Haque (2002b) also reinforces the association with the original *pq* Theory by referring to the single-phase instantaneous powers ($p_{1\phi}$ and $q_{1\phi}$) as the *"single-phase version of instantaneous active and imaginary powers"*, respectively. These expressions are also adopted in this thesis. The reader should, however, keep in mind the distinction between the meaning behind single-phase and three-phase instantaneous powers concepts.

Khadkikar, Chandra and Singh (2009) identified a lack of technical studies regarding single-phase instantaneous powers. These authors proposed a *"generalized single-phase pq theory for active power filtering"*. The proposed improvement consisted of applying a single-phase Phase-Locked Loop (PLL) to track the fundamental voltage of the power supply. The insertion of a PLL in the instantaneous powers calculation algorithm allowed the compensation of undesired effects caused by voltage distortions. That is an aspect that was not covered by previous works regarding the Single-phase *pq* Theory (KHADKIKAR; CHANDRA & SINGH, 2009). Such work also described the usage of the Single-phase *pq* Theory in two different strategies for current control: *"the direct current control technique"* and the *"indirect current control technique"*

(KHADKIKAR; CHANDRA & SINGH, 2009).

The common point between the works of Liu, Yang and Wang (1999), Haque (2002a), Haque (2002b), Saitou and Shimizu (2002) and Khadkikar, Chandra and Singh (2009) is the representation of single-phase voltage and current in the orthogonal stationary $\alpha\beta$ reference frame. Then, these authors apply Akagi's powers definitions to obtain single-phase instantaneous powers in terms of $\alpha\beta$ quantities. The next section discusses the representation of single-phase signals in the $\alpha\beta$ reference frame. An analysis of single-phase instantaneous powers is presented in Section 2.2.2.

2.2.1   SINGLE-PHASE $\alpha\beta$ TRANSFORMATION

The operation of transforming a single-phase signal into the orthogonal stationary reference frame is referred in this work as *"single-phase $\alpha\beta$ transformation"* or, alternatively, as *"a–$\alpha\beta$ transformation"*. This operation is described in different ways in technical literature. Liu, Yang and Wang (1999) defined the a-$\alpha\beta$ transformation as a phase lag corresponding to 90° in the fundamental frequency, as illustrated in the block diagram of Figure 23. Haque (2002a), Haque (2002b), in turn, performed the single-phase $\alpha\beta$ transformation by leading single-phase signals by 90° of the fundamental frequency, as illustrated in Figure 24. A third scheme, shown in Figure 25, was used by Furtado et al. (2014) as an alternative to represent single-phase signals in the $\alpha\beta$ reference frame.

Figure 23 – Single-phase $\alpha\beta$ transformation by delaying signals.
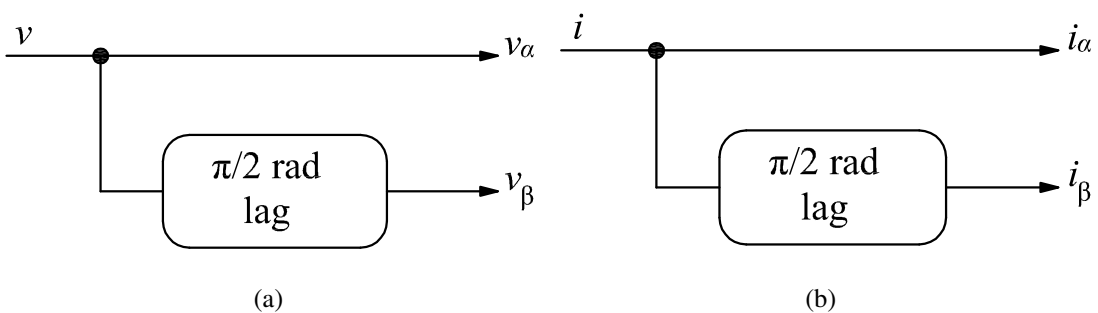
Source: Own authorship.

Figure 24 – Single-phase $\alpha\beta$ transformation by leading signals.
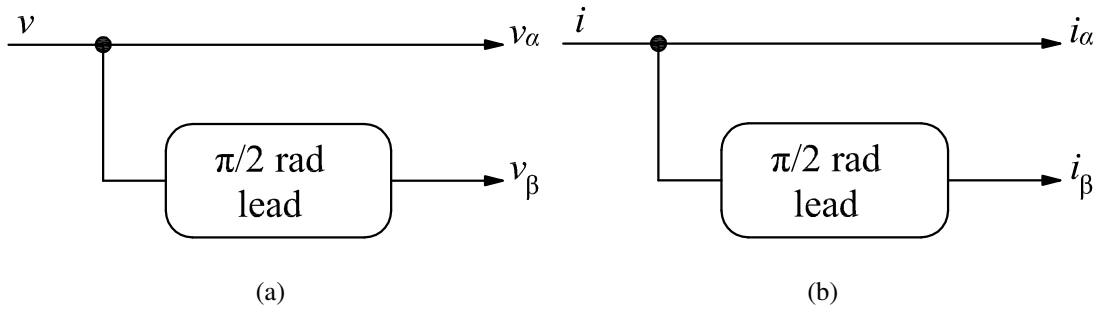
Figure 25 – Alternative single-phase $\alpha\beta$ transformation by lagging signals.
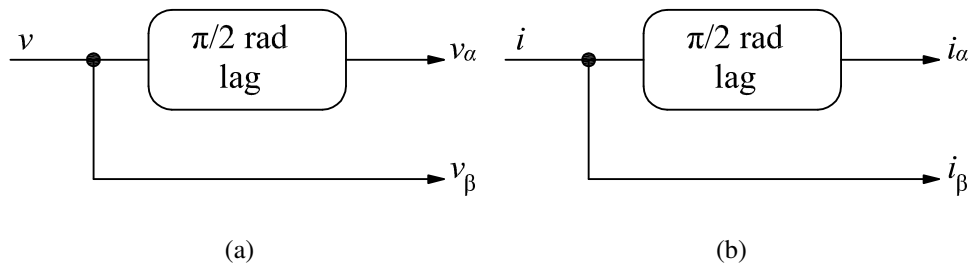
Results obtained for all these three forms of $\alpha\beta$ transformation are equivalent. In practice, the choice between leading or lagging waveforms interferes only in the signal of the calculated single-phase imaginary power.

Different techniques can be employed to implement the 90° phase shifting necessary to the single-phase $\alpha\beta$ transformation. Haque and Ise (2002) described a method based on all-pass filter tuned at the fundamental frequency with the form

$$H(s) = -\frac{1 - T_1 s}{1 + T_1 s},$$

(2.23)

where T_1 is the inverse of fundamental angular frequency ω_1 of the system. This all-pass filter which imposes a 90° advance at the fundamental component of signals, was shown in the Bode plot of Figure 26. However, the single-phase $\alpha\beta$ transformation using $H(s)$ has the disadvantage that the phase shift imposed is not 90° at each harmonic frequencies, which distorts $\alpha\beta$ waveforms and causes errors in power calculations (FURTADO, 2014b).

Figure 26 – Bode plot of $H(s)$ for $\omega_1 = 377$ rad/s.
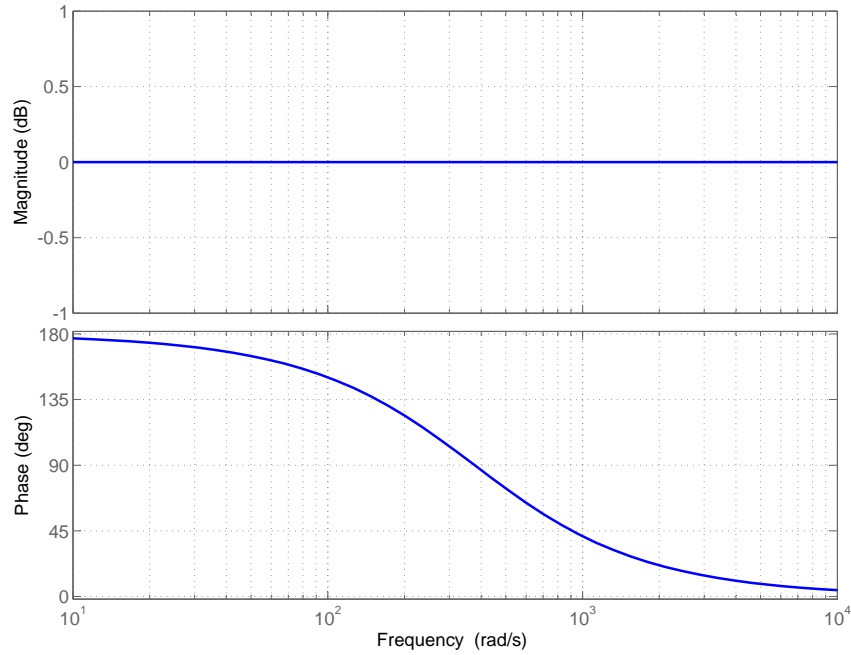
Source: Own authorship.

Furtado et al. (2013), Furtado et al. (2014) combined two alternative methods to perform a–$\alpha\beta$ transformations (FURTADO et al., 2013; FURTADO et al., 2014; FURTADO, 2014b). For current $\alpha\beta$ transformation, a vector was used to store sampled data corresponding to 90° of the signal. Only after $\frac{1}{4}$ of a period the vector starts to be read. This method produces an exact copy of the signal, delayed by 90° at the fundamental frequency. Consequently, the phase shift at harmonic components is $h\frac{\pi}{2}$ rad, where h is the harmonic order. This method was described in more detail by (FURTADO, 2014b).

As discussed by Khadkikar, Chandra and Singh (2009), it may be necessary to extract the fundamental voltage in order to apply the Single-phase pq Theory. For this reason, Furtado (2014b) used a Second-Order Generalized Integrator (SOGI) to implement voltage $\alpha\beta$ transformation. A SOGI system is capable of filtering harmonics for fundamental voltage extraction and, simultaneously, generating a quadrature copy of the filtered signal (RODRIGUEZ et al., 2006) (*i.e.*, performing $\alpha\beta$ transformation).

The methods used to implement single-phase $\alpha\beta$ transformations are all based on shifting the fundamental frequency component of signals by 90°. However, due to the known methods, the phase shift imposed to harmonic components is not 90°. It means that single-phase $\alpha\beta$ quantities are not precisely orthogonal under the presence of harmonic distortions. These properties are different of those observed at three-phase $\alpha\beta$ components obtained with the Clarke transformation (see (2.17) and (2.18)). Therefore, it is expected that single-phase instantaneous

powers behave different if compared with instantaneous active and reactive powers proposed by Akagi. The characteristics and behaviour of single-phase $\alpha\beta$ powers are discussed in next section.

2.2.2 TIME-DOMAIN ANALYSIS OF THE SINGLE-PHASE PQ THEORY

As discussed in the previous section, there are different ways a single-phase $\alpha\beta$ transformation can be implemented. The time-domain analysis presented in this section is based on lagging measured voltages and currents by 90° of the fundamental frequency to obtain the β component, as that illustrated in Figure 23. A factor $\frac{1}{2}$ was included in (2.22) to provide power invariance between classical definitions and the Single-phase pq Theory, resulting in:

$$\begin{bmatrix} p_{1\phi} \\ q_{1\phi} \end{bmatrix} = \begin{bmatrix} \bar{p}_{1\phi} + \tilde{p}_{1\phi} \\ \bar{q}_{1\phi} + \tilde{q}_{1\phi} \end{bmatrix} = \frac{1}{2} \begin{bmatrix} v_\alpha & v_\beta \\ v_\beta & -v_\alpha \end{bmatrix} \begin{bmatrix} i_\alpha \\ i_\beta \end{bmatrix} . \tag{2.24}$$

2.2.2.1 SINUSOIDAL CONDITIONS

Under sinusoidal conditions, single-phase voltage and current are expressed, respectively, as

$$v_a = \sqrt{2}V\sin(\omega t) \tag{2.25}$$

and

$$i_a = \sqrt{2}I\sin(\omega t + \phi_i) . \tag{2.26}$$

These quantities are represented in the $\alpha\beta$ reference frame as

$$\begin{cases} v_\alpha = \sqrt{2}V\sin(\omega t) \\ v_\beta = \sqrt{2}V\sin(\omega t - \pi/2) \end{cases} \tag{2.27}$$

and

$$\begin{cases} i_\alpha = \sqrt{2}I\sin(\omega t + \phi_i) \\ i_\beta = \sqrt{2}I\sin(\omega t + \phi_i - \pi/2) \end{cases} \tag{2.28}$$

Applying the definitions in (2.24), the resulting single-phase instantaneous powers are

$$\begin{cases} p_{1\phi} = \bar{p}_{1\phi} = VI\cos(\phi_i) \\ q_{1\phi} = \bar{q}_{1\phi} = -VI\sin(\phi_i) \end{cases} . \tag{2.29}$$

As discussed by Akagi, Watanabe and Aredes (2007), classical concepts of active and reactive powers in single-phase circuits are based on definitions of average and peak values of a

power expression (*i.e.*, the simple product between voltage and current). The results obtained in this section for $p_{1\phi}$ and $q_{1\phi}$ meet the classical definitions of single-phase active and reactive powers, respectively (AKAGI; WATANABE & AREDES, 2007). Single-phase $\alpha\beta$ powers are constant quantities obtained from instantaneous voltage and current only, with no need of averaging. From this point of view, single-phase instantaneous powers, defined in the $\alpha\beta$ domain, behave similarly as Akagi's three-phase instantaneous powers.

These conditions are exemplified in Figure 27, which illustrates waveforms of sinusoidal single-phase voltage and current.

Figure 27 – Single-phase sinusoidal voltage and current with $V = 127$ V, $I = 35$ A and $\phi_i = -\dfrac{\pi}{6}$ rad.
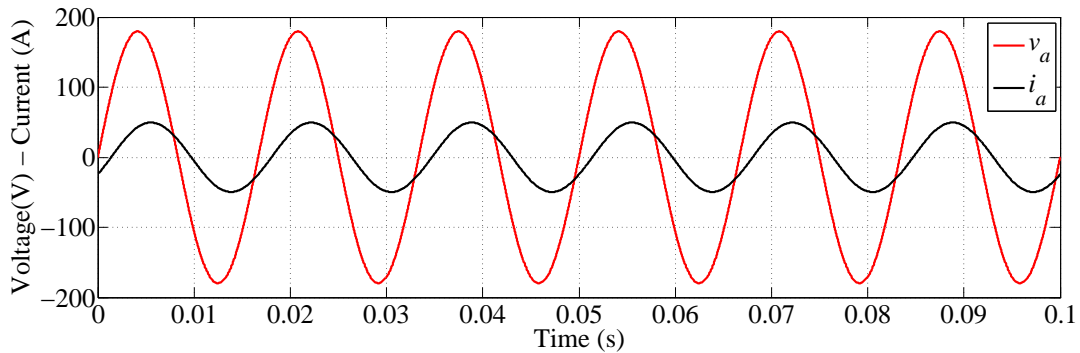
Source: Own authorship.

Figure 28 and Figure 29 show the example single-phase voltage and current, respectively, represented in the orthogonal $\alpha\beta$ reference frame. In this example, the α-component is defined as the original quantity, whereas the β-component is obtained with a $\dfrac{\pi}{2}$ rad delay.

Figure 28 – Single-phase sinusoidal voltage in the $\alpha\beta$ reference frame.
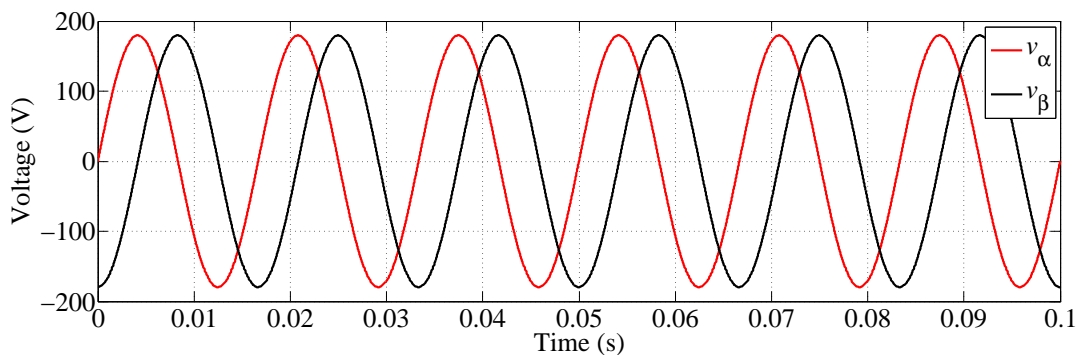
Source: Own authorship.

Figure 29 – Single-phase sinusoidal current in the $\alpha\beta$ reference frame.
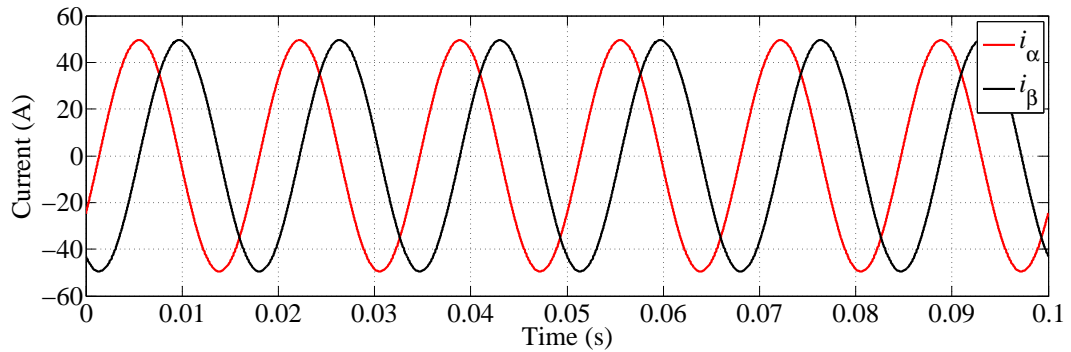
Source: Own authorship.

Finally, Figure 30 shows the single-phase instantaneous powers calculated according to (2.22). It is possible to observe the expected constant behaviour according to (2.29).

Figure 30 – Single-phase instantaneous powers for sinusoidal voltage and current.
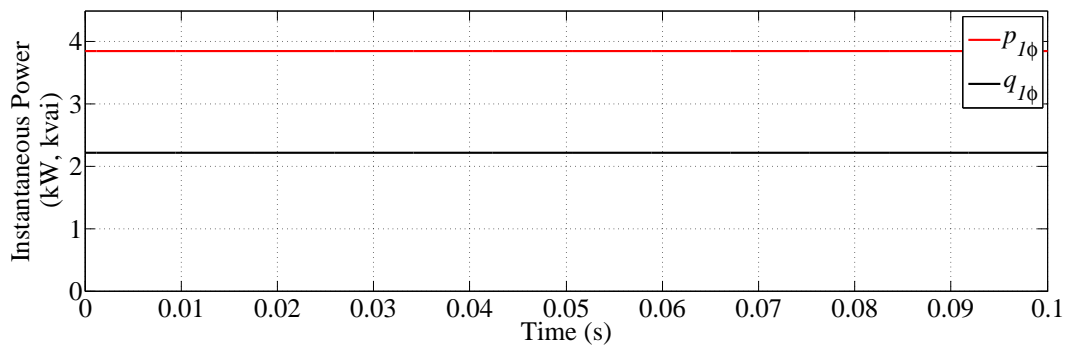
Source: Own authorship.

2.2.2.2 DISTORTED CURRENT CONDITIONS

The next condition in this analysis considers current harmonic distortions. In this case, the voltage is considered to contain only its fundamental component and is expressed as

$$v_a = \sqrt{2}V \sin\left(\omega t + \phi_{v_1}\right) \ . \tag{2.30}$$

The harmonic distorted current waveform is generically expressed by a Fourier series, at which the harmonic order is indicated by the index h:

$$i_a = \sum_{h=1}^{\infty} \sqrt{2}I_h \sin\left[h\omega t + \phi_{i_h}\right] \ . \tag{2.31}$$

The representation of such quantities in the $\alpha\beta$ reference frame is

$$\begin{cases} v_\alpha = & \sqrt{2}V\sin(\omega t + \phi_{v_1}) \\ v_\beta = & \sqrt{2}V\sin(\omega t + \phi_{v_1} - \pi/2) \end{cases} \tag{2.32}$$

and

$$\begin{cases} i_\alpha = & \sum\limits_{h=1}^{\infty} \sqrt{2}I_h \sin[h(\omega t) + \phi_{i_h}] \\ i_\beta = & \sum\limits_{h=1}^{\infty} \sqrt{2}I_h \sin[h(\omega t - \pi/2) + \phi_{i_h}] \end{cases}. \tag{2.33}$$

As previously mentioned, the single-phase $\alpha\beta$ transformation adopted in this analysis is based on lagging signals by $\dfrac{\pi}{2}$ rad of the signal fundamental frequency. Consequently, due to this method, harmonic components are delayed by $h\dfrac{\pi}{2}$ rad. Another important observation to be done is that these $\alpha\beta$ quantities contain all harmonics present in i_a, including triplen and zero-sequence harmonics. These characteristics are not observed in three-phase $\alpha\beta$ quantities obtained through the Clarke transformation (AKAGI; WATANABE & AREDES, 2007).

The calculation of single-phase $\alpha\beta$ powers using (2.24) results in

$$\begin{cases} \bar{p}_{1\phi} = & +V_1 I_1 \cos(\phi_{v_1} - \phi_{i_1}) \\ \\ \tilde{p}_{1\phi} = & +\frac{1}{2}V_1 I_2 \sin(\omega t - \phi_{v_1} + \phi_{i_2}) + \frac{1}{2}V_1 I_2 \cos(\omega t - \phi_{v_1} + \phi_{i_2}) \\ & +\frac{1}{2}V_1 I_2 \sin(3\omega t + \phi_{v_1} + \phi_{i_2}) - \frac{1}{2}V_1 I_2 \cos(3\omega t + \phi_{v_1} + \phi_{i_2}) \\ & -V_1 I_3 \cos(4\omega t + \phi_{v_1} + \phi_{i_3}) \\ & -\frac{1}{2}V_1 I_4 \sin(3\omega t - \phi_{v_1} + \phi_{i_4}) + \frac{1}{2}V_1 I_4 \cos(3\omega t - \phi_{v_1} + \phi_{i_4}) \\ & -\frac{1}{2}V_1 I_4 \sin(5\omega t + \phi_{v_1} + \phi_{i_4}) - \frac{1}{2}V_1 I_4 \cos(5\omega t + \phi_{v_1} + \phi_{i_4}) \\ & +V_1 I_5 \cos(4\omega t - \phi_{v_1} + \phi_{i_5}) \\ & +\frac{1}{2}V_1 I_6 \sin(5\omega t - \phi_{v_1} + \phi_{i_6}) + \frac{1}{2}V_1 I_6 \cos(5\omega t - \phi_{v_1} + \phi_{i_6}) \\ & +\frac{1}{2}V_1 I_6 \sin(7\omega t + \phi_{v_1} + \phi_{i_6}) - \frac{1}{2}V_1 I_6 \cos(7\omega t + \phi_{v_1} + \phi_{i_6}) \\ & -V_1 I_7 \cos(8\omega t + \phi_{v_1} + \phi_{i_7}) \\ & -\frac{1}{2}V_1 I_8 \sin(7\omega t - \phi_{v_1} + \phi_{i_8}) + \frac{1}{2}V_1 I_8 \cos(7\omega t - \phi_{v_1} + \phi_{i_8}) \\ & -\frac{1}{2}V_1 I_8 \sin(9\omega t + \phi_{v_1} + \phi_{i_8}) - \frac{1}{2}V_1 I_8 \cos(9\omega t + \phi_{v_1} + \phi_{i_8}) \\ & +V_1 I_9 \cos(8\omega t - \phi_{v_1} + \phi_{i_9})\dots \end{cases} \tag{2.34}$$

and

$$
\begin{cases}
\bar{q}_{1\phi} = & V_1 I_1 \sin\left(\phi_{v_1} - \phi_{i_1}\right) \\[2ex]
\tilde{q}_{1\phi} = & -\frac{1}{2}V_1 I_2 \sin\left(\omega t - \phi_{v_1} + \phi_{i_2}\right) + \frac{1}{2}V_1 I_2 \cos\left(\omega t - \phi_{v_1} + \phi_{i_2}\right) \\
& -\frac{1}{2}V_1 I_2 \sin\left(3\omega t + \phi_{v_1} + \phi_{i_2}\right) - \frac{1}{2}V_1 I_2 \cos\left(3\omega t + \phi_{v_1} + \phi_{i_2}\right) \\
& -V_1 I_3 \sin\left(4\omega t + \phi_{v_1} + \phi_{i_3}\right) \\
& -\frac{1}{2}V_1 I_4 \sin\left(3\omega t - \phi_{v_1} + \phi_{i_4}\right) - \frac{1}{2}V_1 I_4 \cos\left(3\omega t - \phi_{v_1} + \phi_{i_4}\right) \\
& -\frac{1}{2}V_1 I_4 \sin\left(5\omega t + \phi_{v_1} + \phi_{i_4}\right) + \frac{1}{2}V_1 I_4 \cos\left(5\omega t + \phi_{v_1} + \phi_{i_4}\right) \\
& -V_1 I_5 \sin\left(4\omega t - \phi_{v_1} + \phi_{i_5}\right) \\
& -\frac{1}{2}V_1 I_6 \sin\left(5\omega t - \phi_{v_1} + \phi_{i_6}\right) + \frac{1}{2}V_1 I_6 \cos\left(5\omega t - \phi_{v_1} + \phi_{i_6}\right) \\
& -\frac{1}{2}V_1 I_6 \cos\left(7\omega t + \phi_{v_1} + \phi_{i_6}\right) - \frac{1}{2}V_1 I_6 \sin\left(7\omega t + \phi_{v_1} + \phi_{i_6}\right) \\
& -V_1 I_7 \sin\left(8\omega t + \phi_{v_1} + \phi_{i_7}\right) \\
& -\frac{1}{2}V_1 I_8 \sin\left(7\omega t - \phi_{v_1} + \phi_{i_8}\right) - \frac{1}{2}V_1 I_8 \cos\left(7\omega t - \phi_{v_1} + \phi_{i_8}\right) \\
& -\frac{1}{2}V_1 I_8 \sin\left(9\omega t + \phi_{v_1} + \phi_{i_8}\right) + \frac{1}{2}V_1 I_8 \cos\left(9\omega t + \phi_{v_1} + \phi_{i_8}\right) \\
& -V_1 I_9 \sin\left(8\omega t - \phi_{v_1} + \phi_{i_9}\right) \ldots
\end{cases}
\tag{2.35}
$$

These results show the interaction of voltage and current at the fundamental frequency produce only the constant power parcels $\bar{p}_{1\phi}$ and $\bar{q}_{1\phi}$, as also shown in the previous section. All other power components, produced by the interactions of voltage and currents in different frequencies, are oscillatory with zero average.

The characteristics observed in $p_{1\phi}$ and $q_{1\phi}$ under harmonic distortions are similar to those of three-phase Akagi's instantaneous powers (AKAGI; WATANABE & AREDES, 2007). The power components $\bar{p}_{1\phi}$ and $\bar{q}_{1\phi}$ can be used to separate the fundamental-frequency current in i_a. Also, it is possible to separate the fundamental frequency current in its "active" and "reactive" parcels from $\bar{p}_{1\phi}$ and $\bar{q}_{1\phi}$, respectively. These characteristics are specially useful for algorithms that generate reference currents to be synthesized by APFs and other grid-connected converters (LIU; YANG & WANG, 1999; HAQUE & ISE, 2002; KHADKIKAR; CHANDRA & SINGH, 2009).

Example waveforms are presented in Figure 31, which shows a single-phase sinusoidal voltage and an harmonic distorted and delayed current.

Figure 31 – Single-phase sinusoidal voltage with $V = 127$ V and distorted current with $I_1 = 35$ A, $I_3 = 10$ % and $I_5 = 5$ % of I_1.
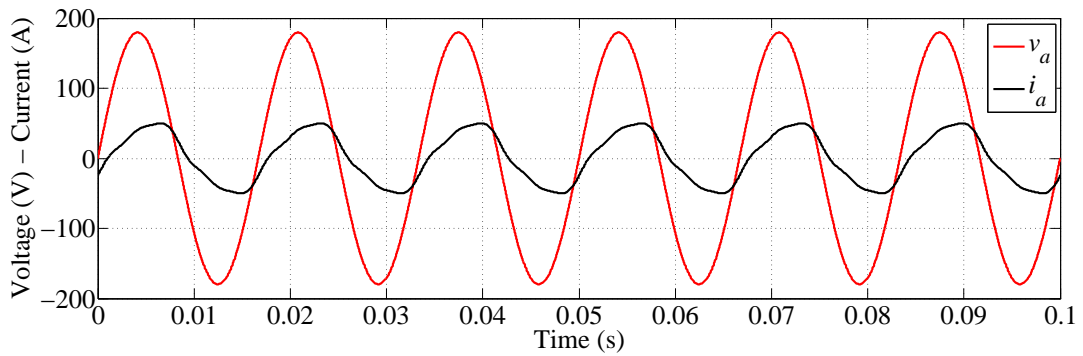
Source: Own authorship.

The representation of these quantities in terms of $\alpha\beta$ coordinates is shown in Figure 32 and Figure 33.

Figure 32 – Single-phase sinusoidal voltage in the $\alpha\beta$ reference frame.
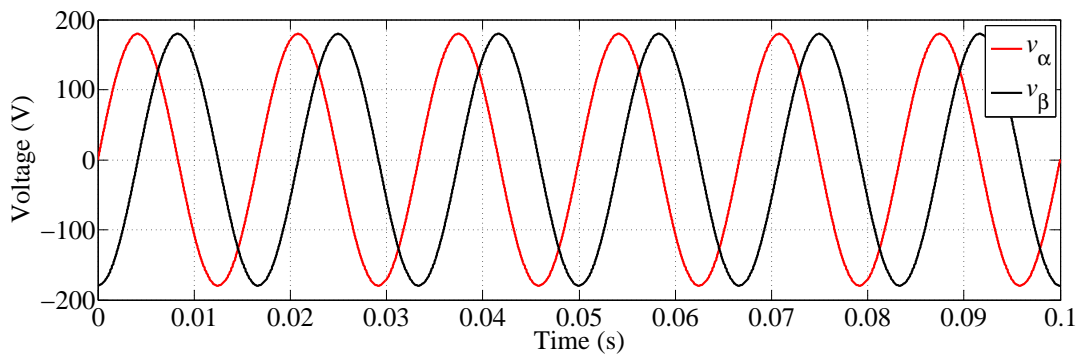
Source: Own authorship.

Figure 33 – Single-phase harmonic distorted current in the $\alpha\beta$ reference frame.
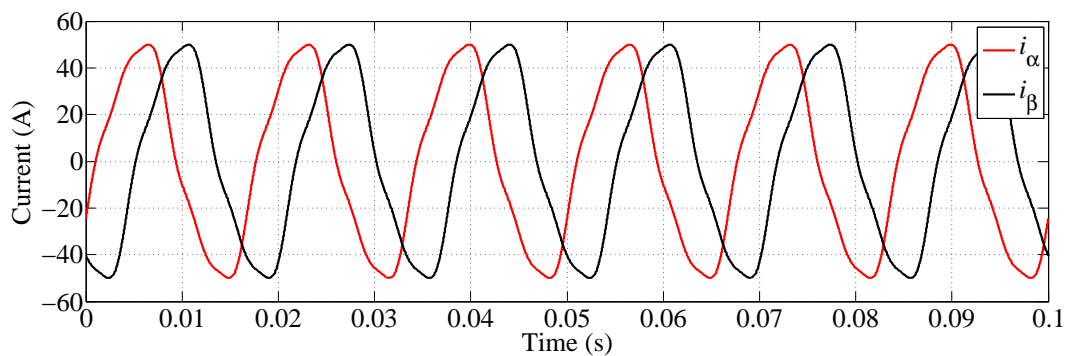
Source: Own authorship.

The single-phase instantaneous powers obtained in this example are illustrated in Figure 34.

It is possible to observe that these powers have non-zero constant components, due to the interaction of fundamental voltage and current. As previously discussed, the oscillations observed in $p_{1\phi}$ and $q_{1\phi}$ are caused by the interactions between the fundamental voltage and harmonic current components.

Figure 34 – Single-phase instantaneous powers under sinusoidal voltage and distorted current conditions.
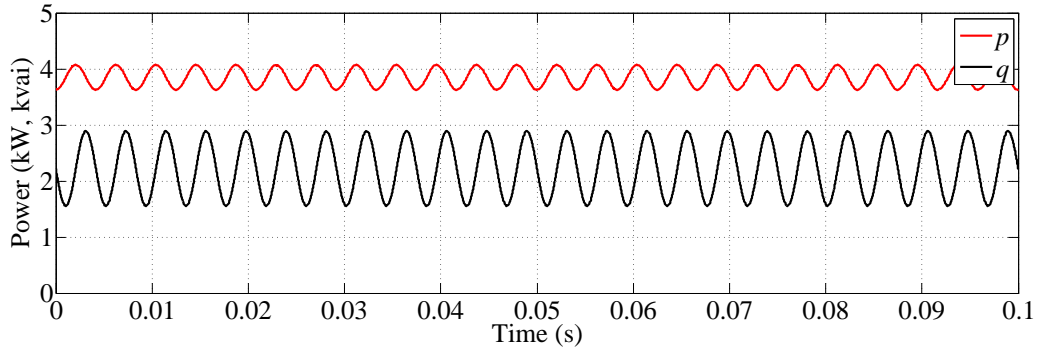
Source: Own authorship.

2.2.2.3 *VOLTAGE AND CURRENT DISTORTIONS*

This section deals with the most general situation, in which both voltage and current present harmonic distortions. In such condition, these quantities can be generically expressed as

$$v_a = \sum_{h=1}^{\infty} \sqrt{2}V_h \sin\left[h\left(\omega t\right) + \phi_{v_h}\right] \tag{2.36}$$

and

$$i_a = \sum_{h=1}^{\infty} \sqrt{2}I_h \sin\left[h\left(\omega t\right) + \phi_{i_h}\right] . \tag{2.37}$$

Applying the single-phase $\alpha\beta$ transformation, the representation of these quantities in the stationary reference frame result in

$$\begin{cases} v_\alpha = \sum_{h=1}^{\infty} \sqrt{2}V_h \sin\left[h\left(\omega t\right) + \phi_{v_h}\right] \\ v_\beta = \sum_{h=1}^{\infty} \sqrt{2}V_h \sin\left[h\left(\omega t - \dfrac{\pi}{2}\right) + \phi_{v_h}\right] \end{cases} \tag{2.38}$$

and

$$\begin{cases} i_\alpha = \sum_{h=1}^{\infty} \sqrt{2}I_h \sin\left[h\left(\omega t\right) + \phi_{i_h}\right] \\ i_\beta = \sum_{h=1}^{\infty} \sqrt{2}I_h \sin\left[h\left(\omega t - \dfrac{\pi}{2}\right) + \phi_{i_h}\right] \end{cases} . \tag{2.39}$$

The resulting expressions for the instantaneous powers $p_{1\phi}$ and $q_{1\phi}$ are quite long and not easy to be simplified. Aiming to facilitate the text reading, these expressions are presented in

Appendix A.

As expected, the behaviour of $\alpha\beta$ powers observed in previous sections are still valid. That is, constant power components $\bar{p}_{1\phi}$ and $\bar{q}_{1\phi}$ are always produced by voltages and currents at the same frequency, whereas the products of harmonics of different orders result in oscillating power components that take part in $\tilde{p}_{1\phi}$ and $\tilde{q}_{1\phi}$.

However, there are characteristics that must be observed for the interactions between voltage and current at the same odd harmonic order. These interactions contribute both to $\bar{p}_{1\phi}$ and $\tilde{p}_{1\phi}$. Furthermore, these interactions never contribute to the imaginary power, despite the phase difference between voltage and current at odd harmonic frequencies. The average imaginary power $\bar{q}_{1\phi}$ is composed exclusively by products of even harmonics and $\tilde{q}_{1\phi}$ is formed by products of harmonics of different orders. Due to this property, it becomes impracticable the separation of second-order harmonic currents that produce constant power components from those which produce oscillating powers.

The conditions analysed in this section are exemplified in Figure 35, at which is possible to observe single-phase voltage and current with harmonic distortions. These quantities were transformed into the $\alpha\beta$ reference frame with a $\dfrac{\pi}{2}$ rad delayed copy, as shown in Figure 36 and Figure 37. The instantaneous single-phase powers obtained under these conditions are shown illustrated in Figure 38. In a comparison with Figure 34, it is possible to observe in Figure 38 the power oscillations introduced by the 7th order harmonic in the voltage waveform.

Figure 35 – Single-phase harmonic distorted voltage with $V_1 = 127$ V and $V_7 = 5$ % of V_1 and current with $I_1 = 35$ A, $I_3 = 10$ % and $I_5 = 5$ % I_1.
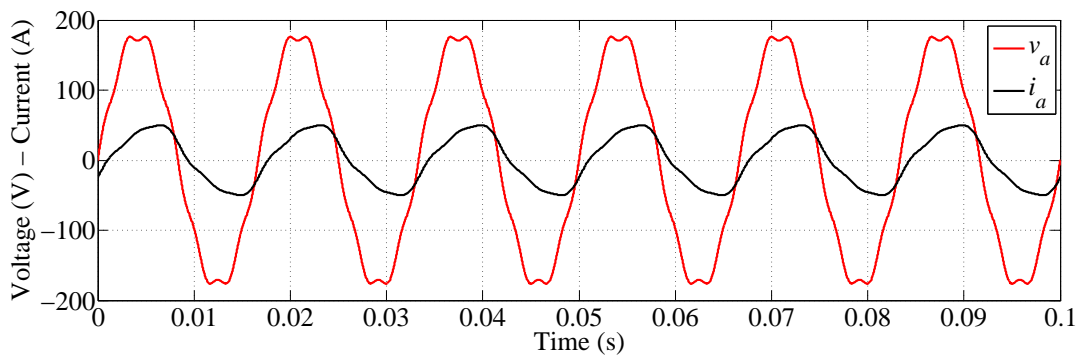
Source: Own authorship.

Figure 36 – Single-phase harmonic distorted voltage in the $\alpha\beta$ reference frame.
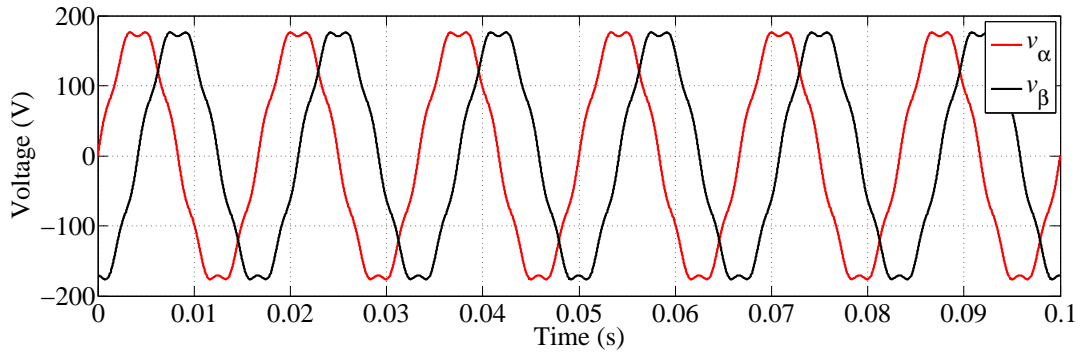
Source: Own authorship.

Figure 37 – Single-phase harmonic distorted current in the $\alpha\beta$ reference frame.
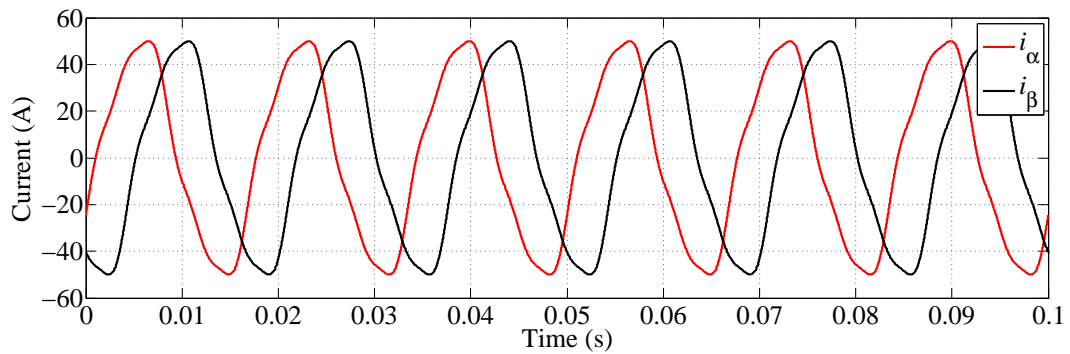
Source: Own authorship.

Figure 38 – Single-phase instantaneous powers under voltage and and current harmonic distortions.
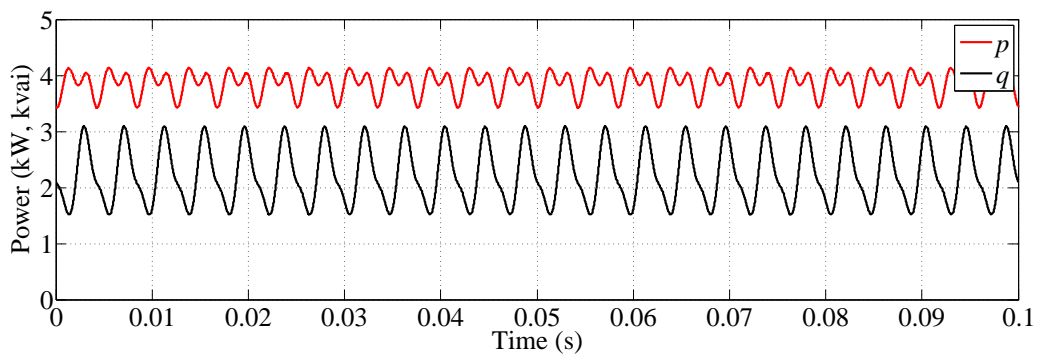
Source: Own authorship.

Another aspect to be regarded is the application of the Single-phase pq Theory to deal with three-phase systems as a superposition of three independent circuits. This sort of approach was used by Liu, Yang and Wang (1999), Saitou and Shimizu (2002), Haque (2002a), Khadkikar, Chandra and Singh (2009) and others. The Single-phase pq Theory neglects unbalances,

negative- and zero-sequence power flows. Therefore, in this sort of approach, it may be not possible to achieve satisfactory compensation from the point of view of a three-phase power supply.

3   INSTANTANEOUS POWERS IN TWO-PHASE THREE-WIRE NETWORKS

3.1   APPLICATIONS IN TWO-PHASE THREE-WIRE POWER CONDITIONING

In previous works, the author of this dissertation studied different methodologies that applied the Single-phase *pq* Theory for power conditioning applications in $2\phi3w$ networks. These works dealt with $2\phi3w$ systems as a superposition of single-phase circuits sharing a common neutral conductor. On the other hand, the control algorithms become long

The first works published in this research treated the active compensation of reactive power and harmonic current filtering of $2\phi3w$ loads. These works discussed the principles behind the idea of two-phase active compensation, suitable power converter topologies and the context at which $2\phi3w$ PC applications could be interesting. Even though each phase was compensated independently, the developed algorithms also included a feature that allowed load balancing between the two involved phases (FURTADO et al., 2013; FURTADO et al., 2014; FURTADO, 2014b).

Afterwards, Furtado et al. (2015a) applied the Single-phase *pq* Theory to implement a grid synchronization and active power injection control strategy for PV systems in $2\phi3w$ networks. This work also showed that power inverters of PV systems can perform simultaneously both power injection and APF functions.

Two different compensation strategies were developed for $2\phi3w$ networks. The first strategy is named Double Single-Phase Strategy (DSPS). Power conditioning with DSPS results in sinusoidal source currents synchronized with phase voltages (FURTADO et al., 2013; FURTADO et al., 2014; FURTADO, 2014b). The second compensation strategy was named Zero Neutral Current Strategy (ZNCS) (FURTADO; RODRIGUES & BARBOSA, 2015b). ZNCS was developed to suppress the flow of neutral currents due to $2\phi3w$ circuits. The application of ZNCS results in sinusoidal source currents synchronized with line voltages and zero neutral current flowing from the source (FURTADO; RODRIGUES & BARBOSA, 2015b). A comparison between DSPS and ZNCS, discussing the pros and cons of each compensation strategy was published by Furtado et al. (2015c).

Even though the Single-phase *pq* Theory was successfully applied for power conditioning

applications for $2\phi 3w$ networks, some limiting aspects were faced in its experimental application. For instance, single-phase algorithms must be implemented twice (once for each phase), which lead to long codes. The representation of two-phase quantities in the $\alpha\beta$, as proposed by Furtado (2014b), demands considerable memory space for data storage. Also, the time needed to perform all calculations for two phases is quite long, which limits sampling and switching frequencies in digital implementation of the algorithm.

Aiming to overcome such issues, this research was directed to investigate and study new tools that can improve control algorithms for $2\phi 3w$ power conditioning equipment, as well as simplify the analysis of the power flow process in $2\phi 3w$ networks. In this context, this chapter describes an adaptation of the *pq* Theory for $2\phi 3w$ electric circuits. This adaptation was firstly published by Furtado, Rodrigues and Barbosa (2015d) and is described and analysed in more detail in this chapter. This approach deals with two-phase systems as an unity, not as superposition of single-phase circuits nor as unbalanced three-phase systems.

3.2 TWO-PHASE $\alpha\beta$ TRANSFORMATION

The three-phase and the single-phase forms of the *pq* Theory presented power definitions based on representations of voltages and currents in an orthogonal stationary $\alpha\beta$ reference frame. The approach proposed in this work relies on a similar idea.

Initially, lets consider a pair of fundamental-frequency two-phase voltages or currents associated with phases *a* and *b*. These quantities can be generically expressed as

$$
\begin{cases}
x_a = \sqrt{2}\, X_a\, \sin\left(\omega t + \phi_a\right) \\
x_b = \sqrt{2}\, X_b\, \sin\left(\omega t + \phi_b\right)
\end{cases}, \tag{3.1}
$$

where x_a and x_b represent instantaneous values of line currents or phase voltages and X_a and X_b represent the rms values of these quantities in phases *a* and *b*, respectively.

It is important to emphasize at this point that the $2\phi 3w$ circuits treated in this work are derivations of three-phase four-wire circuits, at which phase *c* is not accessible. Therefore, since the quantities in (3.1) are part of a three-phase system, they can be mathematically expressed in terms of symmetrical components for three-phase systems described by Fortescue (1918).

In the context of this work, two-phase quantities are regarded as balanced if they have the same amplitude ($X_a = X_b$) and the phase difference between them is $120°$ ($\mid \phi_b - \phi_a \mid = 2\pi/3$). If these conditions are true, this situation is regarded as a "two-phase balance" in this text. However, it must be kept in mind that a two-phase balance does not necessarily mean a balanced

condition in the three-phase system which originated the $2\phi3w$ circuit under analysis.

In these terms, a pair of two-phase balanced fundamental-frequency quantities associated with phases a and b can be represented as

$$\begin{cases} x_a = \sqrt{2}\,X\,\sin(\omega t) \\ x_b = \sqrt{2}\,X\,\sin\left(\omega t - \dfrac{2\pi}{3}\right) \end{cases} . \tag{3.2}$$

The linear transformation (3.3) is proposed to map two-phase voltages and currents from their natural ab reference frame into an orthogonal stationary $\alpha\beta$ reference frame:

$$\begin{bmatrix} x_\alpha \\ x_\beta \end{bmatrix} = \frac{1}{\sqrt{3}} \begin{bmatrix} \sqrt{3} & 0 \\ 1 & 2 \end{bmatrix} \begin{bmatrix} x_a \\ x_b \end{bmatrix}, \tag{3.3}$$

where x_α and x_β represent the quantities expressed in the $\alpha\beta$ reference frame.

Other equation worth to be mentioned at this point is the inverse operation of (3.3), which is used in further sections of this work, expressed as

$$\begin{bmatrix} x_a \\ x_b \end{bmatrix} = \frac{1}{2} \begin{bmatrix} 2 & 0 \\ -1 & \sqrt{3} \end{bmatrix} \begin{bmatrix} x_\alpha \\ x_\beta \end{bmatrix}. \tag{3.4}$$

A vector representation of two-phase quantities in their natural ab coordinates is shown in Figure 39(a). The orientation of vectors $\vec{x}_a$ and $\vec{x}_b$ is fixed, whereas their amplitude correspond to the instantaneous values of x_a and x_b, respectively. It must be noted the absence of a c-axis quantity, which exists in a three-phase system but is not present in $2\phi3w$ circuits studied in this work. An equivalent orthogonal $\alpha\beta$ representation of these vectors can be obtained by applying the linear transformation (3.3). The resulting $\alpha\beta$ representation is illustrated in Figure 39(b). In this coordinate system, vectors $\vec{x}_\alpha$ and $\vec{x}_\beta$ stand for the orthogonal projections of a rotating vector $\vec{x}_{2\phi}$.

Figure 39 – Space vector representation in the *ab* (a) and $\alpha\beta$ (b) reference frames.

<div align="center">(a)   (b)</div>
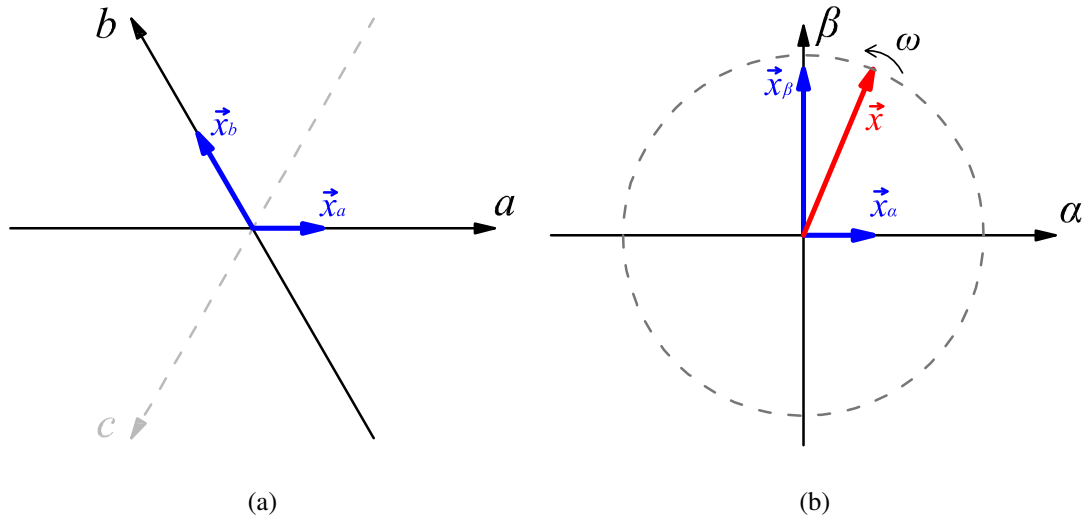
<div align="center">Source: Own authorship.</div>

The rotating vector concept is similar to that employed by Akagi, Watanabe and Aredes (2007) for three-phase systems. The length of $\vec{x}_{2\phi}$ is constant if *ab* quantities are sinusoidal and balanced (*i.e.*, equal in amplitude and phase *a* leading phase *b* by 120 degrees). The rotation with constant amplitude defines a circular trajectory performed by $\vec{x}_{2\phi}$ over the plane, as illustrated in **??**. The presence of harmonics in *ab* quantities would cause oscillations in the length of $\vec{x}_{2\phi}$. Imbalances would make the vector perform an ellipsoidal trajectory. Also, the rotation frequency equals the angular frequency ω of *ab* quantities. Assuming an *a–b–c* phase sequence, $\alpha\beta$ quantities respect an α–β sequence and $\vec{x}_{2\phi}$ rotates in the anticlockwise direction.

The $\alpha\beta$ reference frame is also commonly associated to the complex plane (AKAGI; WATANABE & AREDES, 2007; HAQUE, 2002a), where the α–axis is the Real and β–axis stand for the Imaginary coordinates. In this case the vector $\vec{x}_{2\phi}$ is described as

$$\vec{x}_{2\phi} = x_\alpha + jx_\beta, \tag{3.5}$$

where *j* stands for the imaginary unity.

The relation in (3.3) was initially obtained in this research by means of the decomposition of *ab* vectors on the desired $\alpha\beta$ axis. It was observed later that other approaches converge to the same result. The relation in (3.3) can also be achieved by presupposing the desired $\alpha\beta$ quantities in time-domain and determining the coefficients A, B, C and D of a linear combination of *ab* quantities:

$$\begin{cases} x_\alpha = A\, x_a + B\, x_b = \sqrt{2}X\, \sin(\omega t) \\ x_\beta = C\, x_a + D\, x_b = -\sqrt{2}X\, \cos(\omega t) \end{cases}. \tag{3.6}$$

A third approach is based on the Clarke transformation (2.1). The transformation in (3.3) results if unbalances are neglected and one sets

$$x_c = - (x_a + x_b) . \tag{3.7}$$

As in the original and single-phase *pq* theories, two-phase instantaneous powers are calculated in terms of $\alpha\beta$-represented quantities. The two-phase powers are discussed on the next section.

3.3 TWO-PHASE THREE-WIRE INSTANTANEOUS POWERS

As previously described by Akagi, Watanabe and Aredes (2007) for three-phase systems, the instantaneous complex power is given by the product of the voltage vector and the conjugate current vector. This concept can also be adopted for two-phase instantaneous power:

$$\vec{s}_{2\phi} = \vec{v}_{2\phi} \cdot \vec{i}_{2\phi}^* = \left(v_\alpha + jv_\beta\right) \cdot \left(i_\alpha - ji_\beta\right) , \tag{3.8}$$

where $\vec{s}_{2\phi}$ stands for the two-phase three-wire instantaneous complex power. This definition yields

$$\vec{s}_{2\phi} = \left(v_\alpha i_\alpha + v_\beta i_\beta\right) + j\left(v_\beta i_\alpha - v_\alpha i_\beta\right) . \tag{3.9}$$

Akagi, Kanasawa and Nabae named the real parcel of the complex power as "real power", which unity is watt [W]. The imaginary term of the instantaneous complex power received the name of "imaginary power", given in "volt-ampere imaginary" [vai] (AKAGI; WATANABE & AREDES, 2007). So, this work keeps these nomenclatures and measurement unities for two-phase instantaneous powers.

Writing in matrix form, the calculation of $2\phi3w$ instantaneous powers is expressed as

$$\begin{bmatrix} p_{2\phi} \\ q_{2\phi} \end{bmatrix} = \begin{bmatrix} v_\alpha & v_\beta \\ v_\beta & -v_\alpha \end{bmatrix} \begin{bmatrix} i_\alpha \\ i_\beta \end{bmatrix} , \tag{3.10}$$

where $p_{2\phi}$ is named "two-phase real power" and $q_{2\phi}$ is called "two-phase imaginary power".

It can be shown that, as observed internal signals labelled as "real" and "imaginary" powers, based on the pq Theory for three-phase and single-phase circuits, two-phase powers are composed by an average (constant) and an zero-averaged oscillatory power components:

$$\begin{cases} p_{2\phi} = \bar{p}_{2\phi} + \tilde{p}_{2\phi} \\ q_{2\phi} = \bar{q}_{2\phi} + \tilde{q}_{2\phi} \end{cases} , \tag{3.11}$$

where $\left(\bar{p}_{2\phi}, \bar{q}_{2\phi} \right)$ represent average (constant) values and $\left(\tilde{p}_{2\phi}, \tilde{q}_{2\phi} \right)$ represent zero-averaged oscillating parcels. This characteristic is quite useful in the design of controllers for grid-connected converters. For these applications, it is commonly necessary to determine $\alpha\beta$ currents from predefined instantaneous powers. This operation is done by applying the inverse form of (3.10):

$$
\begin{bmatrix} i_\alpha \\ i_\beta \end{bmatrix} = \frac{2}{v_\alpha^2 + v_\beta^2} \begin{bmatrix} v_\alpha & v_\beta \\ v_\beta & -v_\alpha \end{bmatrix} \begin{bmatrix} p_{2\phi} \\ q_{2\phi} \end{bmatrix}.
\tag{3.12}
$$

3.4 TIME-DOMAIN ANALYSIS OF TWO-PHASE POWERS

A time-domain analysis is presented in this section to demonstrate and discuss specific characteristics that result from the application of the proposed ab–$\alpha\beta$ transformation and $2\phi3w$ instantaneous powers.

3.4.1 SINUSOIDAL BALANCED CONDITIONS

This is the simplest situation, at which two-phase voltages and currents are balanced and include no harmonic components. It is worth emphasizing that, for the context of this work, $2\phi3w$ quantities are considered balanced if they are phase displaced by $2\pi/3$ rad and have equal amplitude and frequency.

The set of two-phase voltages for these conditions can be written as

$$
\begin{cases} v_a = \sqrt{2}V \sin\left(\omega t\right) \\ v_b = \sqrt{2}V \sin\left(\omega t - \dfrac{2\pi}{3}\right) \end{cases},
\tag{3.13}
$$

whereas line currents are expressed as

$$
\begin{cases} i_a = \sqrt{2}I \sin\left(\omega t + \phi_i\right) \\ i_b = \sqrt{2}I \sin\left(\omega t - \dfrac{2\pi}{3} + \phi_i\right) \end{cases}.
\tag{3.14}
$$

Applying the transformation (3.3), the resulting ab–$\alpha\beta$ quantities are

$$
\begin{cases} v_\alpha = \sqrt{2}V \sin\left(\omega t\right) \\ v_\beta = -\sqrt{2}V \cos\left(\omega t\right) \end{cases}
\tag{3.15}
$$

and

$$
\begin{cases} i_\alpha = \sqrt{2}I \sin\left(\omega t\right) \\ i_\beta = -\sqrt{2}I \cos\left(\omega t\right) \end{cases}.
\tag{3.16}
$$

As previously mentioned, these results are comparable to those the Clarke transformation produces for three-phase balanced quantities.

At this point, it interesting to evaluate the instantaneous power in terms of the natural *ab* reference frame:

$$p_{ab} = v_a\, i_a + v_b\, i_b \ , \tag{3.17}$$

where

$$
p_{ab} = 2VI\cos(\phi_i) + VI\cos(\phi_i)\cos\left(2\omega t - \frac{2\pi}{3}\right) \\
- VI\sin(\phi_i)\sin\left(2\omega t - \frac{2\pi}{3}\right) . \tag{3.18}
$$

It is possible to observe a power parcel that flows unidirectionally and is never null, but oscillates around an average value. It is an expected result, since it is exactly the behaviour of a three-phase system if one phase is open. The active power is the average value expressed in (3.18). It can also be noted a power parcel with zero average which amplitude $VI\sin(\phi_i)$ regards the conventional definition of reactive power. Therefore, both conventional active and reactive powers present oscillations. Also, these oscillations are summed with the same frequency 2ω in p_{ab}. This characteristics do not allow an independent and direct observation or measurement of the corresponding active and reactive powers in the circuit.

On the $\alpha\beta$ domain, the calculation of two-phase instantaneous powers by applying (3.10) yields

$$
\begin{cases}
p_{2\phi} = \bar{p}_{2\phi} = 2VI\cos(\phi_i) \\
q_{2\phi} = \bar{q}_{2\phi} = -2VI\sin(\phi_i)
\end{cases} . \tag{3.19}
$$

Furthermore, aiming to illustrate the behaviour of $2\phi 3w$ instantaneous powers under sinusoidal balanced conditions, Figure 40 and Figure 41 show example waveforms of voltages and currents.

Figure 40 – Two-phase three-wire sinusoidal balanced voltages with $V = 127$ V.
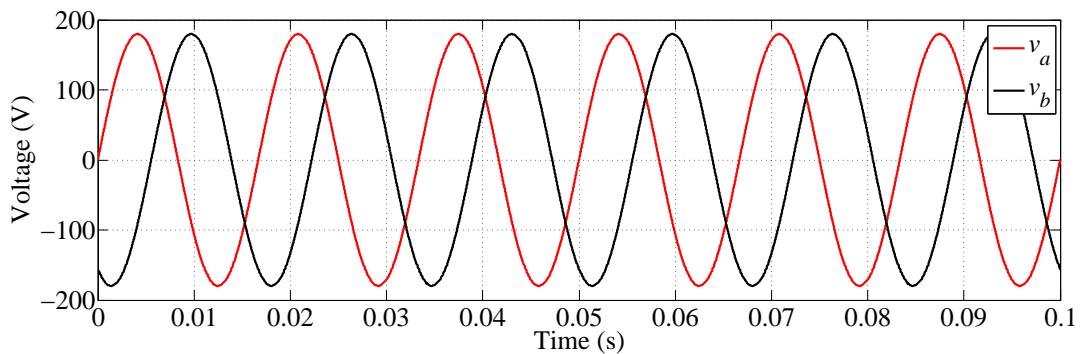
Source: Own authorship.

Figure 41 – Two-phase three-wire sinusoidal balanced currents with $I = 35$ A and $\phi_i = -\dfrac{\pi}{6}$ rad.
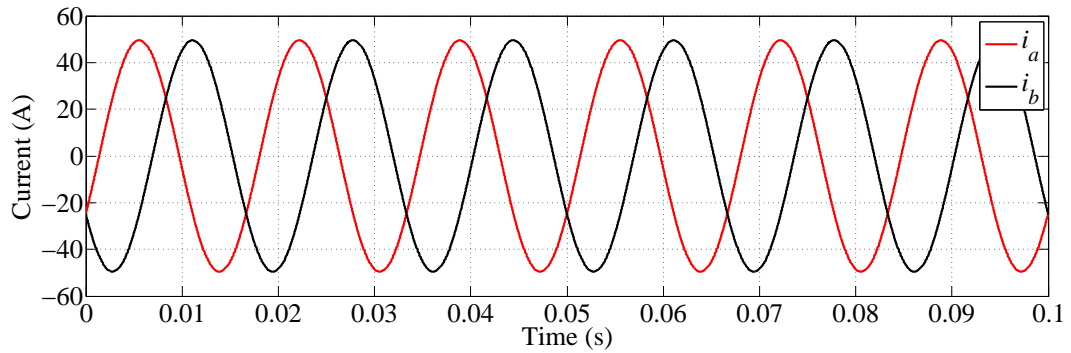
Source: Own authorship.

The $\alpha\beta$ representation of these $2\phi3w$ quantities is shown in Figure 42 and Figure 43. It is possible to observe in these figures the orthogonality between α and β components, achieved by the linear transformation (3.3).

Figure 42 – Two-phase sinusoidal balanced voltages in the $\alpha\beta$ reference frame.
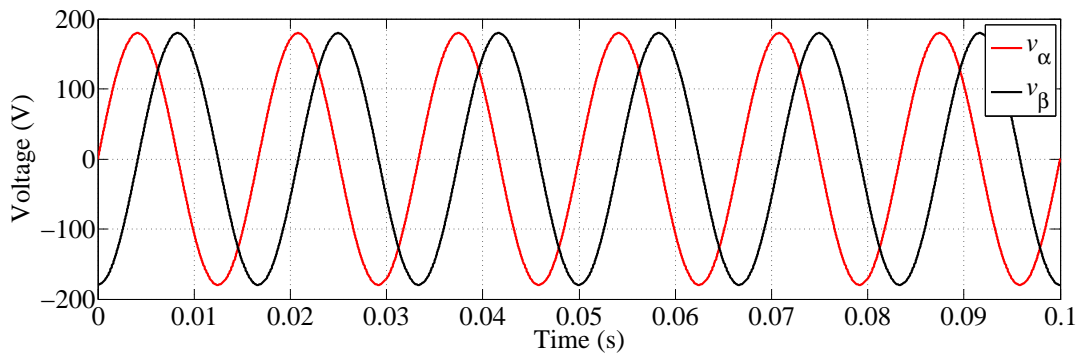
Source: Own authorship.

Figure 43 – Two-phase sinusoidal balanced currents in the $\alpha\beta$ reference frame.
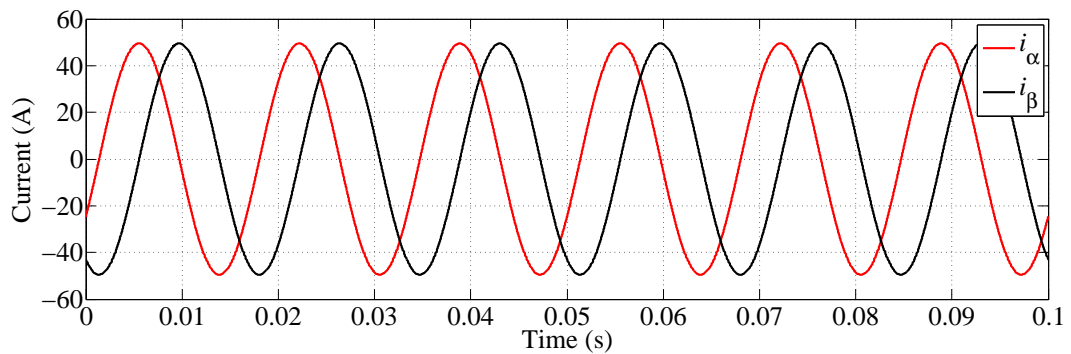
Source: Own authorship.

The $2\phi3w$ instantaneous powers obtained with these quantities are illustrated in Figure 44.

Figure 44 – Two-phase instantaneous powers under voltage and current sinusoidal balanced conditions.
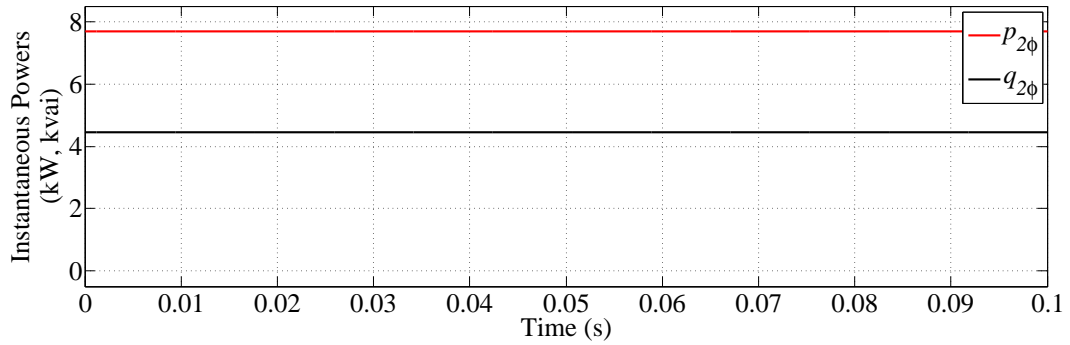
Source: Own authorship.

It can be observed that both $p_{2\phi}$ and $q_{2\phi}$ are constant under sinusoidal balanced conditions. The real power equals the average value in (3.18). As Akagi, Watanabe and Aredes (2007) highlighted for the three-phase pq theory, it is worth mentioning here that $p_{2\phi}$ is obtained from instantaneous voltages and currents, with no need of averaging. The real power corresponds to the average power which flows unidirectionally from the source to the load (AKAGI; WATANABE & AREDES, 2007). The imaginary power $q_{2\phi}$ is related to the conventional definition of reactive power. The two-phase imaginary power is a measurement of the amount of power continuously exchanged between phases a and b. It can be observed that (3.3) and (3.10) provide both voltage/current amplitude and power invariance between ab and $\alpha\beta$ domains.

3.4.2 SINUSOIDAL UNBALANCED CONDITIONS

This section addresses situations at which quantities in phases a and b given in (3.1) do not present the same amplitude or $2\pi/3$ rad phase displacement. It must be clear that this work refers to negative- and zero-sequence components present in three-phase system from which $2\phi3w$ circuits derive.

As previously discussed, $2\phi3w$ circuits in this work are a subset derived from a three-phase four-wire system. Therefore, it is convenient that two-phase quantities are expressed and analysed in terms of symmetrical components (FORTESCUE, 1918). Aiming to ease the interpretation of their influence in two-phase instantaneous powers, separate analysis are presented for negative- and zero-sequence unbalances

3.4.2.1 NEGATIVE-SEQUENCE UNBALANCES

In this context, two-phase sinusoidal voltages with negative-sequence unbalances can be generically expressed as

$$
\begin{cases}
v_a = \sqrt{2}V_+ \sin\left(\omega t\right) + \sqrt{2}V_- \sin\left(\omega t + \phi_{v_-}\right) \\
\\
v_b = \sqrt{2}V_+ \sin\left(\omega t - \dfrac{2\pi}{3}\right) + \sqrt{2}V_- \sin\left(\omega t + \dfrac{2\pi}{3} + \phi_{v_-}\right)
\end{cases}
\tag{3.20}
$$

and currents as

$$
\begin{cases}
i_a = \sqrt{2}I_+ \sin\left(\omega t + \phi_{i_+}\right) + \sqrt{2}I_- \sin\left(\omega t + \phi_{i_-}\right) \\
\\
i_b = \sqrt{2}I_+ \sin\left(\omega t - \dfrac{2\pi}{3} + \phi_{i_+}\right) + \sqrt{2}I_- \sin\left(\omega t + \dfrac{2\pi}{3} + \phi_{i_-}\right)
\end{cases}
\tag{3.21}
$$

The ab–$\alpha\beta$ transformation (3.3) for these quantities yields

$$
\begin{cases}
v_\alpha = \sqrt{2}V_+ \sin\left(\omega t\right) + \sqrt{2}V_- \sin\left(\omega t + \phi_{v_-}\right) \\
v_\beta = -\sqrt{2}V_+ \cos\left(\omega t\right) + \sqrt{2}V_- \cos\left(\omega t + \phi_{v_-}\right)
\end{cases},
\tag{3.22}
$$

and

$$
\begin{cases}
i_\alpha = \sqrt{2}I_+ \sin\left(\omega t + \phi_{i_+}\right) + \sqrt{2}I_- \sin\left(\omega t + \phi_{i_-}\right) \\
i_\beta = -\sqrt{2}I_+ \cos\left(\omega t + \phi_{i_+}\right) + \sqrt{2}I_- \cos\left(\omega t + \phi_{i_-}\right)
\end{cases}.
\tag{3.23}
$$

It can be observed that positive- and negative-sequence components in two-phase $\alpha\beta$ quantities are equivalent to those which result from the Clarke transformation in three-phase systems. The two-phase instantaneous powers which result by substituting these $\alpha\beta$ quantities into (3.10) are

$$
\begin{cases}
\bar{p}_{2\phi} = 2V_+I_+ \cos\left(\phi_{i_+}\right) + 2V_-I_- \cos\left(\phi_{v_-} - \phi_{i_-}\right) \\
\tilde{p}_{2\phi} = -2V_+I_- \cos\left(2\omega t + \phi_{i_-}\right) - 2V_-I_+ \cos\left(2\omega t + \phi_{v_-} + \phi_{i_+}\right)
\end{cases}.
\tag{3.24}
$$

and

$$
\begin{cases}
\bar{q}_{2\phi} = -2V_+I_+ \sin\left(\phi_{i_+}\right) - 2V_-I_- \sin\left(\phi_{v_-} - \phi_{i_-}\right) \\
\tilde{q}_{2\phi} = -2V_+I_- \sin\left(2\omega t + \phi_{i_-}\right) + 2V_-I_+ \sin\left(2\omega t + \phi_{v_-} + \phi_{i_+}\right)
\end{cases}.
\tag{3.25}
$$

The interaction between voltages and currents in the same phase sequence produce average power parcels $\left(\bar{p}_{2\phi} \text{ and } \bar{q}_{2\phi}\right)$, whereas products of voltages and currents with different phase sequences result in oscillating power components $\left(\tilde{p}_{2\phi} \text{ and } \tilde{q}_{2\phi}\right)$. These results are similar to those shown by Akagi, Watanabe and Aredes (2007) for three-phase systems.

Two-phase voltages and currents with negative-sequence unbalances are illustrated in Fi-

gure 45 and Figure 46. The two-phase $\alpha\beta$ representations of these quantities are illustrated in Figure 47 and Figure 48. The instantaneous powers obtained for these conditions are shown in Figure 49, at which is possible to observe the oscillations with frequency 2ω due to the interactions between components of different phase sequences.

Figure 45 – Two-phase sinusoidal negative-sequence unbalanced voltages with $V_+ = 127$ V and $V_- = 10$ % of V_+.
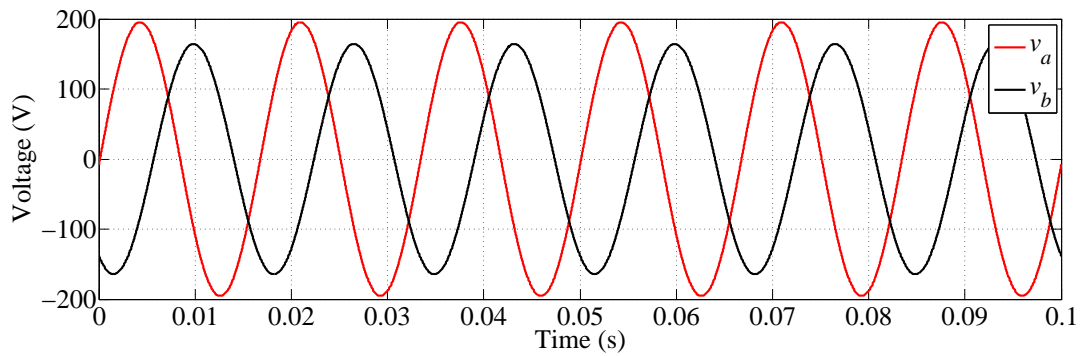
Source: Own authorship.

Figure 46 – Two-phase sinusoidal negative-sequence unbalanced currents with $I_+ = 35$ A and $I_- = 20$ % of I_+.
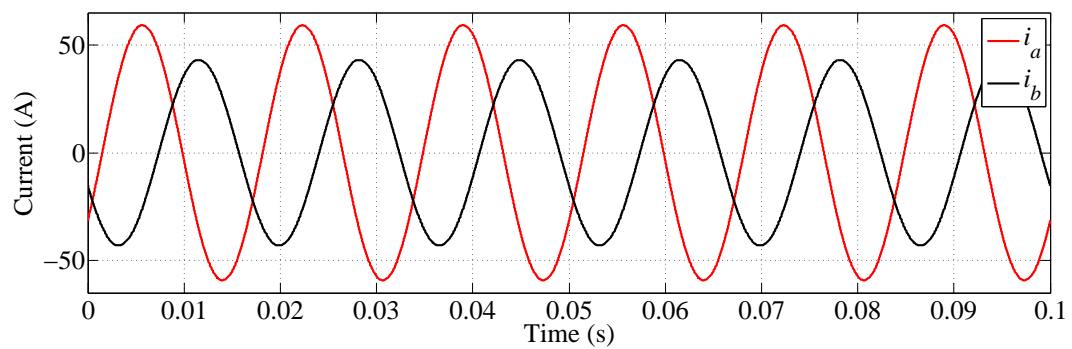
Source: Own authorship.

Figure 47 – Two-phase sinusoidal negative-sequence unbalanced voltages in the $\alpha\beta$ reference frame.
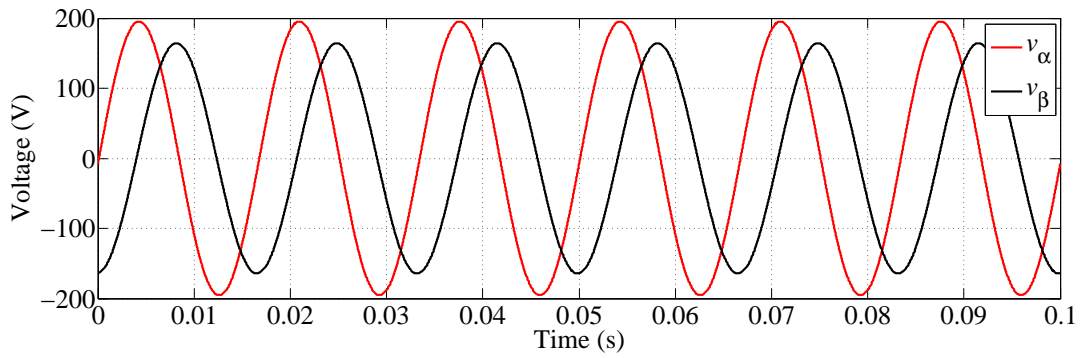
Source: Own authorship.

Figure 48 – Two-phase sinusoidal negative-sequence unbalanced currents in the $\alpha\beta$ reference frame.
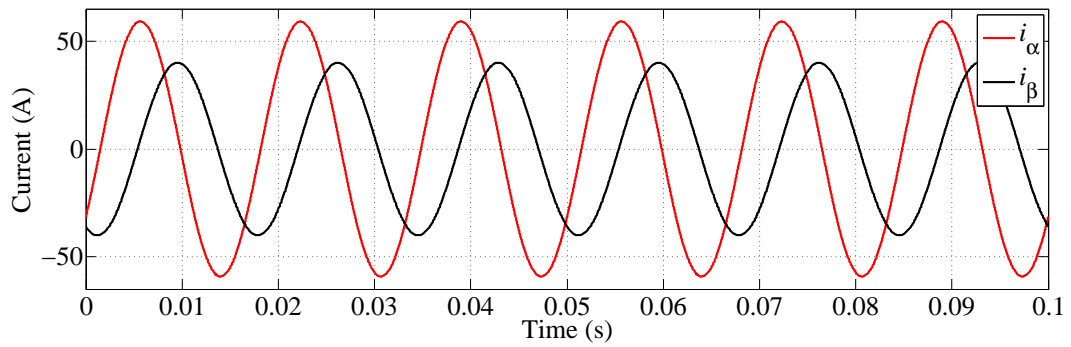
Source: Own authorship.

Figure 49 – Two-phase instantaneous powers under voltage and current sinusoidal negative-sequence unbalanced conditions.
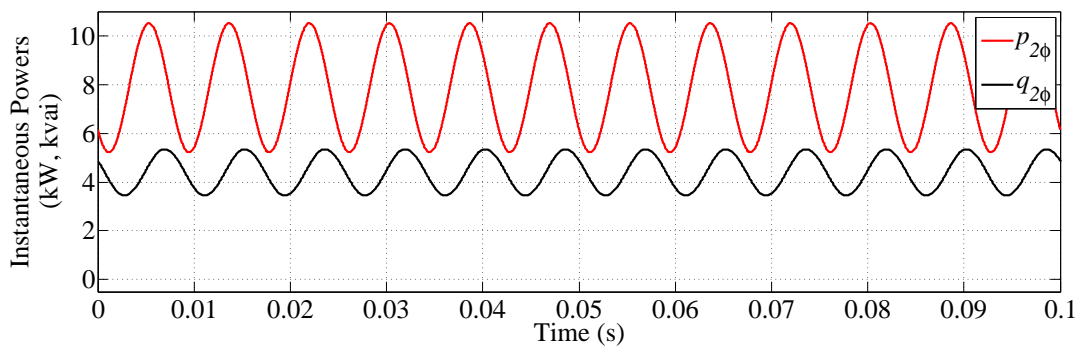
Source: Own authorship.

3.4.2.2 ZERO-SEQUENCE UNBALANCES

Two-phase voltages containing zero-sequence unbalance are expressed as

$$
\begin{cases}
v_a = & \sqrt{2}V_+ \sin(\omega t) + \sqrt{2}V_0 \sin(\omega t + \phi_{v_0}) \\
\\
v_b = & \sqrt{2}V_+ \sin\left(\omega t - \dfrac{2\pi}{3}\right) + \sqrt{2}V_0 \sin(\omega t + \phi_{v_0})
\end{cases}
\tag{3.26}
$$

and currents are written

$$
\begin{cases}
i_a = & \sqrt{2}I_+ \sin\left(\omega t + \phi_{i_+}\right) + \sqrt{2}I_0 \sin(\omega t + \phi_{i_0}) \\
\\
i_b = & \sqrt{2}I_+ \sin\left(\omega t - \dfrac{2\pi}{3} + \phi_{i_+}\right) + \sqrt{2}I_0 \sin(\omega t + \phi_{i_0})
\end{cases}
\tag{3.27}
$$

Applying the ab–$\alpha\beta$ transformation (3.3), the resulting voltages and currents are, respectively,

$$
\begin{cases}
v_\alpha = & \sqrt{2}V_+ \sin(\omega t) + \sqrt{2}V_0 \sin(\omega t + \phi_{v_0}) \\
v_\beta = & -\sqrt{2}V_+ \cos(\omega t) + \sqrt{6}V_0 \sin(\omega t + \phi_{v_0})
\end{cases}
\tag{3.28}
$$

and

$$
\begin{cases}
i_\alpha = & \sqrt{2}I_+ \sin\left(\omega t + \phi_{i_+}\right) + \sqrt{2}I_0 \sin(\omega t + \phi_{i_0}) \\
i_\beta = & -\sqrt{2}I_+ \cos\left(\omega t + \phi_{i_+}\right) + \sqrt{6}I_0 \sin(\omega t + \phi_{i_0})
\end{cases}
\tag{3.29}
$$

It can be noted that two-phase $\alpha\beta$ quantities contain a parcel of zero-sequence components. Unlike the Clarke transformation, the proposed ab–$\alpha\beta$ transformation (3.3) is not able to filter zero-sequence components.

Zero-sequence parcels observed in $\alpha\beta$ voltages and currents also contribute to the power flow process in $2\phi3w$ circuits. Indeed, the instantaneous powers that result by applying (3.28) and (3.29) into (3.10) are:

$$
\begin{cases}
\bar{p}_{2\phi} = & 2V_+I_+ \cos\left(\phi_{i_+}\right) + 2V_+I_0 \cos\left(\phi_{i_0} + \dfrac{\pi}{3}\right) + 2V_0I_+ \cos\left(-\phi_{i_+} + \phi_{v_0} + \dfrac{\pi}{3}\right) \\
& + 4V_0I_0 \cos\left(\phi_{v_0} - \phi_{i_0}\right) \\
\\
\tilde{p}_{2\phi} = & -2V_+I_0 \cos\left(2\omega t + \phi_{i_0} - \dfrac{\pi}{3}\right) - 2V_0I_+ \cos\left(2\omega t + \phi_{i_+} + \phi_{v_0} - \dfrac{\pi}{3}\right) \\
& - 4V_0I_0 \cos\left(2\omega t + \phi_{i_0} + \phi_{v_0}\right)
\end{cases}
\tag{3.30}
$$

and

$$\begin{cases} \bar{q}_{2\phi} = & -2V_+I_+\sin\left(\phi_{i_+}\right) - 2V_+I_0\sin\left(\phi_{i_0} + \frac{\pi}{3}\right) + 2V_0I_+\sin\left(\phi_{v_0} - \phi_{i_+} + \frac{\pi}{3}\right) \\[2ex] \tilde{q}_{2\phi} = & -2V_+I_0\sin\left(2\omega t + \phi_{i_0} - \frac{\pi}{3}\right) - 2V_0I_+\sin\left(2\omega t + \phi_{v_0} + \phi_{i_+} - \frac{4\pi}{3}\right) \end{cases} \quad . \quad (3.31)$$

The waveforms of two-phase voltages and currents containing zero-sequence unbalances are exemplified in Figure 50 and Figure 51, respectively. The representation of these quantities in the $\alpha\beta$ reference frame is also shown in Figure 52 and Figure 53. The two-phase instantaneous powers obtained under zero-sequence distortion conditions are shown in Figure 54. It is possible to observe in this example that $p_{2\phi}$ and $q_{2\phi}$ contain oscillations with frequency 2ω that result from the interaction between positive- and zero-sequence components.

Figure 50 – Two-phase sinusoidal zero-sequence unbalanced voltages with $V_+ = 127$ V and $V_0 = 5$ % of V_+.
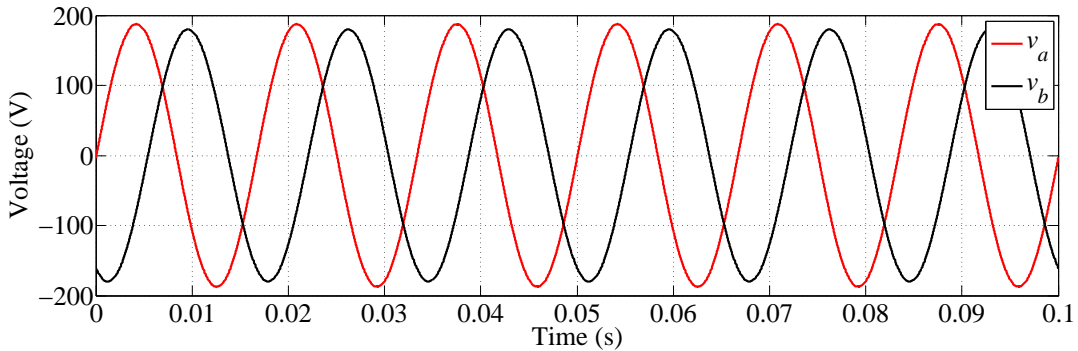
Source: Own authorship.

Figure 51 – Two-phase sinusoidal zero-sequence unbalanced currents with $I_+ = 35$ A and $I_0 = 10$ % of I_+.
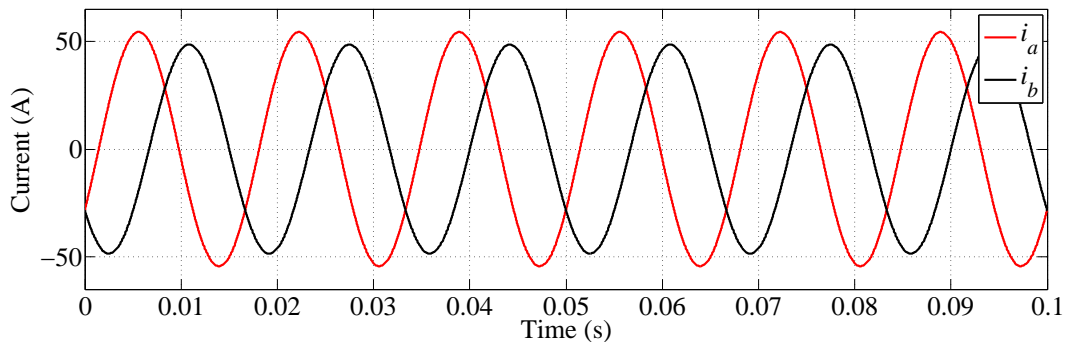
Source: Own authorship.

Figure 52 – Two-phase sinusoidal zero-sequence unbalanced voltages in the $\alpha\beta$ reference frame.
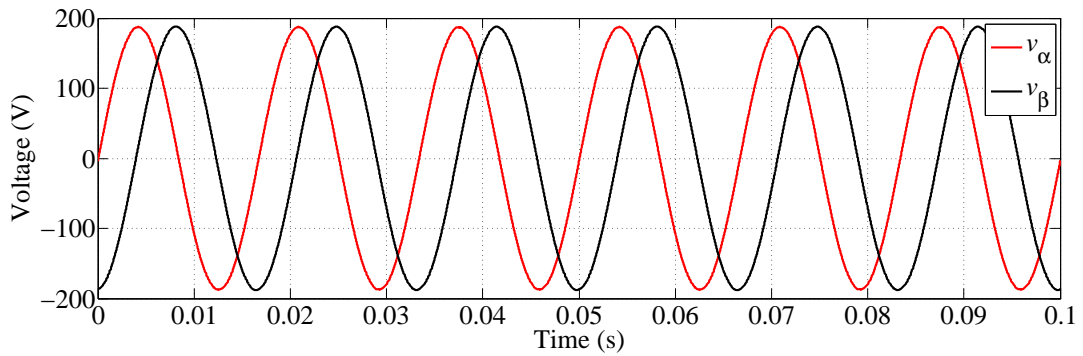
Source: Own authorship.

Figure 53 – Two-phase sinusoidal zero-sequence unbalanced currents in the $\alpha\beta$ reference frame.
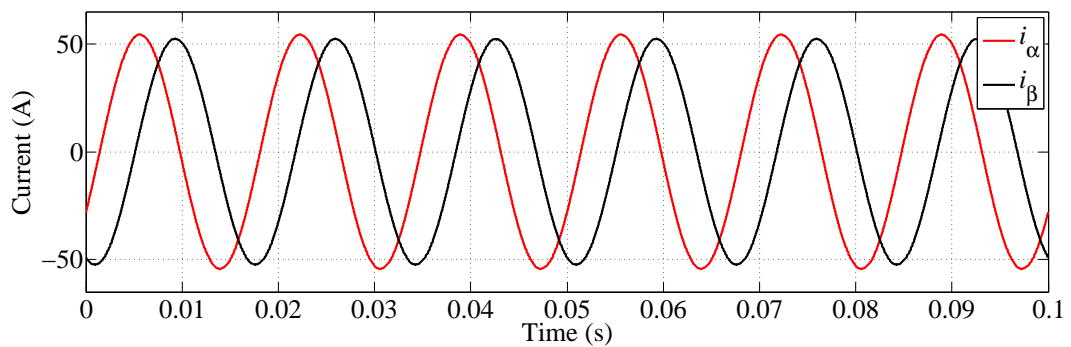
Source: Own authorship.

Figure 54 – Two-phase instantaneous powers under voltage and current sinusoidal zero-sequence unbalanced conditions.
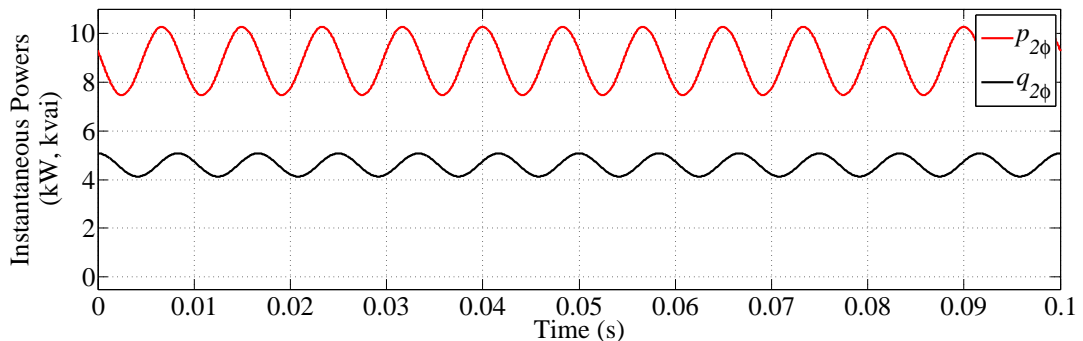
Source: Own authorship.

The expressions and waveforms presented in this section show that zero-sequence voltages and currents interact between themselves and with positive-sequence, producing average and

oscillating real power components. The products of quantities with different phase sequence also produce imaginary power components. It is also possible to show that a similar behaviour can be observed if zero-sequence quantities interact with negative-sequence voltages and currents. However, it can be seen in (3.31) there are no imaginary powers due to the interaction of zero-sequence voltages and currents. These characteristics are not observed in the *pq* Theory applied in three-phase systems (AKAGI; WATANABE & AREDES, 2007).

Power conditioning applications typically require the extraction of average powers related to the fundamental frequency positive-sequence voltages and currents. For this reason, the presence of average powers due to interactions between positive- and zero-sequence components is an undesirable characteristic in $2\phi3w$ instantaneous powers.

3.4.3 HARMONIC DISTORTED CONDITIONS

As previously discussed, the presence of nonlinear loads in power systems is related with undesired harmonic voltage and current distortions. Power conditioning equipment are commonly applied to suppress or reduce the effects of such distortions in power grids (SINGH; AL-HADDAD & CHANDRA, 1999; AKAGI, 2005). In this context, it is important to understand the behaviour of two-phase $\alpha\beta$ powers involving harmonic components.

The analysis regarding harmonics was divided into two parts in this work. The first part considers sinusoidal voltages, whereas currents present harmonic components. This is a common situation in real applications, as discussed in next chapter. The second part discusses the behaviour of $2\phi3w$ powers under the presence of both voltage and current harmonic components.

3.4.3.1 SINUSOIDAL VOLTAGES AND DISTORTED CURRENTS

This is the situation at which phase voltages are purely sinusoidal and displaced by $2\pi/3$ rad, whereas currents are composed by a fundamental-frequency component and an indefinite number of harmonics. These conditions are commonly faced in applications that use only fundamental-frequency positive-sequence voltages to calculate instantaneous powers, as discussed in Chapter 4.

In this case, phase voltages are mathematically expressed as

$$\begin{cases} v_a = & \sqrt{2}V\sin\left(\omega t\right) \\ v_b = & \sqrt{2}V\sin\left(\omega t - \dfrac{2\pi}{3}\right) \end{cases},$$ (3.32)

whereas distorted currents are generically written as

$$
\begin{cases}
i_a = \sum\limits_{h=1}^{\infty} \sqrt{2} I_h \sin \left(h\omega t + \phi_{i_h} \right) \\
i_b = \sum\limits_{h=1}^{\infty} \sqrt{2} I_h \sin \left(h\omega t - h\dfrac{2\pi}{3} + \phi_{i_h} \right)
\end{cases}
. \tag{3.33}
$$

Applying the transformation in (3.3), the resulting voltages and currents in $\alpha\beta$ reference frame are, respectively,

$$
\begin{cases}
v_\alpha = \sqrt{2} V \sin (\omega t) \\
v_\beta = -\sqrt{2} V \cos (\omega t)
\end{cases}
\tag{3.34}
$$

and

$$
\begin{cases}
i_\alpha = \sum\limits_{h=1}^{\infty} \sqrt{2}\, I_h \, \sin \left(h\omega t + \phi_{i_h} \right) \\
i_\beta = \sum\limits_{h=1}^{\infty} \sqrt{\dfrac{2}{3}}\, I_h \left[\sin \left(h\omega t + \phi_{i_h} \right) + 2 \sin \left(h\omega t + \phi_{i_h} - h\dfrac{2\pi}{3} \right) \right]
\end{cases}
. \tag{3.35}
$$

Applying these quantities to calculate two-phase instantaneous powers according to (3.10), are

$$
\begin{cases}
\bar{p}_{2\phi} = 2VI_1 \cos \left(\phi_{i_1} \right) \\
\tilde{p}_{2\phi} = -2VI_2 \cos \left(3\omega t + \phi_{i_2} \right) \\
\qquad + VI_3 \cos \left(2\omega t + \phi_{i_3} \right) - VI_3 \sqrt{3} \sin \left(2\omega t + \phi_{i_3} \right) \\
\qquad - VI_3 \cos \left(4\omega t + \phi_{i_3} \right) - VI_3 \sqrt{3} \sin \left(4\omega t + \phi_{i_3} \right) \\
\qquad + 2VI_4 \cos \left(3\omega t + \phi_{i_4} \right) \\
\qquad - 2VI_5 \cos \left(6\omega t + \phi_{i_5} \right) \\
\qquad + VI_6 \cos \left(5\omega t + \phi i_6 \right) - \sqrt{3} VI_6 \sin \left(5\omega t + \phi_{i_6} \right) \\
\qquad - VI_6 \cos \left(7\omega t + \phi_{i_6} \right) - \sqrt{3} VI_6 \sin \left(7\omega t + \phi_{i_6} \right) \\
\qquad + 2VI_7 \cos \left(6\omega t + \phi_{i_7} \right) \\
\qquad - 2VI_8 \cos \left(9\omega t + \phi_{i_8} \right) \\
\qquad + VI_9 \cos \left(8\omega t + \phi_{i_9} \right) - \sqrt{3} VI_9 \sin \left(8\omega t + \phi_{i_9} \right) \\
\qquad - VI_9 \cos \left(10\omega t + \phi_{i_9} \right) - \sqrt{3} VI_9 \sin \left(10\omega t + \phi_{i_9} \right) \\
\qquad \vdots
\end{cases}
\tag{3.36}
$$

and

$$
\left\{
\begin{aligned}
\bar{q}_{2\phi} =\ & -2VI_1\sin\left(\phi_{i_1}\right) \\
\tilde{q}_{2\phi} =\ & -2VI_2\sin\left(3\omega t+\phi_{i_2}\right) \\
& -\sqrt{3}VI_3\cos\left(2\omega t+\phi_{i_3}\right)-VI_3\sin\left(2\omega t+\phi_{i_3}\right) \\
& +\sqrt{3}VI_3\cos\left(4\omega t+\phi_{i_3}\right)-VI_3\sin\left(4\omega t+\phi_{i_3}\right) \\
& -2VI_4\sin\left(3\omega t+\phi_{i_4}\right) \\
& -2VI_5\sin\left(6\omega t+\phi_{i_5}\right) \\
& -\sqrt{3}VI_6\cos\left(5\omega t+\phi_{i_6}\right)-VI_6\sin\left(5\omega t+\phi_{i_6}\right) \\
& +\sqrt{3}VI_6\cos\left(7\omega t+\phi_{i_6}\right)-VI_6\sin\left(7\omega t+\phi_{i_6}+\phi_{v_1}\right) \\
& -2VI_7\sin\left(6\omega t+\phi_{i_7}\right) \\
& -2VI_8\sin\left(9\omega t+\phi_{i_8}\right) \\
& -\sqrt{3}VI_9\cos\left(8\omega t+\phi_{i_9}\right)-VI_9\sin\left(8\omega t+\phi_{i_9}\right) \\
& +\sqrt{3}VI_9\cos\left(10\omega t+\phi_{i_9}\right)-VI_9\sin\left(10\omega t+\phi_{i_9}\right) \\
& \vdots
\end{aligned}
\right.
\tag{3.37}
$$

As already shown in this work, the products of voltages and currents of the same harmonic order result in average power components $\bar{p}_{2\phi}\ \bar{q}_{2\phi}$. These expressions also show that the interaction between fundamental-frequency voltage with current harmonics produce oscillatory power components. This is an important property for power conditioning applications. It means that, if fundamental-frequency voltages are known, it is possible to isolate fundamental frequency currents in real time throughout the instantaneous power concepts.

The waveforms of sinusoidal voltages used to exemplify these conditions are shown in Figure 55. The two-phase *ab* currents with harmonic distortions are illustrated in the waveforms of Figure 56. The waveforms of these quantities, transformed into the $\alpha\beta$ reference frame, are illustrated in Figure 57 and Figure 58.

The $2\phi 3w$ instantaneous powers obtained in this example are shown in Figure 59, at which is possible to observe oscillations at a few harmonic frequencies. As shown in (3.36) and (3.37), these oscillations are originated in products of voltages and currents in different frequencies.

Figure 55 – Two-phase sinusoidal voltages with $V_1 = 127$ V.
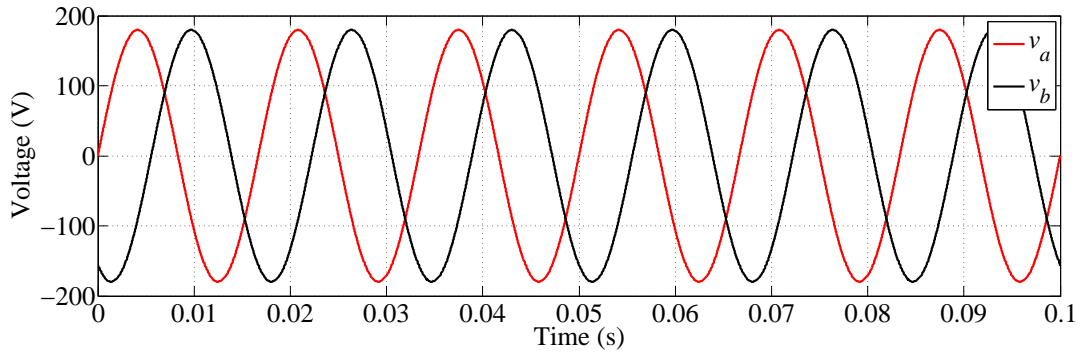
Figure 56 – Two-phase harmonic distorted currents with $I_1 = 35$ A, $I_3 = 10$ % and $I_5 = 5$ % of I_1.
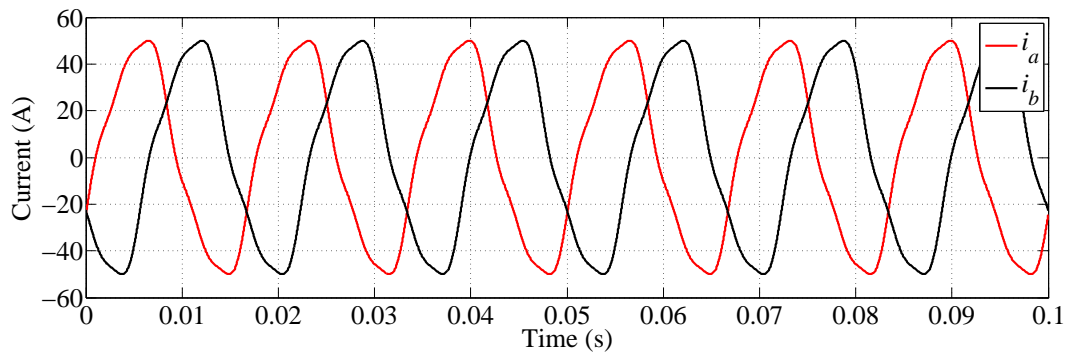
Figure 57 – Two-phase sinusoidal voltages in the $\alpha\beta$ reference frame.
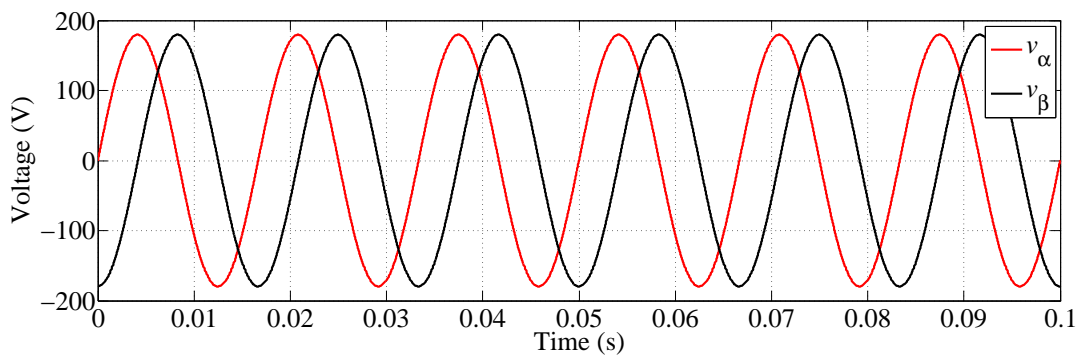
Figure 58 – Two-phase harmonic distorted currents in the $\alpha\beta$ reference frame.
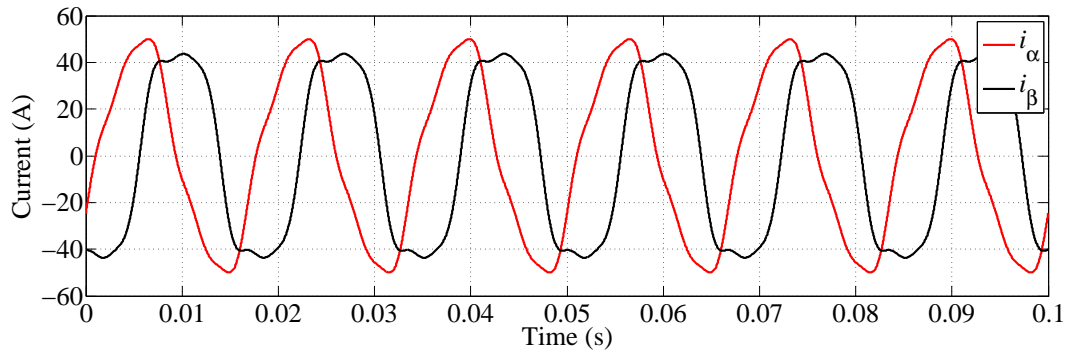
Source: Own authorship.

Figure 59 – Two-phase instantaneous powers under sinusoidal balanced voltages and harmonic distorted current conditions.
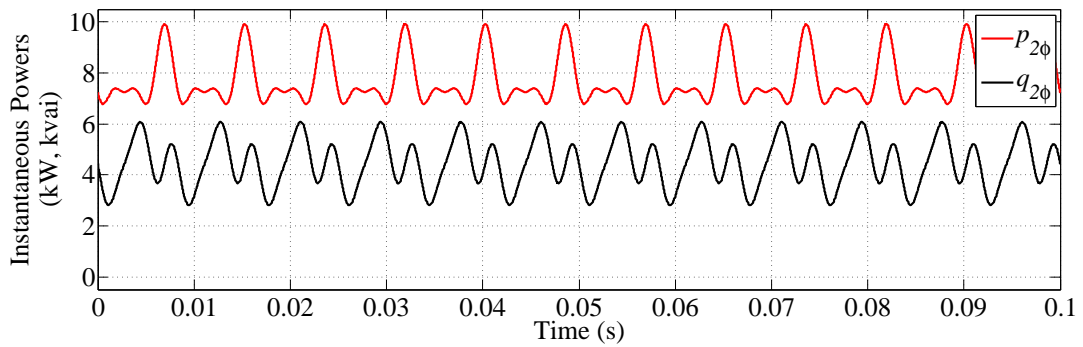
Source: Own authorship.

3.4.3.2 *DISTORTED VOLTAGES AND CURRENTS*

This is the most general case comprising harmonics, which considers both voltages and currents distortions.

In this case, *ab* quantities can be generically expressed as

$$
\begin{cases}
v_a = \displaystyle\sum_{h=1}^{\infty} \sqrt{2}V_h \sin\left(h\omega t + \phi_{v_h}\right) \\
v_b = \displaystyle\sum_{h=1}^{\infty} \sqrt{2}V_h \sin\left(h\omega t - h\dfrac{2\pi}{3} + \phi_{v_h}\right)
\end{cases}
\tag{3.38}
$$

and

$$
\begin{cases}
i_a = \displaystyle\sum_{h=1}^{\infty} \sqrt{2}I_h \sin\left(h\omega t + \phi_{i_h}\right) \\
i_b = \displaystyle\sum_{h=1}^{\infty} \sqrt{2}I_h \sin\left(h\omega t - h\dfrac{2\pi}{3} + \phi_{i_h}\right)
\end{cases}
\; .
\tag{3.39}
$$

These quantities are expressed in $\alpha\beta$ reference frame as

$$
\begin{cases}
v_\alpha = \sum_{h=1}^{\infty} \sqrt{2}\, V_h \,\sin\left(h\omega t + \phi_{v_h}\right) \\[2em]
v_\beta = \sum_{h=1}^{\infty} \sqrt{\frac{2}{3}}\, V_h \left[\sin\left(h\omega t + \phi_{v_h}\right) + 2\sin\left(h\omega t + \phi_{v_h} - h\frac{2\pi}{3}\right)\right]
\end{cases}
\tag{3.40}
$$

and

$$
\begin{cases}
i_\alpha = \sum_{h=1}^{\infty} \sqrt{2}\, I_h \,\sin\left(h\omega t + \phi_{i_h}\right) \\[2em]
i_\beta = \sum_{h=1}^{\infty} \sqrt{\frac{2}{3}}\, I_h \left[\sin\left(h\omega t + \phi_{i_h}\right) + 2\sin\left(h\omega t + \phi_{i_h} - h\frac{2\pi}{3}\right)\right]
\end{cases}
\tag{3.41}
$$

The application of (3.10) to calculate $2\phi 3w$ instantaneous powers result in expressions that are not possible to come out any conclusion due their complexity. For this reason, and aiming to ease the document reading, the resulting expressions for $p_{2\phi}$ and $q_{2\phi}$ are presented in Appendix B.

For $h = 1$, the results equal those shown in the previous section. For most frequencies, interactions between voltages and currents in the same frequency produce constant power components. Interactions between harmonics of different orders result in oscillating power components. On the other hand, two-phase instantaneous powers differ from Akagi, Watanabe and Aredes (2007) three-phase powers regarding triplen harmonics, which present zero-sequence characteristics. It can be seen in Appendix B that the products of triplen harmonics produce $\bar{p}_{2\phi}$ and/or $\tilde{p}_{2\phi}$, but do not produce $q_{2\phi}$.

These conditions are exemplified in the $2\phi 3w$ voltages and currents of Figure 60 and Figure 61, respectively. The $\alpha\beta$ representation of these quantities, according to (3.3) are shown in Figure 62 and Figure 63. The two-phase instantaneous powers $p_{2\phi}$ and $q_{2\phi}$ are shown in Figure 64. Compared to the situation discussed in the previous section, the two-phase powers in Figure 64 present higher oscillations due to the introduction of voltage harmonics.

Figure 60 – Two-phase harmonic distorted voltages with $V_1 = 127$ V and $V_3 = 5$ % of V_1.
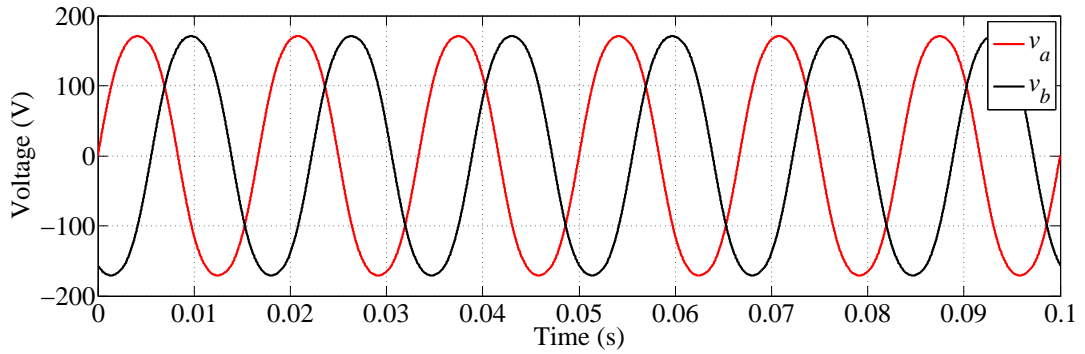
Source: Own authorship.

Figure 61 – Two-phase harmonic distorted currents with $I_1 = 35$ A, $I_3 = 10$ % and $I_5 = 5$ % of I_1.
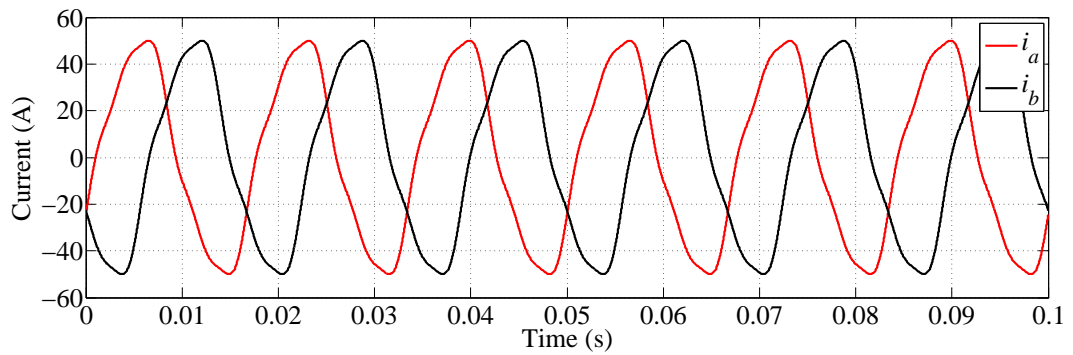
Source: Own authorship.

Figure 62 – Two-phase harmonic-distorted voltages in the $\alpha\beta$ reference frame.
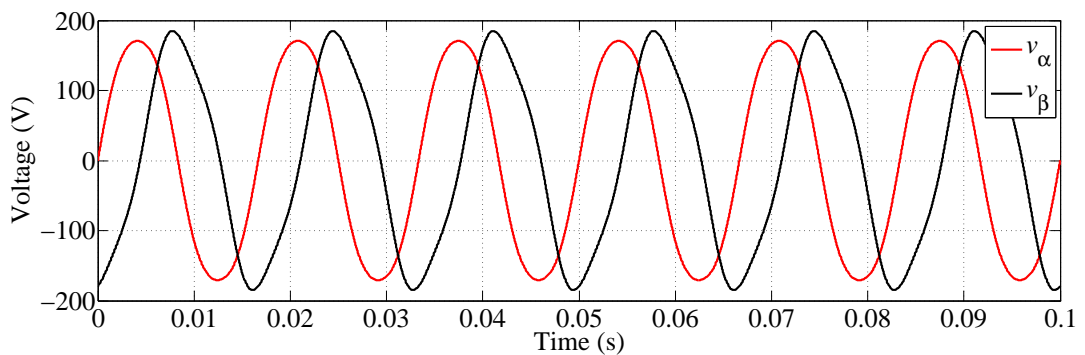
Source: Own authorship.

Figure 63 – Two-phase harmonic distorted currents in the $\alpha\beta$ reference frame.
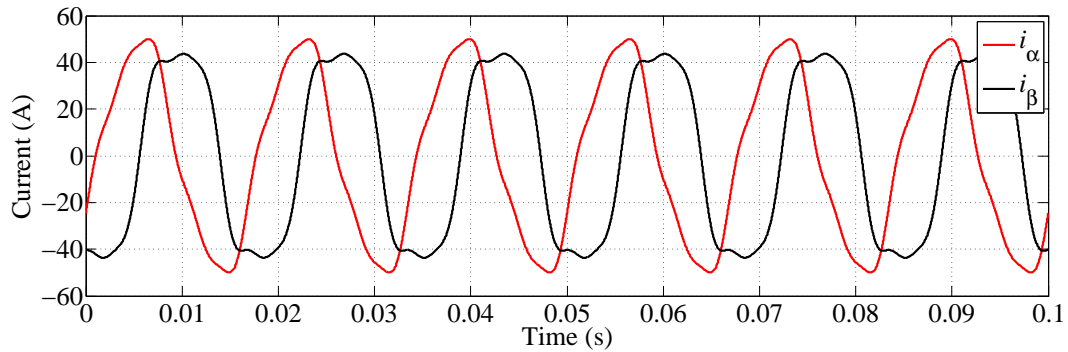
Source: Own authorship.

Figure 64 – Two-phase instantaneous powers under sinusoidal balanced voltages and harmonic distorted current conditions.
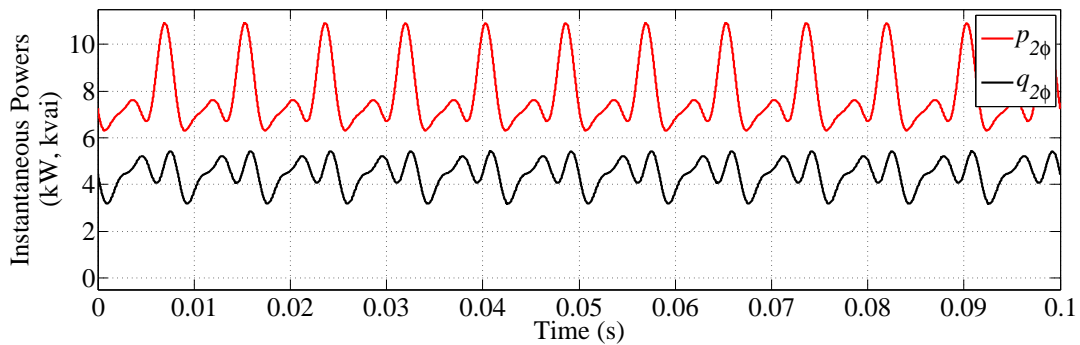
Source: Own authorship.

3.4.4   UNBALANCED AND HARMONIC DISTORTED CONDITIONS

The calculation and analysis of $2\phi3w$ powers involving simultaneously harmonics and un-balances in both voltages and currents is the most general situation to be considered in the context of this work.

The resulting two-phase powers for these conditions are the superposition of the characte-ristics observed in Section 3.4.1, Section 3.4.2, and Section 3.4.3. The complete expressions of $p_{2\phi}$ and $q_{2\phi}$ lead to conclusions which have already been discussed. It can be shown in-teractions between voltages and currents with the same frequency and phase sequence produce constant power components $\bar{p}_{2\phi}$ and $\bar{q}_{2\phi}$. On the other hand, interactions between voltages and currents in different frequencies and/or phase sequence produce oscillatory power components $\tilde{p}_{2\phi}$ and $\tilde{q}_{2\phi}$. The interaction between zero-sequence voltages and currents, including triplen harmonics, produce both constant and oscillating power components.

4 ACTIVE FILTER CONTROL BASED ON TWO-PHASE INSTANTANEOUS POWERS

The concepts of two-phase instantaneous powers in Chapter 3 were conceived as useful tools for the development of control algorithms for PC equipment in $2\phi3w$ circuits as, for instance, for shunt APFs. The synthesis of the currents produced by the active filter aim at performing an specified function, such as harmonic filtering, reactive power compensation, active power injection or combinations of these functions.

Therefore, this chapter describes control algorithms elaborated in this research during the development of this thesis. In this context, the system topology at which such control algorithms apply are generically described in Section 4.1. As the control algorithms presented here need the information of fundamental-frequency positive-sequence voltage, a two-phase positive-sequence detection system is discussed in Section 4.2. Reference current calculation algorithms are separated in two different strategies: Double Single-Phase Strategy (DSPS) and Zero Neutral Current Strategy (ZNCS), as deeply discussed in Section 4.3 and Section 4.4, respectively. The current control system was also modelled using the $2\phi3w$ $\alpha\beta$ proposed in this work. A Model Predictive Controller (MPC) was chosen to implement the $2\phi3w$ APF in this work. This controller is described in detail in Section 4.5. An overview of a $2\phi3w$ control system is presented at the end of this chapter.

4.1 SYSTEM TOPOLOGY

A generic $2\phi3w$ system topology is illustrated in Figure 65. The power source is represented by a three-phase four-wire voltage source with solidly grounded neutral. Furthermore, as expected, three conductors (two phase circuits with neutral return) were used for connecting the loads to the power grid. Phases a and b are adopted for convenience in this work, but any pair of phases can be used. Electrical characteristics of the feeders are represented by the inductances L_s and resistances r_s. It is considered that phase and neutral cables have the same cross-sectional area and physical characteristics (ABNT, 2008).

The two-phase loads were represented by linear and non-linear circuits, with reactive cha-

racteristics or not, equally distributed between phases or not. It is worth remembering that the situation at which loads are equally distributed between phases *a* and *b* is regarded as balanced considering the $2\phi3w$ context, which is not necessarily true considering a three-phase point of view. Load circuits can also be connected phase-to-neutral or phase-to-phase.

Figure 65 – $2\phi3w$ System topology with shunt APF compensation.
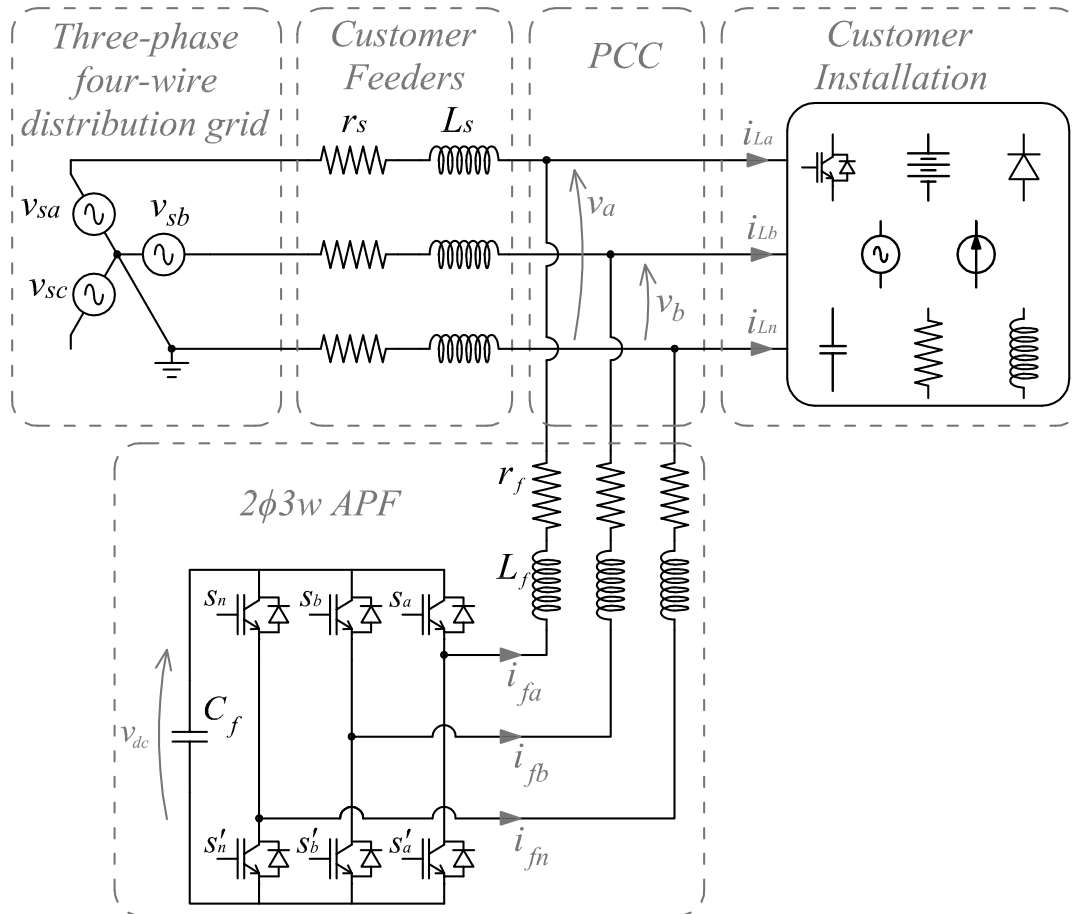
Source: Own authorship.

The power conditioner is basically formed of a DC-link composed of the capacitance C_f, a three-phase VSC and output filters represented by inductances L_f and parasitic resistances r_f. A power source, such as batteries and PV arrays, can also be connected to the DC-link in active power injection applications. The PCC is the node, defined between the power grid and the load, at which the shunt power conditioner is connected.

The measurement of all quantities used in control algorithms is shown in Figure 65. Namely, the instantaneous values of phase voltages at the PCC (v_a, v_b), load line currents (i_{L_a}, i_{L_b}), power conditioner output currents $(i_{f_a}, i_{f_b}, i_{f_n})$ and the DC-link voltage (v_{dc}).

As previously mentioned, the algorithms described in this work aim to calculate the refe-

rence currents which must be synthesized by the shunt power conditioner.

4.2 TWO-PHASE FUNDAMENTAL-FREQUENCY POSITIVE-SEQUENCE DETECTOR

Power conditioning applications typically require synchronization so that power converters can properly operate connected to the grid. Control algorithms based on instantaneous powers commonly need the identification of power components produced by fundamental-frequency positive-sequence quantities, which is important for grid synchronization. It is the case of the sinusoidal source current compensation strategy described by Akagi, Watanabe and Aredes (2007). As discussed by Khadkikar, Chandra and Singh (2009), the application of single-phase *pq* Theory also requires the extraction of fundamental-frequency positive-sequence voltages.

The control algorithms proposed in this work are also sinusoidal source current compensation strategies, which are described in following sections. Therefore, it is necessary the extraction of fundamental-frequency positive-sequence components from $2\phi 3w$ voltages. It is important to keep in mind that symmetrical components referred in this work are those defined for three-phase systems, from which two-phase circuits derive.

There are works with wide literature reviews regarding grid synchronization methods for both single- and three-phase systems (JAALAM et al., 2016; GOLESTAN; GUERRERO & VASQUEZ, 2017; GOLESTAN; GUERRERO & VASQUEZ, 2017b). An interesting method is the Dual Second-Order Generalized Integrator (DSOGI)-PLL (DSOGI-PLL) developed by Rodriguez et al. (2006). This synchronization method proved to be a highly effective tool and has been successfully applied in different contexts (ALMEIDA, 2011; FOGLI, 2014). Even though the DSOGI-PLL was initially developed for three-phase systems, it calculates the positive-sequence component of signals in the $\alpha\beta$ reference frame. This feature represents an opportunity for $2\phi 3w$ applications, considering the two-phase $\alpha\beta$ transformation (3.3) proposed in this work.

In this context, this section describes how the structure of the DSOGI-PLL (RODRIGUEZ et al., 2006) can be adapted for fundamental-frequency positive-sequence detection in $2\phi 3w$ circuits. This adaptation is useful for control algorithms described in next sections of this work.

The positive-sequence detector developed by Rodriguez et al. (2006) is represented in the block diagram of Figure 66. The values ω_r and k are the resonance frequency and the damping factor of the SOGI (RODRIGUEZ et al., 2007). The DSOGI uses the Clarke transformation to take *abc* voltages into the $\alpha\beta$ reference frame. This operation eliminates zero-sequence voltage components, including all triplen harmonics. In sequence, a DSOGI structure receives $\alpha\beta$ voltages and behaves as an harmonic filter and Quadrature Signal Generator (QSG). The

quadrature generation is represented by the operator $q = e^{-j}$. This structure is also referred by Rodriguez et al. (2006) as DSOGI-QSG. Finally, the DSOGI-QSG outputs are used to calculate the $\alpha\beta$ positive-sequence voltages. This part of the algorithm is referred as Positive-Sequence Calculation (PSC) (RODRIGUEZ et al., 2006). The outputs of the DSOGI-PLL are the fundamental-frequency positive-sequence voltages contained in the inputs.

Figure 66 – Three-phase positive-sequence detector DSOGI-PLL.
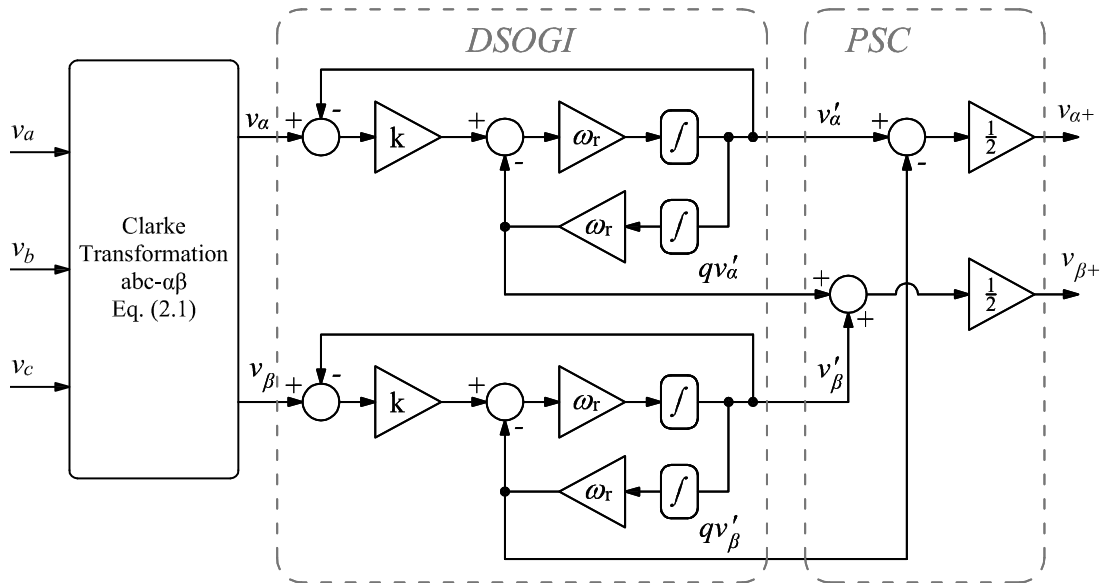
Source: Own authorship.

The proposed $2\phi3w$ adaptation of the DSOGI-PLL is represented in the block diagram of Figure 67. In this case, the Clarke transformation is substituted by the $ab\text{-}\alpha\beta$ transformation described in (3.3).

Figure 67 – Two-phase positive-sequence detector DSOGI-PLL.
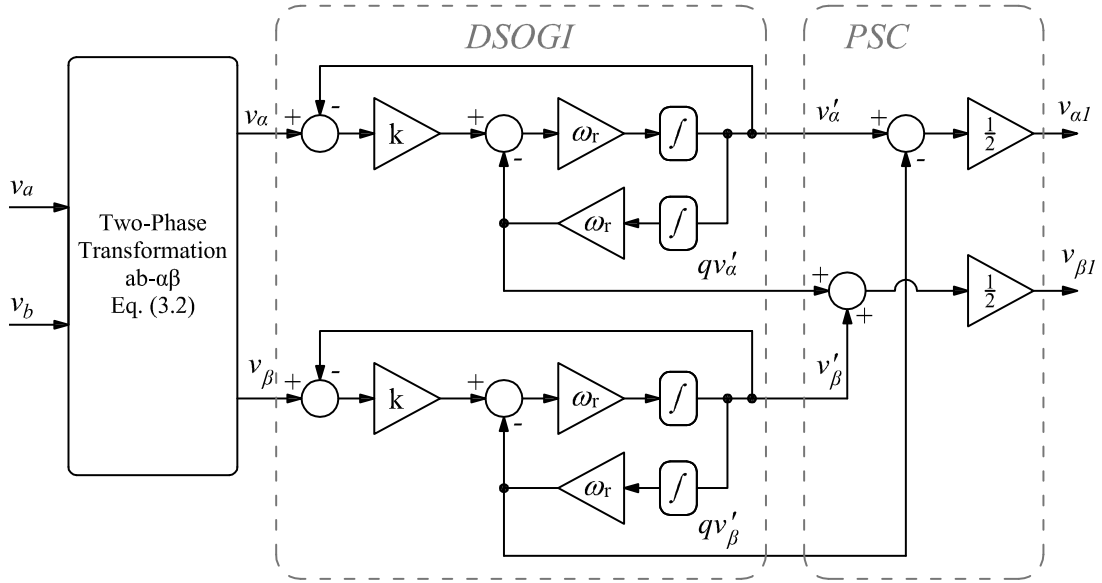
Source: Own authorship.

As previously discussed in Chapter 3, the *ab-αβ* transformation does not eliminate zero-sequence quantities due to the characteristics of the grid voltages in this circuit. Actually, zero-sequence voltages at the input are transmitted into the output $\alpha\beta$ components. This is an undesired characteristic since the objective is isolating the positive-sequence component. Also, it can be observed in a simplified analysis, considering an ideal DSOGI-QSG. In this case, "ideal" refers to the capability of harmonic filtering. Applying in the input a set of two-phase generic unbalanced of voltages expressed as

$$\begin{cases} v_a = \sqrt{2}V_+ \sin(\omega t) + \sqrt{2}V_- \sin(\omega t + \phi_{v_-}) + \sqrt{2}V_0 \sin(\omega t + \phi_{v_0}) \\ \\ v_b = \sqrt{2}V_+ \sin\left(\omega t - \frac{2\pi}{3}\right) + \sqrt{2}V_- \sin\left(\omega t + \frac{2\pi}{3} + \phi_{v_-}\right) + \sqrt{2}V_0 \sin(\omega t + \phi_{v_0}) \end{cases}, \quad (4.1)$$

then these components are transmitted to the DSOGI-QSG output, in the $\alpha\beta$ reference frame as

$$\begin{cases} v_{\alpha_1} = \sqrt{2}V_+ \sin(\omega t) + \sqrt{2}V_0 \sin\left(\omega t + \phi_{v_0} + \frac{\pi}{3}\right) \\ \\ v_{\beta_1} = -\sqrt{2}V_+ \cos(\omega t) + \sqrt{2}V_0 \sin\left(\omega t + \phi_{v_0} - \frac{\pi}{6}\right) \end{cases}. \quad (4.2)$$

The results in (4.2) show that positive-sequence components are correctly extracted from the input of the adapted DSOGI-QSG exactly as expected. Furthermore, there are no negative-sequence components, also as expected. On the other hand, there are zero-sequence-related parcels in the $\alpha\beta$ output signals. The presence of zero-sequence components represent an er-

ror in relation to the desired output, which should contain only positive-sequence. It must be mentioned at this point that the subscript "+" is used to represent the positive-sequence component of voltages, whereas the subscript "1" was chosen to express the output of the two-phase DSOGI-PLL. These labels were adopted due to the presence of zero-sequence components at the adapted DSOGI-PLL outputs.

The proposed two-phase DSOGI-PLL was implemented in a Digital Signal Controller (DSC) and tested in laboratory. Some experimental results were obtained and are presented in Section 5.1.1, as well as the description of the system used for these tests. Preliminary results showed to be satisfactory under real conditions, despite the error caused by zero-sequence components. Indeed, zero-sequence unbalances are commonly neglected in the distribution procedures regulated by the Brazilian National Electricity Agency (In portuguese, Agência Nacional de Energia Elétrica – ANEEL) (ANEEL, 2007). It can be interesting to conduct future studies in this subject to measure the error in neglecting zero-sequence voltage components. The performance of the two-phase DSOGI-PLL under different real voltage conditions could also be evaluated in other $2\phi3w$ consumer installations.

As previously stated, the voltages obtained with the adapted $2\phi3w$ DSOGI-PLL are used by the current reference algorithms proposed in this work, namely the DSPS and ZNCS. These algorithms are discussed in detail in the following sections.

4.3 DOUBLE SINGLE-PHASE STRATEGY

The Double Single-Phase Strategy (DSPS) was the first compensation strategy conceived on this research. It was initially implemented using the single-phase *pq* Theory. Two-phase systems were treated as two superposed single-phase circuits and this is the reason the strategy was named DSPS (FURTADO et al., 2013; FURTADO et al., 2014; FURTADO, 2014b). Afterwards, this strategy was also implemented using $2\phi3w$ instantaneous powers for shunt APF control (FURTADO; RODRIGUES & BARBOSA, 2015d). This compensation strategy is analogous to the *"sinusoidal source current control strategy"* described by Akagi, Watanabe and Aredes (2007).

Therefore, it is expected that the compensated grid currents (i_{sa}, i_{sb}) become with low-harmonic distortion and in phase with phase voltages v_a and v_b, respectively. Also, the amplitude of compensated (source) currents become equalized, even though the load is unbalanced between phases *a* and *b* (FURTADO; RODRIGUES & BARBOSA, 2015d).

Initially, the two-phase DSOGI-PLL is used to extract fundamental-frequency positive-sequence of measured PCC phase voltages v_a and v_b. This operation results in the signals

$v_{\alpha 1}$ and $v_{\beta 1}$ shown in Figure 67 and described in (4.2). The measured load currents i_{La} and i_{Lb} are also transformed into the $\alpha\beta$ reference frame according to (3.3). From this point on, the algorithm is similar to those described by (AKAGI; WATANABE & AREDES, 2007). Voltages and currents in the $\alpha\beta$ reference frame are used to calculate $2\phi 3w$ powers according to (3.10). Low-pass filters are employed to separate oscillating and average power components.

The following step is the determination of compensation powers that must be supplied by the shunt APF. In DSPS, it must provide the oscillating real power $\tilde{p}_{2\phi}$ and the total imaginary power $q_{2\phi}$ demanded by the load. The only load-demanded power component to be supplied by the source is the average real power $\bar{p}_{2\phi}$. A real power parcel p_{dc} must be absorbed to compensate APF losses and regulate the DC-bus voltage v_{dc}. This subject was already treated in this research and reported in detail by Furtado (2014b). In these terms, compensation powers $p_{2\phi}^*$ $q_{2\phi}^*$ to be provided by the shunt APF are expressed as

$$\begin{cases} p_{2\phi}^* = & \tilde{p}_{2\phi} - p_{dc} \\ q_{2\phi}^* = & \bar{q}_{2\phi} + \tilde{q}_{2\phi} \end{cases}.$$

(4.3)

From these compensation powers, the corresponding currents can be obtained according to (3.12):

$$\begin{bmatrix} i_{f\alpha}^* \\ i_{f\beta}^* \end{bmatrix} = \frac{2}{v_\alpha^2 + v_\beta^2} \begin{bmatrix} v_\alpha & v_\beta \\ v_\beta & -v_\alpha \end{bmatrix} \begin{bmatrix} p_{2\phi}^* \\ q_{2\phi}^* \end{bmatrix},$$

(4.4)

where i_α^* and i_β^* are the reference compensation powers in $\alpha\beta$ coordinates. These currents are taken into the *ab* reference frame by applying (3.4):

$$\begin{bmatrix} i_{fa}^* \\ i_{fb}^* \end{bmatrix} = \frac{1}{2} \begin{bmatrix} 2 & 0 \\ -1 & \sqrt{3} \end{bmatrix} \begin{bmatrix} i_{f\alpha}^* \\ i_{f\beta}^* \end{bmatrix}.$$

(4.5)

The third (neutral) reference compensation current can be calculated by the Kirchhoff's law as:

$$i_{fn}^* = -\left(i_{fa}^* + i_{fb}^* \right).$$

(4.6)

The reference compensation currents i_{fa}^*, i_{fb}^* and i_{fn}^* are those which must be synthesized by the $2\phi 3w$ shunt APF at the PCC. These signals are taken into a current control loop, which is discussed in Section 4.5.

Simulation results showing the control of a shunt APF using DSPS are presented and discussed in Chapter 5.

The shunt compensation applying DSPS results in a sinusoidal neutral current

$$i_{sn} = - (i_{sa} + i_{sb}) \tag{4.7}$$

which must be supplied by the power source. The flow of neutral currents in three-phase four-wire distribution systems is related to issues such as the overloading/overheating of neutral conductors and transformers, asymmetric voltage drops, voltage fluctuations and others (BALDA et al., 1997; SREENIVASARAO; AGARWAL & DAS, 2012; ALAM; MUTTAQI & SUTANTO, 2013). Aiming to avoid such problems, the mitigation of neutral currents is a subject of interest in works regarding active power filtering (AKAGI; WATANABE & AREDES, 2007; ALAM; MUTTAQI & SUTANTO, 2013; YUEH et al., 2016; GUPTA; JAIN & DAHIYA, 2014; JAVAID et al., 2016). In this context, another control strategy was developed in this research aiming to mitigate neutral currents caused by $2\phi3w$ loads, in addition to filter current harmonics and compensate reactive power.

4.4 ZERO NEUTRAL CURRENT STRATEGY

The Zero Neutral Current Strategy (ZNCS) was also initially developed using the single-phase pq Theory (FURTADO; RODRIGUES & BARBOSA, 2015d). Afterwards, the strategy was also implemented using the concepts of two-phase instantaneous powers, which is the method described in this section.

In ZNCS, the shunt APF provides the neutral current demanded by the load so that it does not flow from the power source (*i.e.*, the distribution grid). The ZNCS-operated APF also provides the reactive and harmonic power required by the load. The compensated $2\phi3w$ load seen by the grid (*i.e.*, the set Load + APF) behaves as a two-terminal circuit, connected phase-to-phase and drains a sinusoidal current $i_{sa} = -i_{sb}$ in phase with the line voltage v_{ab}. This power conditioning strategy can also be understood as a continuous process at which the APF drains power from the source as a phase-to-phase sinusoidal-current load and, at the same time, provides the total power as demanded by the load.

Initially, measured *ab* quantities are transformed into the $\alpha\beta$ reference frame according to (3.3). Then, the load two-phase real power is calculated according to (3.10) and a low-pass filter is used to separate the average value $\bar{p}_{2\phi}$. The line voltage v_{ab} is calculated and a SOGI structure is employed to eliminate voltage harmonics and to create a quadrature copy of the signal, as shown in Figure 68.

Figure 68 – SOGI used to implement ZNCS.
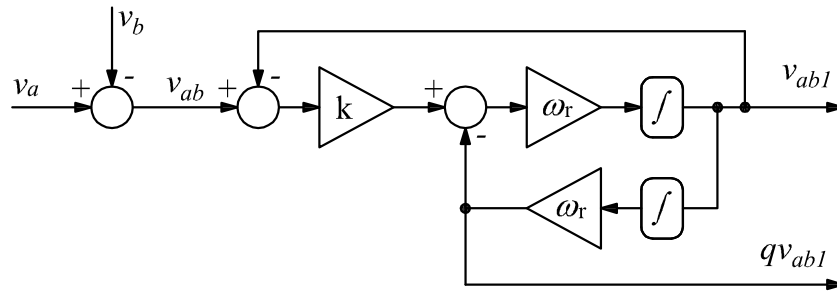
Source: Own authorship.

The APF power input (drawn from the grid) corresponds to two parcels: the average real power $\bar{p}_{2\phi}$ demanded by the load and the power parcel p_{dc} used to regulate the DC-bus voltage, which is generated by an outer control loop. These powers must be drained from the source through a current flowing between phases a and b and in phase with the line voltage v_{ab}. It can be be calculated as

$$i^*_{fab} = \frac{1}{v^2_{ab1} + qv^2_{ab1}} \left(\bar{p}_{2\phi} + p_{dc} \right) v_{ab1} \ . \tag{4.8}$$

The APF power output (provided to the load) is the total power demanded by the load, including reactive and harmonic power. In other words, the APF must provide all the currents demanded by the load. Therefore, the reference compensation currents are expressed as:

$$\begin{cases} i^*_{fa} & = i_{La} - i^*_{fab} \\ i^*_{fb} & = i_{Lb} + i^*_{fab} \\ i^*_{fn} & = - \left(i_{La} + i_{Lb} \right) \end{cases} , \tag{4.9}$$

which are the currents to be synthesized by the shunt APF at the PCC.

As previously described, DSPS and ZNCS algorithms generate compensation currents that must be synthesized by the APF. These reference signals are sent to an inner current control loop, which is responsible for generating driving signals of VSC semiconductor switches so that the reference currents are tracked. The current control loop adopted in this work is described in the next section.

A comparison study regarding DSPS and ZNCS was published by Furtado et al. (2015c). The referred work already showed that both compensation strategies proved to be effective in harmonics filtering, reactive power compensation and load balancing between phases a and b. When ZNCS is applied to two-phase shunt APF control, the power source must provide a higher phase current if compared with DSPS compensation. That is, ZNCS demands higher source currents to transport the same power, which increases conduction losses. On the other

hand, Furtado et al. (2015c) showed that neutral current has nearly the same amplitude of phase currents when the active filter is controlled by the DSPS strategy. Neutral currents contribute to loading neutral conductors and is related to power losses and other issues previously mentioned. Future works regarding this subject can compare DSPS and ZNCS from the two-phase shunt APF point of view. Compensation current levels, the total power processed and dc-link voltage oscillation can be parameters for these studies.

4.5   ADAPTED MODEL PREDICTIVE CONTROLLER FOR CURRENT CONTROL IN $2\phi3W$ GRID-CONNECTED CONVERTERS

It is possible to find in technical literature a wide variety of techniques for current control in shunt APF and other grid-connected converters. As examples of linear controllers, there are Proportional-Integral (PI) controllers in synchronous reference frame (PI-SRF), with multiple rotating integrators (PI-MRI) and with resonant integrators in stationary reference frame (PI-RES). Non-linear techniques are also described for current control, including hysteresis controllers (LAM; WONG & HAN, 2012), Sliding-Mode Controllers (SMCs) (FOGLI et al., 2015), MPCs (RODRIGUEZ et al., 2007; RODRIGUEZ & CORTES, 2012) and controllers based on artificial intelligence (QASIM & KHADKIKAR, 2014).

As discussed by Rodriguez et al. (2007), Rodriguez and Cortes (2012), MPCs present advantages due to the following features: it is based in simple and intuitive concepts, simple digital implementation, making no restrictions to the behaviour of reference signals and dealing naturally with the nonlinear nature of power converters. Due to these characteristics, the MPC showed to be an interesting option for current control in applications of $2\phi3w$ APFs. Therefore, a MPC was chosen in this work to control the output currents of $2\phi3w$ shunt APF.

In general terms, MPCs employ a mathematical model of the system to predict future values of controlled variables for a finite number of possible output states the power converter may assume. These predictions are used to evaluate a predefined cost function for each possible VSC output state. Then the VSC output state to be applied is the one which minimizes the cost function at each sampling period (RODRIGUEZ et al., 2007; RODRIGUEZ & CORTES, 2012). The MPC used in this work also includes dead-time compensation and fixed switching frequency features, which are important characteristics for experimental validation.

In a previous work published during this research (FURTADO et al., 2015a), a three-phase MPC, described by Rodriguez et al. (2007), was adapted for $2\phi3w$ current control. However, that controller was designed based on models of three-phase systems, which is not the case for $2\phi3w$ circuits. The control implementation required the Clarke transformation (2.1) to be ap-

plied in "*abn*" (*i.e.*, phase *a*, phase *b* and neutral) quantities so they could be properly introduced in the controller.

Aiming to make the current control systems simpler in $2\phi3w$ applications, a MPC was designed specifically for two-phase systems by applying the *ab-αβ* transformation (3.3). The following subsections describe the two-phase $\alpha\beta$ models used to design the two-phase $\alpha\beta$ MPC used in this work, the cost function to be minimized, the strategy employed to set a fixed switching frequency and the current controller structure as a whole. The description of the adapted $2\phi3w$ MPC is reported as a conference paper by Furtado and Barbosa (2019).

4.5.1 *VSC MODEL*

The system topology considered to obtain the models used in MPC is shown in Figure 69. It should be noted that the third VSC branch is tagged with the index *n* because, in the context of this work, this leg is connected to the grid neutral conductor. The voltages v_a and v_b represent phase-to-neutral voltages of a three-phase four-wire power grid. The $2\phi3w$ APF is connected to phase *a*, phase *b* and neutral at PCC. The shunt power conditioner is composed by a three-branch VSC, a dc-bus capacitance C_f, and inductive output filters represented by the inductances L_f and their parasitic resistances r_f. The PEC output voltages, measured in relation to the neutral point *N*, are represented by v_{fa}, v_{fb} and v_{fn} (FURTADO & BARBOSA, 2019).

Figure 69 – System topology used to design the predictive current controller.
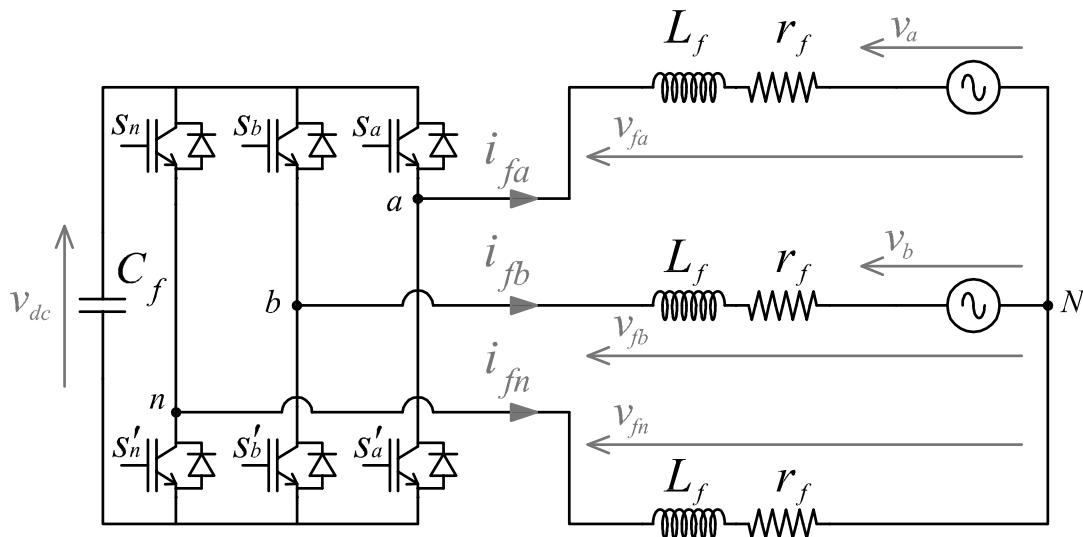
Considering that switches in the same VSC leg work in a complimentary way, the three-leg VSC has eight possible switching states, which are denoted by *x* and numbered from 1 to 8.

Each switching state define a VSC output voltage space vector with components v_{fa}, v_{fb} and v_{fn}. The eight output voltage vectors that can be assumed by a three-leg VSC are described in the *abn* reference frame in Table 2 (FURTADO & BARBOSA, 2019).

Table 2 – Three-leg VSC output vectors expressed in the *abn* reference frame.

Switching	VSC Output		
state (x)	$v_{fa}(x)$	$v_{fb}(x)$	$v_{fn}(x)$
1	0	0	0
2	$\frac{2}{3}v_{dc}$	$-\frac{1}{3}v_{dc}$	$-\frac{1}{3}v_{dc}$
3	$\frac{1}{3}v_{dc}$	$\frac{1}{3}v_{dc}$	$-\frac{2}{3}v_{dc}$
4	$-\frac{1}{3}v_{dc}$	$\frac{2}{3}v_{dc}$	$-\frac{1}{3}v_{dc}$
5	$-\frac{2}{3}v_{dc}$	$\frac{1}{3}v_{dc}$	$\frac{1}{3}v_{dc}$
6	$-\frac{1}{3}v_{dc}$	$-\frac{1}{3}v_{dc}$	$\frac{2}{3}v_{dc}$
7	$\frac{1}{3}v_{dc}$	$-\frac{2}{3}v_{dc}$	$\frac{1}{3}v_{dc}$
8	0	0	0

By using (3.3), the transformation of these voltages into two-phase $\alpha\beta$ components results in the values presented in Table 3 (FURTADO & BARBOSA, 2019). These $\alpha\beta$ voltages are presented to the system model used to predict future values of controlled variables (FURTADO & BARBOSA, 2019).

Table 3 – Three-leg VSC output vectors expressed in two-phase $\alpha\beta$ reference frame.

Switching state (x)	VSC Output	
	$v_{f\alpha}(x)$	$v_{f\beta}(x)$
1	0	0
2	$\dfrac{2}{3}v_{dc}$	0
3	$\dfrac{1}{3}v_{dc}$	$\dfrac{\sqrt{3}}{3}v_{dc}$
4	$-\dfrac{1}{3}v_{dc}$	$\dfrac{\sqrt{3}}{3}v_{dc}$
5	$-\dfrac{2}{3}v_{dc}$	0
6	$-\dfrac{1}{3}v_{dc}$	$-\dfrac{\sqrt{3}}{3}v_{dc}$
7	$\dfrac{1}{3}v_{dc}$	$-\dfrac{\sqrt{3}}{3}v_{dc}$
8	0	0

4.5.2 SYSTEM MODEL FOR PREDICTION

The design of a MPC is based on a discrete model of the system to be controlled (RO-DRIGUEZ et al., 2007; RODRIGUEZ & CORTES, 2012). Aiming to obtain such model, the $2\phi3w$ circuit shown in Figure 69 is mathematically described by the differential equations

$$
\begin{cases}
v_{fa}(t) = L_f \dfrac{d}{dt}i_{fa}(t) + r_f i_{fa}(t) + v_a(t) \\[2mm]
v_{fb}(t) = L_f \dfrac{d}{dt}i_{fb}(t) + r_f i_{fb}(t) + v_b(t) \quad , \\[2mm]
v_{fn}(t) = L_f \dfrac{d}{dt}i_{fn}(t) + r_f i_{fn}(t)
\end{cases}
\tag{4.10}
$$

which can be transformed into two-phase $\alpha\beta$ reference frame using (3.3) (FURTADO & BARBOSA, 2019), resulting in

$$
\begin{cases}
v_{f\alpha}(t) = L_f \dfrac{d}{dt}i_{f\alpha}(t) + r_f i_{f\alpha}(t) + v_\alpha(t) \\[2mm]
v_{f\beta}(t) = L_f \dfrac{d}{dt}i_{f\beta}(t) + r_f i_{f\beta}(t) + v_\beta(t)
\end{cases}
\tag{4.11}
$$

The discretization of this model can be done by using a forward Euler approximation to calculate derivatives (RODRIGUEZ & CORTES, 2012):

$$\frac{d}{dt}i(t) = \frac{i(k+1) - i(k)}{T_s},$$
$$(4.12)$$

where T_s is the sampling period and k is the discrete-time variable.

Other approximations are based on the assumption that sampling frequency is sufficiently higher than grid frequency. It implies that reference currents and grid voltages do not vary considerably in two sampling periods (RODRIGUEZ & CORTES, 2012). Therefore, it is assumed in the discrete model that

$$i^*(k+2) \approx i^*(k+1) \approx i^*(k)$$
$$(4.13)$$

and

$$v(k+2) \approx v(k+1) \approx v(k).$$
$$(4.14)$$

By considering these approximations and substituting (4.12) into (4.10), it is possible to obtain expressions to predict future values of APF currents (RODRIGUEZ & CORTES, 2012):

$$\begin{cases} i^p_{f\alpha}(k+1) = \left(1 - \frac{r_f T_s}{L_f}\right) i_{f\alpha}(k) + \frac{T_s}{L_f}\left[v_{f\alpha}(x) - v_\alpha(k)\right] \\ \\ i^p_{f\beta}(k+1) = \left(1 - \frac{r_f T_s}{L_f}\right) i_{f\beta}(k) + \frac{T_s}{L_f}\left[v_{f\beta}(x) - v_\beta(k)\right] \end{cases},$$
$$(4.15)$$

where the superscript p is used to indicate a model-predicted quantity.

These results are similar to those presented by Rodriguez et al. (2007). The difference is that the model in (4.15) was obtained using only voltages and currents related to phases a and b, which were taken into the $\alpha\beta$ domain using the ab-$\alpha\beta$ transformation in (3.3) (FURTADO & BARBOSA, 2019).

4.5.3 DEAD-TIME COMPENSATION

It is described by Rodriguez and Cortes (2012) that calculation times influence the performance of the MPC due to the delay between the data acquisition and the application of the chosen VSC output. This error causes high-frequency ripple in output currents i_{fa}, i_{fb} and i_{fn}. Aiming to improve the performance of the MPC used in this work, it is implemented a dead-time compensation method as described by Rodriguez and Cortes (2012). This improvement needs the prediction of variables two sampling periods in the future $(k+2)$. These predictions

can be obtained as:

$$
\begin{cases}
i_{f\alpha}^{p}(k+2) = \left(1 - \dfrac{r_f T_s}{L_f}\right) i_{f\alpha}^{p}(k+1) + \dfrac{T_s}{L_f}\left[v_{f\alpha}(x) - v_{\alpha}(k)\right] \\[3mm]
i_{f\beta}^{p}(k+2) = \left(1 - \dfrac{r_f T_s}{L_f}\right) i_{f\beta}^{p}(k+1) + \dfrac{T_s}{L_f}\left[v_{f\beta}(x) - v_{\beta}(k)\right]
\end{cases}
. \qquad (4.16)
$$

Therefore, the MPC used in this work employs the predictions obtained through (4.16) to evaluate the cost function $g(x)$ for each possible switching state (RODRIGUEZ & CORTES, 2012).

4.5.4 COST FUNCTION

After predicting currents for each VSC state x, a cost function is evaluated. The cost function $g(x)$ used in this work is a measurement of the future current error if each switching state x is applied at the present sampling period. This cost function is composed by the sum of absolute errors in the α and β reference frames, considering that reference signals do not change significantly in two sampling periods (RODRIGUEZ et al., 2007; RODRIGUEZ & CORTES, 2012). The cost function is expressed by:

$$
g(x) = \left| i_{f\alpha}^{*}(k) - i_{f\alpha}^{p}(k+2) \right| + \left| i_{f\beta}^{*}(k) - i_{f\beta}^{p}(k+2) \right| \qquad (4.17)
$$

After the cost function is evaluated for $x = 1 \ldots 8$, the value of x which returns the optimum (*i.e.*, minimum) value of $g(x)$ is stored as x_{opt}. Then, switching state the VSC must be set is x_{opt} (RODRIGUEZ et al., 2007; RODRIGUEZ & CORTES, 2012).

4.5.5 FIXED SWITCHING FREQUENCY

According to the general MPC presented by Rodriguez et al. (2007), the switches states are set directly by setting s_a, s_b and s_n (FURTADO & BARBOSA, 2019). This working mode leads to variable switching frequency, which is limited by the sampling frequency (VAZQUEZ et al., 2009; RODRIGUEZ & CORTES, 2012). It causes the current spectrum to present a wide range of high frequency content due to switching (VAZQUEZ et al., 2009; RODRIGUEZ & CORTES, 2012). This characteristic can cause problems such as interferences and difficult the design of passive filters (VAZQUEZ et al., 2009; RODRIGUEZ & CORTES, 2012). Aiming to overcome this issue, Cortés et al. (2008) proposed the use of a band-stop filter at the cost function. A different approach found in literature is the integration between MPC and the fixed switching frequency provided by the Space Vector Modulation (SVM) (VAZQUEZ et al., 2009). In this configuration, the MPC selects the voltage which minimizes the current error. This voltage reference is provided to the

SVM algorithm, which generates the drive signals for VSC switches. SVM presents advantages such as the fixed switching frequency, optimization of converter hardware utilization (BUSO & MATTAVELLI, 2006) and it is so well established that optimal SVM algorithms can be found ready for use in digital signal controllers. Thus, the SVM can be used to generate the VSC output voltages which minimizes the cost function (*i.e.,* the current error) at each sampling period (VAZQUEZ et al., 2009; FURTADO & BARBOSA, 2019).

4.5.6 MPC ALGORITHM

The algorithm to be implemented for the $2\phi 3w$ MPC was reported by Furtado and Barbosa (2019). The first step in this algorithm is to sample the variables: PCC voltages v_a and v_b and APF currents i_{fa}, i_{fb} and i_{fn}. Then VSC output is set according to the switching state $v_f(x_{opt})$, which has been selected in the previous sampling period. Afterwards, the controlled variables are estimated at the instant t_{k+1} according to the system model (4.15). The estimations $i_{fa}^p(k+1)$, $i_{fb}^p(k+1)$ and $i_{fn}^p(k+1)$ are calculated only for the switching state $v_f(x_{opt})$, which was just applied. Then the predictions $i_{fa}^p(k+2)$, $i_{fb}^p(k+2)$ and $i_{fn}^p(k+2)$ and the cost function $g(x)$ are evaluated for each possible VSC switching state ($x = 1, \ldots, 8$). Finally, the switching state which minimizes $g(x)$ is stored as x_{opt} to be used in the next sampling period. The whole MPC algorithm implemented in simulations studies presented in this work is illustrated in Figure 70

Figure 70 – Algorithm of the $2\phi3w$ adapted MPC current controller.
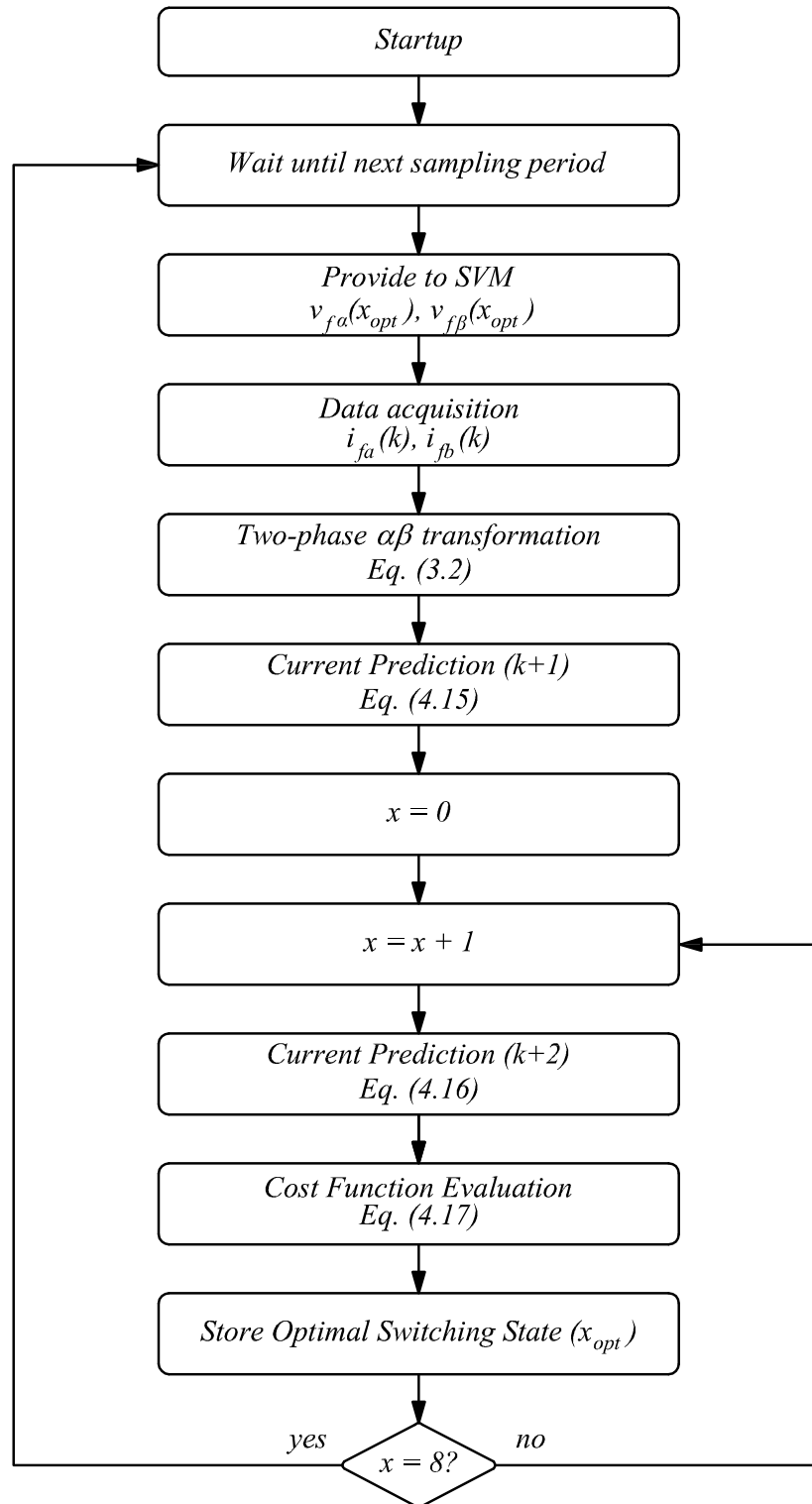
Source: adapted from Furtado and Barbosa (2019).

4.6 GENERAL CONTROL BLOCK DIAGRAM

An overview of the proposed control scheme is illustrated in Figure 71.

Figure 71 – Block diagram of the proposed $2\phi3w$ APF control system.
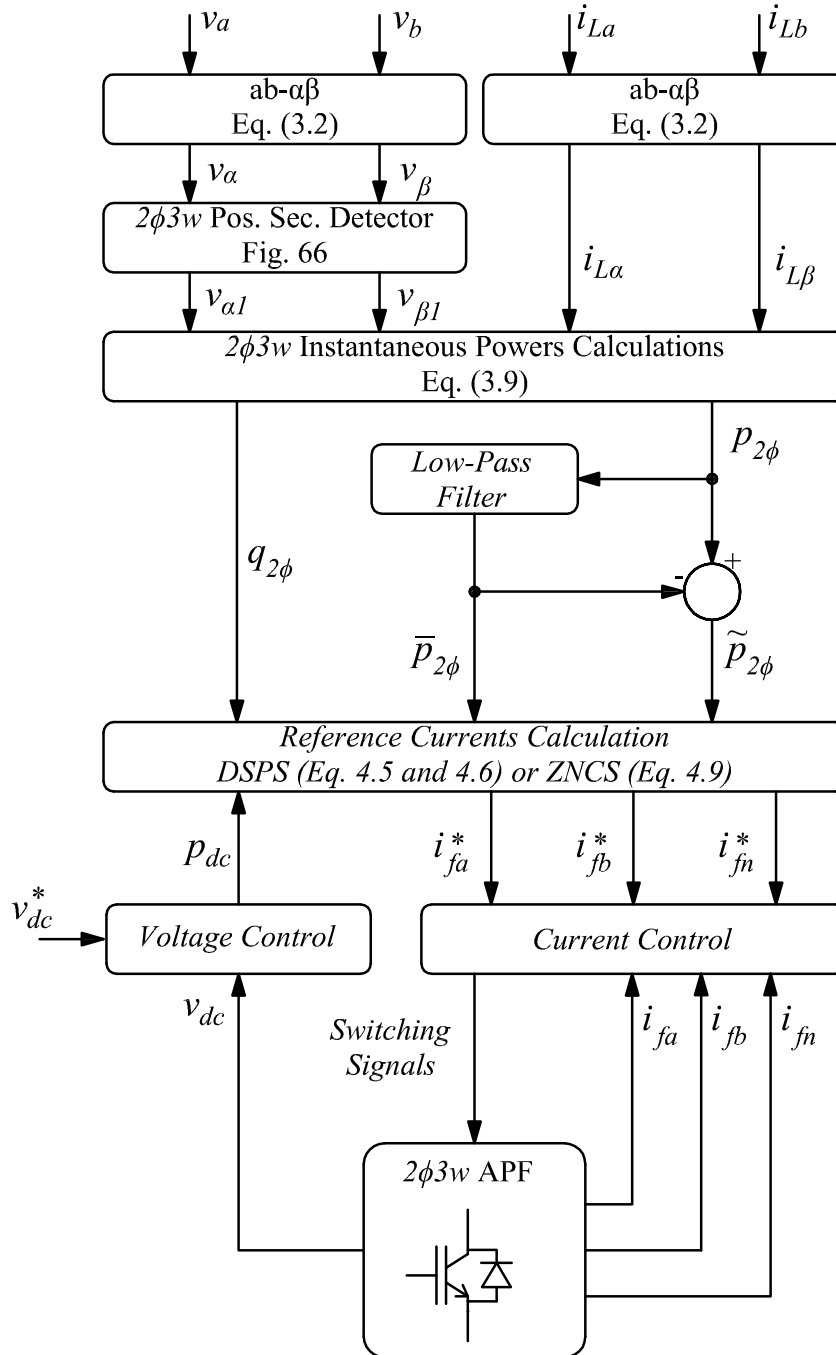
Source: Own authorship.

Simulation studies were performed aiming to validate the $2\phi3w$ shunt APF control techniques proposed in this chapter. The description of the simulated system and the results obtained in digital simulations are presented and discussed in the following chapter.

5   SIMULATION AND EXPERIMENTAL RESULTS

This chapter aims to present and discuss some preliminary results obtained up to this point in this research. An experimental laboratory prototype is used to evaluate the effectiveness of the two-phase positive-sequence detector of Section 4.2 under real voltage conditions. The experimental results obtained are presented in the next section. Simulations are performed to validate the proposed concepts of $2\phi3w$ instantaneous powers as a whole, specially the control systems described in Chapter 4.

5.1   *EXPERIMENTAL RESULTS*

5.1.1   *TWO-PHASE POSITIVE-SEQUENCE DETECTOR*

This section presents some preliminary experimental results obtained with the proposed two-phase adaptation of the DSOGI-PLL discussed in Section 4.2. The experiment was performed under real voltage conditions in an existing experimental setup at the Power Electronics and Automation Group (in Portuguese, *Núcleo de Automação e Eletrônica de Potência*) (NAEP) laboratory of the Federal University of Juiz de Fora (in Portuguese, *Universidade Federal de Juiz de Fora, Brasil*) (UFJF). It is worth mentioning that the experimental setup contained step-down transformers (ratio 4:1) to work with reduced voltages, which does not represent any issue for evaluating the proposed positive-sequence detector. An schematic view of the experimental prototype used is shown in Figure 72.

The positive-sequence detector adapted for $2\phi3w$ systems was implemented in a *TMS320 F28335* DSC. For comparison purposes, the three-phase DSOGI-PLL, as described by Rodriguez et al. (2006) was also implemented in the same laboratory setup. Both algorithms were executed simultaneously. It is important to know that the adapted $2\phi2w$ DSOGI-PLL run with the informations of phase voltages v_a and v_b only. On the other hand, the third phase voltage (v_c) was also measured and provided for the three-phase DSOGI-PLL aiming to compare the results with the proposed $2\phi3w$ adaptation.

Figure 72 – Schematic of the experimental setup.
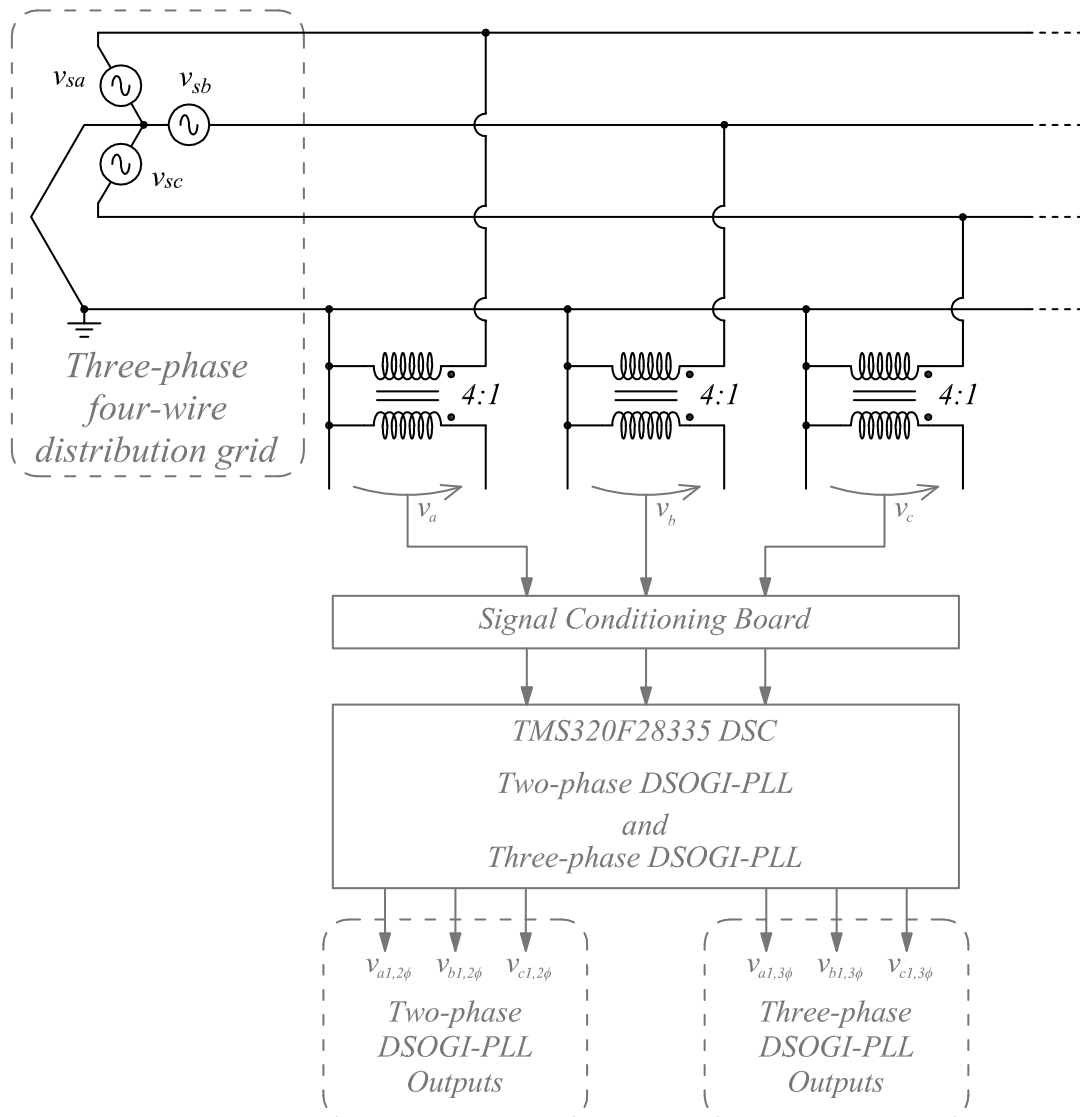
Source: Own authorship.

The data points stored in internal DSC variables were exported to a computer to generate the presented graphs and waveforms. The results obtained are shown in Figure 73 to Figure 75. In these figures, the signals expressed as v_a, v_b and v_c (red waveforms) represent the phase voltage signals measured in the laboratory power supply. The signals $v_{a1,3\phi}$, $v_{b1,3\phi}$ and $v_{c1,3\phi}$ (blue waveforms) are the results obtained through the conventional three-phase DSOGI-PLL. These signals are taken as reference results, as they represent exactly the positive-sequence fundamental-frequency sinusoidal signals, as demonstrated by Rodriguez et al. (2006). Finally, the signals $v_{a1,2\phi}$, $v_{b1,2\phi}$ and $v_{c1,2\phi}$ (black waveforms) in Figure 73 to Figure 75 are the results obtained through the proposed two-phase positive-sequence detector. Even though $v_{c1,2\phi}$ has

no physical/application purpose in $2\phi 3w$ circuits, it was calculated as

$$v_{c1,2\phi} = -(v_{a1,2\phi} + v_{b1,2\phi}) \qquad (5.1)$$

and displayed in Figure 75 to allow the comparison with the correspondent three-phase signal.

Figure 73 – Two-phase positive sequence detection (waveforms - phase a).
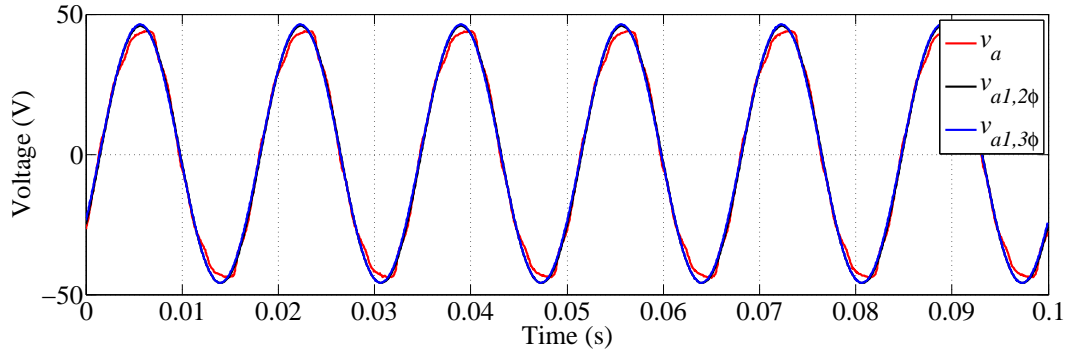
Source: Own authorship.

Figure 74 – Two-phase positive sequence detection (waveforms - phase b).
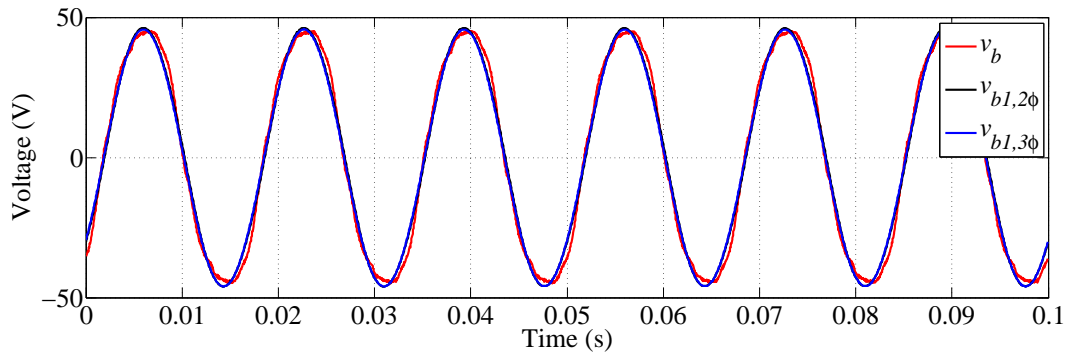
Source: Own authorship.

Figure 75 – Two-phase positive sequence detection (waveforms - phase c).
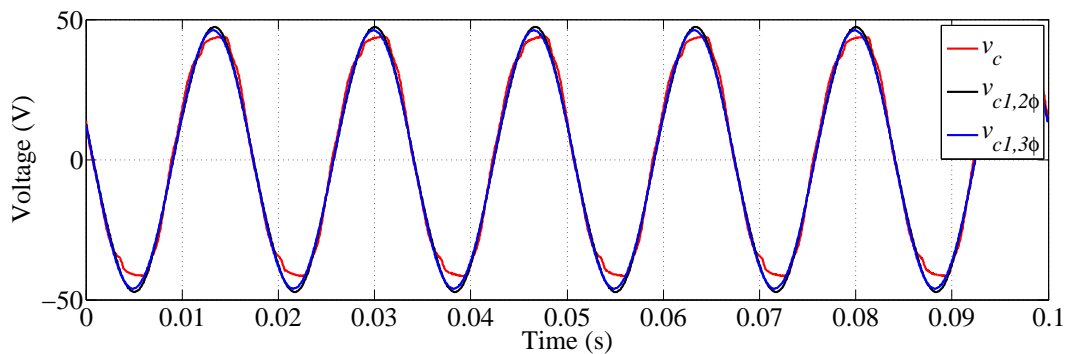
Source: Own authorship.

Aiming to observe these signals in the frequency domain, an offline Fast Fourier Transform (FFT) was applied using the software *Matlab*. The representation in terms of frequencies are shown in Figure 76 to Figure 78. The spectrum is shown up to the 20 th component to ease the observation of the most relevant information.

Figure 76 – Two-phase positive sequence detection (spectrum - phase a).
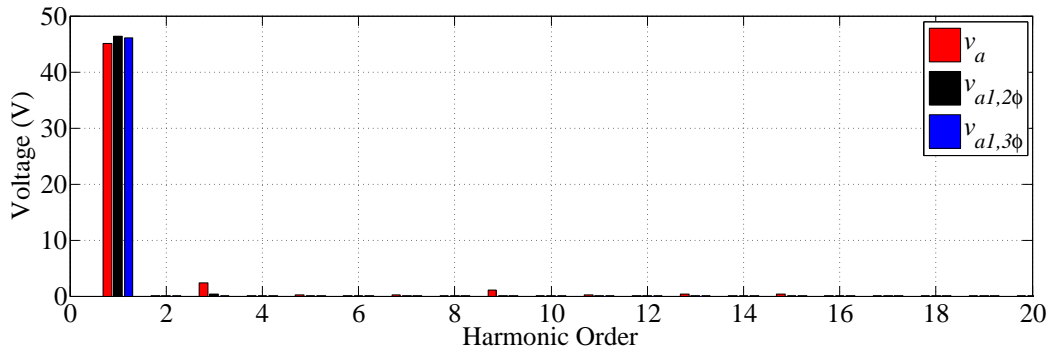
Source: Own authorship.

Figure 77 – Two-phase positive sequence detection (spectrum - phase b).
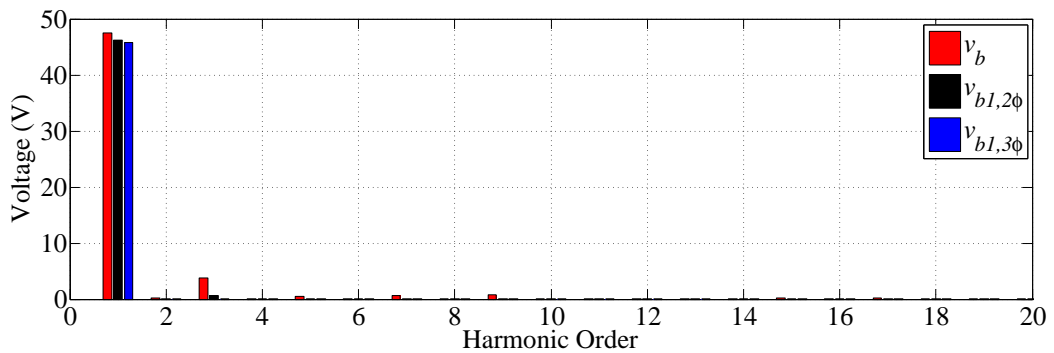
Source: Own authorship.

Figure 78 – Two-phase positive sequence detection (spectrum - phase c).
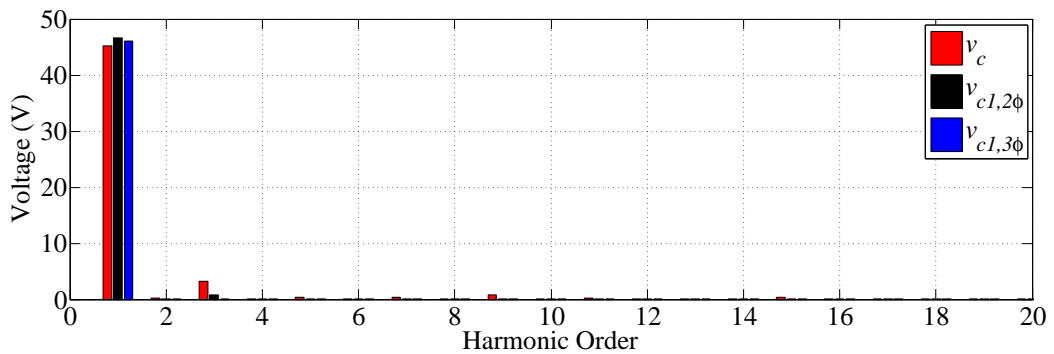
Source: Own authorship.

The presented results show that measured signals (in red) are unbalanced and contain harmonic components, specially the 3rd. The outputs of the three-phase DSOGI-PLL (in blue) contain only the positive-sequence fundamental-frequency component with expressive amplitude. The output of the $2\phi 3w$ DSOGI-PLL presents nearly the same amplitude in the fundamental frequency. The presence of the 3rd harmonic components is also observed, even though they are attenuated in relation to original signals.

It can be observed that the two-phase approach presents an error if compared with the original three-phase DSOGI-PLL. This error is caused by the presence of zero-sequence components in voltages, which cannot be eliminated by the ab-$\alpha\beta$ transformation in (3.3), as discussed in Section 4.2. On the other hand, the preliminary results show that the $2\phi 3w$ adaptation of the DSOGI-PLL could approximate the fundamental-frequency positive-sequence components of measured phase voltage signals. The proposed $2\phi 3w$ DSOGI-PLL can be subject of further investigation, as for example to model and quantify the observed errors and to stablish an error acceptability range for practical applications.

5.2   SIMULATION RESULTS

5.2.1   SIMULATED SYSTEM TOPOLOGY

The topology of the simulated $2\phi 3w$ system is illustrated Figure 79. The power source representing the distribution grid is represented by a three-phase four-wire solidly-grounded voltage source. Three conductors are derived from the grid to feed the load: phases *a* and *b* and the neutral. Neither the load nor the APF any kind of connection to phase *c*, which is considered open in the context of this work. The power cables that connect the load are represented by their equivalent inductances L_s and resistances r_s. The same characteristics are considered for all feeders because the neutral must have the same cross-sectional area as phase conductors in $2\phi 3w$ circuits (ABNT, 2008). The $2\phi 3w$ load is composed by four different circuits, comprising linear and non-linear components. The load is also unbalanced between phases *a* and *b*, *i.e.*, drains different currents in each phase. There are a linear resistive-inductive and a diode rectifier loads connected between phase *a* and neutral. Another diode rectifier circuit is connected between phase *b* and neutral. Finally, a resistive load is connected from phase *a* to phase *b*. The $2\phi 3w$ shunt APF is composed by a three-leg VSC, a DC-link capacitor represented by a capacitance C and output inductive filters represented by inductances L_f and parasitic resistances r_f. The main system parameters used to perform simulation studies are listed in Table 4.

Figure 79 – Simulated system topology.
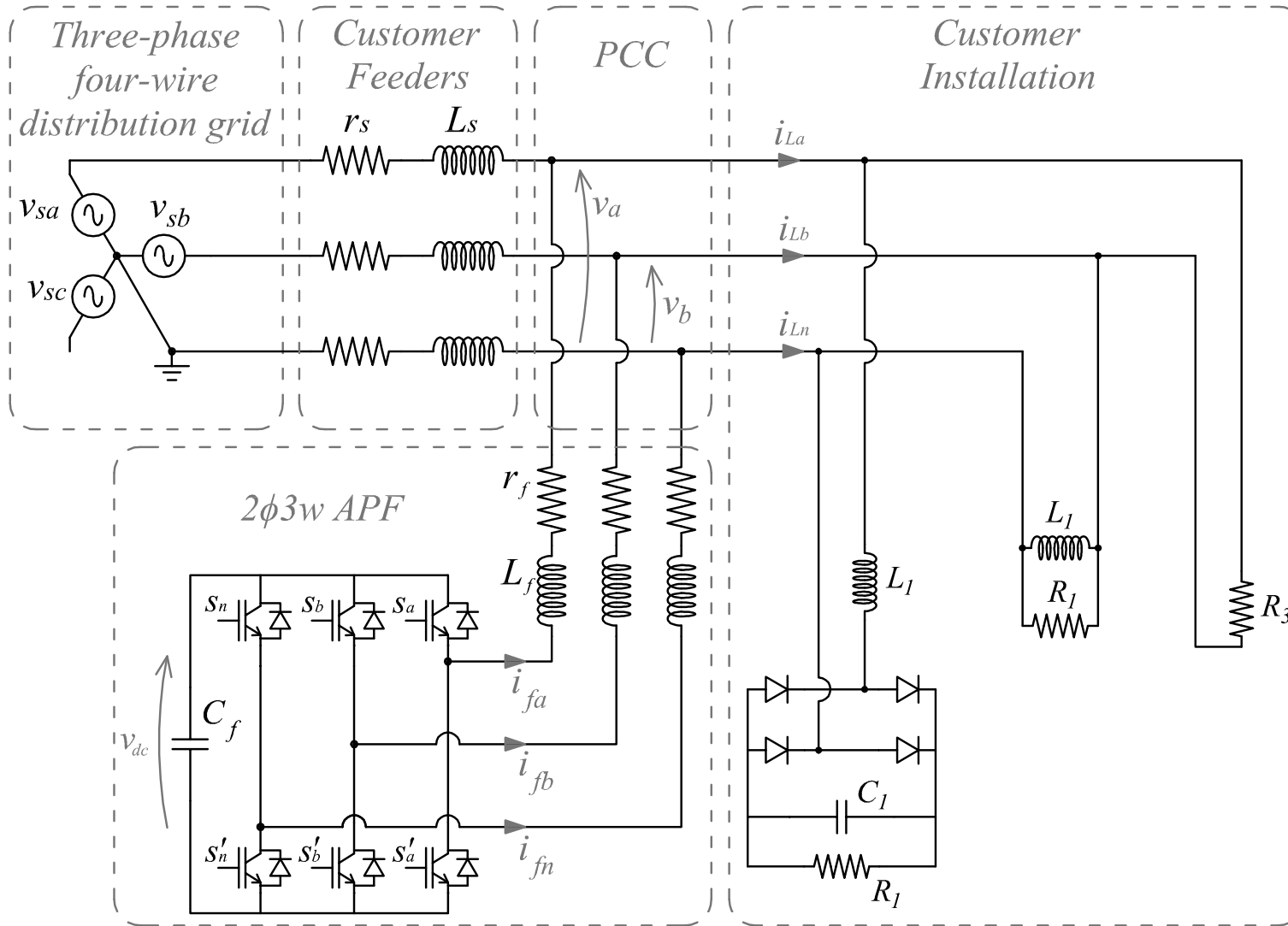
Source: Own authorship.

Table 4 – Simulation setup parameters.

Part of circuit	Description	Value
Mains	phase rms voltage (v_a, v_b)	127 V
	line rms voltage (v_{ab})	220 V
	frequency (f)	60 Hz
	line resistance (R_s)	1 mΩ
	line inductance (L_s)	50.0 μH
$2\phi 3w$ APF	sampling frequency (f_s)	40 kHz
	switching frequency (f_{sw})	40 kHz
	DC voltage (V_{dc})	400 V
	DC-link capacitance (C)	24.2 mF
	output inductance (L_f)	2.5 mH
	output resistance (r_f)	0.1 Ω
Load # 1 (a-n)	Diode Rectifier (nonlinear)	
	Input Inductor (L_1)	2.9 mH
	Output Capacitor (C_1)	100 μF
	Resistive load (R_1)	50 Ω
Load # 2 (b-n)	Parallel RL (linear)	
	Resistance (R_2)	10 Ω
	Inductance (L_2)	20 mH
Load # 3 (a-b)	Resistive (linear)	
	Resistive load (R_3)	10 Ω

5.2.2 SIMULATED LOAD

This section presents the behaviour of currents and powers of the simulated load. The waveforms in this section illustrate the way a generic unbalanced two-phase nonlinear load absorbs power from the grid. These characteristics are important for the sake of comparison with the results of the two-phase shunt compensation in the following sections.

The current drawn by the load in phase a is shown in Figure 80. These are the currents to be provided by the source if no compensation is applied. It can be observed that this current contains harmonic components and is advanced in relation with the phase voltage v_a. The load current waveform in phase b is shown in Figure 81. As the load connected to phase b is resistive-inductive, this current is sinusoidal and lags the phase voltage v_b.

Figure 80 – PCC phase voltage and load current - Phase *a*.
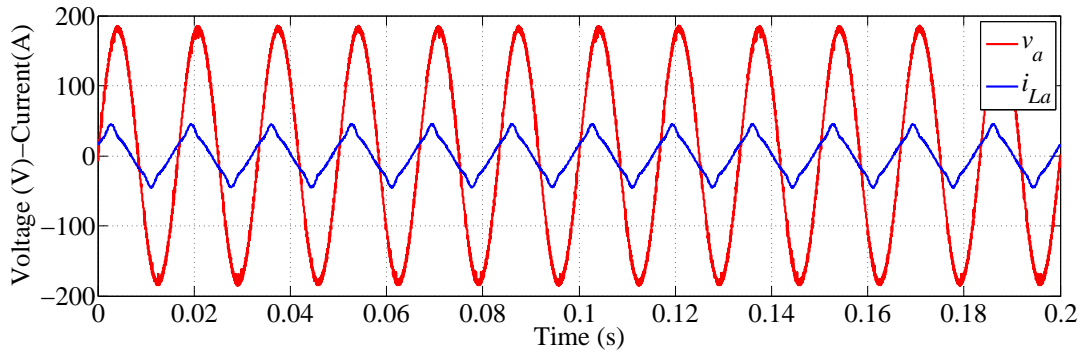
Source: Own authorship.

Figure 81 – PCC phase voltage and load current - Phase *b*.
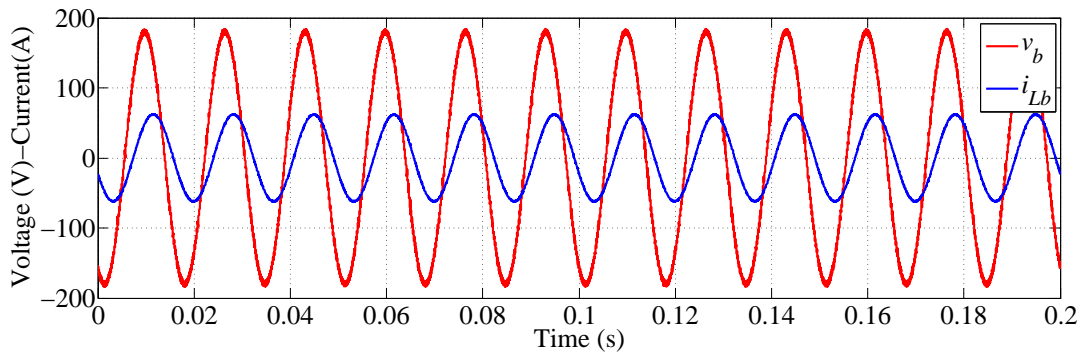
Source: Own authorship.

For the sake of comparison, the load currents i_{La}, i_{Lb} are also illustrated again in Figure 82, which also shows the neutral current i_{Ln} demanded by the load. It is possible to notice in this figure the difference of the amplitude of currents in phases *a* and *b* and in the neutral.

Figure 82 – Load currents - Phases *a*, *b* and neutral.
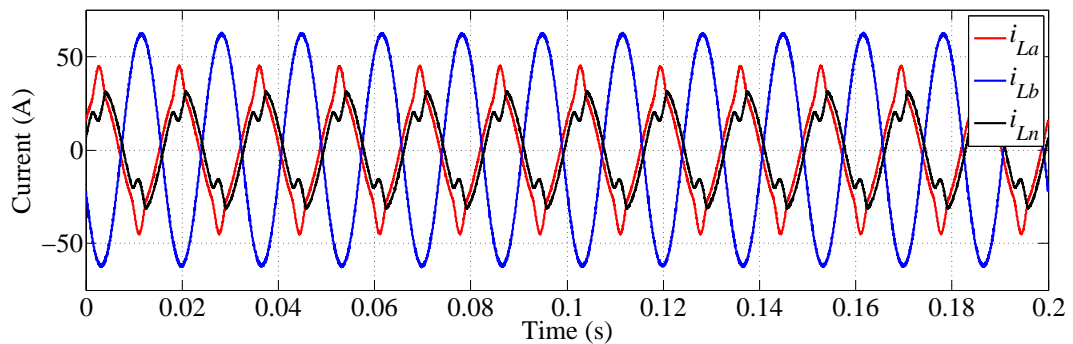
Source: Own authorship.

The harmonic spectrum of load currents is compared with the recommended limits of the

IEEE-519 standard (IEEE, 2014) in Figure 83, Figure 84, and Figure 85. The comparison considers harmonic components up to the 50 th order (IEEE, 2014). It is possible to note that currents i_{La} and i_{Ln} present 3 rd and 5 th harmonics beyond the limits. The 7 th harmonic of i_{Ln} is also higher than recommended. On the other hand, it is possible to observe that i_{Lb} has all harmonic components below the recommended limits.

Figure 83 – Harmonic spectrum of load current - Phase a.
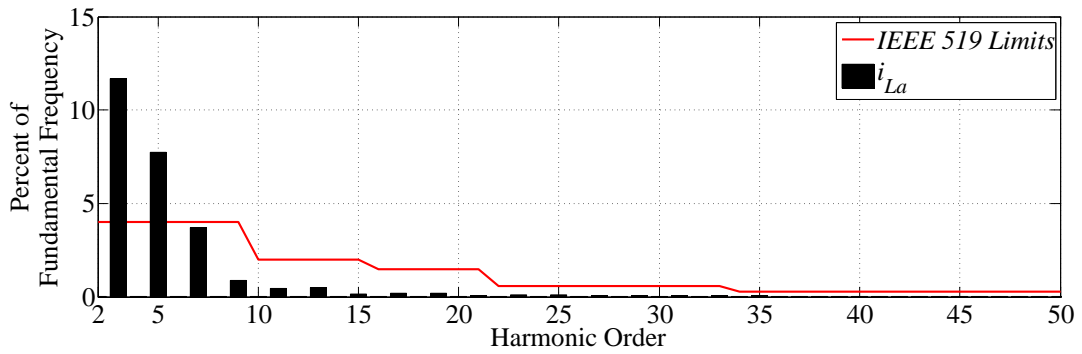
Source: Own authorship.

Figure 84 – Harmonic spectrum of load current - Phase b.
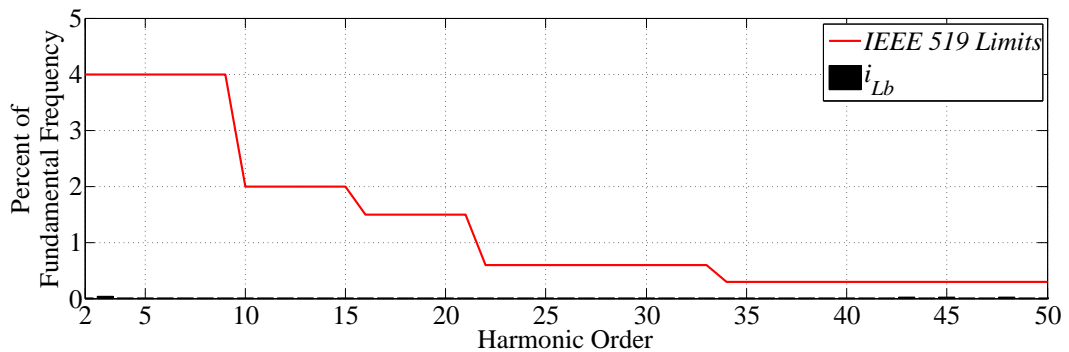
Source: Own authorship.

Figure 85 – Harmonic spectrum of load current - Neutral.
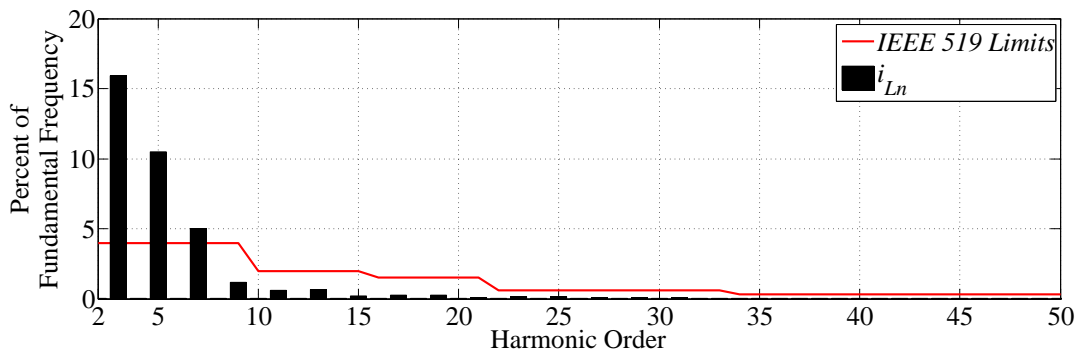
Source: Own authorship.

The load characteristics can also be evaluated quantitatively through currents rms values, Total Harmonic Distortion (THD), the Power Factor (PF) in each phase and the loss due to the feeder resistances R_s. These measurements are listed in Table 5.

Table 5 – Load currents THD, rms values , PF and losses.

Part of Circuit		rms	THD	PF	Loss
Load	Phase *a*	25.97 A	14.51 %	0.8543	0.674 W
	Phase *b*	43.88 A	0.10 %	0.7769	1.925 W
	Neutral	19.35 A	19.71 %	–	0.374 W
	Total	–	–	–	2.973 W

Finally, the two-phase instantaneous powers $p_{2\phi}$ and $q_{L2\phi}$ absorbed by the load are shown in Figure 86. It can be seen that these waveforms present an oscillation twice the grid frequency, caused by load unbalances and the flow of reactive power. These waveforms also contain components in other frequencies due to the current harmonics demanded by the load. It can also be observed that both real and imaginary powers become negative during part of their periods, which indicates the flow of power back to the source during these time intervals.

Figure 86 – Two-phase instantaneous powers demanded by the load.
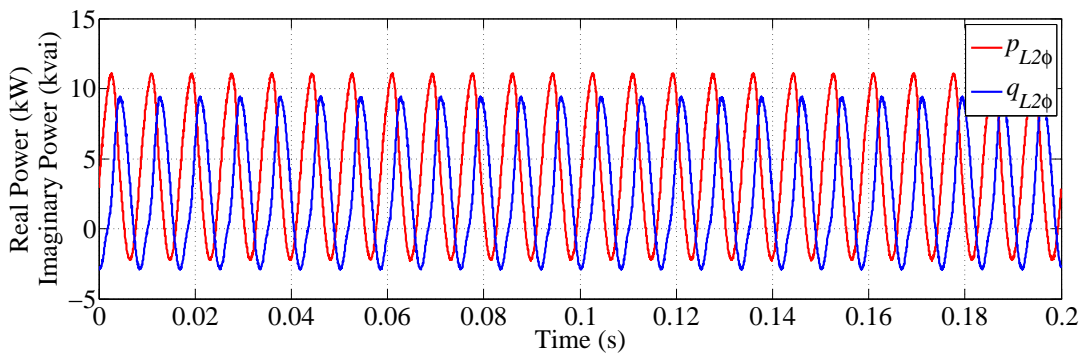
Source: Own authorship.

The effects of $2\phi3w$ shunt compensation are presented, from the source perspective, in the following sections. It is worth commenting that the same load was considered for both DSPS and ZNCS compensation simulations.

5.2.3 *SIMULATION RESULTS OF TWO-PHASE SHUNT COMPENSATION USING THE DOUBLE SINGLE-PHASE STRATEGY*

The compensation currents synthesized by the simulated $2\phi3w$ shunt APF, as well as their reference signals, are illustrated Figure 87, Figure 88 and Figure 89. It can be observed the presence of some high-frequency ripple in APF output currents due to VSC switching. These figures also show that APF currents follow their references, which validates the implemented current control loop using a MPC.

Figure 87 – DSPS compensation - APF current and reference - Phase *a*.
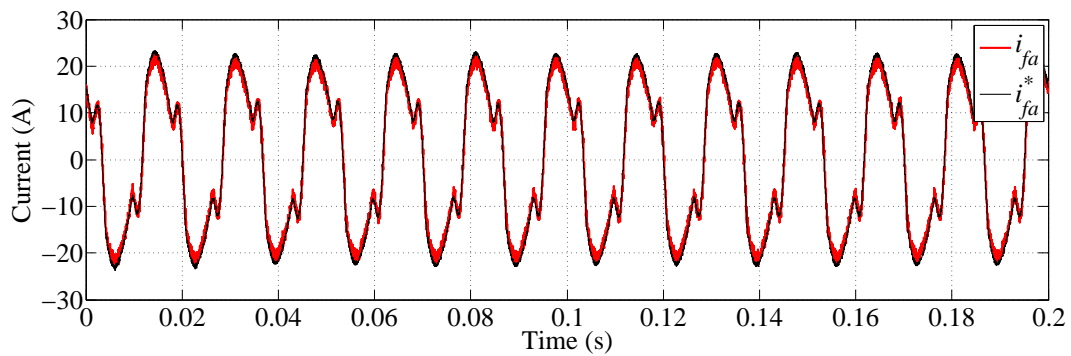
Source: Own authorship.

Figure 88 – DSPS compensation - APF current and reference - Phase *b*.
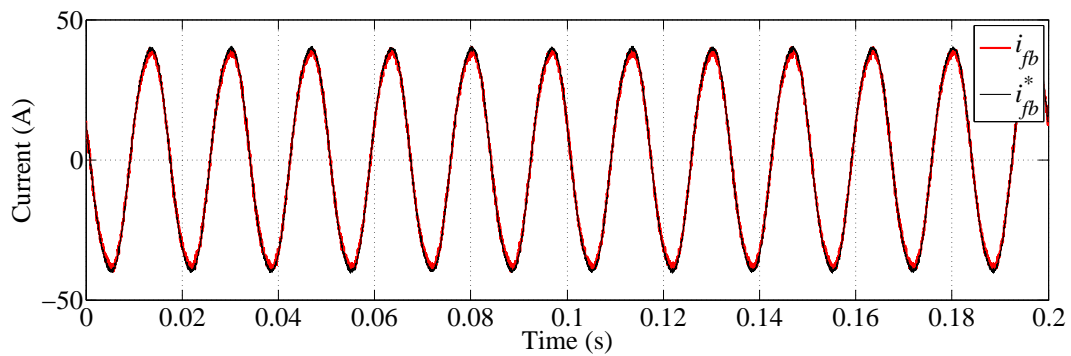
Source: Own authorship.

Figure 89 – DSPS compensation - APF current and reference - Neutral.
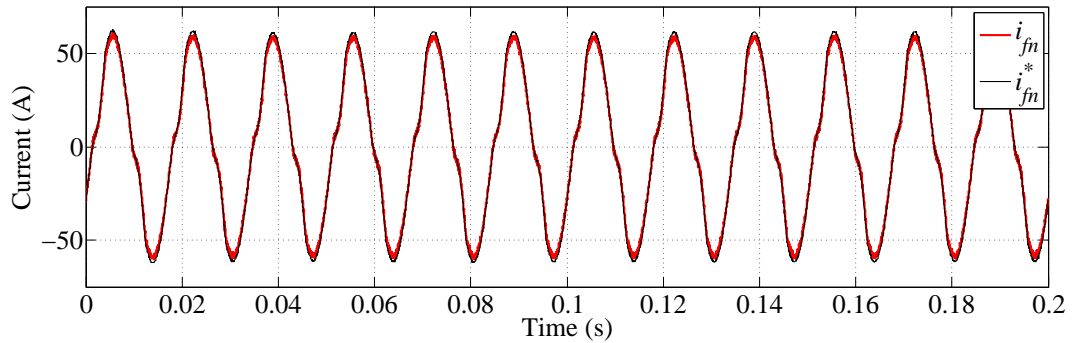
Source: Own authorship.

The main result of DSPS compensation is illustrated in Figure 90 and Figure 91, which show compensated currents provided by the source. It can be seen that phase currents are nearly sinusoidal and in phase with voltages, despite load nonlinear and reactive characteristics.

Figure 90 – DSPS compensation - PCC phase voltage and source current - Phase a.
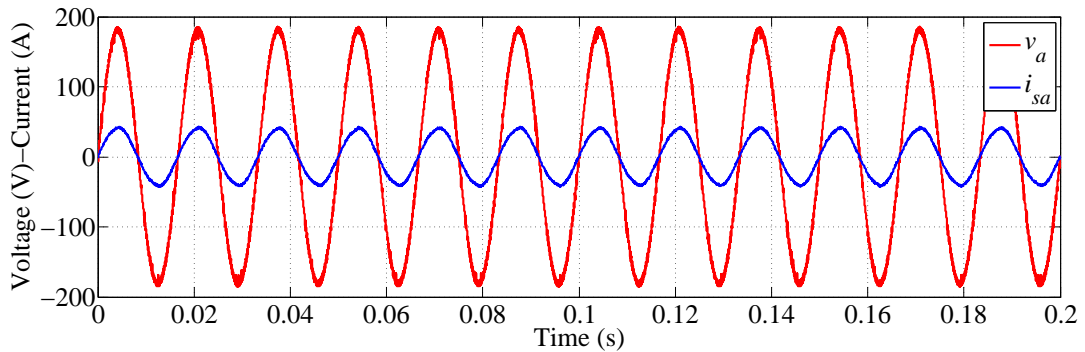
Source: Own authorship.

Figure 91 – DSPS compensation - PCC phase voltage and source current - Phase b.
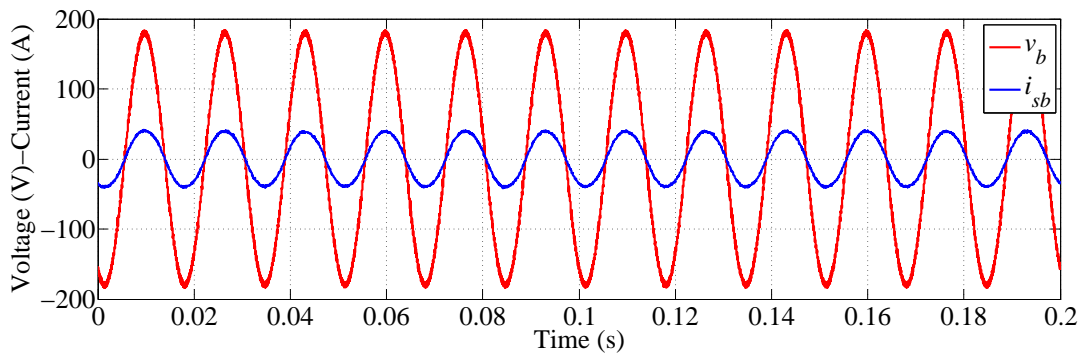
Source: Own authorship.

Phase and neutral currents provided by the source are shown together in Figure 92. It can

be observed that the two-phase APF could reduce significantly the load unbalances. Actually, there is still some unbalance in source currents due to oscillations in the APF DC voltage. These oscillations are transmitted to APF output currents through the inner voltage control loop and, consequently, affect compensated source currents. This is a topic proposed in this work for further investigation.

Figure 92 – DSPS compensation - Source currents - Phases *a*, *b* and neutral.
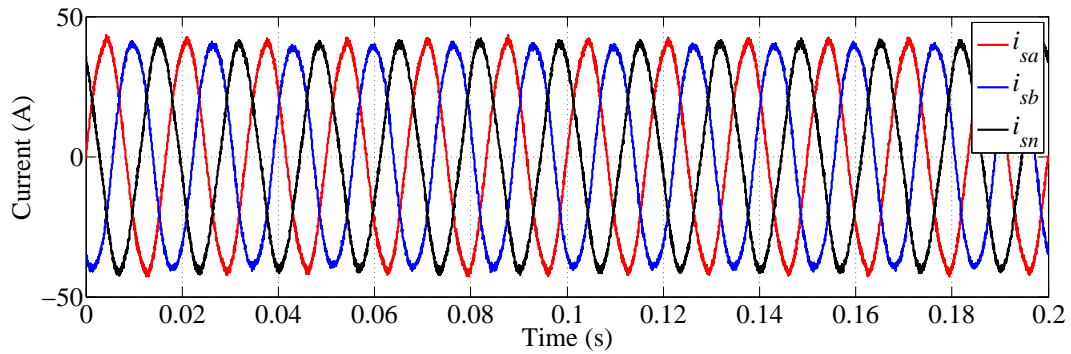
Source: Own authorship.

The harmonic spectrum of source currents obtained with DSPS compensation are presented in Figure 93, Figure 94 and Figure 95. There was some introduction of harmonics, specially the 3rd, in i_{sb} compared with i_{Lb} due to the APF operation. However, all current harmonics in source currents are bellow accepted limits according to IEEE-519 recommendations (IEEE, 2014).

Figure 93 – DSPS compensation - Harmonic spectrum of source current - Phase *a*.
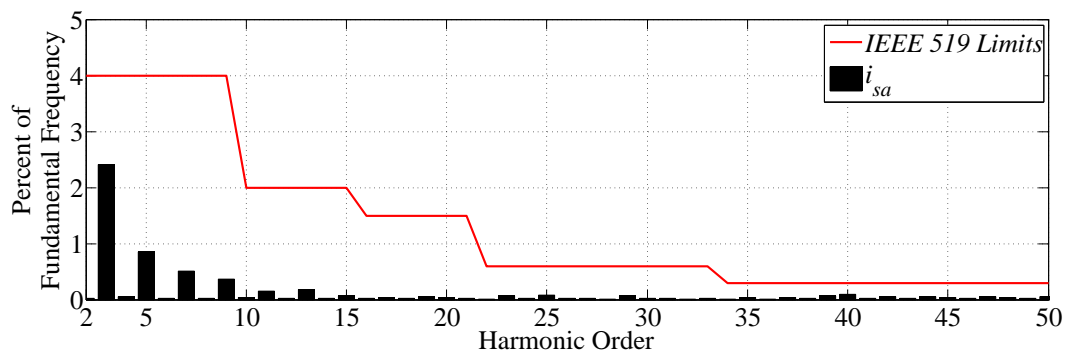
Source: Own authorship.

Figure 94 – DSPS compensation - Harmonic spectrum of source current - Phase *b*.
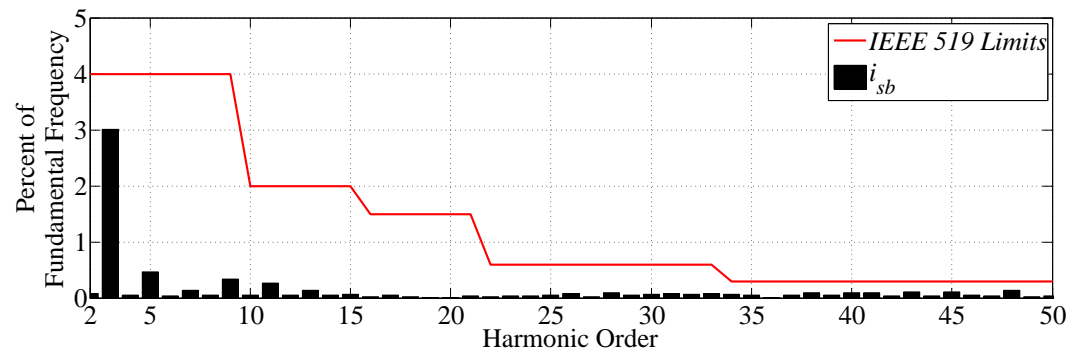
Source: Own authorship.

Figure 95 – DSPS compensation - Harmonic spectrum of source current - Neutral.
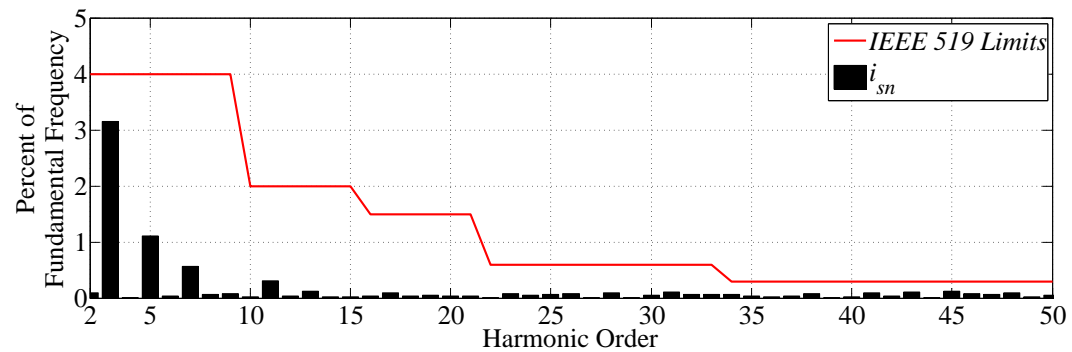
Source: Own authorship.

The information of effective values, harmonic distortion, PF measured in the power source and conduction losses during DSPS compensation are presented in Table 6. These data show the THD of currents was reduced significantly. The THD in phase *b*, which load current was sinusoidal, was increased in acceptable levels due to APF operation. The PF in phases *a* and *b* was increased to nearly the unity. Also, the unbalances in source currents is considerably small compared with load currents. The difference between the highest and the lowest rms values in source currents (*i.e.*, neutral and phase *b*, respectively) is less than 5 %, whereas the same index is 126 % for load currents (compared i_{Lb} versus i_{Ln}). Also, it is possible to observe that conduction losses are reduced to 2.638 W. These numbers represent a reduction of 11.23 % in conduction losses in comparison with 2.973 W of conduction losses observed in the load without compensation, as shown in Table 5.

Table 6 – DSPS compensation - Souce currents THD, rms values and PF.

Part of Circuit		rms	THD	PF	Loss
	Phase *a*	29.61 A	3.21 %	0.9958	0.876 W
Source	Phase *b*	29.04 A	3.43 %	0.9983	0.843 W
(DSPS)	Neutral	30.31 A	3.69 %	–	0.918 W
	Total	–	–	–	2.638 W

The two-phase instantaneous powers, in terms of $\alpha\beta$ quantities, provided by the power source during DSPS compensation are shown in Figure 96.

As all the imaginary power demanded by the load is provided by the APF in DSPS, the source imaginary power $q_{s2\phi}$ is nearly zero. The real power $p_{s2\phi}$ delivered by the source presents an average value and a relatively small oscillating component with twice the grid frequency (2ω). As previously mentioned, the oscillation observed in $p_{s2\phi}$ is related with the control loop of the APF DC-link voltage.

Figure 96 – DSPS compensation - Two-phase instantaneous powers fed by the source.
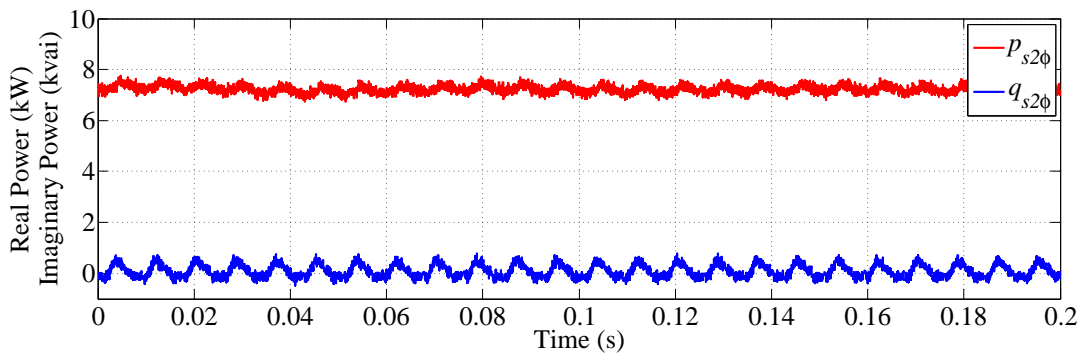
Source: Own authorship.

The powers provided by the source (p_{sab}) and demanded by the load (p_{Lab}), calculated in terms of *ab* voltages and currents, can be compared in Figure 97. It is observed that both have nearly the same average value and present an oscillation with twice the grid frequency, which is a natural condition for a two-phase three-wire circuit. However, due to the APF compensation, the oscillation in the power delivered from the mains is considerably reduced in comparison to the power demanded by the load.

Figure 97 – DSPS compensation - Source and load powers in terms of *ab* quantities.
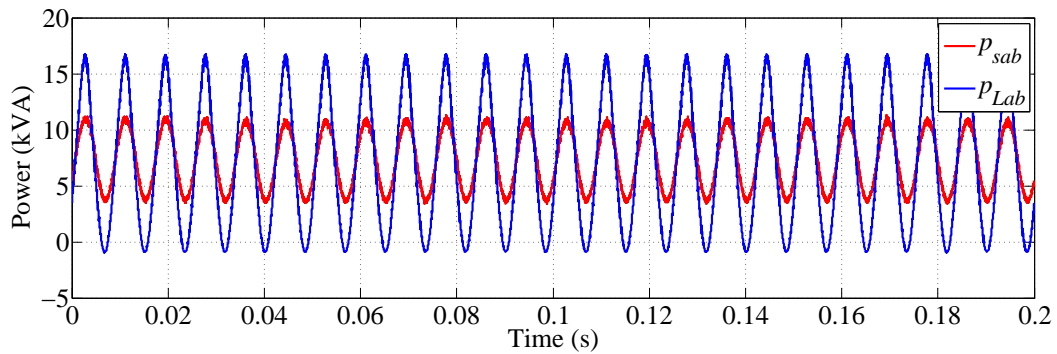
Source: Own authorship.

The difference between source and load powers is provided or absorbed by the $2\phi3w$ shunt APF. When $p_{sab} < p_{Lab}$, energy is taken from the DC-link and injected at PCC. On the other hand, when $p_{sab} > p_{Lab}$, the APF stores energy in the capacitor represented by C_f. This charge-discharge process can be observed in Figure 98, which illustrates the DC-bus voltage V_{dc} in the APF. This figure also shows that the DC voltage, in steady-state, oscillates around its reference value (400 V), which validates the proper working of the inner voltage control loop.

Figure 98 – DSPS compensation - APF DC-bus voltage.
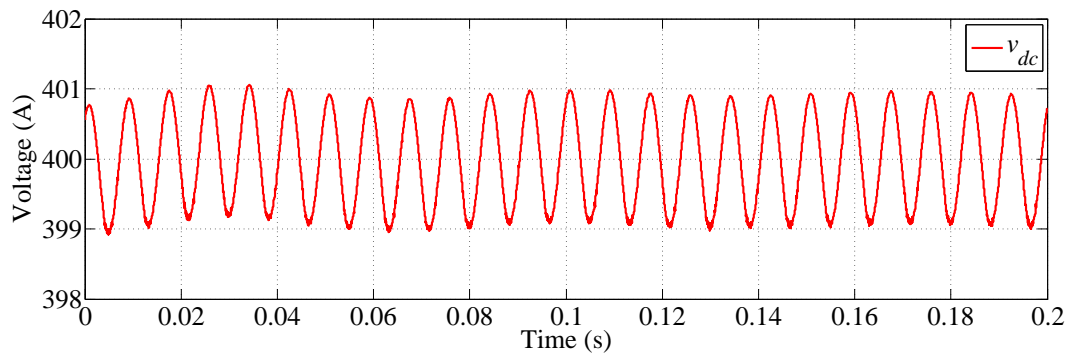
Source: Own authorship.

The results shown in this section demonstrated the effectiveness of the DSPS algorithm proposed in this work to control a two-phase three-wire shunt APF aiming to compensate current harmonics, load unbalances and reactive power. Next section presents and discusses simulation results obtained with ZNCS compensation.

5.2.4 SIMULATION RESULTS OF TWO-PHASE SHUNT COMPENSATION USING THE ZERO NEUTRAL CURRENT STRATEGY

The reference signals and currents synthesized by the $2\phi3w$ APF are illustrated in Figure 99, Figure 100 and Figure 101.

Figure 99 – ZNCS compensation - APF current and reference - Phase a.
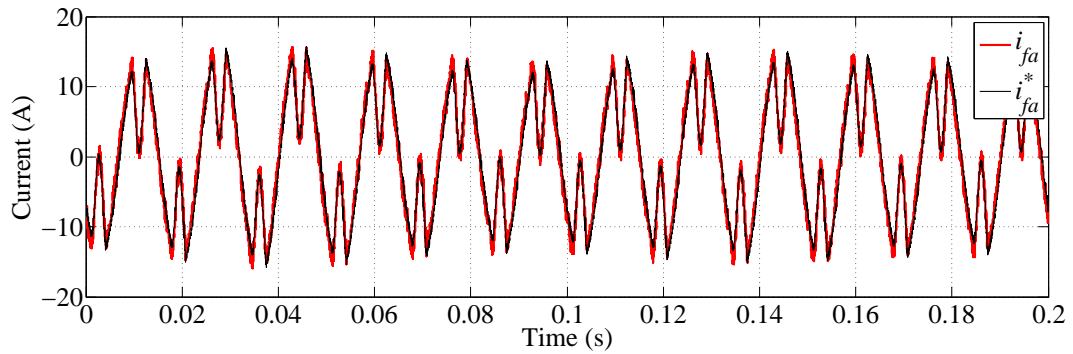
Source: Own authorship.

Figure 100 – ZNCS compensation - APF current and reference - Phase b.
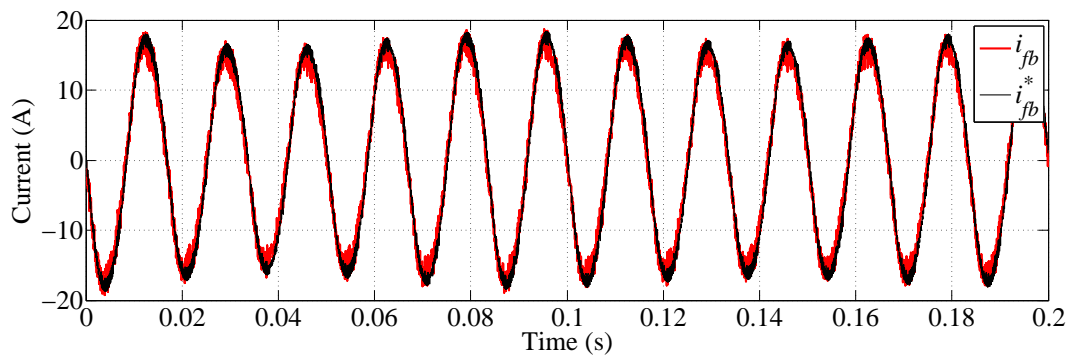
Source: Own authorship.

Figure 101 – ZNCS compensation - APF current and reference - Neutral.
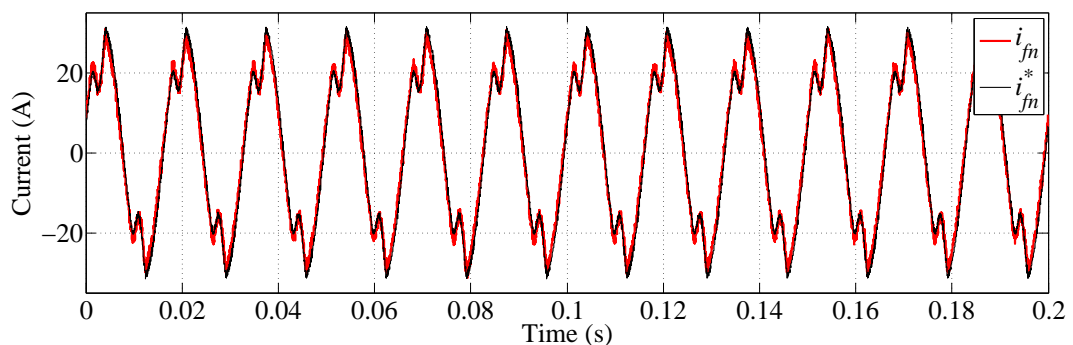
Source: Own authorship.

The compensated phase currents, those provided by the source when ZNCS is applied, are shown in Figure 102 and Figure 103. These currents are sinusoidal, but they are displaced in relation to phase voltages. As previously discussed, the objective in ZNCS is to make the compensated load to behave like a single-phase circuit connected phase-to-phase. Therefore, the source current in phase a is in phase with the line voltage v_{ab} as shown in Figure 104.

Figure 102 – ZNCS compensation - PCC phase voltage and source current - Phase a.
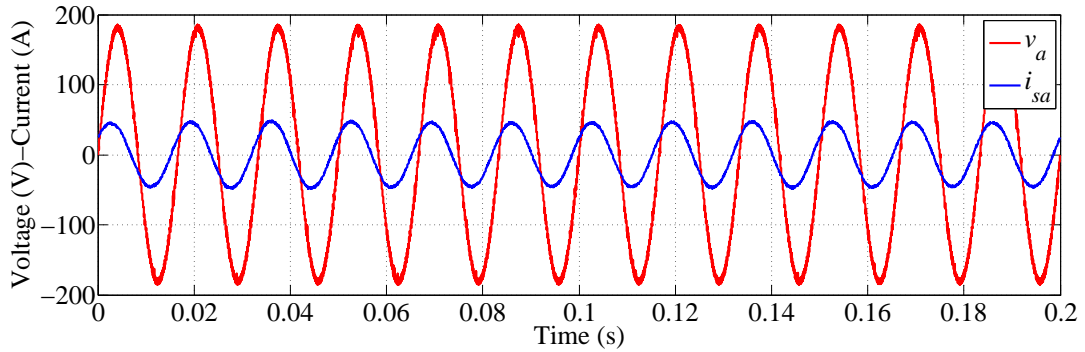
Source: Own authorship.

Figure 103 – ZNCS compensation - PCC phase voltage and source current - Phase b.
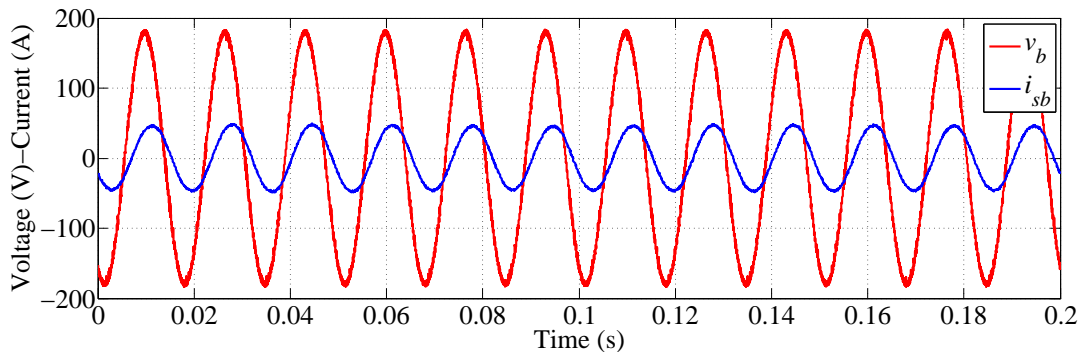
Source: Own authorship.

Figure 104 – ZNCS compensation - PCC line voltage and source current.
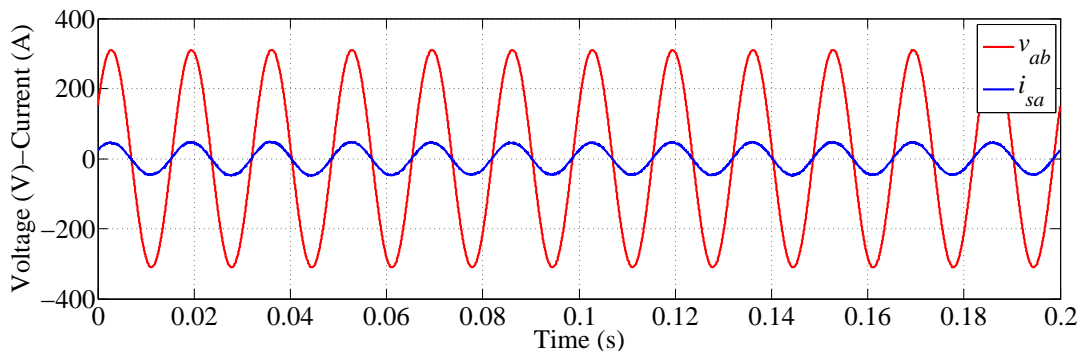
Source: Own authorship.

The current in phase *b* is the negative of i_{sa}, whereas the source neutral current is nearly zero, as shown in Figure 105. These results show the shunt APF, controlled according to the proposed ZNCS, could effectively mitigate the neutral current demanded from the source. Also, currents flowing from source phases are sinusoidal and with nearly the same amplitude, despite load nonlinearities and unbalances.

Figure 105 – ZNCS compensation - Source currents - Phases *a*, *b* and neutral.
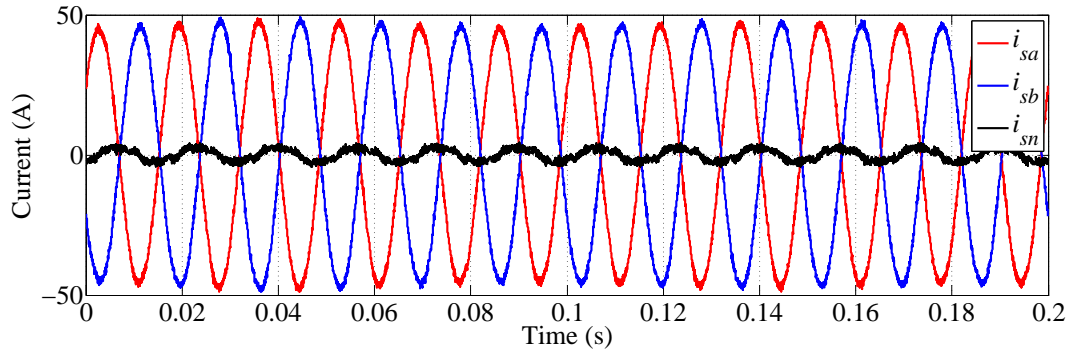
Source: Own authorship.

The harmonic spectrum of phase currents provided by the source in ZNCS compensation is shown in Figure 106 and Figure 107. The harmonic spectrum of the neutral current is not shown in this case because it is basically composed by high-frequency harmonics and switching noise. It can be observed that all harmonic components in i_{sa} and i_{sb} are below IEEE-519 recommended limits (IEEE, 2014).

Figure 106 – ZNCS compensation - Harmonic spectrum of source current - Phase *a*.
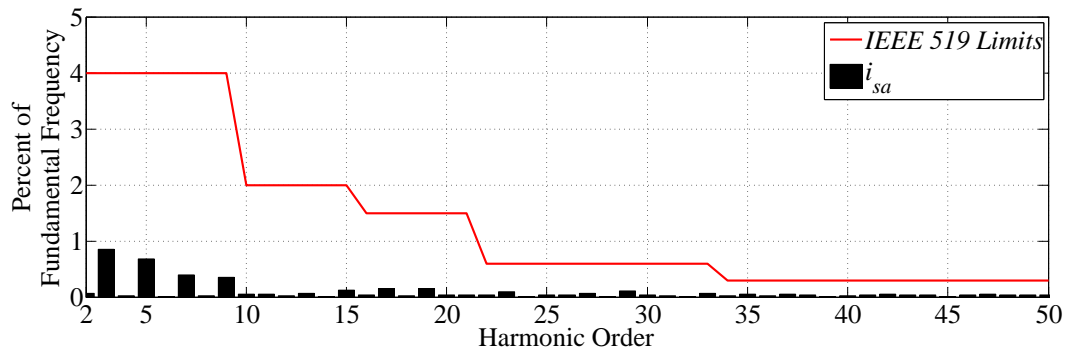
Source: Own authorship.

Figure 107 – ZNCS compensation - Harmonic spectrum of source current - Phase *b*.
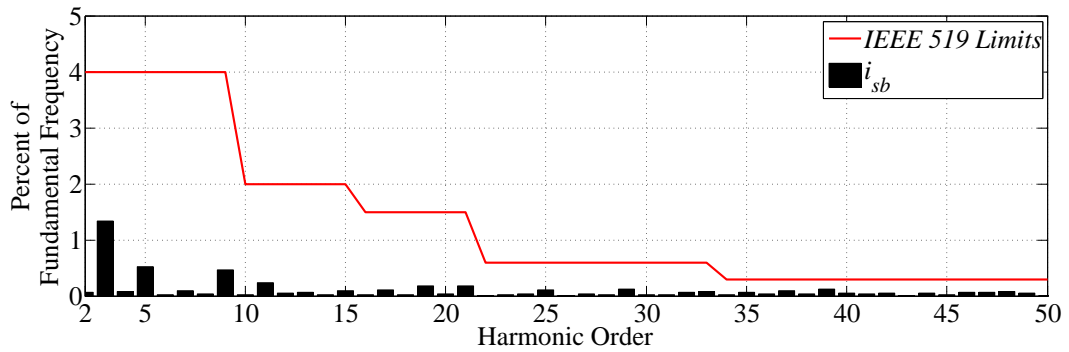
Source: Own authorship.

The two-phase instantaneous powers, defined in terms of $\alpha\beta$ voltages and currents, provided by the power source in ZNCS compensation are shown in Figure 108. It is interesting to observe that $p_{s2\phi}$ oscillates with twice the grid frequency around an average value, whereas the imaginary power $q_{s2\phi}$ oscillates with zero average.

Figure 108 – ZNCS compensation - Two-phase instantaneous powers fed by the source.
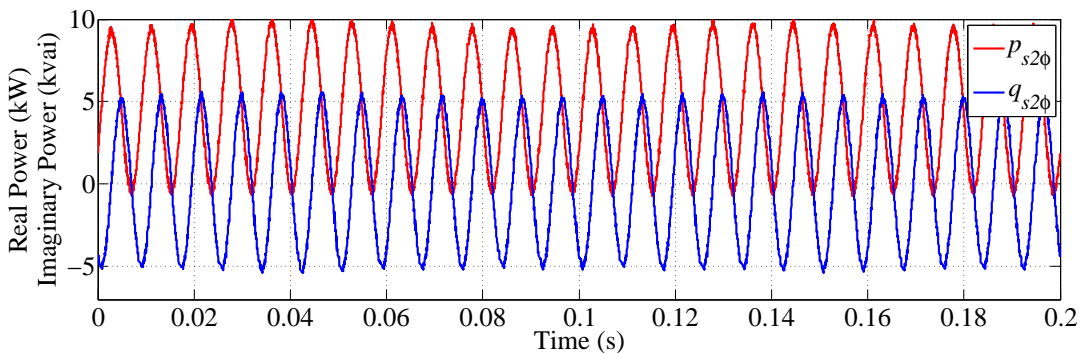
Source: Own authorship.

The load and source powers, calculated in *ab* reference frame, can be compared in Figure 109. It can be noticed that the compensated source power does not become negative, which happens during part of the period in load currents.

Figure 109 – ZNCS compensation - *ab* Power fed by the source.
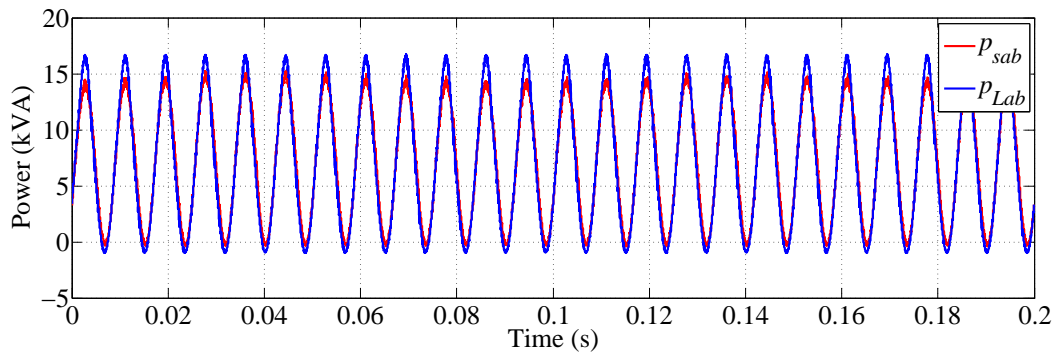
Source: Own authorship.

In this strategy, the 2ϕ3*w* APF absorbs power like single-phase circuit connected phase-to-phase at PCC. The waveform of the APF DC-bus voltage during ZNCS operation is illustrated in Figure 110. It can be observed a permanent 120 Hz oscillation. In this case, a low-frequency damped oscillation is also observed because, compared to the waveform shown in Figure 98, the DC-voltage control response in ZNCS is slower.

Figure 110 – ZNCS compensation - APF DC-bus voltage.
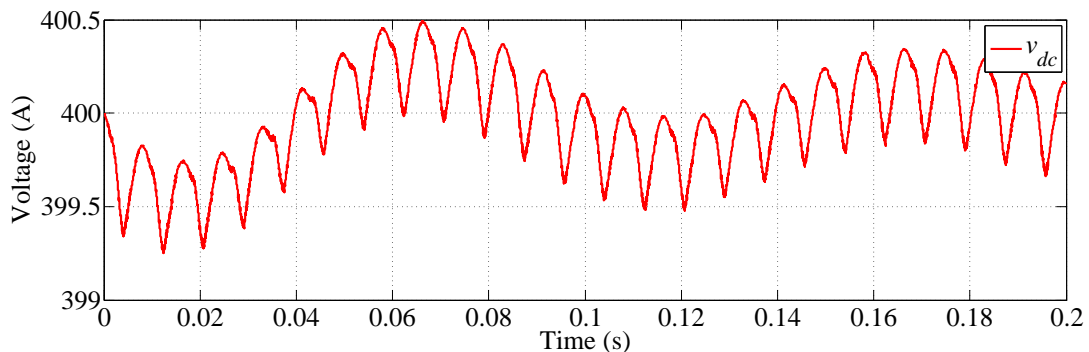
Source: Own authorship.

Finally, the simulation results obtained with ZNCS compensation are expressed numerically in Table 7. It can be observed the reduced THD of phase currents, as well as the nearly equal rms value. The neutral current is considerably small compared to the current flowing through source phases. The high THD of the neutral current is due to the reduced value of its fundamental frequency, since this current is mostly composed by residual harmonics and switching noise. For the ZNCS compensation, the PF is measured using current in phase *a* and the phase-to-phase voltage. The result shown in Table 7 confirms that the compensated source current is in phase with the phase-to-phase voltage. Also, the total conduction losses in ZNCS compensation are 27.35 % smaller than the losses observed in the load without compensation.

Table 7 – ZNCS compensation - Source currents THD, rms values and PF.

Part of Circuit		rms	THD	PF	Loss
Source (ZNCS)	Phase *a*	32.81 A	2.45 %	–	1.076 W
	Phase *b*	32.92 A	2.50 %	–	1.083 W
	Neutral	0.77 A	–	–	0.000 W
	Line *a–b*	–	–	0.9917	–
	Total	–	–	–	2.159 W

5.2.5 *COMPARISON OF COMPENSATION STRATEGY*

Previous sections showed the operation of a $2\phi3w$ shunt APF using two compensation strategies: DSPS and ZNCS. A comparison between the effects of these two compensation strategies was previously published by Furtado et al. (2015c). Aiming to illustrate the comparison of these compensation strategies in the context of this work, the simulation results presented in previous sections are repeated together in Table 8.

Table 8 – Load currents THD, rms values and PF.

Part of Circuit		rms	THD	PF	Loss
Phase *a*	Load	25.97 A	14.51 %	0.8543	0.674 W
	Source (DSPS)	29.61 A	3.21 %	0.9958	0.876 W
	Source (ZNCS)	32.81 A	2.45 %	–	1.076 W
Phase *b*	Load	43.88 A	0.10 %	0.7769	1.925 W
	Source (DSPS)	29.04 A	3.43 %	0.9983	0.843 W
	Source (ZNCS)	32.92 A	2.50 %	–	1.083 W
Neutral	Load	19.35 A	19.71 %	–	0.374 W
	Source (DSPS)	30.31 A	3.69 %	–	0.918 W
	Source (ZNCS)	0.77 A	–	–	0.000 W

Regarding some differences observed in compensation strategies, it can be seen that in ZNCS compensation, a higher phase current level is demanded from the source. On the other hand, the load flowing through the neutral in DSPS equals phase currents, which can cause power losses in the neutral conductor. However, it can be observed that both strategies could

reduce the THD of currents in phase a, which feeds a nonlinear load circuit, whereas the harmonic distortion in phase b was kept in acceptable levels. It is also shown that load unbalances were also compensated in both compensation strategies, since the current level in both source phases is nearly equal. Additionally, the PF seen by the source is close to the unity in both DSPS and ZNCS compensation.

This chapter described the system topology considered for studies in this research. Preliminary experimental results were presented aiming to validate the working principle of the proposed two-phase positive sequence detector based on the SOGI-PLL. Simulation results were also presented to show the effectiveness of the algorithms proposed to control a $2\phi3w$ shunt APF to compensate a load with nonlinear, reactive and unbalanced characteristics.

Next chapter presents the final discussions of this work, as well as the subjects proposed for future studies.

6 FINAL REMARKS AND FUTURE STUDIES

6.1 CONCLUSIONS

The main contribution of this research is the proposal of the use of two-phase three-wire power electronic converters for grid-connected applications of power conditioning. These converters may be useful to perform power conditioning functions in electrical installations fed by two phases and neutral derived from a three-phase four-wire distribution network. This kind of circuit topology is typically used for residential and small commercial consumers, which are present in large number in electric networks. Therefore, $2\phi3w$ power converters are an interesting resource for the integration of these consumers in a scenario of constant modernization of electric power networks.

In this context, this doctoral thesis proposed concepts for instantaneous power definitions for two-phase three-wire circuits derived from three-phase four-wire networks. A bibliography review discussed the definitions of instantaneous powers in three-phase and single-phase electric circuits, namely the *pq* Theory and the single-phase *pq* Theory. The review also discussed briefly the application of these concepts in algorithms for reference current calculation for electronic power conditioning equipment.

A linear transformation was proposed to represent two-phase voltages and currents in the orthogonal $\alpha\beta$ reference frame. The proposed two-phase powers are calculated in terms of instantaneous values of $\alpha\beta$ voltages and currents. A time-domain analysis was presented aiming to investigate the meaning of each two-phase instantaneous power component. The nature of $2\phi3w$ instantaneous powers were compared with the powers in the *pq* Theory and with those defined in the single-phase *pq* Theory. It was discussed that, in general terms, interactions between voltages and currents in the same frequency and phase sequence generate constant powers. On the other hand, interactions between voltages and currents with different frequencies and/or phase sequences produce oscillating power components. However, it could be observed that the interactions between zero-sequence components, including triplen harmonics, with components in the same and/or other frequencies may produce both constant and oscillating power parcels.

This is the main difference between the proposed $2\phi3w$ powers and those in the original form of the *pq* Theory.

It was also described the application of two-phase power definitions in the design of control algorithms conceived for $2\phi3w$ electronic power conditioners, specially for shunt active power filters. It was shown in this work that grid-connected $2\phi3w$ converters may be controlled to work according to two different strategies: Double Single-Phase Strategy (DSPS) and the Zero Neutral Current Strategy (ZNCS). In DSPS, $2\phi3w$ converter act as a superposition of two single-phase converters. Applied to shunt APF control, this strategy results in source phase currents with sinusoidal waveforms and in phase with each phase voltage. In ZNCS, $2\phi3w$ converters work as a single-phase converter connected phase-to-phase, with no neutral current demanded from the source. Applied to shunt APF control, ZNCS results in source phase currents with sinusoidal waveforms and in phase with each phase voltage.

A DSOGI-PLL-based $2\phi3w$ fundamental-frequency positive-sequence detector was developed for two-phase control algorithms. This detector is useful in the design of control systems for grid-connected converters. The algorithm was implemented in an laboratory prototype. Experimental results showed the system worked satisfactorily under real voltage distortion and imbalance conditions, despite the error caused existing by zero-sequence components.

A $2\phi3w$ MPC was designed to implement the current control loop for two-phase grid-connected converters. Simulation studies were presented to validate the proposed power concepts and their application in the design of a control system of a $2\phi3w$ shunt APF. The APF could provide harmonic currents and the reactive power demanded by the load, avoiding it to flow from the source. It was shown the considerable difference of THD and PF between load (without compensation) and (compensated) grid quantities. Furthermore, simulation studies have shown that the APF reduced two-phase imbalances, so that the source could provide currents with nearly the same amplitude in phases *a* and *b*. In ZNCS compensation, it was also shown that the compensated source current is nearly zero in the neutral conductor, as expected. Due to this feature, the control of active filters with ZNCS compensation is specially interesting for applications that aim to avoid or reduce zero-sequence voltage unbalances and their adverse effects in distribution systems and microgrids. Therefore, simulation results have shown the effectiveness of both DSPS and ZNCS for two-phase shunt compensation.

6.2 PUBLICATIONS

This section presents a list of submitted and published works during the development of this research.

6.2.1 JOURNAL PUBLICATIONS

FURTADO, P. C. de S.; RODRIGUES, M. C. B. P.; BRAGA, H. A. C.; BARBOSA, P. G. Two-phase three-wire shunt active power filter control by using the single-phase p-q theory. Revista Eletrônica de Potência. v. 19, n. 3, p. 303–311, August 2014.

6.2.2 CONFERENCE PUBLICATIONS

FURTADO, P. C. de S.; BARBOSA, P. G. Model predictive controller for two-phase three-wire grid-connected converters. In: 2019 IEEE 15th Brazilian Power Electronics Conference and 5th Southern Power Electronics Conference (COBEP/SPEC) (Accepted for publication). 2019. p. 1–5.

RODRIGUES, M. C. B. P.; FURTADO, P. C. de S.; RODRIGUES, C. R. B. S.; FERREIRA, R. A. F.; FERREIRA, A. A. ; BARBOSA, P. G. ; BRAGA, H. A. C.; Development of a small-signal model for a two-phase three-wire active power filter. In: 2017 Brazilian Power Electronics Conference (COBEP), 2017. p. 1–7.

FURTADO, P. C. de S.; FOGLI, G. A.; ALMEIDA, P. M.; BARBOSA, P. G.; OLIVEIRA, J. G. Topology and control of a two-phase residential pv system with load compensation capability. In: 24th International Symposium on Industrial Electronics (ISIE). 2015. p. 1127–1132.

FURTADO, P. C. de S.; BARBOSA, P. G.; RODRIGUES, M. C. B. P. A shunt active compensation strategy with zero neutral current in two-phase three-wire systems. In: IEEE PowerTech Eidhoven. 2015. p. 1–5.

FURTADO, P. C. de S.; RODRIGUES, M. C. B. P.; BARBOSA, P. G.; Adaptation of the instantaneous power theory for two-Phase three-wire systems and its application in shunt active power filters. In: 2015 IEEE 13th Brazilian Power Electronics Conference and 1st Southern Power Electronics Conference (COBEP/SPEC). 2015. p. 1–5.

FURTADO, P. C. de S.; RODRIGUES, M. C. B. P.; BARBOSA, P. G.; A comparison of two-phase three-wire shunt compensation strategies. In: 2015 IEEE 13th Brazilian Power Electronics Conference and 1st Southern Power Electronics Conference (COBEP/SPEC). 2015. p. 1–5.

FURTADO, P. C. de S.; RODRIGUES, M. C. B. P.; BRAGA, H. A. C.; BARBOSA, P. G. Two-phase, three-wire shunt active power filter using the single-phase P-Q theory. In: 12th Brazilian Power Electronics Conference (COBEP). 2013. p. 1245–1250.

RODRIGUES, M. C. B. P.; FURTADO, P. C. de S.; RODRIGUES, R. B. S.; FERREIRA, A. A.; BARBOSA, P. G.; Development of a small-signal model for a two-phase three-wire

active power filter. Accepted for Publication In: 2017 IEEE 13th Brazilian Power Electronics Conference(COBEP). 2017. p. 1–5.

6.3 *PROPOSALS FOR FUTURE STUDIES*

Aiming to give continuity to this research, the following studies are proposed:

i. To make field measurements of zero-sequence and triplen harmonic voltages in real distribution network, aiming evaluate the error caused by zero-sequence components in two-phase powers and to measure the influence of these components in the adapted $2\phi 3w$ positive-sequence detector;

ii. To compare proposed compensation strategies DSPS ZNCS considering APF current levels, the total power processed and dc-link voltage oscillation, for example. These studies can be useful to limit the amount of power which can be processed by two-phase power conditioners;

iii. To improve the inner control loop aiming to reduce the oscillation in the APF DC-bus voltage;

iv. To implement the proposed control systems in a new laboratory setup and obtain further experimental results;

v. To present experimental results comprising active power injection applications, as well as transient results;

REFERENCES

ABNT, Associação Brasileira de Normas Técnicas. Abnt nbr 5410:2004 - instalações elétricas de baixa tensão. p. 1–209, 2008.

AES ELETROPAULO. Fornecimento de energia elétrica em tensão secundária de distribuição (lig-bt). (Online) Available at: <https://www.aeseletropaulo.com.br/padroes-e-normas-tecnicas/manuais-normas-tecnicas-e-de-seguranca/Documents/LIG BT 2014/LIG BT 12° edição - 2014.pdf>. Access on: 31 March 2016, 2014.

AKAGI, H. Active harmonic filters. *Proceedings of the IEEE*, v. 93, n. 12, p. 2128–2141, Dec 2005.

AKAGI, H.; KANAZAWA, Y.; NABAE, A. Generalized theory of the instantaneous reactive power in three-phase circuits. In: *International Power Electronics Conference (IPEC)*. 1983. v. 83, p. 1375–1386.

AKAGI, H.; KANAZAWA, Y.; NABAE, A. Instantaneous reactive power compensators comprising switching devices without energy storage components. *IEEE Transactions on Industry Applications*, n. 3, p. 625–630, 1984.

AKAGI, H.; WATANABE, E. H.; AREDES, M. *Instantaneous power theory and applications to power conditioning*. : John Wiley & Sons, 2007.

ALAM, M. J. E.; MUTTAQI, K. M.; SUTANTO, D. Effectiveness of traditional mitigation strategies for neutral current and voltage problems under high penetration of rooftop pv. In: *2013 IEEE Power Energy Society General Meeting*. 2013. p. 1–5.

ALMEIDA, P. M. de. *Modelagem e controle de conversores fonte de tensão utilizados em sistemas de geração fotovoltaicos conectados à rede elétrica de distribuição*. 2011.

AMPLA. Fornecimento de energia elétrica em tensão secundária - padrão de fornecimento de energia elétrica. (Online) Available at: <https://www.ampla.com/media/202870/fornecimento de energia elétrica em tensão secundária.docx.pdf>. Access on: 31 March 2016, 2011.

ANEEL, Agência Nacional de Energia Elétrica. Resolução normativa no.482, de 17 de abril de 2012. ANEEL, 2012.

ANEEL, P. d. D. d. E. Elétrica no sistema elétrico nacional–prodist: Módulo 8-qualidade de energia elétrica. *Revisão*, v. 5, p. 76, 2007.

ANTONIOU, D.; TZIMAS, A.; ROWLAND, S. M. Transition from alternating current to direct current low voltage distribution networks. *IET Generation, Transmission & Distribution*, v. 9, n. 12, p. 1391–1401, 2015.

ASIMINOAEL, L.; BLAABJERG, F.; HANSEN, S. Detection is key - harmonic detection methods for active power filter applications. *IEEE Industry Applications Magazine*, v. 13, n. 4, p. 22–33, 2007.

BALDA, J. C. et al. Measurements of neutral currents and voltages on a distribution feeder. *IEEE Transactions on Power Delivery*, v. 12, n. 4, p. 1799–1804, Oct 1997.

BLAABJERG, F.; CHEN, Z.; KJAER, S. Power electronics as efficient interface in dispersed power generation systems. *IEEE Transactions on Power Electronics*, v. 19, n. 5, p. 1184–1194, Sept 2004.

BOLLEN, M. H. et al. Power quality aspects of smart grids. In: *International conference on renewable energies and power quality (ICREPQ'10)*. 2010. p. 1–6.

BUENO, H. et al. Shunt active power filter for harmonic compensation of two-phase nonlinear loads. In: *IEEE PES Transmission Distribution Conference and Exposition - Latin America (PES T D-LA)*. 2014. p. 1–6.

BUSO, S.; MATTAVELLI, P. *Digital control in power electronics*. : Morgan & Claypool, 2006.

CELG-D, CELG Distribuição. Fornecimento de energia elétrica em tensão secundária de distribuição - revisão 3. (Online) Available at: <https://www.celg.com.br/arquivos/dadosTecnicos/normasTecnicas/NTC04.pdf>. Access on: 07 April 2016, 2008.

CEMIG, Companhia Energética de Minas Gerais. Norma de distribuição 5.1: Fornecimento de energia elétrica em tensão secundária - rede de distribuição aérea - edificações individuais. Companhia Energética de Minas Gerais, 2013.

CHAKRABORTY, S.; SIMÕES, M. G.; KRAMER, W. E. *Power electronics for renewable and distributed energy systems*. : Springer, 2013.

CLASTRES, C. Smart grids: another step towards competition, energy security and climate change objectives. *Energy Policy*, v. 39, n. 9, p. 5399–5408, 2011.

COLAK, I. et al. A comparative study of harmonic extraction methods for single phase shunt active power filter. In: *International Conference on Power Engineering, Energy and Electrical Drives (POWERENG)*. 2011. p. 1–4.

COPEL, Companhia Paraense de Energia. Normas técnicas copel: fornecimento em tensão secundária de distribuição (ntc 901100). (Online) Available at: <http://www.copel.com/hpcopel/normas/ntcarquivos.nsf/4F0C269A3EBCF33B0325 7F800070D966/$FILE/NTC 901100 Fornecimento em Tensão Secundária.pdf>. Access on: 31 March 2016, 2016.

CORTÉS, P. et al. Predictive current control strategy with imposed load current spectrum. *IEEE Transactions on power Electronics*, v. 23, n. 2, p. 612–618, 2008.

CPFL, Companhia Paulista de Força e Luz. Fornecimento em tensão secundária de distribuição. CPFL Energia, 2012.

EMADI, A. Transportation 2.0. *IEEE Power and Energy Magazine*, v. 9, n. 4, p. 18–29, July 2011.

EMADI, A.; NASIRI, A.; BEKIAROV, S. B. *Uninterrupted power supplies and active power filters*. : CRC Press, 2005.

ESSENTIAL ENERGY. Supply standards: electricity supply standard. (Online) Available at: <https://www.essentialenergy.com.au/asset/cms/pdf/aasp/CEOP8026.pdf>. Access on: 30 March 2016, 2011.

FAJARDO, M. et al. Two-phase active power filter direct current control with capacitor voltages estimation and balance. In: *IEEE Workshop on Power Electronics and Power Quality Applications (PEPQA)*. 2015. p. 1–6.

FANG, X. et al. Smart grid - the new and improved power grid: a survey. *IEEE Communications Surveys Tutorials*, v. 14, n. 4, p. 944–980, Apr 2012.

FARHANGI, H. The path of the smart grid. *IEEE Power and Energy Magazine*, v. 8, n. 1, p. 18–28, 2010.

FERREIRA, A. A. *Sistema supervisório de gestão de múltiplas fontes de suprimento para aplicações em veículos elétricos*. Tese (Doutorado) — Universidade Estadual de Campinas, 2007.

FOGLI, G. A. *Integração de um grupo motor gerador diesel em uma rede secundária de distribuição através de um conversor estático de tensão*. Dissertação (Mestrado) — Federal University of Juiz de Fora, 2014.

FOGLI, G. A. et al. Sliding mode control of a shunt active power filter with indirect current measurement. In: *2015 IEEE 13th Brazilian Power Electronics Conference and 1st Southern Power Electronics Conference (COBEP/SPEC)*. 2015. p. 1–5.

FORTESCUE, C. L. Method of symmetrical co-ordinates applied to the solution of polyphase networks. *Transactions of the American Institute of Electrical Engineers*, v. 37, n. 2, p. 1027–1140, 1918.

FURTADO, P. C. de S. *Controle de um filtro ativo de potência bifásico a três fios utilizando a teoria p-q monofásica*. Dissertação (Mestrado) — Federal University of Juiz de Fora, 2014b.

FURTADO, P. C. de S.; BARBOSA, P. G. Model predictive controller for two-phase three-wire grid-connected converters. *2019 IEEE 15th Brazilian Power Electronics Conference and 5th Southern Power Electronics Conference (COBEP/SPEC) (Accepted for publication)*, 2019.

FURTADO, P. C. de S. et al. Topology and control of a two-phase residential pv system with load compensation capability. In: *The 24th International Symposium on Industrial Electronics (ISIE)*. 2015a. p. 1127–1132.

FURTADO, P. C. de S.; RODRIGUES, M. do C. B. P.; BARBOSA, P. G. A shunt active compensation strategy with zero neutral current in two-phase three-wire systems. In: *IEEE Eindhoven PowerTech*. 2015b. p. 1–5.

FURTADO, P. C. de S.; RODRIGUES, M. do C. B. P.; BARBOSA, P. G. Adaptation of the instantaneous power theory for two-phase three-wire systems and its application in shunt active power filters. In: *2015 IEEE 13th Brazilian Power Electronics Conference and 1st Southern Power Electronics Conference (COBEP/SPEC)*. 2015d. p. 1–5.

FURTADO, P. C. de S. et al. Two-phase, three-wire shunt active power filter using the single-phase p-q theory. In: *Brazilian Power Electronics Conference (COBEP)*. 2013. p. 1245–1250.

FURTADO, P. C. de S. et al. Two-phase three-wire shunt active power filter control by using the single-phase p-q theory. *Eletrônica de Potência*, v. 19, n. 3, p. 303–311, Aug 2014.

FURTADO, P. C. de S. et al. A comparison of two-phase three-wire shunt compensation strategies. In: *2015 IEEE 13th Brazilian Power Electronics Conference and 1st Southern Power Electronics Conference (COBEP/SPEC)*. 2015c. p. 1–6.

GALUS, M. D. et al. The role of electric vehicles in smart grids. *Wiley Interdisciplinary Reviews: Energy and Environment*, v. 2, n. 4, p. 384–400, 2013.

GIL-DE-CASTRO, A. et al. Harmonics from household equipment and different lamp technologies. In: *The 8th International Conference on Compatibility and Power Electronics (CPE)*. 2013. p. 1–6.

GOLESTAN, S.; GUERRERO, J.; VASQUEZ, J. Single-phase plls: A review of recent advances. *IEEE Transactions on Power Electronics*, PP, n. 99, p. 1–1, 2017b.

GOLESTAN, S.; GUERRERO, J. M.; VASQUEZ, J. C. Three-phase plls: A review of recent advances. *IEEE Transactions on Power Electronics*, v. 32, n. 3, p. 1894–1907, March 2017.

GRAINGER, J. J.; STEVENSON, W. D. *Power system analysis*. : McGraw-Hill, 1994.

GUERRERO, J. M. et al. Distributed generation: toward a new energy paradigm. *IEEE Industrial Electronics Magazine*, v. 1, n. 4, p. 52–64, 2010.

GUPTA, A.; JAIN, D.; DAHIYA, S. Neutral current compensation techniques in autonomous wind energy sources. *International Journal of Energy and Environmental Engineering*, v. 5, n. 4, p. 357–363, 2014.

HAQUE, M. T. Single-phase pq theory. In: *IEEE 33rd Annual Power Electronics Specialists Conference (PESC'02)*. 2002. v. 4, p. 1815–1820.

HAQUE, M. T. Single-phase pq theory for active filters. In: *IEEE Region 10 Conference on Computers, Communications, Control and Power Engineering (TENCON'02)*. 2002. v. 3, p. 1941–1944.

HAQUE, M. T.; ISE, T. Implementation of single-phase pq theory. In: IEEE. *Power Conversion Conference (PCC-Osaka 2002)*. 2002. v. 2, p. 761–765.

HARDIE, S.; WATSON, N. The effect of new residential appliances on power quality. In: *The 20th Australasian Universities Power Engineering Conference (AUPEC)*. 2010. p. 1–6.

HATZIARGYRIOU, N. et al. Microgrids. *IEEE Power and Energy Magazine*, v. 5, n. 4, p. 78–94, 2007.

HOJABRI, H.; MOKHTARI, H. A new power quality enhancement method for two-phase loads. In: *International Conference on Power Electronics, Drives and Energy Systems (PEDES)*. 2006. p. 1–5.

IEA, International Energy Agency. Technology roadmap: electric and plug-in hybrid electric vehicles. (Online) Available at: <http://www.iea.org/publications/freepublications/publication/EV_PHEV_Roadmap.pdf>. Access on: 16 February 2016, 2011.

IEEE, Standards Association. Ieee recommended practice and requirements for harmonic control in electrical power systems - redline. p. 1–213, 2014.

JAALAM, N. et al. A comprehensive review of synchronization methods for grid-connected converters of renewable energy source. *Renewable and Sustainable Energy Reviews*, v. 59, p. 1471 – 1481, 2016.

JAVAID, M. S. et al. Direct control of three-phase smart load for neutral current mitigation. In: *2016 19th International Multi-Topic Conference (INMIC)*. 2016. p. 1–6.

JUSTO, J. J. et al. Ac-microgrids versus dc-microgrids with distributed energy resources: a review. *Renewable and Sustainable Energy Reviews*, v. 24, p. 387–405, 2013.

KHADKIKAR, V.; CHANDRA, A.; SINGH, B. N. Generalised single-phase pq theory for active power filtering: simulation and dsp-based experimental investigation. *Power Electronics, IET*, v. 2, n. 1, p. 67–78, 2009.

KIM, H.; AKAGI, H. The instantaneous power theory based on mapping matrices in three-phase four-wire systems. In: *Power Conversion Conference (PCC Nagaoka 1997)*. 1997. v. 1, p. 361–366.

KIM, H.; AKAGI, H. The instantaneous power theory on the rotating p-q-r reference frames. In: *IEEE International Conference on Power Electronics and Drive Systems (PEDS'99)*. 1999. v. 1, p. 422–427.

KOOHI-KAMALI, S. et al. Emergence of energy storage technologies as the solution for reliable operation of smart power systems: a review. *Renewable and Sustainable Energy Reviews*, v. 25, p. 135–165, 2013.

LAM, C. S.; WONG, M. C.; HAN, Y. D. Hysteresis current control of hybrid active power filters. *IET Power Electronics*, v. 5, n. 7, p. 1175–1187, August 2012. ISSN 1755-4535.

LIGHT. Regulamentação para fornecimento de energia elétrica a consumidores em baixa tensão (recon-bt). (Online) Available at: <http://www.light.com.br/Repositorio/Recon/RECON_BT_ERRATA_OUTUBRO_2014_FINAL.pdf>. Access on: 31 March 2016, 2014.

LIU, J.; YANG, J.; WANG, Z. A new approach for single-phase harmonic current detecting and its application in a hybrid active power filter. In: *The 25th Annual Conference of the IEEE Industrial Electronics Society (IECON'99)*. 1999. v. 2, p. 849–854.

MARAFÃO, F. P. et al. A influência da referência de tensão na avaliação de indicadores de qualidade de energia. *IEEE Latin America Transactions*, p. 81–88, 2008.

MOHAN, N.; UNDELAND, T.; ROBBINS, W. P. *Power Electronics: Converters, Applications and Design*. 2nd. ed. : John Wiley & Sons Inc., 1995.

MONFARED, M.; GOLESTAN, S. Control strategies for single-phase grid integration of small-scale renewable energy sources: A review. *Renewable and Sustainable Energy Reviews*, v. 16, n. 7, p. 4982–4993, 2012.

NEENAN, B.; HEMPHILL, R. C. Societal benefits of smart metering investments. *The Electricity Journal*, v. 21, n. 8, p. 32–45, 2008.

NOROOZIAN, R.; GHAREHPETIAN, G. B. An investigation on combined operation of active power filter with photovoltaic arrays. *International Journal of Electrical Power & Energy Systems*, v. 46, p. 392–399, 2013.

PAREDES, H. K. M. *Influência do referencial de tensão na avaliação da qualidade de energia elétrica*. 2006.

PENG, F. Z.; LAI, J.-S. Generalized instantaneous reactive power theory for three-phase power systems. *IEEE Transactions on Instrumentation and Measurement*, v. 45, n. 1, p. 293–297, 1996.

POWERWATER CORPORATION. Np007: Service rules. (Online) Available at: <https://www.powerwater.com.au/__data/assets/pdf_file/0013/13531/qdoc2008_171_ power_networks_np_007_service_rules.pdf>. Access on: 30 March 2016, 2008.

QASIM, M.; KHADKIKAR, V. Application of artificial neural networks for shunt active power filter control. *IEEE Transactions on Industrial Informatics*, v. 10, n. 3, p. 1765–1774, Aug 2014.

RIBEIRO, P. F. et al. Energy storage systems for advanced power applications. *Proceedings of the IEEE*, v. 89, n. 12, p. 1744–1756, Dec 2001.

RICHARDSON, D. B. Electric vehicles and the electric grid: a review of modeling approaches, impacts, and renewable energy integration. *Renewable and Sustainable Energy Reviews*, v. 19, p. 247–254, 2013.

ROBERTS, B. P.; SANDBERG, C. The role of energy storage in development of smart grids. *Proceedings of the IEEE*, v. 99, n. 6, p. 1139–1144, 2011.

RODRIGUES, M. do C. B. P. *Integração de um filtro ativo de potência monofásico e bifásico ao sistema de propulsão de um veículo elétrico*. Tese (Doutorado) — Universidade Federal de Juiz de Fora, 2014.

RODRIGUES, M. do C. B. P. et al. Conexão de veículos elétricos à rede de energia elétrica para recarga de baterias: uma visão geral. *Eletrônica de Potência*, v. 19, n. 2, p. 194–207, May 2014.

RODRIGUEZ, J.; CORTES, P. *Predictive control of power converters and electrical drives*. : John Wiley & Sons, 2012.

RODRIGUEZ, J. et al. Predictive current control of a voltage source inverter. *IEEE Transactions on Industrial Electronics*, v. 54, n. 1, p. 495–503, Feb 2007.

RODRIGUEZ, P. et al. New positive-sequence voltage detector for grid synchronization of power converters under faulty grid conditions. In: *Power Electronics Specialists Conference*. 2006. p. 1–7.

SAITOU, M.; SHIMIZU, T. Generalized theory of instantaneous active and reactive powers in single-phase circuits based on hilbert transform. In: *IEEE 33rd Annual Power Electronics Specialists Conference (PESC'02)*. 2002. v. 3, p. 1419–1424.

SHORT, T. A. *Electric power distribution handbook*. : CRC press, 2014.

SINGH, B.; AL-HADDAD, K.; CHANDRA, A. A review of active filters for power quality improvement. *IEEE Transactions on Industrial Electronics*, v. 46, n. 5, p. 960–971, Oct 1999.

SREENIVASARAO, D.; AGARWAL, P.; DAS, B. Neutral current compensation in three-phase, four-wire systems: A review. *Electric Power Systems Research*, Elsevier, v. 86, p. 170–180, 2012.

TANAKA, T. et al. Smart charger for electric vehicles with power-quality compensator on single-phase three-wire distribution feeders. *IEEE Transactions on Industry Applications*, v. 49, n. 6, p. 2628–2635, 2013.

TEODORESCU, R.; LISERRE, M.; RODRIGUEZ, P. *Grid converters for photovoltaic and wind power systems*. : John Wiley & Sons, 2011.

U.S. Department of Energy. Smart grid. (Online) Available at: <http://energy.gov/oe/services/technology-development/smart-grid>. Access on: 21 January, 2016.

USTUN, T. S.; OZANSOY, C.; ZAYEGH, A. Recent developments in microgrids and example cases around the world: a review. *Renewable and Sustainable Energy Reviews*, v. 15, n. 8, p. 4030–4041, 2011.

VAZQUEZ, S. et al. Model predictive control with constant switching frequency using a discrete space vector modulation with virtual state vectors. In: IEEE. *2009 IEEE International Conference on Industrial Technology*. 2009. p. 1–6.

VAZQUEZ, S. et al. Energy storage systems for transport and grid applications. *IEEE Transactions on Industrial Electronics*, v. 57, n. 12, p. 3881–3895, Dec 2010.

WATANABE, E.; STEPHAN, R.; AREDES, M. New concepts of instantaneous active and reactive powers in electrical systems with generic loads. *IEEE Transactions on Power Delivery*, v. 8, n. 2, p. 697–703, abr. 1993.

WATSON, N. R.; SCOTT, T. L.; HIRSCH, S. Implications for distribution networks of high penetration of compact fluorescent lamps. *IEEE Transactions on Power Delivery*, v. 24, n. 3, p. 1521–1528, July 2009.

WESTERN POWER DISTRIBUTION AU; HORIZON POWER AU. Western australian distribution connections manual. (Online) Available at: <http://www.westernpower.com.au/documents/WA_Distribution_Connections_Manual.pdf>. Access on: 30 March 2016, 2015.

WESTERN POWER DISTRIBUTION UK. Information for electrical installers. (Online) Available at: <https://www.westernpower.co.uk/Connections/Information-for-Electrical-Installers.aspx>. Access on: 30 March 2016, 2016.

WISCONSIN ELECTRIC POWER COMPANY. Rate book for electric service. (Online) Available at: <http://www.dleg.state.mi.us/mpsc/electric/ratebooks/wisconsinelectric/we3cur.pdf>. Access on: 30 March 2016, 2012.

WU, C. et al. A negative sequence compensation method based on a two-phase three-wire converter for a high-speed railway traction power supply system. *IEEE Transactions on Power Electronics*, v. 27, n. 2, p. 706–717, Feb 2012.

YAZDANI, A.; IRAVANI, R. *Voltage-sourced converters in power systems*. : John Wiley & Sons, 2010.

YILMAZ, M.; KREIN, P. Review of battery charger topologies, charging power levels, and infrastructure for plug-in electric and hybrid vehicles. *IEEE Transactions on Power Electronics*, v. 28, n. 5, p. 2151–2169, May 2013.

YILMAZ, M.; KREIN, P. Review of the impact of vehicle-to-grid technologies on distribution systems and utility interfaces. *IEEE Transactions on Power Electronics*, v. 28, n. 12, p. 5673–5689, Dec 2013.

YU, X. et al. The new frontier of smart grids. *IEEE Industrial Electronics Magazine*, v. 5, n. 3, p. 49–63, Sept 2011.

YUEH, T. et al. The reverse zero-sequence current compensation strategy for back-to-back active power conditioners. In: *2016 IEEE Energy Conversion Congress and Exposition (ECCE)*. 2016. p. 1–6.

APPENDIX A – SINGLE-PHASE INSTANTANEOUS POWERS UNDER DISTORTED VOLTAGE AND CURRENT

$$
\begin{aligned}
\bar{p}_{1\phi} = \; & +V_1 I_1 \cos\left(\phi_{i_1} - \phi_{v_1}\right) + V_2 I_2 \cos\left(\phi_{i_2} - \phi_{v_2}\right) + V_3 I_3 \cos\left(\phi_{v_3} - \phi_{i_3}\right) \\
& +V_4 I_4 \cos\left(\phi_{i_4} - \phi_{v_4}\right) + V_5 I_5 \cos\left(\phi_{v_5} - \phi_{i_6}\right) \dots
\end{aligned}
$$

$$
\begin{aligned}
\tilde{p}_{1\phi} = \; & +\tfrac{1}{2} V_1 I_2 \sin\left(\omega t - \phi_{v_1} + \phi_{i_2}\right) + \tfrac{1}{2} V_1 I_2 \cos\left(\omega t - \phi_{v_1} + \phi_{i_2}\right) \\
& +\tfrac{1}{2} V_1 I_2 \sin\left(3\omega t + \phi_{v_1} + \phi_{i_2}\right) - \tfrac{1}{2} V_1 I_2 \cos\left(3\omega t + \phi_{v_1} + \phi_{i_2}\right) \\
& -V_1 I_3 \cos\left(4\omega t + \phi_{v_1} + \phi_{i_3}\right) \\
& -\tfrac{1}{2} V_1 I_4 \sin\left(3\omega t - \phi_{v_1} + \phi_{i_4}\right) + \tfrac{1}{2} V_1 I_4 \cos\left(3\omega t - \phi_{v_1} + \phi_{i_4}\right) \\
& -\tfrac{1}{2} V_1 I_4 \sin\left(5\omega t + \phi_{v_1} + \phi_{i_4}\right) - \tfrac{1}{2} V_1 I_4 \cos\left(5\omega t + \phi_{v_1} + \phi_{i_4}\right) \\
& +V_1 I_5 \cos\left(4\omega t - \phi_{v_1} + \phi_{i_6}\right) \\
& +\tfrac{1}{2} V_1 I_6 \sin\left(5\omega t - \phi_{v_1} + \phi_{i_6}\right) + \tfrac{1}{2} V_1 I_6 \cos\left(5\omega t - \phi_{v_1} + \phi_{i_6}\right) \\
& +\tfrac{1}{2} V_1 I_6 \sin\left(7\omega t + \phi_{v_1} + \phi_{i_6}\right) - \tfrac{1}{2} V_1 I_6 \cos\left(7\omega t + \phi_{v_1} + \phi_{i_6}\right) \\
& -V_1 I_7 \cos\left(8\omega t + \phi_{v_1} + \phi_{i_7}\right) \\
& -\tfrac{1}{2} V_1 I_8 \sin\left(7\omega t - \phi_{v_1} + \phi_{i_8}\right) + \tfrac{1}{2} V_1 I_8 \cos\left(7\omega t - \phi_{v_1} + \phi_{i_8}\right) \\
& -\tfrac{1}{2} V_1 I_8 \sin\left(9\omega t + \phi_{v_1} + \phi_{i_8}\right) - \tfrac{1}{2} V_1 I_8 \cos\left(9\omega t + \phi_{v_1} + \phi_{i_8}\right) \\
& +V_1 I_9 \cos\left(8\omega t - \phi_{v_1} + \phi_{i_9}\right) \dots \\[6pt]
& +\tfrac{1}{2} V_2 I_1 \sin\left(\omega t + \phi_{v_2} - \phi_{i_1}\right) + \tfrac{1}{2} V_2 I_1 \cos\left(\omega t + \phi_{v_2} - \phi_{i_1}\right) \\
& +\tfrac{1}{2} V_2 I_1 \sin\left(3\omega t + \phi_{v_2} + \phi_{i_1}\right) - \tfrac{1}{2} V_2 I_1 \cos\left(3\omega t + \phi_{v_2} + \phi_{i_1}\right) \\
& -V_2 I_2 \cos\left(4\omega t + \phi_{v_2} + \phi_{i_2}\right) \\
& +\tfrac{1}{2} V_2 I_3 \sin\left(\omega t - \phi_{v_2} + \phi_{i_3}\right) + \tfrac{1}{2} V_2 I_3 \cos\left(\omega t - \phi_{v_2} + \phi_{i_3}\right) \\
& -\tfrac{1}{2} V_2 I_3 \sin\left(5\omega t + \phi_{v_2} + \phi_{i_3}\right) - \tfrac{1}{2} V_2 I_3 \cos\left(5\omega t + \phi_{v_2} + \phi_{i_3}\right) \\
& -\tfrac{1}{2} V_2 I_5 \sin\left(3\omega t - \phi_{v_2} + \phi_{i_6}\right) + \tfrac{1}{2} V_2 I_5 \cos\left(3\omega t - \phi_{v_2} + \phi_{i_6}\right) \\
& +\tfrac{1}{2} V_2 I_5 \sin\left(7\omega t + \phi_{v_2} + \phi_{i_6}\right) - \tfrac{1}{2} V_2 I_5 \cos\left(7\omega t + \phi_{v_2} + \phi_{i_6}\right) \\
& +V_2 I_6 \cos\left(4\omega t - \phi_{v_2} + \phi_{i_6}\right) - V_2 I_6 \cos\left(8\omega t + \phi_{v_2} + \phi_{i_6}\right) \\
& +\tfrac{1}{2} V_2 I_7 \sin\left(5\omega t - \phi_{v_2} + \phi_{i_7}\right) + \tfrac{1}{2} V_2 I_7 \cos\left(5\omega t - \phi_{v_2} + \phi_{i_7}\right) \\
& -\tfrac{1}{2} V_2 I_7 \sin\left(9\omega t + \phi_{v_2} + \phi_{i_7}\right) - \tfrac{1}{2} V_2 I_7 \cos\left(9\omega t + \phi_{v_2} + \phi_{i_7}\right) \\
& -\tfrac{1}{2} V_2 I_9 \sin\left(7\omega t - \phi_{v_2} + \phi_{i_9}\right) + \tfrac{1}{2} V_2 I_9 \cos\left(7\omega t - \phi_{v_2} + \phi_{i_9}\right) \\
& +\tfrac{1}{2} V_2 I_9 \sin\left(11\omega t + \phi_{v_2} + \phi_{i_9}\right) - \tfrac{1}{2} V_2 I_9 \cos\left(11\omega t + \phi_{v_2} + \phi_{i_9}\right) \dots \\[6pt]
& -V_3 I_1 \cos\left(4\omega t + \phi_{v_3} + \phi_{i_1}\right) \\
& +\tfrac{1}{2} V_3 I_2 \sin\left(\omega t + \phi_{v_3} - \phi_{i_2}\right) + \tfrac{1}{2} V_3 I_2 \cos\left(\omega t + \phi_{v_3} - \phi_{i_2}\right) \\
& -\tfrac{1}{2} V_3 I_2 \sin\left(5\omega t + \phi_{v_3} + \phi_{i_2}\right) - \tfrac{1}{2} V_3 I_2 \cos\left(5\omega t + \phi_{v_3} + \phi_{i_2}\right) \\
& +\tfrac{1}{2} V_3 I_4 \sin\left(\omega t - \phi_{v_3} + \phi_{i_4}\right) + \tfrac{1}{2} V_3 I_4 \cos\left(\omega t - \phi_{v_3} + \phi_{i_4}\right) \\
& +\tfrac{1}{2} V_3 I_4 \sin\left(7\omega t + \phi_{v_3} + \phi_{i_4}\right) - \tfrac{1}{2} V_3 I_4 \cos\left(7\omega t + \phi_{v_3} + \phi_{i_4}\right) \\
& -V_3 I_5 \cos\left(8\omega t + \phi_{v_3} + \phi_{i_6}\right) \\
& -\tfrac{1}{2} V_3 I_6 \sin\left(3\omega t - \phi_{v_3} + \phi_{i_6}\right) + \tfrac{1}{2} V_3 I_6 \cos\left(3\omega t - \phi_{v_3} + \phi_{i_6}\right) \\
& -\tfrac{1}{2} V_3 I_6 \sin\left(9\omega t + \phi_{v_3} + \phi_{i_6}\right) - \tfrac{1}{2} V_3 I_6 \cos\left(9\omega t + \phi_{v_3} + \phi_{i_6}\right) \\
& +V_3 I_7 \cos\left(4\omega t - \phi_{v_3} + \phi_{i_7}\right) \\
& +\tfrac{1}{2} V_3 I_8 \sin\left(5\omega t - \phi_{v_3} + \phi_{i_8}\right) + \tfrac{1}{2} V_3 I_8 \cos\left(5\omega t - \phi_{v_3} + \phi_{i_8}\right) \\
& +\tfrac{1}{2} V_3 I_8 \sin\left(11\omega t + \phi_{v_3} + \phi_{i_8}\right) - \tfrac{1}{2} V_3 I_8 \cos\left(11\omega t + \phi_{v_3} + \phi_{i_8}\right) \\
& -V_3 I_9 \cos\left(12\omega t + \phi_{v_3} + \phi_{i_9}\right) \dots
\end{aligned}
\tag{A.1}
$$

$$-\frac{1}{2}V_4I_1\sin\left(3\omega t+\phi_{v_4}-\phi_{i_1}\right)+\frac{1}{2}V_4I_1\cos\left(3\omega t+\phi_{v_4}-\phi_{i_1}\right)$$
$$-\frac{1}{2}V_4I_1\sin\left(5\omega t+\phi_{v_4}+\phi_{i_1}\right)-\frac{1}{2}V_4I_1\cos\left(5\omega t+\phi_{v_4}+\phi_{i_1}\right)$$
$$+\frac{1}{2}V_4I_3\sin\left(\omega t+\phi_{v_4}-\phi_{i_3}\right)+\frac{1}{2}V_4I_3\cos\left(\omega t+\phi_{v_4}-\phi_{i_3}\right)$$
$$+\frac{1}{2}V_4I_3\sin\left(7\omega t+\phi_{v_4}+\phi_{i_3}\right)-\frac{1}{2}V_4I_3\cos\left(7\omega t+\phi_{v_4}+\phi_{i_3}\right)$$
$$-V_4I_4\cos\left(8\omega t+\phi_{v_4}+\phi_{i_4}\right)$$
$$+\frac{1}{2}V_4I_5\sin\left(\omega t-\phi_{v_4}+\phi_{i_6}\right)+\frac{1}{2}V_4I_5\cos\left(\omega t-\phi_{v_4}+\phi_{i_6}\right)$$
$$-\frac{1}{2}V_4I_5\sin\left(9\omega t+\phi_{v_4}+\phi_{i_6}\right)-\frac{1}{2}V_4I_5\cos\left(9\omega t+\phi_{v_4}+\phi_{i_6}\right)$$
$$+\frac{1}{2}V_4I_7\cos\left(3\omega t-\phi_{v_4}+\phi_{i_7}\right)-\frac{1}{2}V_4I_7\sin\left(3\omega t-\phi_{v_4}+\phi_{i_7}\right)$$
$$+\frac{1}{2}V_4I_7\sin\left(11\omega t+\phi_{v_4}+\phi_{i_7}\right)-\frac{1}{2}V_4I_7\cos\left(11\omega t+\phi_{v_4}+\phi_{i_7}\right)$$
$$+\frac{1}{2}V_4I_9\sin\left(5\omega t-\phi_{v_4}+\phi_{i_9}\right)+\frac{1}{2}V_4I_9\cos\left(5\omega t-\phi_{v_4}+\phi_{i_9}\right)$$
$$-\frac{1}{2}V_4I_9\sin\left(13\omega t+\phi_{v_4}+\phi_{i_9}\right)-\frac{1}{2}V_4I_9\cos\left(13\omega t+\phi_{v_4}+\phi_{i_9}\right)\dots$$

$$+V_5I_1\cos\left(4\omega t+\phi_{v_5}-\phi_{i_1}\right)$$
$$+\frac{1}{2}V_5I_2\cos\left(3\omega t+\phi_{v_5}-\phi_{i_2}\right)-\frac{1}{2}V_5I_2\sin\left(3\omega t+\phi_{v_5}-\phi_{i_2}\right)$$
$$+\frac{1}{2}V_5I_2\sin\left(7\omega t+\phi_{v_5}+\phi_{i_2}\right)-\frac{1}{2}V_5I_2\cos\left(7\omega t+\phi_{v_5}+\phi_{i_2}\right)$$
$$-V_5I_3\cos\left(8\omega t+\phi_{v_5}+\phi_{i_3}\right)$$
$$+\frac{1}{2}V_5I_4\cos\left(\omega t+\phi_{v_5}-\phi_{i_4}\right)+\frac{1}{2}V_5I_4\sin\left(\omega t+\phi_{v_5}-\phi_{i_4}\right)$$
$$-\frac{1}{2}V_5I_4\sin\left(9\omega t+\phi_{v_5}+\phi_{i_4}\right)-\frac{1}{2}V_5I_4\cos\left(9\omega t+\phi_{v_5}+\phi_{i_4}\right)$$
$$+\frac{1}{2}V_5I_6\sin\left(\omega t-\phi_{v_5}+\phi_{i_6}\right)+\frac{1}{2}V_5I_6\cos\left(\omega t-\phi_{v_5}+\phi_{i_6}\right)$$
$$+\frac{1}{2}V_5I_6\sin\left(11\omega t+\phi_{v_5}+\phi_{i_6}\right)-\frac{1}{2}V_5I_6\cos\left(11\omega t+\phi_{v_5}+\phi_{i_6}\right)$$
$$-V_5I_7\cos\left(12\omega t+\phi_{v_5}+\phi_{i_7}\right)$$
$$+V_4I_8\cos\left(4\omega t-\phi_{v_4}+\phi_{i_8}\right)-V_4I_8\cos\left(12\omega t+\phi_{v_4}+\phi_{i_8}\right)$$
$$-\frac{1}{2}V_5I_8\sin\left(3\omega t-\phi_{v_5}+\phi_{i_8}\right)+\frac{1}{2}V_5I_8\cos\left(3\omega t-\phi_{v_5}+\phi_{i_8}\right)$$
$$-\frac{1}{2}V_5I_8\sin\left(13\omega t+\phi_{v_5}+\phi_{i_8}\right)-\frac{1}{2}V_5I_8\cos\left(13\omega t+\phi_{v_5}+\phi_{i_8}\right)$$
$$+V_5I_9\cos\left(4\omega t-\phi_{v_5}+\phi_{i_9}\right)\dots$$

$$\bar{q}_{1\phi}=\quad -V_1I_1\sin\left(\phi_{i_1}-\phi_{v_1}\right)+V_3I_3\sin\left(\phi_{i_3}-\phi_{v_3}\right)-V_5I_5\sin\left(\phi_{i_6}-\phi_{v_5}\right)\dots$$

$$\bar{q}_{1\phi}=\quad -\frac{1}{2}V_1I_2\sin\left(\omega t-\phi_{v_1}+\phi_{i_2}\right)+\frac{1}{2}V_1I_2\cos\left(\omega t-\phi_{v_1}+\phi_{i_2}\right)$$
$$-\frac{1}{2}V_1I_2\sin\left(3\omega t+\phi_{v_1}+\phi_{i_2}\right)-\frac{1}{2}V_1I_2\cos\left(3\omega t+\phi_{v_1}+\phi_{i_2}\right)$$
$$-V_1I_3\sin\left(4\omega t+\phi_{v_1}+\phi_{i_3}\right)$$
$$-\frac{1}{2}V_1I_4\sin\left(3\omega t-\phi_{v_1}+\phi_{i_4}\right)-\frac{1}{2}V_1I_4\cos\left(3\omega t-\phi_{v_1}+\phi_{i_4}\right)$$
$$-\frac{1}{2}V_1I_4\sin\left(5\omega t+\phi_{v_1}+\phi_{i_4}\right)+\frac{1}{2}V_1I_4\cos\left(5\omega t+\phi_{v_1}+\phi_{i_4}\right)$$
$$-V_1I_5\sin\left(4\omega t-\phi_{v_1}+\phi_{i_6}\right)$$
$$-\frac{1}{2}V_1I_6\sin\left(5\omega t-\phi_{v_1}+\phi_{i_6}\right)+\frac{1}{2}V_1I_6\cos\left(5\omega t-\phi_{v_1}+\phi_{i_6}\right)$$
$$-\frac{1}{2}V_1I_6\cos\left(7\omega t+\phi_{v_1}+\phi_{i_6}\right)-\frac{1}{2}V_1I_6\sin\left(7\omega t+\phi_{v_1}+\phi_{i_6}\right)$$
$$-V_1I_7\sin\left(8\omega t+\phi_{v_1}+\phi_{i_7}\right)$$
$$-\frac{1}{2}V_1I_8\sin\left(7\omega t-\phi_{v_1}+\phi_{i_8}\right)-\frac{1}{2}V_1I_8\cos\left(7\omega t-\phi_{v_1}+\phi_{i_8}\right)$$
$$-\frac{1}{2}V_1I_8\sin\left(9\omega t+\phi_{v_1}+\phi_{i_8}\right)+\frac{1}{2}V_1I_8\cos\left(9\omega t+\phi_{v_1}+\phi_{i_8}\right)$$
$$-V_1I_9\sin\left(8\omega t-\phi_{v_1}+\phi_{i_9}\right)\dots$$

(A.2)

$$+\frac{1}{2}V_2I_1\sin\left(\omega t+\phi_{v_2}-\phi_{i_1}\right)-\frac{1}{2}V_2I_1\cos\left(\omega t+\phi_{v_2}-\phi_{i_1}\right)$$
$$+\frac{1}{2}V_2I_1\sin\left(3\omega t+\phi_{v_2}+\phi_{i_1}\right)+\frac{1}{2}V_2I_1\cos\left(3\omega t+\phi_{v_2}+\phi_{i_1}\right)$$
$$+\frac{1}{2}V_2I_3\sin\left(\omega t-\phi_{v_2}+\phi_{i_3}\right)-\frac{1}{2}V_2I_3\cos\left(\omega t-\phi_{v_2}+\phi_{i_3}\right)$$
$$-\frac{1}{2}V_2I_3\sin\left(5\omega t+\phi_{v_2}+\phi_{i_3}\right)+\frac{1}{2}V_2I_3\cos\left(5\omega t+\phi_{v_2}+\phi_{i_3}\right)$$
$$-V_2I_4\cos\left(2\omega t-\phi_{v_2}+\phi_{i_4}\right)+V_2I_4\cos\left(6\omega t+\phi_{v_2}+\phi_{i_4}\right)$$
$$-\frac{1}{2}V_2I_5\sin\left(3\omega t-\phi_{v_2}+\phi_{i_6}\right)-\frac{1}{2}V_2I_5\cos\left(3\omega t-\phi_{v_2}+\phi_{i_6}\right)$$
$$+\frac{1}{2}V_2I_5\sin\left(7\omega t+\phi_{v_2}+\phi_{i_6}\right)+\frac{1}{2}V_2I_5\cos\left(7\omega t+\phi_{v_2}+\phi_{i_6}\right)$$
$$+\frac{1}{2}V_2I_7\sin\left(5\omega t-\phi_{v_2}+\phi_{i_7}\right)-\frac{1}{2}V_2I_7\cos\left(5\omega t-\phi_{v_2}+\phi_{i_7}\right)$$
$$-\frac{1}{2}V_2I_7\sin\left(9\omega t+\phi_{v_2}+\phi_{i_7}\right)+\frac{1}{2}V_2I_7\cos\left(9\omega t+\phi_{v_2}+\phi_{i_7}\right)$$
$$-\frac{1}{2}V_2I_9\sin\left(7\omega t-\phi_{v_2}+\phi_{i_9}\right)-\frac{1}{2}V_2I_9\cos\left(7\omega t-\phi_{v_2}+\phi_{i_9}\right)$$
$$-V_2I_8\cos\left(6\omega t-\phi_{v_2}+\phi_{i_8}\right)+V_2I_8\cos\left(10\omega t+\phi_{v_2}+\phi_{i_8}\right)$$
$$+\frac{1}{2}V_2I_9\sin\left(11\omega t+\phi_{v_2}+\phi_{i_9}\right)+\frac{1}{2}V_2I_9\cos\left(11\omega t+\phi_{v_2}+\phi_{i_9}\right)\dots$$

$$+ V_3 I_1 \sin\left(4\omega t + \phi_{v_3} + \phi_{i_1}\right)$$

$$- \tfrac{1}{2} V_3 I_2 \sin\left(\omega t + \phi_{v_3} - \phi_{i_2}\right) + \tfrac{1}{2} V_3 I_2 \cos\left(\omega t + \phi_{v_3} - \phi_{i_2}\right)$$

$$+ \tfrac{1}{2} V_3 I_2 \sin\left(5\omega t + \phi_{v_3} + \phi_{i_2}\right) - \tfrac{1}{2} V_3 I_2 \cos\left(5\omega t + \phi_{v_3} + \phi_{i_2}\right)$$

$$+ \tfrac{1}{2} V_3 I_4 \sin\left(\omega t - \phi_{v_3} + \phi_{i_4}\right) - \tfrac{1}{2} V_3 I_4 \cos\left(\omega t - \phi_{v_3} + \phi_{i_4}\right)$$

$$+ \tfrac{1}{2} V_3 I_4 \sin\left(7\omega t + \phi_{v_3} + \phi_{i_4}\right) + \tfrac{1}{2} V_3 I_4 \cos\left(7\omega t + \phi_{v_3} + \phi_{i_4}\right)$$

$$+ V_3 I_5 \sin\left(8\omega t + \phi_{v_3} + \phi_{i_6}\right)$$

$$+ V_3 I_6 \tfrac{1}{2} \sin\left(3\omega t - \phi_{v_3} + \phi_{i_6}\right) + V_3 I_6 \tfrac{1}{2} \cos\left(3\omega t - \phi_{v_3} + \phi_{i_6}\right)$$

$$+ V_3 I_6 \tfrac{1}{2} \sin\left(9\omega t + \phi_{v_3} + \phi_{i_6}\right) - V_3 I_6 \tfrac{1}{2} \cos\left(9\omega t + \phi_{v_3} + \phi_{i_6}\right)$$

$$+ V_3 I_7 \sin\left(4\omega t - \phi_{v_3} + \phi_{i_7}\right)$$

$$+ \tfrac{1}{2} V_3 I_8 \sin\left(5\omega t - \phi_{v_3} + \phi_{i_8}\right) - \tfrac{1}{2} V_3 I_8 \cos\left(5\omega t - \phi_{v_3} + \phi_{i_8}\right)$$

$$+ \tfrac{1}{2} V_3 I_8 \sin\left(11\omega t + \phi_{v_3} + \phi_{i_8}\right) + \tfrac{1}{2} V_3 I_8 \cos\left(11\omega t + \phi_{v_3} + \phi_{i_8}\right)$$

$$+ V_3 I_9 \sin\left(12\omega t + \phi_{v_3} + \phi_{i_9}\right) \ldots$$

$$+ \tfrac{1}{2} V_4 I_1 \sin\left(3\omega t + \phi_{v_4} - \phi_{i_1}\right) + \tfrac{1}{2} V_4 I_1 \cos\left(3\omega t + \phi_{v_4} - \phi_{i_1}\right)$$

$$+ \tfrac{1}{2} V_4 I_1 \sin\left(5\omega t + \phi_{v_4} + \phi_{i_1}\right) - \tfrac{1}{2} V_4 I_1 \cos\left(5\omega t + \phi_{v_4} + \phi_{i_1}\right)$$

$$+ V_4 I_2 \cos\left(2\omega t + \phi_{v_4} - \phi_{i_2}\right) - V_4 I_2 \cos\left(6\omega t + \phi_{v_4} + \phi_{i_2}\right)$$

$$- \tfrac{1}{2} V_4 I_3 \sin\left(\omega t + \phi_{v_4} - \phi_{i_3}\right) + \tfrac{1}{2} V_4 I_3 \cos\left(\omega t + \phi_{v_4} - \phi_{i_3}\right)$$

$$- \tfrac{1}{2} V_4 I_3 \sin\left(7\omega t + \phi_{v_4} + \phi_{i_3}\right) - \tfrac{1}{2} V_4 I_3 \cos\left(7\omega t + \phi_{v_4} + \phi_{i_3}\right)$$

$$- \tfrac{1}{2} V_4 I_5 \sin\left(\omega t - \phi_{v_4} + \phi_{i_6}\right) + \tfrac{1}{2} V_4 I_5 \cos\left(\omega t - \phi_{v_4} + \phi_{i_6}\right)$$

$$+ \tfrac{1}{2} V_4 I_5 \sin\left(9\omega t + \phi_{v_4} + \phi_{i_6}\right) - \tfrac{1}{2} V_4 I_5 \cos\left(9\omega t + \phi_{v_4} + \phi_{i_6}\right)$$

$$+ V_4 I_6 \cos\left(2\omega t - \phi_{v_4} + \phi_{i_6}\right) - V_4 I_6 \cos\left(10\omega t + \phi_{v_4} + \phi_{i_6}\right)$$

$$+ \tfrac{1}{2} V_4 I_7 \sin\left(3\omega t - \phi_{v_4} + \phi_{i_7}\right) + \tfrac{1}{2} V_4 I_7 \cos\left(3\omega t - \phi_{v_4} + \phi_{i_7}\right)$$

$$- \tfrac{1}{2} V_4 I_7 \sin\left(11\omega t + \phi_{v_4} + \phi_{i_7}\right) - \tfrac{1}{2} V_4 I_7 \cos\left(11\omega t + \phi_{v_4} + \phi_{i_7}\right)$$

$$- \tfrac{1}{2} V_4 I_9 \sin\left(5\omega t - \phi_{v_4} + \phi_{i_9}\right) + \tfrac{1}{2} V_4 I_9 \cos\left(5\omega t - \phi_{v_4} + \phi_{i_9}\right)$$

$$+ \tfrac{1}{2} V_4 I_9 \sin\left(13\omega t + \phi_{v_4} + \phi_{i_9}\right) - \tfrac{1}{2} V_4 I_9 \cos\left(13\omega t + \phi_{v_4} + \phi_{i_9}\right) \ldots$$

$$+ V_5 I_1 \sin\left(4\omega t + \phi_{v_5} - \phi_{i_1}\right)$$

$$+ \tfrac{1}{2} V_5 I_2 \sin\left(3\omega t + \phi_{v_5} - \phi_{i_2}\right) + \tfrac{1}{2} V_5 I_2 \cos\left(3\omega t + \phi_{v_5} - \phi_{i_2}\right)$$

$$- \tfrac{1}{2} V_5 I_2 \sin\left(7\omega t + \phi_{v_5} + \phi_{i_2}\right) - \tfrac{1}{2} V_5 I_2 \cos\left(7\omega t + \phi_{v_5} + \phi_{i_2}\right)$$

$$- V_5 I_3 \sin\left(8\omega t + \phi_{v_5} + \phi_{i_3}\right)$$

$$+ \tfrac{1}{2} V_5 I_4 \sin\left(\omega t + \phi_{v_5} - \phi_{i_4}\right) - \tfrac{1}{2} V_5 I_4 \cos\left(\omega t + \phi_{v_5} - \phi_{i_4}\right)$$

$$- \tfrac{1}{2} V_5 I_4 \sin\left(9\omega t + \phi_{v_5} + \phi_{i_4}\right) + \tfrac{1}{2} V_5 I_4 \cos\left(9\omega t + \phi_{v_5} + \phi_{i_4}\right)$$

$$- \tfrac{1}{2} V_5 I_6 \sin\left(\omega t - \phi_{v_5} + \phi_{i_6}\right) + \tfrac{1}{2} V_5 I_6 \cos\left(\omega t - \phi_{v_5} + \phi_{i_6}\right)$$

$$- \tfrac{1}{2} V_5 I_6 \sin\left(11\omega t + \phi_{v_5} + \phi_{i_6}\right) - \tfrac{1}{2} V_5 I_6 \cos\left(11\omega t + \phi_{v_5} + \phi_{i_6}\right)$$

$$- V_5 I_7 \sin\left(12\omega t + \phi_{v_5} + \phi_{i_7}\right)$$

$$- \tfrac{1}{2} V_5 I_8 \sin\left(3\omega t - \phi_{v_5} + \phi_{i_8}\right) - \tfrac{1}{2} V_5 I_8 \cos\left(3\omega t - \phi_{v_5} + \phi_{i_8}\right)$$

$$- \tfrac{1}{2} V_5 I_8 \sin\left(13\omega t + \phi_{v_5} + \phi_{i_8}\right) + \tfrac{1}{2} V_5 I_8 \cos\left(13\omega t + \phi_{v_5} + \phi_{i_8}\right)$$

$$- V_5 I_9 \sin\left(4\omega t - \phi_{v_5} + \phi_{i_9}\right) \ldots$$

APPENDIX B – TWO-PHASE INSTANTANEOUS POWERS UNDER DISTORTED VOLTAGES AND CURRENTS

$$
\begin{aligned}
\bar{p}_{2\phi} = \ & +2V_1 I_1 \cos\left(\phi_{i_1} - \phi_{v_1}\right) \\
& +2V_2 I_2 \cos\left(\phi_{i_2} - \phi_{v_2}\right) \\
& +4V_3 I_3 \cos\left(\phi_{i_3} - \phi_{v_3}\right) \\
& +2V_4 I_4 \cos\left(\phi_{i_4} - \phi_{v_4}\right) \\
& +2V_5 I_5 \cos\left(\phi_{i_5} - \phi_{v_5}\right) \\
& +4V_6 I_6 \cos\left(\phi_{i_6} - \phi_{v_6}\right) \dots
\end{aligned}
$$

$$
\begin{aligned}
\tilde{p}_{2\phi} = \ & -2V_1 I_2 \cos\left(3\omega t + \phi_{i_2} + \phi_{v_1}\right) \\
& +V_1 I_3 \cos\left(2\omega t + \phi_{i_3} - \phi_{v_1}\right) - \sqrt{3}V_1 I_3 \sin\left(2\omega t + \phi_{i_3} - \phi_{v_1}\right) \\
& -V_1 I_3 \cos\left(4\omega t + \phi_{i_3} + \phi_{v_1}\right) - \sqrt{3}V_1 I_3 \sin\left(4\omega t + \phi_{i_3} + \phi_{v_1}\right) \\
& +2V_1 I_4 \cos\left(3\omega t + \phi_{i_4} - \phi_{v_1}\right) \\
& -2V_1 I_5 \cos\left(6\omega t + \phi_{i_5} + \phi_{v_1}\right) \\
& +V_1 I_6 \cos\left(5\omega t + \phi i_6 - \phi_{v_1}\right) - \sqrt{3}V_1 I_6 \sin\left(5\omega t + \phi_{i_6} - \phi_{v_1}\right) \\
& -V_1 I_6 \cos\left(7\omega t + \phi_{i_6} + \phi_{v_1}\right) - \sqrt{3}V_1 I_6 \sin\left(7\omega t + \phi_{i_6} + \phi_{v_1}\right) \\
& +2V_1 I_7 \cos\left(6\omega t + \phi_{i_7} - \phi_{v_1}\right) \\
& -2V_1 I_8 \cos\left(9\omega t + \phi_{i_8} + \phi_{v_1}\right) \\
& +V_1 I_9 \cos\left(8\omega t + \phi_{i_9} - \phi_{v_1}\right) - \sqrt{3}V_1 I_9 \sin\left(8\omega t + \phi_{i_9} - \phi_{v_1}\right) \\
& -V_1 I_9 \cos\left(10\omega t + \phi_{i_9} + \phi_{v_1}\right) - \sqrt{3}V_1 I_9 \sin\left(10\omega t + \phi_{i_9} + \phi_{v_1}\right) \dots \\[6pt]
& -2V_2 I_1 \cos\left(3\omega t + \phi_{i_1} + \phi_{v_2}\right) \\
& +V_2 I_3 \cos\left(\omega t + \phi_{i_3} - \phi_{v_2}\right) + \sqrt{3}V_2 I_3 \sin\left(\omega t + \phi_{i_3} - \phi_{v_2}\right) \\
& -V_2 I_3 \cos\left(5\omega t + \phi_{i_3} + \phi_{v_2}\right) + \sqrt{3}V_2 Y_3 \sin\left(5\omega t + \phi_{i_3} + \phi_{v_2}\right) \\
& -2V_2 I_4 \cos\left(6\omega t + \phi_{i_4} + \phi_{v_2}\right) \\
& +2V_2 I_5 \cos\left(3\omega t + \phi_{i_5} - \phi_{v_2}\right) \\
& +V_2 I_6 \cos\left(4\omega t + \phi_{i_6} - \phi_{v_2}\right) + \sqrt{3}V_2 I_6 \sin\left(4\omega t + \phi_{i_6} - \phi_{v_2}\right) \\
& -V_2 I_6 \cos\left(8\omega t + \phi_{i_6} + \phi_{v_2}\right) + \sqrt{3}V_2 I_6 \sin\left(8\omega t + \phi_{i_6} + \phi_{v_2}\right) \\
& -2V_2 I_7 \cos\left(9\omega t + \phi_{i_7} + \phi_{v_2}\right) \\
& +2V_2 I_8 \cos\left(6\omega t + \phi_{i_8} - \phi_{v_2}\right) \\
& +V_2 I_9 \cos\left(7\omega t + \phi_{i_9} - \phi_{v_2}\right) + \sqrt{3}V_2 I_9 \sin\left(7\omega t + \phi_{i_9} - \phi_{v_2}\right) \\
& -V_2 I_9 \cos\left(11\omega t + \phi_{i_9} + \phi_{v_2}\right) + \sqrt{3}V_2 I_9 \sin\left(11\omega t + \phi_{i_9} + \phi_{v_2}\right) \dots \\[6pt]
& +V_3 I_1 \cos\left(2\omega t - \phi_{i_1} + \phi_{v_3}\right) - \sqrt{3}V_3 I_1 \sin\left(2\omega t - \phi_{i_1} + \phi_{v_3}\right) \\
& -V_3 I_1 \cos\left(4\omega t + \phi_{i_1} + \phi_{v_3}\right) - \sqrt{3}V_3 I_1 \sin\left(4\omega t + \phi_{i_1} + \phi_{v_3}\right) \\
& +V_3 I_2 \cos\left(\omega t - \phi_{i_2} + \phi_{v_3}\right) + \sqrt{3}V_3 I_2 \sin\left(\omega t - \phi_{i_2} + \phi_{v_3}\right) \\
& -V_3 I_2 \cos\left(5\omega t + \phi_{i_2} + \phi_{v_3}\right) + \sqrt{3}V_3 I_2 \sin\left(5\omega t + \phi_{i_2} + \phi_{v_3}\right) \\
& -4V_3 I_3 \cos\left(6\omega t + \phi_{i_3} + \phi_{v_3}\right) \\
& +V_3 I_4 \cos\left(\omega t + \phi_{i_4} - \phi_{v_3}\right) + \sqrt{3}V_3 I_4 \sin\left(\omega t + \phi_{i_4} - \phi_{v_3}\right) \\
& -V_3 I_4 \cos\left(7\omega t + \phi_{i_4} + \phi_{v_3}\right) - \sqrt{3}V_3 I_4 \sin\left(7\omega t + \phi_{i_4} + \phi_{v_3}\right) \\
& +V_3 I_5 \cos\left(2\omega t + \phi_{i_5} - \phi_{v_3}\right) - \sqrt{3}V_3 I_5 \sin\left(2\omega t + \phi_{i_5} - \phi_{v_3}\right) \\
& -V_3 I_5 \cos\left(8\omega t + \phi_{i_5} + \phi_{v_3}\right) + \sqrt{3}V_3 I_5 \sin\left(8\omega t + \phi_{i_5} + \phi_{v_3}\right) \\
& +4V_3 I_6 \cos\left(3\omega t + \phi_{i_6} - \phi_{v_3}\right) \\
& -4V_3 I_6 \cos\left(9\omega t + \phi_{i_6} + \phi_{v_3}\right) \\
& +V_3 I_7 \cos\left(4\omega t + \phi_{i_7} - \phi_{v_3}\right) + \sqrt{3}V_3 I_7 \sin\left(4\omega t + \phi_{i_7} - \phi_{v_3}\right) \\
& -V_3 I_7 \cos\left(10\omega t + \phi_{i_7} + \phi_{v_3}\right) - \sqrt{3}V_3 I_7 \sin\left(10\omega t + \phi_{i_7} + \phi_{v_3}\right) \\
& +V_3 I_8 \cos\left(5\omega t + \phi_{i_8} - \phi_{v_3}\right) - \sqrt{3}V_3 I_8 \sin\left(5\omega t + \phi_{i_8} - \phi_{v_3}\right) \\
& -V_3 I_8 \cos\left(11\omega t + \phi_{i_8} + \phi_{v_3}\right) + \sqrt{3}V_3 I_8 \sin\left(11\omega t + \phi_{i_8} + \phi_{v_3}\right) \\
& +4V_3 I_9 \cos\left(6\omega t + \phi_{i_9} - \phi_{v_3}\right) \\
& -4V_3 I_9 \cos\left(12\omega t + \phi_{i_9} + \phi_{v_3}\right) \dots
\end{aligned}
$$

$$(\text{B.1})$$

$$+2V_4I_1\cos\left(3\omega t-\phi_{i_1}+\phi_{v_4}\right)$$
$$-2V_4I_2\cos\left(6\omega t+\phi_{i_2}+\phi_{v_4}\right)$$
$$+V_4I_3\cos\left(\omega t-\phi_{i_3}+\phi_{v_4}\right)+\sqrt{3}V_4I_3\sin\left(\omega t-\phi_{i_3}+\phi_{v_4}\right)$$
$$-V_4I_3\cos\left(7\omega t+\phi_{i_3}+\phi_{v_4}\right)-\sqrt{3}V_4I_3\sin\left(7\omega t+\phi_{i_3}+\phi_{v_4}\right)$$
$$-2V_4I_5\cos\left(9\omega t+\phi_{i_5}+\phi_{v_4}\right)$$
$$+V_4I_6\cos\left(2\omega t+\phi_{i_6}-\phi_{v_4}\right)-\sqrt{3}V_4I_6\sin\left(2\omega t+\phi_{i_6}-\phi_{v_4}\right)$$
$$-V_4I_6\cos\left(10\omega t+\phi_{i_6}+\phi_{v_4}\right)-\sqrt{3}V_4I_6\sin\left(10\omega t+\phi_{i_6}+\phi_{v_4}\right)$$
$$+2V_4I_7\cos\left(3\omega t+\phi_{i_7}-\phi_{v_4}\right)$$
$$-2V_4I_8\cos\left(12\omega t+\phi_{i_8}+\phi_{v_4}\right)$$
$$+V_4I_9\cos\left(5\omega t+\phi_{i_9}-\phi_{v_4}\right)-\sqrt{3}V_4I_9\sin\left(5\omega t+\phi_{i_9}-\phi_{v_4}\right)$$
$$-V_4I_9\cos\left(13\omega t+\phi_{i_9}+\phi_{v_4}\right)-\sqrt{3}V_4I_9\sin\left(13\omega t+\phi_{i_9}+\phi_{v_4}\right)\dots$$

$$-2V_5I_1\cos\left(6\omega t+\phi_{i_1}+\phi_{v_5}\right)$$
$$+2V_5I_2\cos\left(3\omega t-\phi_{i_2}+\phi_{v_5}\right)$$
$$+V_5I_3\cos\left(2\omega t-\phi_{i_3}+\phi_{v_5}\right)-\sqrt{3}V_5I_3\sin\left(2\omega t-\phi_{i_3}+\phi_{v_5}\right)$$
$$-V_5I_3\cos\left(8\omega t+\phi_{i_3}+\phi_{v_5}\right)+\sqrt{3}V_5I_3\sin\left(8\omega t+\phi_{i_3}+\phi_{v_5}\right)$$
$$-2V_5I_4\cos\left(9\omega t+\phi_{i_4}+\phi_{v_5}\right)$$
$$+V_5I_6\cos\left(\omega t+\phi_{i_6}-\phi_{v_5}\right)+\sqrt{3}V_5I_6\sin\left(\omega t+\phi_{i_6}-\phi_{v_5}\right)$$
$$-V_5I_6\cos\left(11\omega t+\phi_{i_6}+\phi_{v_5}\right)+\sqrt{3}V_5I_6\sin\left(11\omega t+\phi_{i_6}+\phi_{v_5}\right)$$
$$-2V_5I_7\cos\left(12\omega t+\phi_{i_7}+\phi_{v_5}\right)$$
$$+2V_5I_8\cos\left(3\omega t+\phi_{i_8}-\phi_{v_5}\right)$$
$$+V_5I_9\cos\left(4\omega t+\phi_{i_9}-\phi_{v_5}\right)+\sqrt{3}V_5I_9\sin\left(4\omega t+\phi_{i_9}-\phi_{v_5}\right)$$
$$-V_5I_9\cos\left(14\omega t+\phi_{i_9}+\phi_{v_5}\right)+\sqrt{3}V_5I_9\sin\left(14\omega t+\phi_{i_9}+\phi_{v_5}\right)\dots$$

(B.2)

$$+V_6I_1\cos\left(5\omega t-\phi_{i_1}+\phi_{v_6}\right)-\sqrt{3}V_6I_1\sin\left(5\omega t-\phi_{i_1}+\phi_{v_6}\right)$$
$$-V_6I_1\cos\left(7\omega t+\phi_{i_1}+\phi_{v_6}\right)-\sqrt{3}V_6I_1\sin\left(7\omega t+\phi_{i_1}+\phi_{v_6}\right)$$
$$+V_6I_2\cos\left(4\omega t-\phi_{i_2}+\phi_{v_6}\right)+\sqrt{3}V_6I_2\sin\left(4\omega t-\phi_{i_2}+\phi_{v_6}\right)$$
$$-V_6I_2\cos\left(8\omega t+\phi_{i_2}+\phi_{v_6}\right)+\sqrt{3}V_6I_2\sin\left(8\omega t+\phi_{i_2}+\phi_{v_6}\right)$$
$$+4V_6I_3\cos\left(3\omega t-\phi_{i_3}+\phi_{v_6}\right)+V_6I_4\cos\left(2\omega t-\phi_{i_4}+\phi_{v_6}\right)$$
$$-4V_6I_3\cos\left(9\omega t+\phi_{i_3}+\phi_{v_6}\right)-V_6I_4\cos\left(10\omega t+\phi_{i_4}+\phi_{v_6}\right)$$
$$-\sqrt{3}V_6I_4\sin\left(2\omega t-\phi_{i_4}+\phi_{v_6}\right)$$
$$-\sqrt{3}V_6I_4\sin\left(10\omega t+\phi_{i_4}+\phi_{v_6}\right)$$
$$+V_6I_5\cos\left(\omega t-\phi_{i_5}+\phi_{v_6}\right)+\sqrt{3}V_6I_5\sin\left(\omega t-\phi_{i_5}+\phi_{v_6}\right)$$
$$-V_6I_5\cos\left(11\omega t+\phi_{i_5}+\phi_{v_6}\right)+\sqrt{3}V_6I_5\sin\left(11\omega t+\phi_{i_5}+\phi_{v_6}\right)$$
$$-4V_6I_6\cos\left(12\omega t+\phi_{i_6}+\phi_{v_6}\right)$$
$$+V_6I_7\cos\left(\omega t+\phi_{i_7}-\phi_{v_6}\right)+\sqrt{3}V_6I_7\sin\left(\omega t+\phi_{i_7}-\phi_{v_6}\right)$$
$$-V_6I_7\cos\left(13\omega t+\phi_{i_7}+\phi_{v_6}\right)-\sqrt{3}V_6I_7\sin\left(13\omega t+\phi_{i_7}+\phi_{v_6}\right)$$
$$+V_6I_8\cos\left(2\omega t+\phi_{i_8}-\phi_{v_6}\right)-\sqrt{3}V_6I_8\sin\left(2\omega t+\phi_{i_8}-\phi_{v_6}\right)$$
$$-V_6I_8\cos\left(14\omega t+\phi_{i_8}+\phi_{v_6}\right)+\sqrt{3}V_6I_8\sin\left(14\omega t+\phi_{i_8}+\phi_{v_6}\right)$$
$$+4V_6I_9\cos\left(3\omega t+\phi_{i_9}-\phi_{v_6}\right)$$
$$-4V_6I_9\cos\left(15\omega t+\phi_{i_9}+\phi_{v_6}\right)\dots$$

$$\bar{q}_{2\phi} = \begin{aligned}
& -2V_1 I_1 \sin\left(\phi_{i_1} - \phi_{v_1}\right) \\
& +2V_2 I_2 \sin\left(\phi_{i_2} - \phi_{v_2}\right) \\
& -2V_4 I_4 \sin\left(\phi_{i_4} - \phi_{v_4}\right) \\
& +2V_5 I_5 \sin\left(\phi_{i_5} - \phi_{v_5}\right) \ldots
\end{aligned}$$

$$\bar{q}_{2\phi} = \begin{aligned}
& -2V_1 I_2 \sin\left(3\omega t + \phi_{i_2} + \phi_{v_1}\right) \\
& -\sqrt{3}V_1 I_3 \cos\left(2\omega t + \phi_{i_3} - \phi_{v_1}\right) - V_1 I_3 \sin\left(2\omega t + \phi_{i_3} - \phi_{v_1}\right) \\
& +\sqrt{3}V_1 I_3 \cos\left(4\omega t + \phi_{i_3} + \phi_{v_1}\right) - V_1 I_3 \sin\left(4\omega t + \phi_{i_3} + \phi_{v_1}\right) \\
& -2V_1 I_4 \sin\left(3\omega t + \phi_{i_4} - \phi_{v_1}\right) \\
& -2V_1 I_5 \sin\left(6\omega t + \phi_{i_5} + \phi_{v_1}\right) \\
& -\sqrt{3}V_1 I_6 \cos\left(5\omega t + \phi_{i_6} - \phi_{v_1}\right) - V_1 I_6 \sin\left(5\omega t + \phi_{i_6} - \phi_{v_1}\right) \\
& +\sqrt{3}V_1 I_6 \cos\left(7\omega t + \phi_{i_6} + \phi_{v_1}\right) - V_1 I_6 \sin\left(7\omega t + \phi_{i_6} + \phi_{v_1}\right) \\
& -2V_1 I_7 \sin\left(6\omega t + \phi_{i_7} - \phi_{v_1}\right) \\
& -2V_1 I_8 \sin\left(9\omega t + \phi_{i_8} + \phi_{v_1}\right) \\
& -\sqrt{3}V_1 I_9 \cos\left(8\omega t + \phi_{i_9} - \phi_{v_1}\right) - V_1 I_9 \sin\left(8\omega t + \phi_{i_9} - \phi_{v_1}\right) \\
& +\sqrt{3}V_1 I_9 \cos\left(10\omega t + \phi_{i_9} + \phi_{v_1}\right) - V_1 I_9 \sin\left(10\omega t + \phi_{i_9} + \phi_{v_1}\right) \ldots \\[1em]
& +2V_2 I_1 \sin\left(3\omega t + \phi_{i_1} + \phi_{v_2}\right) \\
& -\sqrt{3}V_2 I_3 \cos\left(\omega t + \phi_{i_3} - \phi_{v_2}\right) + V_2 I_3 \sin\left(\omega t + \phi_{i_3} - \phi_{v_2}\right) \\
& +\sqrt{3}V_2 I_3 \cos\left(5\omega t + \phi_{i_3} + \phi_{v_2}\right) + V_2 I_3 \sin\left(5\omega t + \phi_{i_3} + \phi_{v_2}\right) \\
& +2V_2 I_4 \sin\left(6\omega t + \phi_{i_4} + \phi_{v_2}\right) \\
& +2V_2 I_5 \sin\left(3\omega t + phi_{i_5} - \phi_{v_2}\right) \\
& -\sqrt{3}V_2 I_6 \cos\left(4\omega t + \phi_{i_6} - \phi_{v_2}\right) + V_2 I_6 \sin\left(4\omega t + \phi_{i_6} - \phi_{v_2}\right) \\
& +\sqrt{3}V_2 I_6 \cos\left(8\omega t + \phi_{i_6} + \phi_{v_2}\right) + V_2 I_6 \sin\left(8\omega t + \phi_{i_6} + \phi_{v_2}\right) \\
& +2V_2 I_7 \sin\left(9\omega t + \phi_{i_7} + \phi_{v_2}\right) \\
& +2V_2 I_8 \sin\left(6\omega t + \phi_{i_8} - \phi_{v_2}\right) \\
& -\sqrt{3}V_2 I_9 \cos\left(7\omega t + \phi_{i_9} - \phi_{v_2}\right) + V_2 I_9 \sin\left(7\omega t + \phi_{i_9} - \phi_{v_2}\right) \\
& +\sqrt{3}V_2 I_9 \cos\left(11\omega t + \phi_{i_9} + \phi_{v_2}\right) + V_2 Y_9 \sin\left(11\omega t + \phi_{i_9} + \phi_{v_2}\right) \ldots \\[1em]
& +\sqrt{3}V_3 I_1 \cos\left(2\omega t - \phi_{i_1} + \phi_{v_3}\right) + V_3 I_1 \sin\left(2\omega t - \phi_{i_1} + \phi_{v_3}\right) \\
& -\sqrt{3}V_3 I_1 \cos\left(4\omega t + \phi_{i_1} + \phi_{v_3}\right) + V_3 I_1 \sin\left(4\omega t + \phi_{i_1} + \phi_{v_3}\right) \\
& +\sqrt{3}V_3 I_2 \cos\left(\omega t - \phi_{i_2} + \phi_{v_3}\right) - V_3 I_2 \sin\left(\omega t - \phi_{i_2} + \phi_{v_3}\right) \\
& -\sqrt{3}V_3 I_2 \cos\left(5\omega t + \phi_{i_2} + \phi_{v_3}\right) - V_3 I_2 \sin\left(5\omega t + \phi_{i_2} + \phi_{v_3}\right) \\
& +\sqrt{3}V_3 I_4 \cos\left(\omega t + \phi_{i_4} - \phi_{v_3}\right) - V_3 I_4 \sin\left(\omega t + \phi_{i_4} - \phi_{v_3}\right) \\
& -\sqrt{3}V_3 I_4 \cos\left(7\omega t + \phi_{i_4} + \phi_{v_3}\right) + V_3 I_4 \sin\left(7\omega t + \phi_{i_4} + \phi_{v_3}\right) \\
& +\sqrt{3}V_3 I_5 \cos\left(2\omega t + \phi_{i_5} - \phi_{v_3}\right) + V_3 I_5 \sin\left(2\omega t + \phi_{i_5} - \phi_{v_3}\right) \\
& -\sqrt{3}V_3 I_5 \cos\left(8\omega t + \phi_{i_5} + \phi_{v_3}\right) - V_3 I_5 \sin\left(8\omega t + \phi_{i_5} + \phi_{v_3}\right) \\
& +\sqrt{3}V_3 I_7 \cos\left(4\omega t + \phi_{i_7} - \phi_{v_3}\right) - V_3 I_7 \sin\left(4\omega t + \phi_{i_7} - \phi_{v_3}\right) \\
& -\sqrt{3}V_3 I_7 \cos\left(10\omega t + \phi_{i_7} + \phi_{v_3}\right) + V_3 I_7 \sin\left(10\omega t + \phi_{i_7} + \phi_{v_3}\right) \\
& +\sqrt{3}V_3 I_8 \cos\left(5\omega t + \phi_{i_8} - \phi_{v_3}\right) + V_3 I_8 \sin\left(5\omega t + \phi_{i_8} - \phi_{v_3}\right) \\
& -\sqrt{3}V_3 I_8 \cos\left(11\omega t + \phi_{i_8} + \phi_{v_3}\right) - V_3 I_8 \sin\left(11\omega t + \phi_{i_8} + \phi_{v_3}\right) \ldots \\[1em]
& +2V_4 I_1 \sin\left(3\omega t - \phi_{i_1} + \phi_{v_4}\right) \\
& -2V_4 I_2 \sin\left(6\omega t + \phi_{i_2} + \phi_{v_4}\right) \\
& -\sqrt{3}V_4 I_3 \cos\left(\omega t - \phi_{i_3} + \phi_{v_4}\right) + V_4 I_3 \sin\left(\omega t - \phi_{i_3} + \phi_{v_4}\right) \\
& +\sqrt{3}V_4 I_3 \cos\left(7\omega t + \phi_{i_3} + \phi_{v_4}\right) - V_4 I_3 \sin\left(7\omega t + \phi_{i_3} + \phi_{v_4}\right) \\
& -2\sin\left(9\omega t + \phi_{i_5} + \phi_{v_4}\right)V_4 I_5 \\
& -\sqrt{3}V_4 I_6 \cos\left(2\omega t + \phi_{i_6} - \phi_{v_4}\right) - V_4 I_6 \sin\left(2\omega t + \phi_{i_6} - \phi_{v_4}\right) \\
& +\sqrt{3}V_4 I_6 \cos\left(10\omega t + \phi_{i_6} + \phi_{v_4}\right) - V_4 I_6 \sin\left(10\omega t + \phi_{i_6} + \phi_{v_4}\right) \\
& -2V_4 I_7 \sin\left(3\omega t + \phi_{i_7} - \phi_{v_4}\right) \\
& -2V_4 I_8 \sin\left(12\omega t + \phi_{i_8} + \phi_{v_4}\right) \\
& -\sqrt{3}V_4 I_9 \cos\left(5\omega t + \phi_{i_9} - \phi_{v_4}\right) - V_4 I_9 \sin\left(5\omega t + \phi_{i_9} - \phi_{v_4}\right) \\
& +\sqrt{3}V_4 I_9 \cos\left(13\omega t + \phi_{i_9} + \phi_{v_4}\right) - V_4 I_9 \sin\left(13\omega t + \phi_{i_9} + \phi_{v_4}\right) \ldots \\[1em]
& +2V_5 I_1 \sin\left(6\omega t + \phi_{i_1} + \phi_{v_5}\right) \\
& -2V_5 I_2 \sin\left(3\omega t - \phi_{i_2} + \phi_{v_5}\right) \\
& -\sqrt{3}V_5 I_3 \cos\left(2\omega t - \phi_{i_3} + \phi_{v_5}\right) - V_5 I_3 \sin\left(2\omega t - \phi_{i_3} + \phi_{v_5}\right) \\
& +\sqrt{3}V_5 I_3 \cos\left(8\omega t + \phi_{i_3} + \phi_{v_5}\right) + V_5 I_3 \sin\left(8\omega t + \phi_{i_3} + \phi_{v_5}\right) \\
& +2V_5 I_4 \sin\left(9\omega t + \phi_{i_4} + \phi_{v_5}\right) \\
& -\sqrt{3}V_5 I_6 \cos\left(\omega t + \phi_{i_6} - \phi_{v_5}\right) + V_5 I_6 \sin\left(\omega t + \phi_{i_6} - \phi_{v_5}\right) \\
& +\sqrt{3}V_5 I_6 \cos\left(11\omega t + \phi_{i_6} + \phi_{v_5}\right) + V_5 I_6 \sin\left(11\omega t + \phi_{i_6} + \phi_{v_5}\right) \\
& +2V_5 I_7 \sin\left(12\omega t + \phi_{i_7} + \phi_{v_5}\right) \\
& +2V_5 I_8 \sin\left(3\omega t + \phi_{i_8} - \phi_{v_5}\right) \\
& -\sqrt{3}V_5 I_9 \cos\left(4\omega t + \phi_{i_9} - \phi_{v_5}\right) + V_5 I_9 \sin\left(4\omega t + \phi_{i_9} - \phi_{v_5}\right) \\
& +\sqrt{3}V_5 I_9 \cos\left(14\omega t + \phi_{i_9} + \phi_{v_5}\right) + V_5 I_9 \sin\left(14\omega t + \phi_{i_9} + \phi_{v_5}\right) \ldots
\end{aligned}$$

(B.3)

$$
\begin{aligned}
&+\sqrt{3}V_6I_1\cos\left(5\omega t-\phi_{i_1}+\phi_{v_6}\right)+V_6I_1\sin\left(5\omega t-\phi_{i_1}+\phi_{v_6}\right)\\
&-\sqrt{3}V_6I_1\cos\left(7\omega t+\phi_{i_1}+\phi_{v_6}\right)+V_6I_1\sin\left(7\omega t+\phi_{i_1}+\phi_{v_6}\right)\\
&+\sqrt{3}V_6I_2\cos\left(4\omega t-\phi_{i_2}+\phi_{v_6}\right)-V_6I_2\sin\left(4\omega t-\phi_{i_2}+\phi_{v_6}\right)\\
&-\sqrt{3}V_6I_2\cos\left(8\omega t+\phi_{i_2}+\phi_{v_6}\right)-V_6I_2\sin\left(8\omega t+\phi_{i_2}+\phi_{v_6}\right)\\
&+\sqrt{3}V_6I_4\cos\left(2\omega t-\phi_{i_4}+\phi_{v_6}\right)+V_6I_4\sin\left(10\omega t+\phi_{i_4}+\phi_{v_6}\right)\\
&-\sqrt{3}V_6I_4\cos\left(10\omega t+\phi_{i_4}+\phi_{v_6}\right)+V_6I_4\sin\left(2\omega t-\phi_{i_4}+\phi_{v_6}\right)\\
&+\sqrt{3}V_6I_5\cos\left(\omega t-\phi_{i_5}+\phi_{v_6}\right)-V_6I_5\sin\left(\omega t-\phi_{i_5}+\phi_{v_6}\right)\\
&-\sqrt{3}V_6I_5\cos\left(11\omega t+\phi_{i_5}+\phi_{v_6}\right)-V_6I_5\sin\left(11\omega t+\phi_{i_5}+\phi_{v_6}\right)\\
&+\sqrt{3}V_6I_7\cos\left(\omega t+\phi_{i_7}-\phi_{v_6}\right)-V_6I_7\sin\left(\omega t+\phi_{i_7}-\phi_{v_6}\right)\\
&-\sqrt{3}V_6I_7\cos\left(13\omega t+\phi_{i_7}+\phi_{v_6}\right)+V_6I_7\sin\left(13\omega t+\phi_{i_7}+\phi_{v_6}\right)\\
&+\sqrt{3}V_6I_8\cos\left(2\omega t+\phi_{i_8}-\phi_{v_6}\right)+V_6I_8\sin\left(2\omega t+\phi_{i_8}-\phi_{v_6}\right)\\
&-\sqrt{3}V_6I_8\cos\left(14\omega t+\phi_{i_8}+\phi_{v_6}\right)-V_6I_8\sin\left(14\omega t+\phi_{i_8}+\phi_{v_6}\right)\cdots
\end{aligned}
\tag{B.4}
$$

APPENDIX C – VOLTAGE MEASUREMENT

Paredes (2006) and Marafão et al. (2008) investigated how the choice of the reference point for voltage measurement may influence power calculations and power quality assessment in three-phase electric systems. These works basically discussed two approaches for three-phase voltage measurement:

i. phase voltages in relation with the neutral conductor (v_a, v_b and v_c); and

ii. phase and neutral voltages in relation with an external virtual point (v_{ao}, v_{bo}, v_{co} and v_{no}).

Figure 111 – Three-phase system with voltage measurement methods discussed by Paredes (2006) and Marafão et al. (2008).
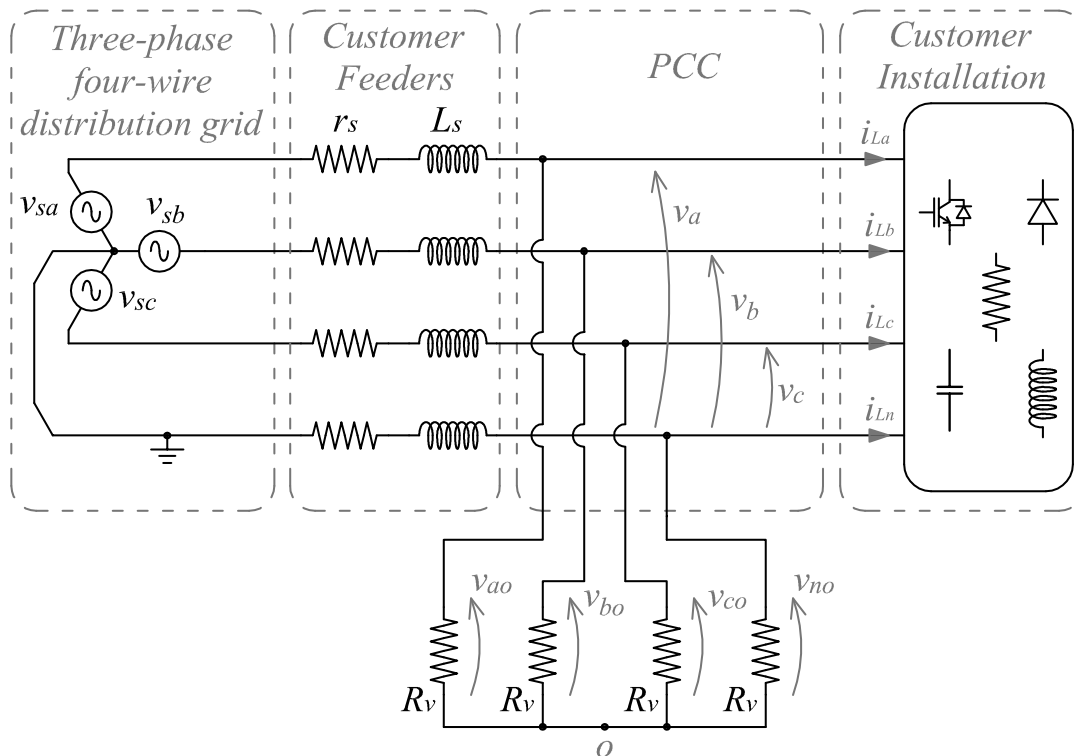
These measurement methods are generically illustrated in Figure 111. The virtual point (regarded as "*o*" in this work) taken as voltage reference in the second method is the common

point of auxiliary resistances R_v. For proper voltage measurements, these resistances must be much higher than load impedances (PAREDES, 2006; MARAFÃO et al., 2008). It can also be observed that the method *"i"* employs three voltage transducers, whereas the second method requires the additional measurement of the neutral voltage in relation to the point o (PAREDES, 2006; MARAFÃO et al., 2008).

Aiming to understand the relationship between both approaches, Paredes (2006) and Marafão et al. (2008) showed mathematically and in simulation studies the convergences and divergences of each measurement method. Phase-to-neutral measurements v_a, v_b and v_c are exactly the voltages applied to load terminals, expressed generically as

$$\begin{cases} v_a = & v_{a+} + v_{a-} + v_0 \\ v_b = & v_{b+} + v_{b-} + v_0 \\ v_c = & v_{c+} + v_{c-} + v_0 \end{cases}, \tag{C.1}$$

where v_{a+}, v_{b+} and v_{c+} stand for positive-sequence, v_{a-}, v_{b-} and v_{c-} stand for the negative-sequence and v_0 is the zero-sequence voltage.

The measurements of phase voltages in relation to the point o contain positive- and negative-sequence components, as well as an attenuated parcel of the zero-sequence voltage component. The neutral voltage v_{no} is proportional to the zero-sequence voltages, including triplen harmonics. The results obtained are expressed as

$$\begin{cases} v_{ao} = & v_{a+} + v_{a-} + \dfrac{1}{4}v_0 \\[2mm] v_{bo} = & v_{b+} + v_{b-} + \dfrac{1}{4}v_0 \\[2mm] v_{co} = & v_{c+} + v_{c-} + \dfrac{1}{4}v_0 \\[2mm] v_{no} = & -\dfrac{3}{4}v_0 \end{cases}. \tag{C.2}$$

These expressions also show that both measurement approaches provide equal results if there are no zero-sequence voltages in the grid. A method was also presented to equalize both measurement methodologies (PAREDES, 2006; MARAFÃO et al., 2008). The authors concluded that the measurement of voltages in relation to the virtual point o seems to be more interesting in high-voltage three-phase three-wire systems (PAREDES, 2006; MARAFÃO et al., 2008). Measurements using the neutral conductor as reference seem to be more suitable for three-phase four-wire low-voltage systems with unbalances and harmonic distortions. This method also

present the advantage of needing one less voltage transducer if compared to the other measurement method (PAREDES, 2006; MARAFÃO et al., 2008).

Aiming to choose the most appropriate voltage measurement approach for the calculation of the two-phase powers proposed in this work, the application of both these measurement methods was investigated for $2\phi 3w$ systems. The achievements of such studies are described in detail in the following subsections.

C.1 NEUTRAL CONDUCTOR AS REFERENCE

In this voltage measurement approach, the neutral conductor is adopted as reference. Voltage sensors are connected at PCC between each phase (*a* and *b*) and the neutral conductor, as illustrated in Figure 112. The two-phase voltage signals are represented in this work as v_a and v_b. These are the voltages actually applied to load terminals in relation to the neutral conductor.

Figure 112 – Voltage measurement with neutral conductor as reference.
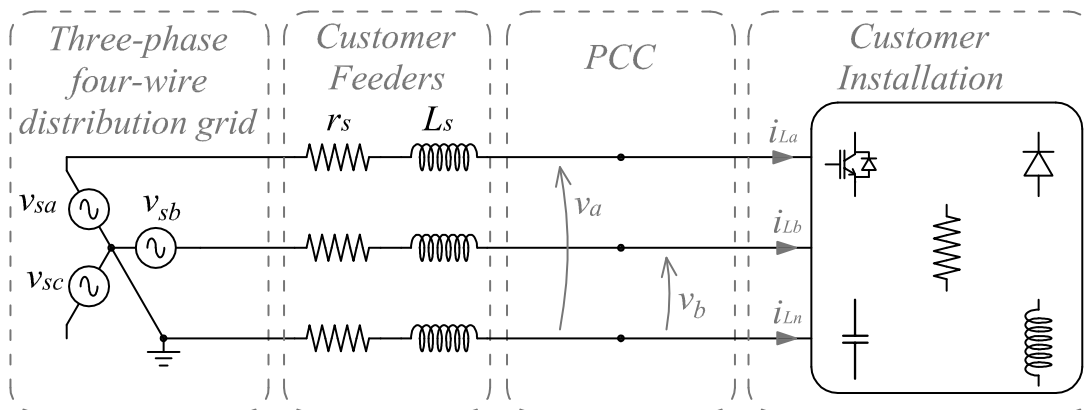
In the context of this work, $2\phi 3w$ circuits are ramifications originated from three-phase four-wire grids. Therefore, two-phase voltages can be mathematically expressed in terms of symmetrical components that may exist in three-phase system which originated the studied $2\phi 3w$ circuit. Following this assumption, the two-phase voltages measured at PCC taking the neutral conductor as reference can be generically written as

$$\begin{cases} v_a = v_{a+} + v_{a-} + v_0 \\ v_b = v_{b+} + v_{b-} + v_0 \end{cases}. \tag{C.3}$$

Similarly to what happens in three-phase systems (PAREDES, 2006; MARAFÃO et al., 2008), two-phase voltages measured taking the neutral conductor as reference are the voltages actually applied to load terminals.

C.2   EXTERNAL VIRTUAL POINT AS REFERENCE

As previously mentioned, an alternative method for voltage measurement employs three resistors R_v connected between the conductors at PCC (phases and neutral) and a common (virtual) point (PAREDES, 2006; MARAFÃO et al., 2008) named "o" in this work. This measurement approach is illustrated for $2\phi 3w$ circuits in Figure 113. The voltage signals obtained with this method at phase a, phase b and neutral are represented by v_{ao}, v_{bo} and v_{no}, respectively.

Figure 113 – Two-phase voltage measurement using the neutral point as reference.
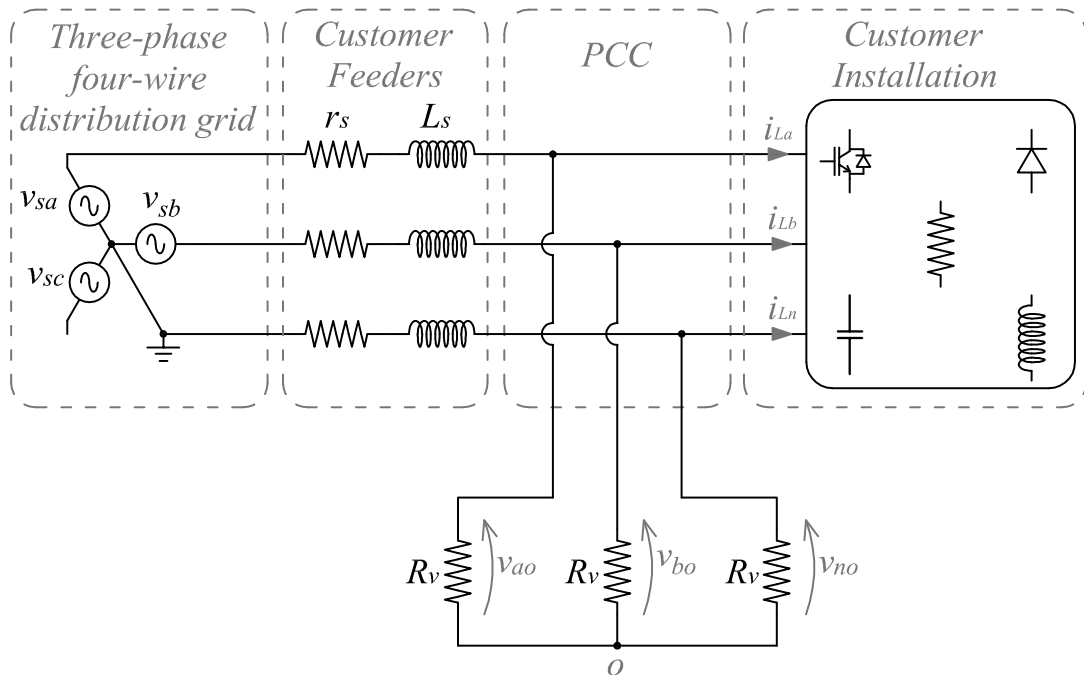
Aiming to understand the meaning of v_{ao}, v_{bo} and v_{co}, this measurement system can represented in the simplified circuit shown in Figure 114.

Figure 114 – Simplified circuit for voltage measurement approaches in $2\phi 3w$ circuits.
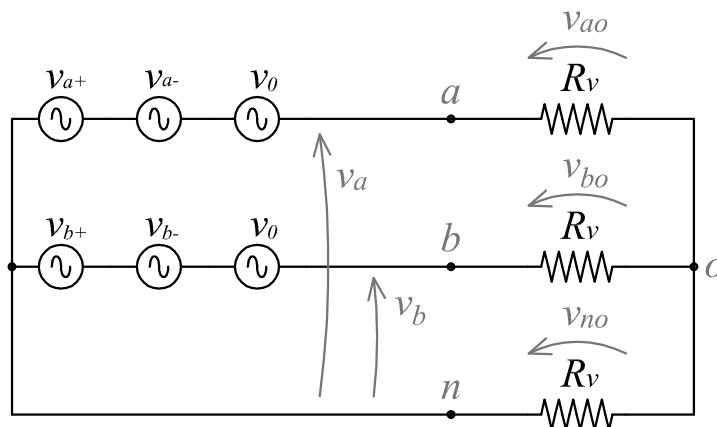
Applying the same analysis methodology used by Paredes (2006) and Marafão et al. (2008), it is possible to verify that two-phase virtual-point-referenced voltage measurements are expressed as

$$
\begin{cases}
v_{ao} = & +\dfrac{2}{3}v_{a+} + \dfrac{2}{3}v_{a-} - \dfrac{1}{3}v_{b+} - \dfrac{1}{3}v_{b-} + \dfrac{1}{3}v_0 \\[2ex]
v_{bo} = & -\dfrac{1}{3}v_{a+} - \dfrac{1}{3}v_{a-} + \dfrac{2}{3}v_{b+} + \dfrac{2}{3}v_{b-} + \dfrac{1}{3}v_0 \\[2ex]
v_{no} = & -\dfrac{1}{3}v_{a+} - \dfrac{1}{3}v_{a-} - \dfrac{1}{3}v_{b+} - \dfrac{1}{3}v_{b-} - \dfrac{2}{3}v_0
\end{cases} ,
\tag{C.4}
$$

where it is possible to observe that measured quantities contain positive-, negative- and zero-sequence components from phases a and b. Also, it can be verified that

$$
v_{ao} + v_{bo} + v_{no} = 0.
\tag{C.5}
$$

Furthermore, (C.3) and (C.4) can be combined to write a linear relationship between the two measurement methods discussed

$$
\begin{bmatrix} v_{ao} \\ v_{bo} \\ v_{no} \end{bmatrix} = \frac{1}{3} \begin{bmatrix} 2 & -1 \\ -1 & 2 \\ -1 & -1 \end{bmatrix} \begin{bmatrix} v_a \\ v_b \end{bmatrix}
\tag{C.6}
$$

or, in the inverse operation, as

$$
\begin{bmatrix} v_a \\ v_b \end{bmatrix} = \begin{bmatrix} 2 & 1 \\ 1 & 2 \end{bmatrix} \begin{bmatrix} v_{ao} \\ v_{bo} \end{bmatrix}.
\tag{C.7}
$$

C.2.1 *TWO-PHASE INSTANTANEOUS POWERS USING VOLTAGES REFERENCED TO A VIRTUAL POINT "O"*

Aiming to investigate the possibility of using the results in (C.4) to calculate the two-phase instantaneous powers as proposed in Chapter 3, it is interesting to observe the condition at which two-phase voltages and currents are sinusoidal and balanced. In this condition, phase-to-neutral voltages, are generically expressed as

$$
\begin{cases}
v_a = & \sqrt{2}V_+ \sin(\omega t) \\[2ex]
v_b = & \sqrt{2}V_+ \sin\left(\omega t - \dfrac{2\pi}{3}\right)
\end{cases} ,
\tag{C.8}
$$

that can be applied into (C.6) to obtain the voltage measurements taking the virtual point "*o*" as reference, which results in

$$
\begin{cases}
v_{ao} = & \dfrac{2\sqrt{2}}{3} V_+ \sin(\omega t) + \dfrac{\sqrt{2}}{3} V_+ \cos\left(\omega t - \dfrac{\pi}{6}\right) \\[3mm]
v_{bo} = & -\dfrac{\sqrt{2}}{3} V_+ \sin(\omega t) - \dfrac{2\sqrt{2}}{3} V_+ \cos\left(\omega t - \dfrac{\pi}{6}\right) \\[3mm]
v_{no} = & -\dfrac{\sqrt{2}}{3} V_+ \sin(\omega t) + \dfrac{\sqrt{2}}{3} V_+ \cos\left(\omega t - \dfrac{\pi}{6}\right)
\end{cases}
. \tag{C.9}
$$

Applying the linear transformation described in (3.3) to *ab* quantities, it is possible to represent these voltages in the $\alpha\beta$ coordinates:

$$
\begin{cases}
v_{\alpha o} = & \dfrac{2\sqrt{2}}{3} V_+ \sin(\omega t) + \dfrac{\sqrt{2}}{3} V_+ \cos\left(\omega t - \dfrac{\pi}{6}\right) \\[3mm]
v_{\beta o} = & -\dfrac{\sqrt{6}}{6} V_+ \sin(\omega t) - \dfrac{\sqrt{2}}{2} V_+ \cos(\omega t)
\end{cases}
. \tag{C.10}
$$

It is interesting to mention here that

$$
\int_0^{2\pi} v_{\alpha o} \cdot v_{\beta o}\, d(\omega t) \neq 0, \tag{C.11}
$$

which means that $v_{\alpha o}$ and $v_{\beta o}$ are not orthogonal, even though orthogonality is expected for $\alpha\beta$ quantities.

As also stated in Section 3.4.1, two-phase sinusoidal balanced two-phase currents are generically expressed in *ab* coordinates as

$$
\begin{cases}
i_a = & \sqrt{2}I_+ \sin\left(\omega t + \phi_{i_+}\right) \\[2mm]
i_b = & \sqrt{2}I_+ \sin\left(\omega t - \dfrac{2\pi}{3} + \phi_{i_+}\right)
\end{cases}
. \tag{C.12}
$$

and in the $\alpha\beta$ reference frame as

$$
\begin{cases}
i_\alpha = & \sqrt{2}I_+ \sin\left(\omega t + \phi_{i_+}\right) \\[3mm]
i_\beta = & -\sqrt{2}I_+ \cos\left(\omega t + \phi_{i_+}\right)
\end{cases}
. \tag{C.13}
$$

Using (C.13) and (C.10) to calculate two-phase powers according to (3.10) yields

$$
\begin{cases}
\bar{p}_{2\phi o} = -\dfrac{\sqrt{3}}{6} V_+ I_+ \sin\left(\phi_{i_+}\right) + \dfrac{7}{6} V_+ I_+ \cos\left(\phi_{i_+}\right) + \dfrac{1}{3} V_+ I_+ \sin\left(\phi_{i_+} + \dfrac{\pi}{6}\right) \\[3mm]
\tilde{p}_{2\phi o} = +\dfrac{\sqrt{3}}{6} \sin\left(2\omega t + \phi_{i_+}\right) - \dfrac{1}{6} \cos\left(2\omega t + \phi_{i_+}\right) + \dfrac{1}{3} \sin\left(2\omega t + \phi_{i_+} - \dfrac{\pi}{6}\right) \\[3mm]
\bar{q}_{2\phi o} = -\dfrac{7}{6} V_+ I_+ \sin\left(\phi_{i_+}\right) - \dfrac{\sqrt{3}}{6} V_+ I_+ \cos\left(\phi_{i_+}\right) + \dfrac{1}{3} V_+ I_+ \cos\left(\phi_{i_+} + \dfrac{\pi}{6}\right) \\[3mm]
\tilde{q}_{2\phi o} = +\dfrac{1}{6} V_+ I_+ \sin\left(\phi_{i_+} + 2\omega t\right) + \dfrac{\sqrt{3}}{6} V_+ I_+ \cos\left(\phi_{i_+} + 2\omega t\right) + \\[3mm]
\qquad\qquad +\dfrac{1}{3} V_+ I_+ \cos\left(2\omega t + \phi_{i_+} - \dfrac{\pi}{6}\right)
\end{cases}
\tag{C.14}
$$

It is possible to observe that, using voltages referenced to the virtual point "o", two-phase instantaneous powers $p_{2\phi}$ and $q_{2\phi}$ present both average and oscillating values. This characteristic is undesired for PC applications in the context of this work. The reason is because it complicates the separation of fundamental-frequency positive-sequence components under unbalances and harmonic distortions. Also, it was shown that two-phase $\alpha\beta$ voltages calculated using (3.3) are not orthogonal when measurements are made using the virtual point "o" as reference. Therefore, it can be concluded that such method of voltage measurement is not adequate for the methodology proposed in this work to deal with powers in two-phase three-wire circuits.

For the reasons discussed above, it is adopted in this work the measurement of $2\phi3w$ voltages taking the neutral conductor as reference, as described in Section C.1. The two-phase instantaneous powers obtained with this measurement method are described in detail in Chapter 3.